OPTIMISATION OF SOLAR DESALINATION PROCESS

An investigation of the critical parameters affecting solar still water production in the context of a developing country

Dissertation in fulfilment of the Master of Engineering Degree requirements (Mechanical)

Student:

Alexander Gorrie, 72769698

UNIVERSITY OF CANTERBURY

Primary Supervisor:

Dr Dirk Pons

UNIVERSITY OF CANTERBURY

Secondary Supervisor:

Dr Paul Docherty

UNIVERSITY OF CANTERBURY

Secondary Supervisor:

David Maples

ARA INSTITUTE OF CANTERBURY

Industry Client:

John Wilson

SUNSHINE SOLAR

2015 - 2016

Abstract

There is a global need for people to have access to enough potable water to meet their daily needs. However, in developing countries water distribution infrastructure is often inadequate to meet demand. Water demand is anticipated to increase as a result of urbanisation, population growth and climate change. The solutions considered must be feasible for those subject to water scarcity.

The current work is concerned with development of a solar desalination still to increase water security in developing countries. Design focus has been on the technical and sociocultural factors which are most important for optimising performance and community acceptance of a still. The work has particular focus toward applications in South Pacific nations where electricity supply, available capital and technical expertise are more limited than in more developed countries.

The influence of several environmental, design and operational factors on water productivity have been tested as part of the current work. This testing led to the formulation of an equation set defining system dynamics. The equations were based on fundamental heat transfer and thermodynamics principles. Solar still desalination is an active field of research and a range of empirical and semi-empirical equations have been presented in prior literature. The studies offering a thermodynamic basis for the equations are relatively few. No prior work was found to have integrated relative humidity as a system variable within the equation set, although it has been acknowledged that internal humidity in the still is below saturated. The current work addresses relative humidity as a significant system variable for the equation formulation and the models have excellent fit to the data as a result.

The key factors of influence were extracted from the empirical and model-building phase and consolidated into a series of design implications for practitioners focussing on solar stills and their design. These implications also considered the socio-cultural dimensions which are critical factors independent of the unit functionality. A framework was formulated which described a general new product design process, tailored specifically for application in developing countries. This framework was then applied to the solar still case, thereby presenting an implementation pathway relevant for practitioners in the field.

Contents

All schematic and photographic images produced by A. Gorrie unless otherwise stated

1 Introduction

1.1 Thesis Project Outline

This thesis is concerned with developing and evaluating the two solar desalination unit concepts presented by Sunshine Solar and with investigating parameters critical to unit productivity. The work involved has culminated to determining a systems-level representation of the thermodynamic system performance of the desalination unit concepts. There was a specific focus on investigating a design solution for application in South Pacific nations.

1.2 Overview of Active Desalination Systems

Solar desalination systems are broadly classified as either active or passive. An active system has one or more powered components; motors, actuators, condensers or pumps; integrated in the design which assist in distilling the water. These active components are typically powered by the local electrical grid or through photo-voltaic (PV) cells. Large scale active desalination plants exist and have a variety of operating mechanisms, including Multi-Stage Flash, Multi-Effect Distillation, Vapour Compression and Reverse Osmosis. These processes produce potable water with high efficiency as a result of the electrical or fossil fuel power consumption, but are not viable for the socio-geographic context for this project. Limiting factors for large scale plants are the high capital and operational costs, high energy demand and require skilled operators and technicians. Active systems have been given lower priority than passive systems based on suitability in the intended context.

1.3 Overview of Passive Desalination Systems

A passive system utilises the ambient conditions; local solar radiation, wind flow, humidity, and water and air temperatures; to promote evaporation and condensation of saline or brackish water (henceforth referred to as brine water). The typical design for a passive solar desalination unit; henceforth referred to as a still, is provided in Figure 2.2. The general functional elements of the still comprise of an insulated basin containing the brine water enclosed with a transparent cover surface. As the sun heats the basin and brine water, the water evaporates and condenses on the cover surface, while the salt remains in the basin. The geometry of the cover surface promotes the condensate to collect at an outlet pipe. Some stills have multiple basins or extra layers of cover surface in which secondary condensation-evaporation cycles may occur. The main point of difference between solar stills is the cover geometry. However there are several design, operational and climatic parameters that influence the rate of distilled water production. These parameters influence different geometries to different extents.

1.4 Project Context

The client has proposed two conceptual designs as detailed below. The intention with each is that the unit be placed in a lagoon for the basin to be filled with brine water by the incoming tide. The evaporation and condensation processes function the same as per conventional stills.

The first concept is intended to operate at sub-atmospheric pressures; henceforth referred to as the Low Pressure concept, shown in Figure 1.4.1. Once the basin cavity is filled with brine water, the cavity volume is increased under sealed conditions. This volume increase causes a proportional decrease in internal pressure, which lowers the evaporation temperature of the brine water inside. A lower evaporation temperature means evaporation is initiated faster and therefore increases daily distilled water productivity. The feasibility of the Low Pressure concept depends on how easy it is in establishing and maintaining the isolated low pressure region. The foreseeable issues are maintaining seals, removing accumulated salt and the determining a suitable source of mechanical work to provide the volume increase.

| (*a*) | (*b*) |
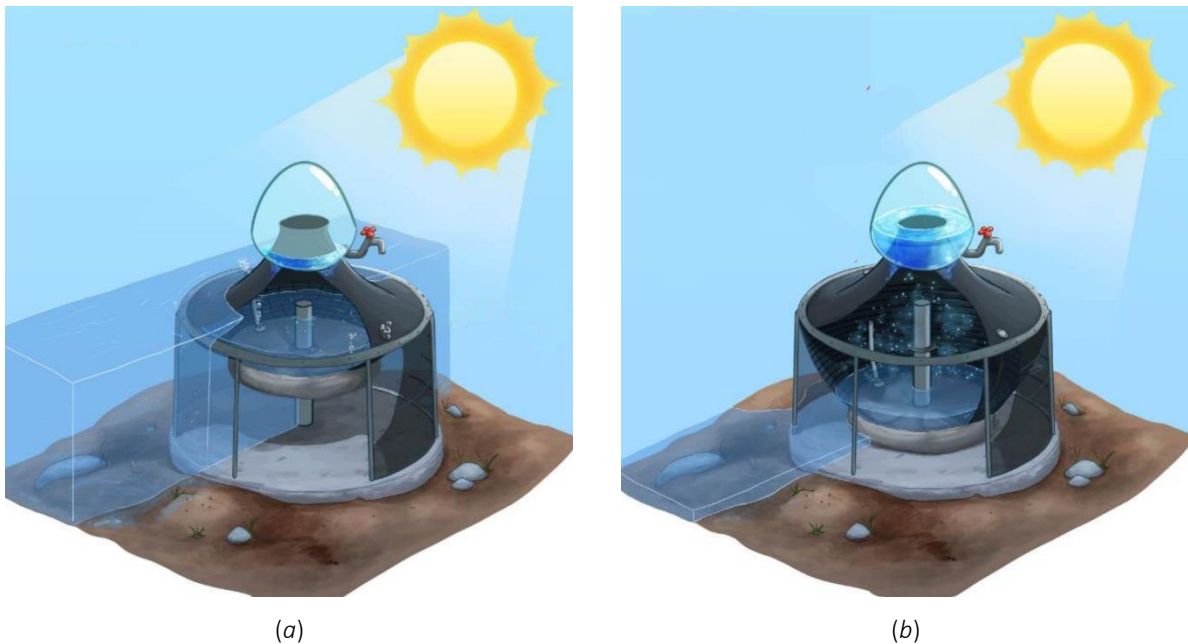
Figure 1.4.1: Initial conceptual schematic of Low Pressure Still filling at atmospheric pressure during high tide (*a*) and undergoing low pressure operation during low tide (*b*). Concept Image: Sunshine Solar

The second concept is open to the atmosphere; henceforth the Open Air concept, shown in Figure 1.4.2. This functionality differs from all other stills and desalination systems researched. The radiation absorption and condensate collection surfaces, are distinct from each other and separated from the basin. The condensate collection volume is open to the air at the top to facilitate convective airflow throughout the unit. When compared against the Low Pressure concept, the Open Air concept is considerably simpler. There are no volume changing elements, seals or valves required and the next high tide washes salt from the basin.

BRINE WATER DISH FILLED BY HIGH TIDE
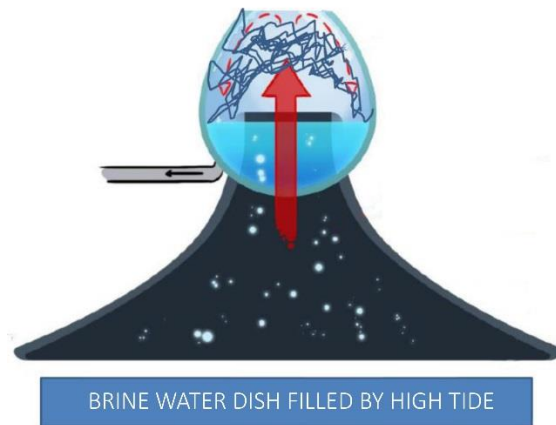
Figure 1.4.2: Initial conceptual schematic of Open-Air Still showing tide-filled brine dish and absorptive wick material. Concept Image: Sunshine Solar

There are currently no passive desalination systems designed specifically for use in the South Pacific, and Sunshine Solar has identified this as the niche market that the system will cater for. The high solar radiation and ambient temperatures in the South Pacific, as well as the relatively low population density, and high proportion of coastal communities are all factors that support the case for developing solar still technology for this context.

For the analyses undertaken in this project, it was judged necessary to select a particular Pacific nation and relate the findings and design developments to the environmental conditions specific to that nation. Tonga was selected on the basis of quantity and quality of available meteorological data. This decision was arbitrary, and the same design, experimentation and modelling process could be applied to any choice of Pacific nation.

The main concern for implementing a reliable design is the severity of sun, rain and wind that is common in South Pacific islands. The design must be sufficient to either withstand the expected environmental stresses, or be easily repaired by locals, using readily available materials. Developing a solution that suits the intended socio-geographic context is a critical facet of the project and design decisions have been made with this context in mind.

1.5 Client Background

Sunshine Solar is a Christchurch-based business that provides solar water heating solutions using Evacuated Tube, Flat Plate, and Hot Water Heat Pump technologies. The business provides both installations and retrofits to residential and commercial buildings, motels and schools across New Zealand. Sunshine Solar conducts ongoing research, development and testing programmes in conjunction with Ara Institute of Canterbury and the University of Canterbury (UC). Alongside the solar technologies, Sunshine Solar also provide underfloor heating and micro hydro services. Although the technology is being developed for Sunshine Solar, this project has been made possible through funding from Callaghan Innovation.

1.6 Situation under Examination: Client Need

The purpose of this project is to clarify relationships between parameters for the Sunshine Solar concepts and to devise a mathematical model that describes the system behaviour characteristics. The project has ascertained which parameters are of critical importance and which may be neglected to optimise distillate productivity. The systems-level model developed has built on the existing body of knowledge where applicable, as several aspects of the proposed designs are similar to existing technology. There are other aspects; passive low pressure operation and open system design; which differ from previous designs studied in the literature. Due to the novel operational principles, experimental validation was required to ensure the relationships obtained had some basis in reality.

From a technological perspective, the optimal solution exhibited the highest evaporation and condensation rates of all designs tested. From an economic perspective, and for practicality of maintenance, the solution had to utilize materials readily available to the islands where it is intended to be implemented. From a social suitability perspective, the solution had to operate using mechanisms that can be understood by the lay person; the level of complexity involved would not require a specialist in order to operate and maintain. It was acknowledged that a small degree of training may be necessary to give local people the knowledge to correctly operate the unit.

The aim was to validate the functionality of the conceptual designs and clarify enough of the solution space to inform the client what design parameters are most relevant to the optimising productivity within the intended context. This aim was realised with the completion of the mathematical model capturing the functional design.

2   Research and Literature Review

This chapter summarises the results of relevant studies and considers the limitations of the conclusions with respect to the project outcomes. The elements of heat transfer in a typical still have been classified [1] conceptually, although the accompanying equations defining the relationships presented in the literature often lacked a strong basis in first principles thermodynamics. It has been proposed that optimisation of parameters is location dependent [1]. The absence of focus on a South Pacific context in prior studies means that determining optimal design parameters for this context is a relatively unexplored field. The majority of prior studies have been conducted in the Middle East, Africa and India, which have different environmental conditions to what is expected in the context of the current study. The purpose of the preliminary research was to determine which factors influence distillate productivity and to what extent. The parameters investigated in this chapter has been broadly categorised as either the Climatic or Design parameters to most clearly represent whether their influence on the system is fully controllable or not.

Broadly speaking, productivity is a function of both the rate of evaporation of brine water in the basin and the rate of condensation on the collector surface. Factors that influence these rates have been reviewed, with accompanying effects on performance and relevant remarks, by Muthu *et al.* [2], and Muftah *et al.* [3].

The solar distillation process has been split into five main elements by Xiao *et al.* [4], redrawn in Figure 2.1. Solar radiation is absorbed by the brine and the basin plate, heat transfer occurs from the basin to the brine, from the brine to the condensation surface and from the condensation surface to the surroundings. Proposed design modifications have been incorporated in their relevant stages in Figure 2.1.
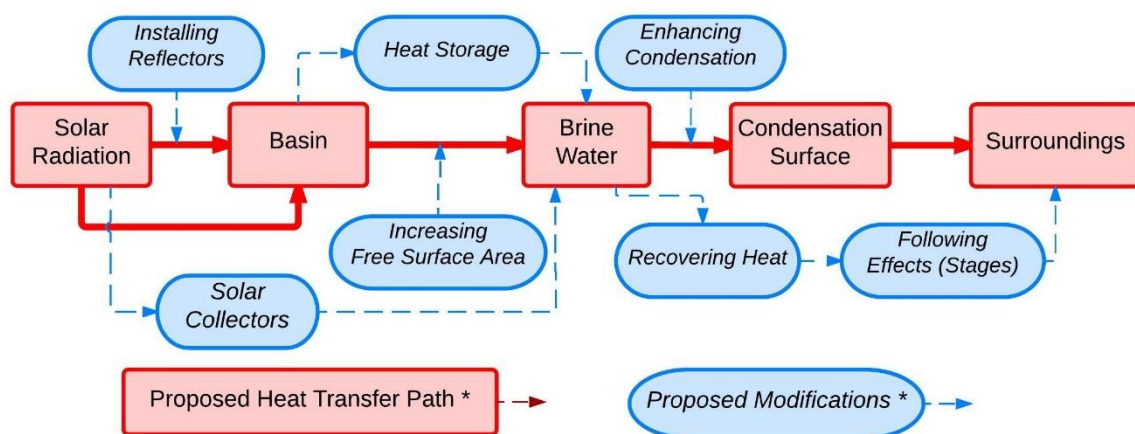
Figure 2.1: Solar Desalination Heat Transfer Process (* Xiao *et al.* [4])

The accompanying Figure 2.2 details functional elements of a Single Slope Solar Still (SSSS), which are typical for all stills. The nomenclature used within the literature review is presented below in Tables 2.1 and 2.2.
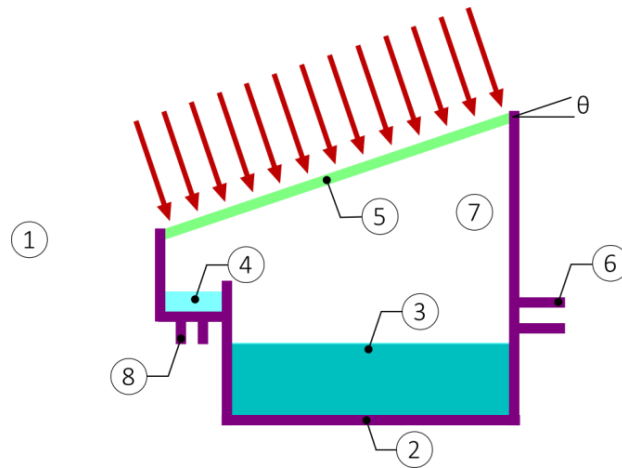
Figure 2.2: Schematic of SSSS detailing functional elements with respect to the nomenclature.

Table 2.1: Nomenclature of solar still functional components and related elements		
No. in Diagram	Subscript	Definition
1	*a*	Ambient Air / Surroundings
2	*B*	Basin
3	*BW*	Brine Water
4	*DW*	Distilled Water
5	*GC*	(Glass) Condensation Surface
6	*i*	Brine Water Inlet
7	*ia*	Internal Air
8	*o*	Distilled Water Outlet
-	*conv*	Convection
-	*evap*	Evaporation
-	*rad*	Radiation
-	*fg* (T_{evap})	Heat of Vaporisation at Evaporation Temperature
-	*Pa*	Saturated Vapour at Room Temperature
-	*w*	Saturated at Water Surface temperature
-	*r*	Room Temperature and Humidity
-	*T*	Total
-	*S*	Saline Water
-	*L*	Loss
-	*INC*	Incident

Table 2.2: Nomenclature assigned to terms presented in the literature		
Term	SI Units	Definition
A	m^2	Area
C	$J/(kg\ K)$	Specific Heat Capacity
d	cm	Brine Depth
$\dot{E}$	kg/m^2h	Evaporation Rate
ΔH_{vap}	kJ/kg	Latent heat of vaporisation
h	W/m^2K	Heat Transfer Coefficient
I	$MJ/m^2/day$	Solar Irradiation
k	$W/(m\ K)$	Thermal Conductivity
M	g/mol	Molecular Weight
$\dot{m}$	kg/s	Mass Production Rate
m	kg	Mass
P	kPa	Partial Pressure of Water Vapour
P_D	$L/m^2/day$	Daily Water Productivity
Q	W	Heat Transfer Energy
T	$°C$	Temperature
ΔT	$°C$	Temperature difference
t	s	Time
V	m/s	Wind Velocity
W	kg (vapour) $/\ kg$ (air)	Specific Humidity
δ/L	m/m	Brine-Depth to Frontal-Still-Height Ratio
ϑ	°	Inclination Angle

2.1   Climatic Parameters

The following parameters all relate to the environment in which the still is placed and act independent to the design or operational configuration of the still.

2.1.1   Relative Humidity of Air

Empirical testing of a triangular solar still (TrSS), by Ahsan *et al* [5] has indicated that the relative humidity of the air inside the still was below saturated, despite high humidity conditions prevalent in Malaysia where testing was conducted. This result indicates that it is not safe to assume saturation. Therefore humid air properties must be integrated into the associated numerical model to correctly capture the dynamics [5], and this adds further complexity.

2.1.2   Solar Radiation

Daily distilled water productivity is directly proportional to the degree of solar radiation incident [5, 6], at least for the case of rectangular and planar surfaces, and this variable has been identified as the most critical parameter to distillate productivity [6, 7]. Whether the same relationships apply for a spherical/hemispherical collector is not addressed in the literature. The meta-analysis conducted by Khalifa *et al*. [6] correlated data from several studies to provide a broader understanding of the effects of the four most relevant performance parameters (solar radiation, brine depth, inclination angle, addition of dye). The correlated equations can be expected to only be valid for the specific situational variables: passive basin stills in operation between the latitudes of 20°-35° N, fabricated from galvanised iron with a 5-10 *cm* thick insulation layer of polystyrene or material of equivalent conductivity [6]. The relationship between distillate productivity and incident energy is given as equation (2.1.2.1).

$$P_D = 0.0036\,I^2 + 0.0701I + 0.2475 \tag{2.1.2.1}$$

where daily water productivity (P_D) is related to the incident solar radiation (I). The equation is limited to solar flux exposures between 8-30 $MJ/m^2/day$ and has a regression coefficient of 0.76. Distillate productivity ranged between $1.0 - 6.0$ $L/m^2/day$ according to the presented data [6]. As the form of equation (2.1.2.1) indicates, it is a power-law fit to empirical data. There is no reason to believe that the underlying mechanics actually abide by this relationship.

A lag time of approximately an hour exists between the peaks in solar radiation and distilled water production [5]. Over a 30 hour test period, productivity was seen to decrease by approximately 44 *%* on a cloudy day as compared to a sunny day [8], all other test parameters remaining constant.

2.1.3 Ambient Air and Water Temperatures

For a given still, elevating the ambient air temperature increases production [5, 9]. Productivity increases ranging from anywhere between 8 % due a temperature rise from 23 to 33 °C, to 288 % due to a temperature rise from 28.6 to 33 °C [5]. An explicit relationship relating ambient air temperature to distillate productivity has not been established. It seems likely that the effect would be dependent on how effectively the absorber can raise the temperature of the brine water, as the evaporation and condensation processes are driven by the temperature gradient between the brine water and ultimately the ambient temperature. In context, it is highly unlikely that the condensing surface will be maintained at a temperature cooler than ambient without active componentry.

The relationship between distillate productivity and brine water temperature is proportional from 20 − 35 °C, above which point the output becomes progressively less dependent on brine temperature [9]. If the brine water could be pre-heated to 40 − 45 °C, the system yield would be expected to increase [10]. This yield increase has been quantified as 8 % more distilled water when the initial temperature is 40 °C rather than 20 °C [9]. Several studies [3, 11] have suggested that the converse relationship is true for brine temperatures in the range of 45 − 65 °C. At a given wind velocity within this range, increasing the temperature causes substantial increase in productivity as shown in Figure 2.1.3.
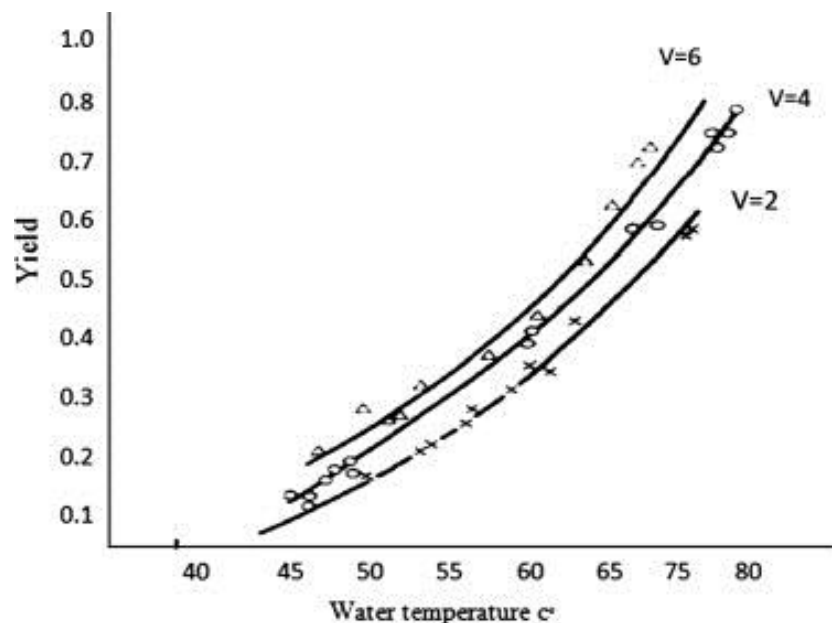
Figure 2.1.3: Variation in distillate productivity (yield) based on wind velocity and brine water temperature [3].

2.1.4   Wind Velocity

There are conflicting results regarding effect of wind velocity on distilled water productivity. Numerical simulations conducted by Nafey *et al*. [7], showed that an increase in wind velocity decreased productivity. The trend presented is not directly proportional and productivity is effectively unchanged beyond a threshold velocity. The argument presented is that increasing the wind velocity reduces the ratio of evaporative heat transfer coefficient to glass-ambient convective coefficient [7]. This result means that for a given rate of convective heat transfer from the still, the evaporative heat transfer is reduced as the wind velocity increases. Less effective evaporation means lower distillate productivity.

Experimental results from Dimri *et al*. [12] indicate that the converse relationship with velocity exists. As before, productivity remains unchanged after a threshold velocity, although this velocity now corresponds to a maximum productivity. The argument is that as velocity increases, convective heat transfer between the glass and ambient air increases. This effect is driven by both the greater cover-to-brine temperature difference and the increased convective heat transfer coefficient [12]. The threshold velocity was determined as independent of still shape, operation mode (active vs. passive) and heat capacity of brine, although it did exhibit seasonal dependence [13].

It has been proposed that a critical brine mass exists, which may account for both phenomena [13]. Above a brine mass of 45 *kg*, still productivity increases with velocity up until the threshold, and below it, productivity decreases with velocity until the threshold. Productivity has been shown to vary between $2.2 - 4.3$ $L/m^2/day$ over the tested range of brine depths and wind velocities [13]. The velocity threshold for a SSSS has been determined as approximately 10 *m/s* [13-15], above which the cover-to-brine temperature difference becomes progressively less dependent on velocity.

2.1.5   Water Salinity and Contaminant Content

The effect of water salinity on distillate production is relatively limited in terms of quantitative relationships. It is generally observed that distilled water production decreases with increased salinity [16, 17]. Experimental results from Akash *et al*. [16] indicate that the productivity-salinity relationship is non-linear and that the detrimental effects on performance become progressively less pronounced at higher salt concentrations. The dependence of distillate production on salinity appears minimal whilst the salinity content lies between 35 - 65 *%* as shown in Figure 2.1.5. The low salinity region, below 35 *%* salt content, has been given little attention in this study.   Considering only the $35 - 65$ *%* range identified, the average production is 5.01 ± 0.09 *L/day*, however this figure changes significantly to 4.9 ± 0.3 *L/day* once the 75 *%* salinity data point is incorporated. This result is indicative that there is a change in system dynamics somewhere between 65 and 75 *%* salinity for the energy input and environmental conditions present during testing.
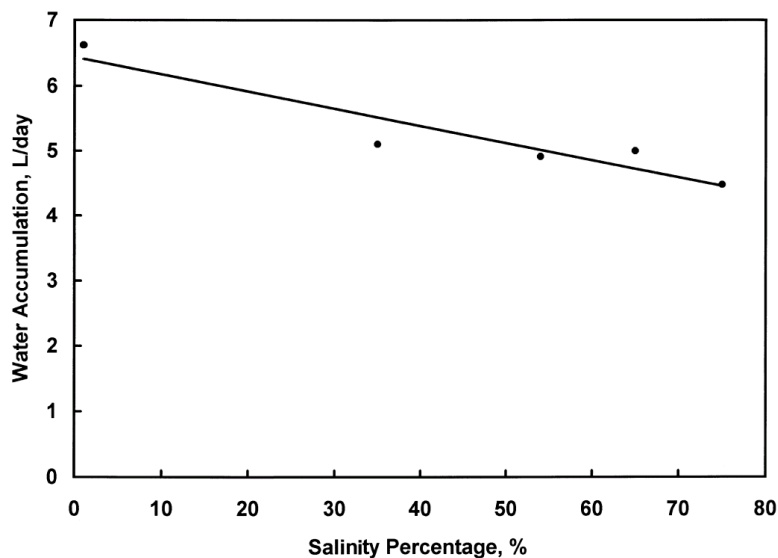
Figure 2.1.5: Effect of salt concentration on distillate production [16]

Figure 2.1.5 provided with permission from the content publisher, Elsevier. License Number: 3887830135567. Refer to Appendix 01 for full license details.

Experimental results presented by Mahdi *et al* indicate that the relationship between efficiency and salinity is effectively linear for water salinity ranging between $0 - 5$ *%* by weight [18].

Experimentation carried out by Abu-Hijleh *et al*. investigated how brine salinity influenced the evaporative efficacy of sponges placed in the basin. The saline concentrations tested corresponded to fresh, brackish and seawater local to Jordan. The accompanying explanation indicated that the increased density and reduced vapour pressure of brine water reduced the effectiveness of the capillary forces in raising this to the evaporative surfaces of the inserted sponges [17] The underlying mechanisms of how salinity influences water production were not addressed in any of the papers studied.

The efficacy of the solar still design at removing other water contaminants has been investigated [19]. Untreated water samples were collected from various boreholes in Nigeria and gave a realistic basis to the contaminant quantities and varieties. All tested samples contained *coli* form bacteria in quantities that the study classified as a 'heavily contaminated microbial load' (2.6×10^4 *cfu/ml*[1]). The samples also contained calcium carbonate (267 *mg/L*) in excess of the World Health Organisation guideline recommendation of 80 *mg/L*. The distilled water exhibited no trace of either microbial or mineral contaminant according to the results [19]. This outcome indicates that the solar still may be considered a viable solution for treatment of water containing other contaminants than exclusively sea salts. The solar still capacity to remove chemical contaminants (petrochemical or fertiliser compounds) is unknown and offers scope for further study. This has been judged beyond the scope of the current project as the intended recipient nations in the Pacific have access to an abundance of seawater, so salt removal is the main priority.

---

[1] 1 *cfu* = 1 colony forming unit

2.2   Design Parameters

The following parameters all relate to the design configuration or operating conditions of the still. These parameters are all predetermined and are independent of the environment the still is placed in.

2.2.1   Brine Depth in Basin

Water with a lower volumetric heat absorption capacity reaches a higher temperature faster and therefore promotes more rapid evaporation. This outcome became more apparent as the initial brine depth in the basin was reduced [1, 5]. Reducing brine depth causes distillate productivity to be initiated earlier and at a greater rate during daylight hours than stills with greater brine depths [7]. However, the system has a reduced thermal storage capacity and after sunset, productivity rates decrease quickly. Conversely, a deeper basin exhibits a longer lag time in productivity after sunrise, but continues to produce into the night [20]. For a given location; where the amount of incident solar radiation is the same, deeper brine depths will have lower temperatures [1]. Deeper brine depth test cases exhibited less variation in temperature than tests at shallower depths due to the greater volumetric heat capacity of the water [1, 20]. Deeper brine depths also act to moderate abrupt changes in solar intensity, namely passing cloud cover.

For a SSSS, the glass cover surface absorbs incident radiation faster than the brine and consequently heats up a faster rate. This condition establishes an inverse temperature gradient (cover surface hotter than brine surface) to what is desired. A deeper brine depth increases the time needed for the temperature to exceed the cover temperature [20], which delays the initial producitivity onset. For the 0.04 - 0.18 m range of depths tested by Tiwari *et al*. [20], the thermal storage is sufficient for the brine temperautre to remain above the cover temperature throughout the night until sunrise the next day. The test with 0.04 m depth exhibits both the highest daily productivity (1.174 kg/m^2) and the highest efficiency (18.9 %). This result raises the question of whether lower depths are worth focussing on.

With increasing brine depth between 0.04 − 0.16 m, the evaporative and convective heat transfer coefficients both reduce in magnitude at a given instance in time and display significantly less variation, reaching almost constant values at the greatest depths. The general form of the heat transfer relationship is given as equation (2.2.1.1), between the heat source (1) and the heat sink (2).

$$Q_{1-2} = h_{1-2}\,\Delta T_{1-2}$$
<div align="right">(2.2.1.1)</div>

where the energy flux (Q) depends on temperature difference (ΔT) and heat transfer coefficient (h). The energy flux is directly proportional to the heat transfer coefficient for a given temperature difference. The heat transfer coefficients at 0.18 m brine depth are greater than all but the 0.04 m. Despite the greater evaporative heat transfer coefficient, the yield at 0.18 m is considerably less than at 0.04 m due to the lower cover-to-brine temperature difference; typical of greater brine depths [20]. Yield is the product of the evaporative heat transfer coefficient and the cover-to-brine temperature difference. The smaller temperature difference delays productivity and negates any benefit achieved through energy storage overnight [20].

The numerical simulations for varying brine depth match the experimental results closely [7]. The data correlation conducted by Khalifa *et al*. [6] formulated the distillate productivity (P_D) relationship as shown equation (2.2.1.2)

$$P_D = 3.884 \, e^{-0.0458 \, d} \tag{2.2.1.2}$$

where (P_D) is exponentially dependent on brine depth (d). The exponential term suggests that the depth has a cumulative effect on productivity. Equation (2.2.1.2) has a regression coefficient of 0.83 and is limited to brine depths in the range of 1-10 *cm*. The correlation indicated that brine depth alone could influence productivity by up to 33 *%.*

Residual questions concerning brine depth are regarding whether an optimal brine depth exists based on mass of brine and day – night temperature range. An optimal mass that would promote productivity during sunlight hours and prolong it during darkness hours through thermal storage has not been investigated using South Pacific environmental conditions.

For a SSSS, 45 *kg* is the proposed critical mass of brine water based on wind velocity effects [13]. At sub-critical brine water masses, the water does not have sufficient thermal storage capacity to maintain a high temperature [14]. As the airflow promotes convection at the cover surface and lowers the temperature, the brine water temperature also drops. The thermal differential decreases similarly after sunset, when there is little or no energy incident on the brine. Both instances result in a reduced cover-to-brine temperature difference and less evaporation on the glass surface. Super-critical masses are sufficient to establish a thermal storage effect so the brine temperature remains high even when the surface cover temperature drops [13]. The increased temperature difference promotes convective and evaporative heat transfer.

2.2.2 Inclination Angle

For SSSS, too low of an inclination angle will severely reduce condensate collection and promote dripping back into the brine [8]. Conversely, too great of an inclination angle will delay distilled water productivity according to equation (2.2.2.1). When the inclination angle becomes too great, reflection losses increase when the sun is high [1, 8]. The effect of the inclination angle on productivity exhibits seasonal variability, which has been attributed to the declinational angle of the earth [7]. To account for this variability, the incline must be as small as possible in summer and as large as possible in winter to ensure the incident radiation strikes as normal to the cover surface as possible. Seasonal variability in the intended South Pacific context is expected to be less pronounced than the study Nafey *et al*. conducted in Suez City, Egypt [7], as the former is more equatorial.

It has been concluded in a meta-analysis conducted by Khalifa [21] that optimum inclination angle is close to the latitude of the angle of the site, on the basis of the trends observed in 20 prior experimental and theoretical studies. This result supersedes the data correlation published two years prior [6] which concluded that 30 ° was the optimum inclination angle for productivity and inclination angle alone could influence productivity by up to 63 *%*.

An equation for the daily water productivity that produces values with less than ±5 *%* error from experimental results for an inclined plane still [7] has been presented as equation (2.2.2.1).

$$P_D = -1.39 + 0.248\,I + 0.033\,T_a - 0.017\,V - 0.008\theta - 1.2\frac{\delta}{l} \qquad (2.2.2.1)$$

where daily water productivity (P_D) is a function of ambient air temperature (T_a), wind velocity (V), glass inclination angle (ϑ), solar irradiation (I) and brine-depth-to-frontal-still-height ratio (δ/L). The model is simple and assumes linear dependence of the parameters studied. Increasing ambient temperature and solar radiation increase productivity, whereas increasing wind velocity inclination angle and depth to height ratio all decrease productivity. The equation is limited to the weather conditions of the Suez Gulf area, where the study was conducted. The nature of this equation is an empirical curve-fitting approach and does not necessarily capture the underlying physical mechanisms or attempt to relate to a first principles approach.

2.2.3   Condensate Surface Material

The influence of different condensaton surfaces on distilled water productivity has been studied. The most critical design parameter for selecting the condensation surface material is the contact angle between the water droplet and the reflecting surface. The most critical phenomenon influencing productivity is the reflection of solar irradiation from the still surface [22]. As the surface reflectivity is increased, the amount of solar radiation energy that penetrates far enough to be absorbed by the brine water and basin decreases so the primary energy transferral path is reduced. The contact surface angle that the water droplets make with the surface also alters surface reflectivity and transmissivity.

Droplet growth by coalescence occurs when surface coverage is around 30 % and is characterised by a self-repeating growth pattern such that the volume of condensed water is statistically identical to that at a later point in time [22]. This growth regime is desirable as it reaches a maximum value and remains constant.

Experiments comparing polyethylene terephthalate (PET) and glass reflecting surfaces yielded that the former promoted droplet condensation whereas the latter promoted puddle-shaped condensation. The latter regime promotes more light to pass through the surface and subsequently increases the solar energy incident to the brine in the still [1, 22]. As expected, a larger temperature difference between the brine and ambient air may be achieved using the glass reflection surface [22] which facilitates more effective heat transfer.

Glass and PET exhibited the lowest contact angles of all reflection surface materials tested [22]; 30 ° and 71 ° repsectively. This result indicated that the desired film-like condensation would occur to the greatest extent in these materials, and in the glass more so than the PET. A higher contact angle retards both condensate movement toward the collection point and transmittance of radiation to the brine [22]. The inclination angle of the collector surface has not been found to significantly impact the transmittance of radiation [22]. Previous studies raise questions about whether a hydrophilic coating could be applied to PET or other plastics to replicate the contact angle of glass.

Condensation mode, surface material and thickness of water film do not affect the heat transfer through a condensation surface [22]. Droplet growth in the initial nucleation stage is slow compared to the migration and coalescence growth stages. Periodic wiping of the condensation surface constrains droplet growth from reaching the final stages, retarding distillate productivity and outweighing any benefits associated with removing condensate [22].

Condensation increases as the internal cover surface becomes cooler [1]. This condition may be imposed by maintaining a film of flowing water over the surface [1] or constructing a still with a second effect (or basin) in parallel with the first [23]. A water film increases the efficiency by increasing both evaporative and convective heat transfer, and hence the temperature difference betweeen water and glass surface. The second effect still involves enclosing the water film (wf) so that any evaporation is captured by a secondary condensate collector, shown in Figure 2.2.3.
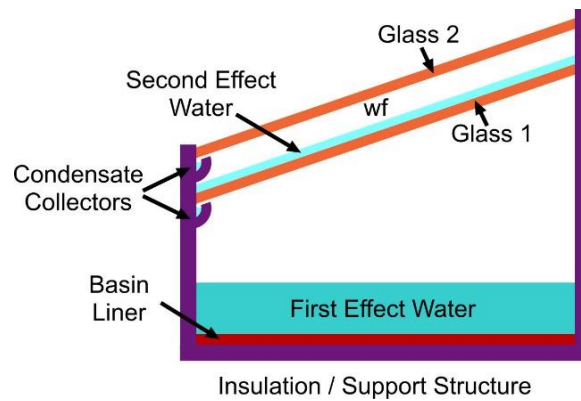
Figure 2.2.3: Schematic of Double Effect (Regenerative) Solar Still.

The energy balance equations for a Double Effect Solar Still (DESS) are extensively covered by Zurigat *et al.*, [23]. It was concluded that productivity for the DESS was 20 *%* higher than for a conventional SSSS. The results show that productivity occurs during the same time interval for both stills, however the DESS exhibits a greater rate. It has been noted that the integration of flowing water over the cover is effective only when properly designed [24]. A poor design; which inevitably reduces solar radiation trnasmitted to the basin [4], may significantly lower the efficiency. The potential complexities added in assuring the design can be fabricated and maintained to remain more efficient reduce the viability of implementing a water film or second effect. Active pumping seems necessary to achieve the desired water film.

2.2.4 Thermal Energy Storage

Thermal energy storage mechanisms increase water productivity for cloudy days and after sunset by prolonging a larger temperature difference. The evaporation rate of brine water is proportional to only the bulk temperature and the free surface area [25], and several low-cost means to maximise these parameters have been investigated.

The implementation of a suspended baffle plate reduced preheating time and prolonged distillate productivity after sunset hours, as the water below the plate remained at a higher temperature than the water above and acted as heat source [26]. Performance was found to be maximised with no vents in the baffle and the lowest possible brine mass above the plate . The production increase was quantified to be between 18 – 20 % [26]. The study investigated stationary plate configurations only and there is scope to investigate whether a buoyant plate would further increase productivity without adding unnecessary complexity.

The addition of black volcanic rocks to the basin improved productivity by 60 % compared to an unmodified still. The rocks did not exhibit corrosion during the study, unlike the other metallic absorbers tested [27], and would be viable options within the economic and geographic contexts of many South Pacific islands.

Phase Change Materials (PCM) are another thermal storage medium that has been investigated [28, 29]. The heat of the sun melts the PCM, storing energy as latent heat, which is then released during cooler periods to continue to drive evaporation through cloudy periods or overnight. It has been suggested by Ansari *et al.* that when the maximum brine water temperature is close to the melting temperature of the PCM, the thermal storage is best [29]. Equations detailing the energy balance for PCM charging and discharging, as well as for the case without PCM have been evaluated by El-Sebaii *et al* [28].

2.2.5 Cavity Space

The majority of experimental studies conducted have been focussed on SSSS [5, 7, 12-14, 22, 26, 27]. The ratio of brine volume to air cavity volume is dependent on both the brine depth, and the inclination angle of the glass. If the cavity between the brine water surface and condensing surface is large, there is a greater volume of air to become saturated, so distillate productivity takes longer to start [8]. Minimising the air cavity volume inside in the system would help to initiate distillate production as early as possible.

2.2.6 Collector Geometry

Efficiency in SSSS is lost due to the shadowing effects of the basin walls which decrease the solar radiation incident on the brine or baseplate. A hemispherical collector has been studied that offers more omnidirectional collection [30]. Active stills with both point-focus and line-focus parabolic collector surfaces have been studied [31, 32] although these are typically coupled with tracking technology, which adds a significant level of instrumentation, control and electromechanical drive systems and are unlikely to be feasible for the present context.

The only study that experimentally considered a parabolic collector surface was conducted by Yadav *et al*. [33], the results were concerned primarily with thermal profiles of various points of an Inverted Absorber Line Axis Compound Parabolic Concentrating Solar Still (IACPC), and the solar radiation incident over the course of a day. Daily distillate production was 3.04 L/m^2 for the apparatus [33] based on a total collection area of 0.132 m^2. A computational study with similar still geometry (IACPC) conducted by Kothdiwala *et al*. [34] was concerned with investigating optical properties of the still. The inherent complexity in typical inverted absorbers is the need for high quality reflective surfaces to transfer the incident radiation energy [34], as the geometry forces a higher number of internal reflections than what occurs in a SSSS.

Stills with single and double slopes and cylindrical collectors have been modified to contain a slowly rotating hollow drum in the basin [35], powered by solar panels. The metal drum was open at the ends and collected a thin film of brine water on both the inner and outer surfaces as it rotated. The high temperature of the drum promoted evaporation and the movement maintained film formation. The available evaporative surface increased substantially with the inclusion of inner and outer drum surfaces, while adding no extra volume to the still. Performance testing of different drum materials yielded that aluminium sheet with a mat black coat of paint had the most desirable water and heat absorption properties of those tested [35].

Comparing double slope stills with and without the inclusion of the drum, productivity increased by by 145 – 190 *%* depending on month of testing. The increased evaporative surface area is continually renewed and effects of increasing salinity concentration are mitigated as the brine surface is continually broken. Brine depth becomes a more significant parameterwith the inclusion of a rotating drum as heat transfer to the water occurs from both the drum and basin and further couples the heat transfer dynamics [35]. The impact of changing an operational or climatic variable was dependent on the cover geometry used [35].

Experimental comparison between productivity of a SSSS and a Double Slope Solar Still (DSSS) at different orientations indicate that North-South configurations produce more distillate than East-West configurations [36]. It would be a useful benchmark to run parallel tests with SSSS, DSSS and the proposed curved/parabolic cover geometries to assess how they compare under identical conditions.

Performance of a particular design may be benchmarked against the correlation results of Khalifa *et al.* [6], which contains productivity data correlated from several studies on the bases of solar radiation flux, inclination angle (applicable to SSSS) and brine depth.

2.2.7   Absorber Area

Equations characterising evaporative and convective heat transfer between the brine water and glass cover have been utilised by Muthu Manokar *et al.* [2]   and reproduced as equations (2.2.7.1 - 3). All terms and subscripts are detailed in Tables 2.1 - 2.2.

$$Q_{(evap\ BW-GC)} = h_{(evap\ BW-GC)}\ A_B\ (P_{BW} - P_{GC}) \tag{2.2.7.1}$$

$$h_{(evap\ BW-GC)} = \frac{M_{DW} h_{fg} P_T}{M_a C_{Pa}\ (P_T - P_{BW})(P_T - P_{GC})}\ h_{(conv\ BW-GC)} \tag{2.2.7.2}$$

$$h_{(conv\ BW-GC)} = 0.884 \left[T_{BW} - T_{GC} + \frac{(P_{BW} - P_{GC})(T_{BW} + 273.15)}{268900 - P_{BW}} \right]^{\frac{2}{3}} \tag{2.2.7.3}$$

The incident solar radiation is absorbed by both the brine water and the liner of the basin [2], so the solar absorptivity of the basin liner must be high to promote the desired heat transfer. Thermal conductivity (k) is the critical parameter that must be considered in conjunction with absorptivity, as the chosen basin material must be able to capture as much incident radiation as possible then effectively conduct this energy off to the adjacent brine water to facilitate evaporation of the brine. Both aluminium (k = 200 *W/mK*) and copper (k = 390 *W/mK*) are considerably more conductive than galvanised steel (k = 48 *W/mK*), although they are significantly more costly [2]. The basin is generally fabricated from metal sheet or plastic [37].

The basin typically reflects about 11 *%* of incident radiation [1, 38], this loss may be reduced through the addition of dye to the brine water [23]. The dye addition acts to directly increase the absorptivity of the brine, rather than modifying the basin properties. Although a significant performance increase could be attained through this absorption modification [1, 23], the suitability of dye within the proposed context is marginal. The Low Pressure concept may benefit, as it contains a fully enclosed internal space, however the Open Air concept does not have the same spatial boundaries and therefore would not retain the dye within the still collector.

The addition of porous materials such as sponge cubes [17] or a floating blackened jute wick [39] has been considered. The porosity of the sponges act to reduce surface tension between water molecules, promoting evaporation. The jute wick exhibits good capillary action and salt accumulation in the fibres was restricted by arranging the wick into a corrugated shape [39]. A floating wick overcomes the issue of a partial dry surface that

detriments productivity in the more common basin-mounted wick arrangement. The floating wick remained wet throughout all test conditions and therefore increased productivity through continual evaporation. The detrimental aspect of using a wick is that it needs regular refurbishment for maintained system efficiency [40].

2.2.8 Operating Pressure and Temperature

Gude *et al* [41] have conducted a study on low pressure, low temperature desalination with a focus on both the first and second laws of thermodynamics. A theoretical approach has been employed based on the first law of thermodynamics (energy conservation in an isolated system) as shown in equation (2.2.8.1).

$$\frac{\dot{m}_{DW}}{\dot{m}_s} = \frac{\frac{(Q_i - Q_l)}{\dot{m}_s} + h_s - h_{BW}}{\Delta H_{vap(T_{evap})} + h_{DW} - h_{BW}} \tag{2.2.8.1}$$

where the distillate productivity ($\dot{m}_{DW}/\dot{m}_s$) is dependent on component energy fluxes (Q), heat transfer coefficients (h), saline water feed rate ($\dot{m}_s$) and the latent heat of vaporisation (ΔH_{vap}). Refer to Table 2.2 for subscript nomenclature. The difference between saline and brine water is that the saline water flows into the system prior to the heat exchange processes and brine water flows out as the by-product of the exchange. This equation was used to create freshwater production contours for a given heat input [41]. The production depended on both evaporative temperature and rate of saline water inflow, as shown in Figure 2.2.8.
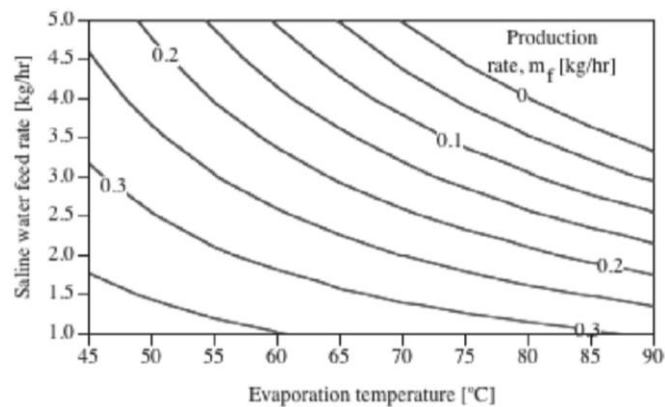
Figure 2.2.8: Distillate Production Contours for Constant 1000 *kJ/h* heat input [41].

Figure 2.2.8 provided with permission from the content publisher, Elsevier. License Number: 3887830467846. Refer to Appendix 01 for full license details.

A comparative case study using these data was also presented, concluding that the specific energy requirement is dependent on the temperature difference [41]. For a given heat input of 1000 *kJ/kg*, the specific energy requirements are 683 *kJ/kg* and 209 *kJ/kg* when the operating temperature differences are 65 *°C* and 25 *°C*, respectively. This analysis was conducted considering Carnot Efficiencies; not simply the quantity of energy used, but also the quality. On this basis, the analysis indicates that the process is less energy intensive if evaporation occurs at a lower temperature.

Two approaches to capitalise on this phenomenon were proposed [41]. The first approach splits the external heat addition process into multiple stages to decrease the overall temperature range; the heat rejected during condensation is recovered to preheat the saline water inflow. The second approach involves maintaining a low operating pressure so that evaporation occurs at lower temperatures. This approach requires the input of additional mechanical energy to maintain the low pressure region, and as such, Gude *et al.* dismiss the viability of the approach on the grounds that mechanical energy is more valuable than heat energy, so inputting mechanical energy is less thermodynamically efficient. This outcome provides a strong thermodynamic basis for dismissing the viability of the Low Pressure option.

If the saline water and fresh water volumes are connected, vapour will distil from the fresh water to the saline water, as the former has a slightly higher vapour pressure. This process may be reversed if the saline volume is heated, and effects are appreciable using a temperature difference of approximately 15 *°C*. Solar heat is suitable to provide this sort of differential [41].

The experimental setup arranged by Gude *et al.* required both a large space for the apparatus and precise water levels in the discharge tanks, neither of which are desirable for the proposed project. The evaporation chamber was approximately 10 *m* above the free surface of the water to create a Torricellian Vacuum[2]. The discharge removal rates ensured constant water levels in the tanks to enable continual desalination without input of mechanical energy for fluid transfer or maintaining the vacuum.

Testing indicated that the average specific energy consumption was 3450 *kJ/kg* as opposed to the 5040 *kJ/kg* for a SSSS unit [41]. The study was concerned with idealised conditions and to provide a higher degree of realism, sensible heat requirements and fugitive emissions[3] need to be accounted for.

Equations characterising the relationship between evaporation rate, air density, specific humidity and partial pressure have been evaluated by Shah [42]. The temperature effect has been implied with inclusion of the density terms. The equations obtained addressed the concern that relationships derived in prior studies fail to model conditions outside those tested. The study was conducted concerning indoor swimming pools although it was stated that the relationships 'may be used for other indoor pools with calm water surfaces'. This proviso has deemed the findings presented relevant to apply to the solar still situation. The concept that a difference in humidity exists between surfaces of interest is the important aspect inferred from this work. The formula derived by from a mass and heat transfer basis is presented as equation (2.2.8.2).

$$\dot{E} = 35\rho_w(\rho_w - \rho_r)^{\frac{1}{3}}(W_w - W_r) \qquad (2.2.8.2)$$

---

[2] Same principle as a mercury barometer
[3] Fugitive emissions are gaseous emissions due to leaks.

where the evaporation rate ($\dot{E}$) is a function of the air density (ρ) and specific humidity (W) at both saturation conditions (w), and the conditions of the room (r). This formula is limited to cases where internal velocity ranges from 0.05 m/s to 0.15 m/s. The ASHRAE method, also presented by Shah [42], explicitly relates pressure and velocity to evaporation rate as shown in equation (2.2.8.3).

$$\dot{E} = \frac{(0.089+0.0782V)(P_r - P_w)}{2\Delta H_{vap}}$$
(2.2.8.3)

where the evaporation rate ($\dot{E}$) is a function of the air velocity (V), the latent heat of vaporisation (ΔH_{vap}) and the pressure difference between the conditions of the room (P_r) and saturation conditions (P_w). Both equations (2.2.8 – 3) require a density difference greater than 0.02 kg/m^3 between air in the bulk cavity space and at the evaporative surface. A 15 % increase factor must be applied for cases where the density difference is less than this amount. It is assumed the air density in the bulk cavity space is equal or greater than that at the surface

The literature concerning how evaporation rates depend on temperature is sparse. The relationship is described on a computational fluid dynamics basis by Lorenzini *et al*. [43], however the study is concerned with droplet evaporation rather than bulk surface evaporation. It was assumed that the results of this study were translatable to the surface evaporation case of the solar still. No evidence was found on the contrary. The relationship is approximately linear, which the author has attributed to the linear dependence between temperature and the convective term in an evaporation process. Throughout the temperature range of 27 *°C* to 47 *°C*, the percentage evaporation rate was found to increase from 6.2 % to 8.5 %; which represents a rate of increase of 0.113 *% / °C*. This temperature range was deemed relevant for operation as encompasses what several studies cite as the 'low operating temperature range' [41, 44].

It has been found throughout the literature that low pressure systems generally utilize active components rather than operating in a fully passive manner [41, 44-48]. Even cases where the vacuum is passively established through the water column heights, pumps or heat exchangers are necessary to ensure the necessary temperature difference is present. An experimental study conducted by Muthunayagam *et al*. concluded that desalination of seawater at typical ocean surface temperatures is feasible using a low pressure flash vaporisation process where the vapour is condensed using cool water pumped from the ocean depths [44]. A theoretical study conducted by Hosseini *et al*. accentuated the benefits of implementing a low pressure system to utilize the waste heat from another industrial process in an ammonia plant [46]. The applications of these studies are toward larger scale operations than what the client desired for the context of this project and the reliance of the low pressure process on active components is not aligned with the original design intent.

2.2.9 Previous Solar Trough Studies

Trough systems were beyond the scope for this project due to the necessary level of complexity in their designs. However, a brief investigation of these systems was conducted in order to extract relevant information back to the context and scope of the project.

A derivation of the SSSS principle is the Parabolic Trough Concentrator (PTC). A typical PTC system is was used for the experimental study conducted by by Orfi *et al*. The schematic representation of this system has been redrawn in Figure 2.2.9. The operational principle involves heating the brine water using the PTC prior to injection into an evaporation chamber. The fresh water from the evaporation chamber is then passed through a condenser which acted as a preheater for subsequent brine water flowing into the PTC. This operating principle is not significantly more complex than what occurs in a SSSS. The focus with this aspect of the research was ascertaining whether the performance enhancements of concentrated solar radiation were able to be obtained through passive means.
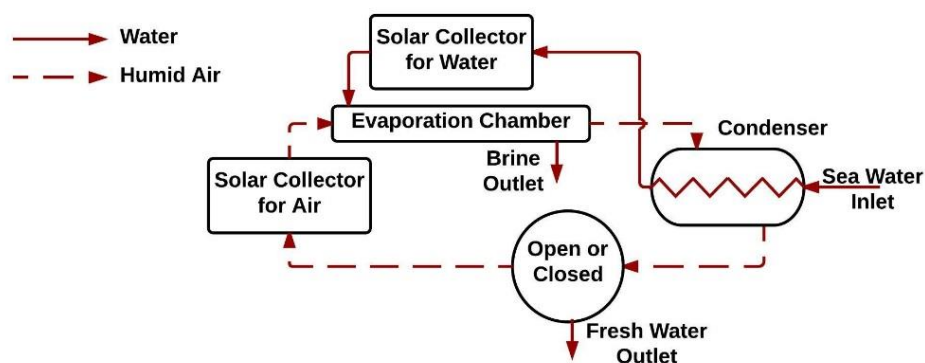
Figure 2.2.9: Schematic diagram of desalination system [49].

This trough is fabricated so the solar radiation is focussed onto the brine pipe that runs longitudinally down it. Air is separately heated in another PTC and the two fluids mix in an evaporator to reach a saturated vapour state at the evaporator outlet. The vapour is then condensed, using incoming brine water, wherein distilled water is produced. The air cycle may be open or closed.

Mohamed *et al*. [50] theoretically studied a PTC system operating similar to the system described by Orfi *et al*. The system contained several machine elements; an evaporator, a condenser, a circulating pump, an air blower and a pre-heater. This systems configurations used by both Mohamed *et al*. and Orfi *et al*. have complexity beyond what is desired for the project context; however the mass and energy balances used have been deemed relevant as they indicate which parameters need to be considered in the system analysis and modelling [49, 50]. The first part of the model described by parabolic concentrator dynamics using spatial and temporal partial derivatives while the second part describes basic equations to define the Humidification Dehumidification Desalination System (HDDS).

The dynamic system model analysis assumed incompressibility of the fluid, negligible pressure drop across the collector tubes, a well-insulated system, atmospheric operating conditions and a constant ambient temperature during working hours. The model represented a set of non-linear partial differential equations describing the temperature distributions of the fluid, receiver and glass surface with respect to time and flow direction. The system solution indicated the dynamic response of the fluid, absorber and glass surface temperatures which allowed instantaneous thermal efficiency of the collector to be determined. A Crank-Nicholson finite difference explicit-implicit method was found to be more stable than other methods trialled. The HDDS equation formulation included the heat exchanger energy balance, humidification and dehumidification processes and the boundary conditions. It was assumed that the system operated adiabatically at steady state under atmospheric pressure. Seawater was assumed to have identical psychrometric properties to fresh water, which were obtained from ASHRAE charts and used for the psychometric component of the analysis.

Decreased performance in winter months was observed and attributed to both lower values and shorter times of solar radiation. The percentage production time on a seasonal basis for the system was found to oscillate between 42 % in summer to 29 % in winter [50] for radiation characteristics representative of the Kingdom of Saudi Arabia. It has been evaluated that the design may be modified so a greater proportion of time is productive, through either thermal storage or alteration of the operating parameters of the system. The reflectivity of the mirror is equal to the effective transmissivity of the parabolic trough collector. The latent heat of vaporisation may be determined using the Clapeyron relationship from tabulated saturation pressure and temperature data [50].

It has been made clear by Mohamed *et al*. [50] that if the system is designed to operate using inflow water at sea temperature, then no preheating is required. Omission of the preheater unit reduces system complexity. To relate this finding back to the specific situation under examination, weather data from Tonga was accessed. Meteorological data compiled over the last 21 years[4] gave the average annual sea surface temperature in Tonga as 26.3 ± 1.4 *°C*. A proviso was also given that 'temperatures close to the shore may vary several degrees from the open sea averages, especially near river mouths or after heavy rain or long offshore winds'.

A HDDS review was conducted by Parekh *et al*. [51] indicating almost all previous studies agreed that air flow rate was insignificant on productivity. The brine water flow rate, however, was found to be of much greater significance. These factors alone indicate that if conventional PTC systems are investigated for the project, the complexity will increase substantially as one of the critical operational parameters becomes a fluid flow rate. Control of the fluid flow rate necessitates some form of pump or valve system. In turn, additions to the system

---

[4] http://www.surf-forecast.com/breaks/Peaking/seatemp

such as this require, at the very least, more components and tighter tolerances at interfaces to prevent leakage altering flow rate.

2.3   Methods of Analysis

The methodologies typically evident in the literature are as follows.

2.3.1   Empirical Testing

The majority of studies considered are fully experimentally based [1-3, 5-7, 10-12, 15, 17, 20, 22, 25, 27, 30-36, 39, 41, 44, 51, 52], although some validate theoretical system models experimentally [8, 21, 40]. The lack of overruling governing equations in the desalination field has meant that most studies require an empirical basis for validation. These experimental studies are focussed on elucidating the relationships between one or two parameters and distillate productivity. The physics governing the system is often simply arrived by applying curves-of-best-fit to the experimental data sets [2]. This result is clear from the nature of the equations presented throughout Chapters 2.1 – 2.2, polynomials and exponentials feature frequently. These equations are valid, but the lack of a first-principle, physical basis means that the empirical results are the extent of the collective knowledge.

Solar still designs are typically simple enough that a test rig replicates the still geometry adequately so he rigs are not abstracted representations of what they are modelling. The vast majority of testing is conducted *in natura*, which couples the results to the environmental conditions of test location.

The more comprehensive studies detail not only the experimental apparatus used, but also the geographic location that testing has been conducted at. This secondary information is important as it has been proposed that productivity and still performance characteristics are very much location dependent [1].

2.3.2   Physics Modelling

The situation has also been addressed from a theoretical basis, sometimes with no coupling experimental validation section [4, 9, 13, 14, 23, 24, 26, 28, 29, 46, 49, 50, 53]. The theoretical basis begins with a mass or energy balance and generally splits terms into radiative, convective and evaporative terms and a transient term. These relationships are typically of the form given by equation (2.3.2.1).

$$Q_{INC\,i} = \sum_{j=1}^{N}(Q_{cond\,i-j} + Q_{conv\,i-j} + Q_{rad\,i-j} + m_i C_i \frac{dT_i}{dt}) \qquad (2.3.2.1)$$

where the total energy transfer between element *i* ($Q_{INC\,i}$) and all elements *j* of an *N* element system representation is the sum of all conductive (Q_{cond}), convective (Q_{conv}), and radiative (Q_{rad}) heat transfer processes occurring as well as the transient temperature change. This transient term describes the rate of temperature change of element *i* ($\frac{dT}{dt}$), proportional to the mass (*m*) and specific heat (C_P) of that element. Several studies have integrated empirically based formulae to determine the heat transfer coefficients into the energy balances [2, 4, 8, 53]. These empirical additions are extensively covered by Xiao *et al* [4].

2.3.3 Finite Element Modelling

There were few studies on solar stills that presented a Finite Element Analysis. An implicit finite difference method was coupled with the Tridiagonal Matrix Algorithm using a one minute time step to solve the non-linear ordinary differential equations studied by Zurigat *et al.* [23]. The Crank-Nicholson explicit-implicit method (weighting factor of 0.5) was used by Mohamed *et al.* [50] to obtain finite difference solutions for the exit temperature of the collector throughout the course of a day. The system productivity was simulated through a using programming platform VISUAL BASIC. This study was concerned with investigating the effects of different working conditions and different solar radiation characteristics on system productivity. A forward finite difference scheme was employed by Kamal [8] to represent the transient thermal behaviour associated with the sensible heat term[5] in the utilised governing equations. The context of the study conducted by Kamal was to investigate whether the simulation model matched experimental results for Doha operating conditions. Although the model was simplified, the simulation results were concordant with experimental results when the inclination angle was close to the optimum value.

---

[5] Sensible heat is energy transferral manifested through a temperature rise, as opposed to latent heat which is manifested through phase change.

2.4 Identified Gaps in Current Studies

Thermal storage, insulation composition, thermo-optical properties of condensing covers and still geometry have been identified as areas toward which research should be focussed in order to decrease the costs of distilled water produced [52]. The literature review has highlighted several other gaps in the underlying knowledge. The gaps may be defined broadly as relating to design configuration or to the physical mechanics of the system. Design-based gaps involve the optimisation of existing models, specifically with regards to changing a system parameter such as the brine level, collector geometry or material. Mechanics-based gaps involve modelling and validating the physics underlying the system dynamics mathematically and experimentally.

2.4.1 Identified Design Gaps

2.4.1.1 Optimal Brine Mass and Depth

The effect of brine depth on daytime productivity has been considered for SSSS [54], TrSS [9] and curved reflector inverted collector [55] still geometries. The notion of an optimal brine mass that maximises both sunlight evaporation and overnight thermal storage has been proposed for the SSSS [13]. The proposed units have an absorption surface below the condensation surface, which makes them closer to inverted collectors than any other design in the reviewed literature. A need was identified to address the optimal brine mass considering both day and night productivity based on brine depth for the proposed design geometry.

2.4.1.2 Optimisation of Parabolic Collector Surface Geometry

With only two exceptions [33, 34] all studies in the literature review concerned with passive stills have considered flat collector surfaces. PTC technologies have been investigated [49-51] for the more complex HDDS arrangements, which all involve active components. Geometric aspects of the active HDDS proposed could be translated to a passive still which is more aligned to the context. A need was identified that addressed the effectiveness of line-concentrating parabolic collection surfaces compared against conventional flat surfaces for the proposed still geometry and passive functionality.

2.4.1.3 Effect of Relative Air Cavity Size

The time taken for the air inside the still to reach steady state moisture content; and therefore begin evaporating, depends on the ratio of air volume to brine volume [8]. A need was identified that addressed the effect of changing this volume ratio to minimize the lag time from when the sun begins heating the brine to when distillate is first produced.

2.4.1.4 Applying Situational Specificity to the Design

No studies have focussed specifically on the South Pacific situation in terms of climatic conditions and feasible fabrication materials. It has been shown that there is not a set of parameters that are globally optimal [1]; design optimisation is situationally specific. As such, the particular meteorological conditions of the intended location will influence the design. The identified need was focussed on relating the brine depth to expected productivity using the solar radiation, ambient temperature and humidity characteristics of the South Pacific. This need relates to both design and mechanics.

2.4.2 Identified Mechanical Gaps

2.4.2.1 Investigating Open-System Operation

One of the proposed units is novel in the respect that exists as an open system. All other desalination units studied exist as closed systems with definite internal and external interfaces and boundaries. This identified need focussed on addressing the effectiveness of an open desalination unit compared to more conventional, closed system designs.

2.4.2.2 Integrating Humid Air Parameters into Equations

It was noted in a recent (2014) study by Ahsan *et al.* [5] that the air inside the still was far below saturated, although saturated air properties were used to describe the system. This identified need was focussed on the integration of humid air properties into existing condensation and evaporation equations to give more realistic system models. The only other study making mention of humidity was conducted by Shah [42] and is concerned with evaporation of water from calm pools. The extent to which the results were translatable to the solar still context was not explicitly addressed. No other studies pertaining directly to the desalination context were found to mention the air condition within the unit being below saturated.

2.4.2.3 Investigating More Hydrophilic Condensate Surfaces

The contact angle between condensate and the condensation surface is critical for still productivity as indicated by Bhardwaj *et al.* [22]. The study quantifies that glass provides the most desirable contact angle, followed by PET. PET would provide a cheaper and more robust condensate surface solution for the South Pacific context. The identified need was focussed on investigating making PET surfaces more hydrophilic to replicate the physical properties of glass, providing higher condensation rates.

2.4.2.4 Investigating Wind Velocity and Solar Radiation Relationship

Significant study has gone into determining the effect of wind velocity on the productivity of a still [12-15] and it has been generally agreed that a threshold velocity exists. Beyond this threshold, no appreciable productivity gain is achieved despite velocity increases. A need was identified that focussed on addressing how the threshold wind velocity depends on amount solar radiation flux incident on the still, specific to the South Pacific environmental conditions.

2.4.2.5 Investigating Feasibility Low Pressure Operating Region

It has been accepted that a lower evaporation temperature increases productivity for a given amount of incident energy [41]. Lower evaporating temperatures are realised at lower pressures, however a low pressure system has not yet been developed that aligns with the socio-geographic scope of the project. This identified need was focussed on specifying the low pressure region parameters and assessing how easily and practicably the design could be implemented and maintained in context.

3 Methodology

3.1 Purpose

The client provided conceptual designs for a low-pressure solar still and an open-air solar still. The impetus for the project was to better understand the underlying physical principles of passive solar desalination, to inform future design efforts.

For the specific situation under examination the most pressing need was to obtain quantitative knowledge of which climatic, operational and design parameters had the greatest influence on maximising still productivity for the chosen still geometry and consolidate these critical parameters into a set of governing equations.

Several gaps in the solar desalination theory limit the understanding of how different parameters affect performance, and these have been outlined in Chapter 2.4. It has been acknowledged that even parameters which are well documented for conventional desalination units may have different effects on the proposed designs, due to novel geometry and functionality. The project is focussed on addressing a gap that will ensure reliable distillate productivity. Solution reliability has been a critical success metric throughout the project, considering the intended socioeconomic context. A combination of experimental and simulation results has helped to direct the performance optimization process in an informed manner.

3.2 Approach

The approach involved a preliminary investigation into identifying the underlying engineering mechanics and the key variables that determine performance. This work was intended to theoretically determine, from the literature, what relationships and principles have already been established for solar desalination. The next activity, and in parallel with the first, was developing a conceptual design that embodied the intended system functionality, and sets out the system architecture at a high level of abstraction. The subsequent work stream was empirical testing, which quantified the parameter values and relationships apparent. The fourth activity was the development of a theoretical model of the thermodynamic behaviour, including the role of key variables and their effect on system productivity. This model was based primarily on first principle engineering mechanics, although relies on some semi-empirical formulations.

Refer to Figure 3.3 for the entire schematic detailing the plan of action for the project, which has been decomposed into five main phases. These identified phases have been detailed in Chapters 3.2.1 − 5. Each phase contains functional elements or decisions that had to be addressed to progress the project. These elements have been detailed to give a full overview of the work entailed within the project.

Elements of Phase 4 (P4) and the entirety of Phase 5 (P5) have been declared beyond project scope as they have sufficient complexity to be standalone projects. Nonetheless these phases must be considered during prior design development work as they represent the direction that the work has to move toward. The focus of this project has been evaluating the concepts provided and exploring the solution space rather than reaching the embodiment design stage of development. The omitted sections offer a starting point for subsequent iterations of the project.

3.2.1 P1: Preliminary Research & Investigation

The first phase in the project was to formulate a first-principles model based on the literature. This model was necessary because it informed the subsequent experimental design, instrumentation plan, and modelling. This process is shown in Figure 3.2.1, and elaborated following.
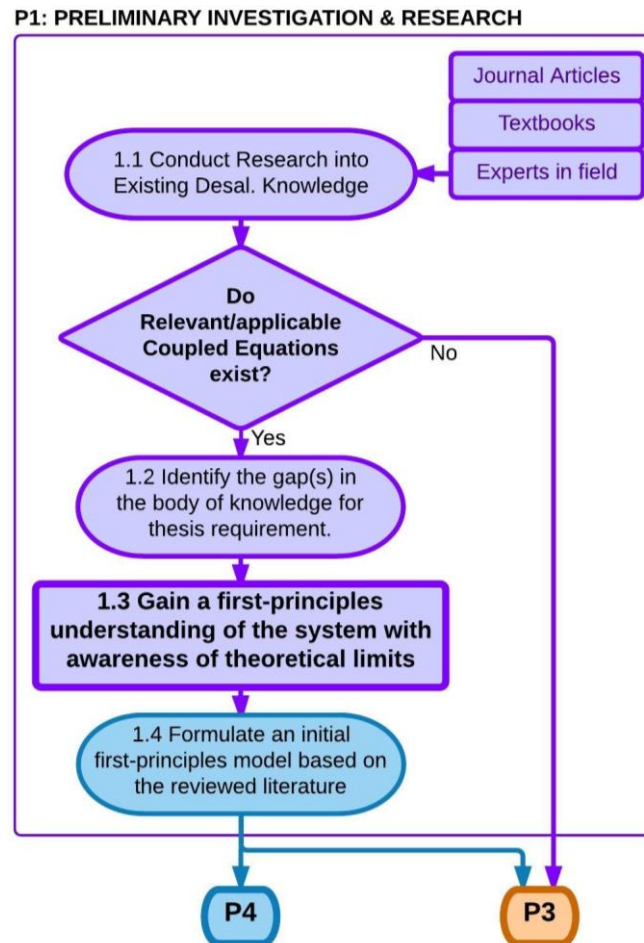
Figure 3.2.1: Work flow for the process to formulate a first-principles model from the literature.

P1.1: Relevant literature on both active and passive solar desalination systems was examined and critiqued. This research determined which design elements have been addressed in sufficient detail within prior studies to use the derived relationships, and which aspects require further clarification through testing and simulation.

P1.2: The research clarified that governing equations exist but the validity of applying these to the proposed design concepts was uncertain. Therefore the project went straight to a first principles experimental phase (P3) to ascertain relationships. Relevant equations from the literature were utilised to inform the data collection process so that it built upon the insights of previous work.

As the particular design problem has not been solved before, gaps within the relevant body of knowledge were known to exist. These gaps may either arise from the results of prior studies; wherein test cases can be modified to reflect the context of the problem; or address factors that are simply not apparent in prior studies.

P1.3: The outcome for this phase was evaluating of the collective body of knowledge related to solar desalination. The research confirmed what the current limits to the theory were and therefore provided direction for the empirical testing to extend these limits in ways meaningful to the project. The project was initially focussed around current desalination theory to optimise the available time and gain an awareness of what testing was new and what was redundant.

P1.4: The formalisation of this phase outcome was arriving at an initial representation of the system as a heat transfer model, as detailed in Chapter 5.1. Elements identified in prior literature were combined using a first principles basis. This outcome initiated the framework for subsequent model building in P4 and helped to inform the instrumentation and testing regime in P3.

3.2.2 P2: Conceptual Design Confirmation

The second phase of the project was ensuring the commercial relevance of the research agenda. This process is shown in Figure 3.2.2 and elaborated following.
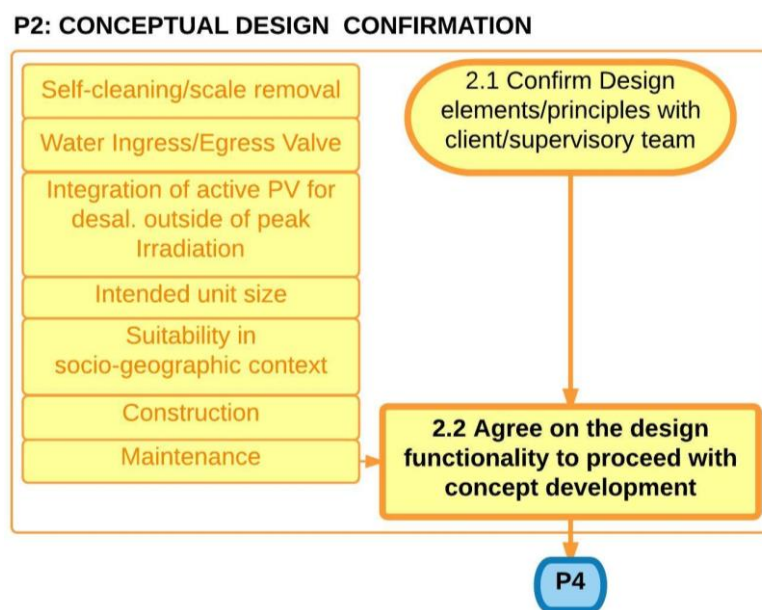
Figure 3.2.2: Workflow for the process of clarifying and confirming function design elements and principles.

P2.1: Concurrent to the research phase, functional elements of the proposed designs were critiqued and the mechanisms providing these were confirmed. This evaluation process involved discussions with both the supervisors and the client. The concepts provided by Sunshine Solar were evaluated and adapted as necessary in light of research conducted in prior studies.

P2.2: The functional design considerations included the list shown in the P2 schematic. The outcome of this phase was evaluation and clarification of the concepts developed for the client such that the project captured the initial design intent.

3.2.3   P3: Empirical Testing

The third phase in the project was to design and build a test apparatus, specify the necessary instrumentation for data collection and obtain sufficient data to both inform further development of the system model and clarify the influence of each tested system parameter. This process is shown in Figure 3.2.3, and elaborated following.
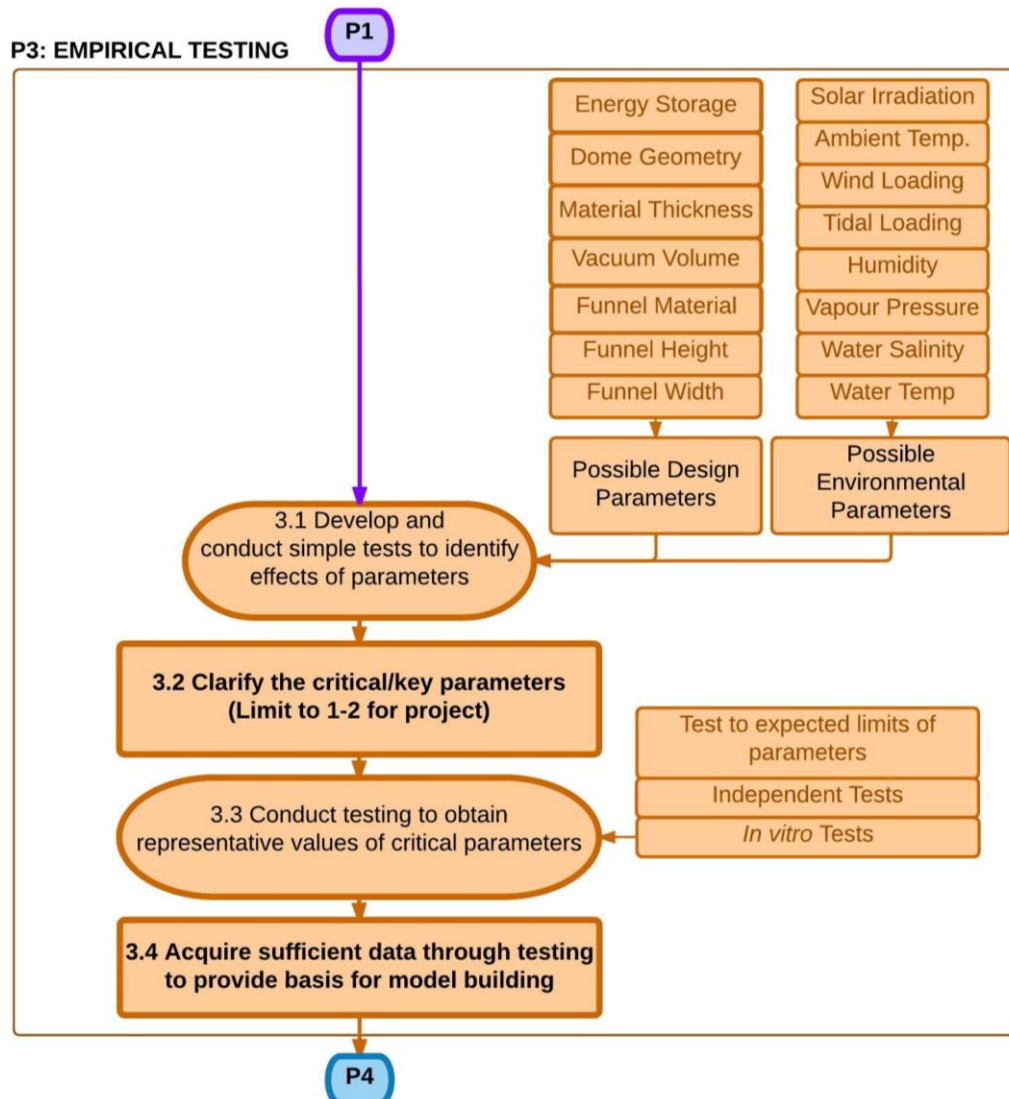
Figure 3.2.3: Workflow for the emprical testing process to identify and relate critical parameters.

P3.1: The first phase of testing was concerned with obtaining the relationships between key operational, design and environmental parameters for the specific geometry of the concepts of interest. The tests were conducted primarily *in vitro*, although supplementary solar tests were also conducted. The experimental regime was designed to keep the parameters as independent as possible for simplicity. The test rig was a slightly abstracted representation of the proposed concept geometry. It was evaluated as more important to obtain a large and varied amount of representative data early on rather than spend time fabricating an intricate and complex test rig at the expense of losing data collection time.

35

P3.2: The relative effects of the parameters of interest were obtained through the initial testing. The most critical parameters were explicitly identified and provided the basis for the subsequent design development. Critical parameters have been defined as those which have the greatest influence on evaporation and condensation rates of the brine water.

P3.3 – 3.4: Once the critical parameters were identified, sufficient data was collected through a series of informed tests for use in building the theoretical system model during Phase 4.

3.2.3.1   Methodology involved with P3.1: *In Vitro* Testing

The *in vitro* testing involved simulating expected Tongan weather conditions. This testing procedure allowed identical test conditions to be established for the entire range of experiments. The approach allowed parameters were evaluated independently without daily variation as experienced *in natura*.

A halogen lighting array with dichroic filters was designed and built to provide an approximation of the solar radiation spectral profile into the brine basin. This lighting source was the preferable option considering the project budget. Halogen lamp filament glows considerably than dimmer than the 6000 *K* of the sun, and as a result produces more infrared (IR) and less ultra violet (UV) light. The dichroic coating on the bulbs acted to reflect the visible and UV wavelengths toward the basin, but allowed a proportion of the IR to pass through [56] which helped to bring the spectrum incident on the brine basin closer to the solar spectrum.

The radiation intensity was captured using a pyranometer. An axial-flow fan simulated a simple wind profile. The water put into the basin for evaporation had a controlled initial temperature and salinity. The ambient air temperature was maintained at approximately 23 *°C* inside the laboratory space. The 'environmental' conditions were matched to expected Tongan conditions as closely as possible to ensure contextually relevant results. (For more on insolation characteristics see Chapter 4.1.4)

A representative test rig was fabricated for the experimental phase that captured the design intent of the concepts, but had simpler geometry. The rig was modular enough to switch between modelling different concept configurations. The rig design and construction methods were selected with an awareness that future modulation could be necessary to test other identified aspects of the system.

The test regime was designed to vary only one parameter of interest (*i.e.* water depth in the basin, simulated solar intensity, cover material) while all others are held constant. The test focus was to keep the procedure lean and simple while accumulating as much reliable data early on as possible.

3.2.3.2 Instrumentation required for P3.1: In Vitro Testing

Thermocouples measured temperature at points of interest on the rig (basin, internal and external faces of absorption surface, internal and external faces of condensation surface, internal air, ambient air and brine water). Hygrometers measured relative humidity at both the evaporation and condensation surfaces. A pressure transducer measured the differential between the interior and exterior rig pressures. The masses of brine and distillate water collected were measured on load cells. A pyranometer captured the radiation flux incident on the brine water. Further details on the instrumentation and data acquisition apparatus (DAQ) are provided in Chapter 4.2.2.

3.2.4 P4: Design Development & Optimisation

The fourth phase in the project was to refine the first-principles model using the data obtained through testing and develop it through to a systems level representation that captured the behaviour occurring. This process is shown in Figure 3.2.4, and elaborated following.
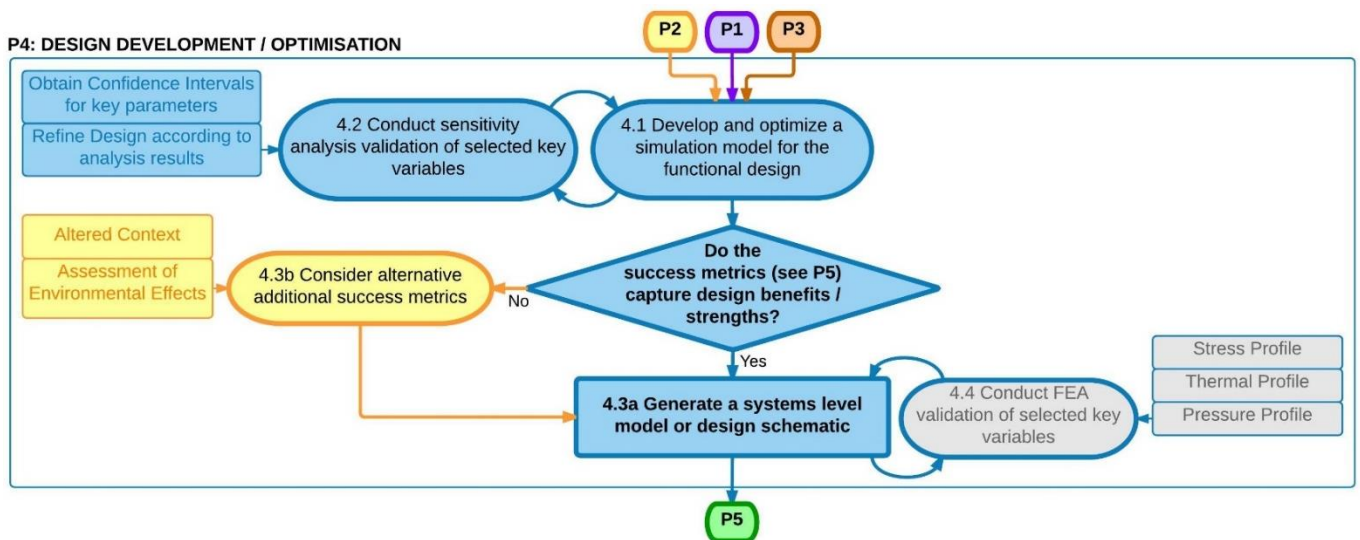
Figure 3.2.4: Workflow for model-building and validation.

P4.1: The theoretical (P1) and empirical (P3) knowledge acquired, in conjunction with the client-directed design concept (P2) was integrated into developing a model that described thermodynamic behaviour of the concept.

P4.2: A sensitivity analysis was conducted to identify the effects of perturbing model elements from their identified values. This analysis helped to inform the relative influence of parameters on system performance.

P4.3: The success metrics were initially defined as financial cost, performance and suitability in context. The first two were quantifiable and directly comparable against other desalination systems. The contextual suitability is bounded by a maximum cost and minimum performance. This third metric related to socio-cultural design implications and the relevant work is pertaining to this is presented in Chapter 4.3.8.

It was initially proposed to conduct an Assessment of Environmental Effects (AEE) or other comparable analysis to highlight particular concept strengths if the initial success metrics failed to capture them. As an alternative, it was also proposed that another context may need to be considered to locate the socio-geographic niche that best suits the concepts. These concerns were only applicable if the concepts showed significant performance potential after the testing and modelling phase.

P4.4: FEA was identified as a necessary component for completion of the design optimisation, but not critical for the concept evaluation work included in this project. This project was concerned primarily with concept proof and solution space exploration, not analysis of embodied design. The model developed described the systems level behaviour of the desalination unit concept. The knowledge captured could be used in future iterations of the project to inform the construction a Computer Aided Design (CAD) model and conduct Finite Element Analysis (FEA) to determine the component-level behaviour and conditions.

3.2.5   P5: System Level Prototype Testing (beyond scope)

This phase was evaluated as being beyond project scope, however it is the direction that current and future work will move toward. As such, this project has considered what is involved with subsequent prototyping so that the development process remained relevant to a greater outcome than just completion of the current project. The prototype testing process is outlined in Figure 3.2.5 and elaborated following.
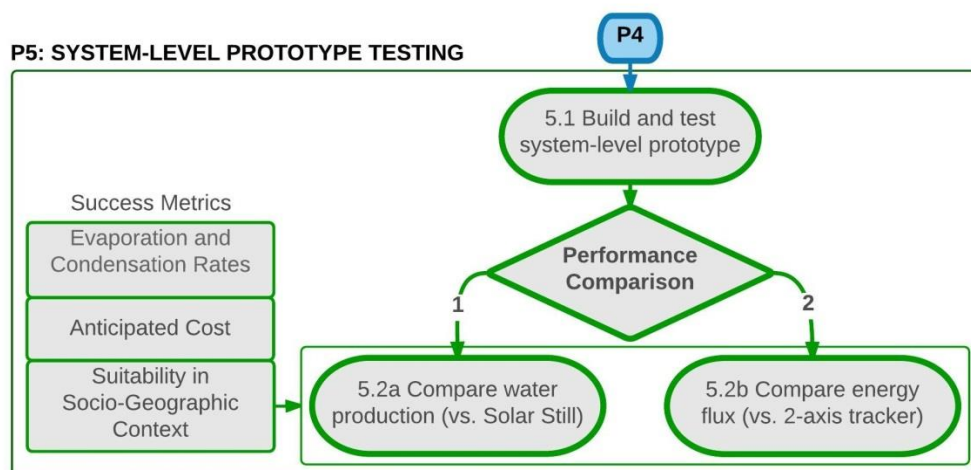
Figure 3.2.5: Proposed workflow for subsequent prototype testing (beyond scope).

P5.1: The model produced in P4 shall be sufficiently complete to allow a prototype to be fabricated using the embedded information. The component details such as bolt dimensions, tolerances and seals will not necessarily be included during this phase in order to speed up prototype testing. *In natura* tests may be conducted at the Ara Institute of Canterbury solar facility. The proceeding description details the methods expected in this sub-phase.

P5.2: Concept performance is proposed to be assessed one of two ways. The first option is the comparing the distilled water volume produced over a given time period between the developed design and a conventional solar still design. The second option is comparing the incident solar energy flux between the developed design and the 2-axis tracker at the Ara solar facility. The success metrics are based on both performance and contextual suitability.

3.2.5.1   Method Proposed for P5.1: *In Natura* Testing (beyond scope)

Once the *in vitro* testing and mathematical modelling produce concordant results that have been validated and optimized through sensitivity and finite element analyses, a prototype test rig will be purpose built for *in natura* testing. This test phase will examine the functional concept in its entirety rather than representative functional aspects as with prior *in vitro* tests.

This *in natura* test regime will allow for a greater degree of realism than the prior *in vitro* testing. The solar testing facility at Ara Institute of Canterbury will be utilised to compare the prototype with either a conventional solar still or the Ara two-axis solar tracker. The performance benchmark has been judged as the amount of distilled water produced over a given timeframe.

3.3 Integrated Project Plan Schematic

The overall research plan for this project, integrating the above individual phases, is shown in Figure 3.3. This provides the system level architecture.
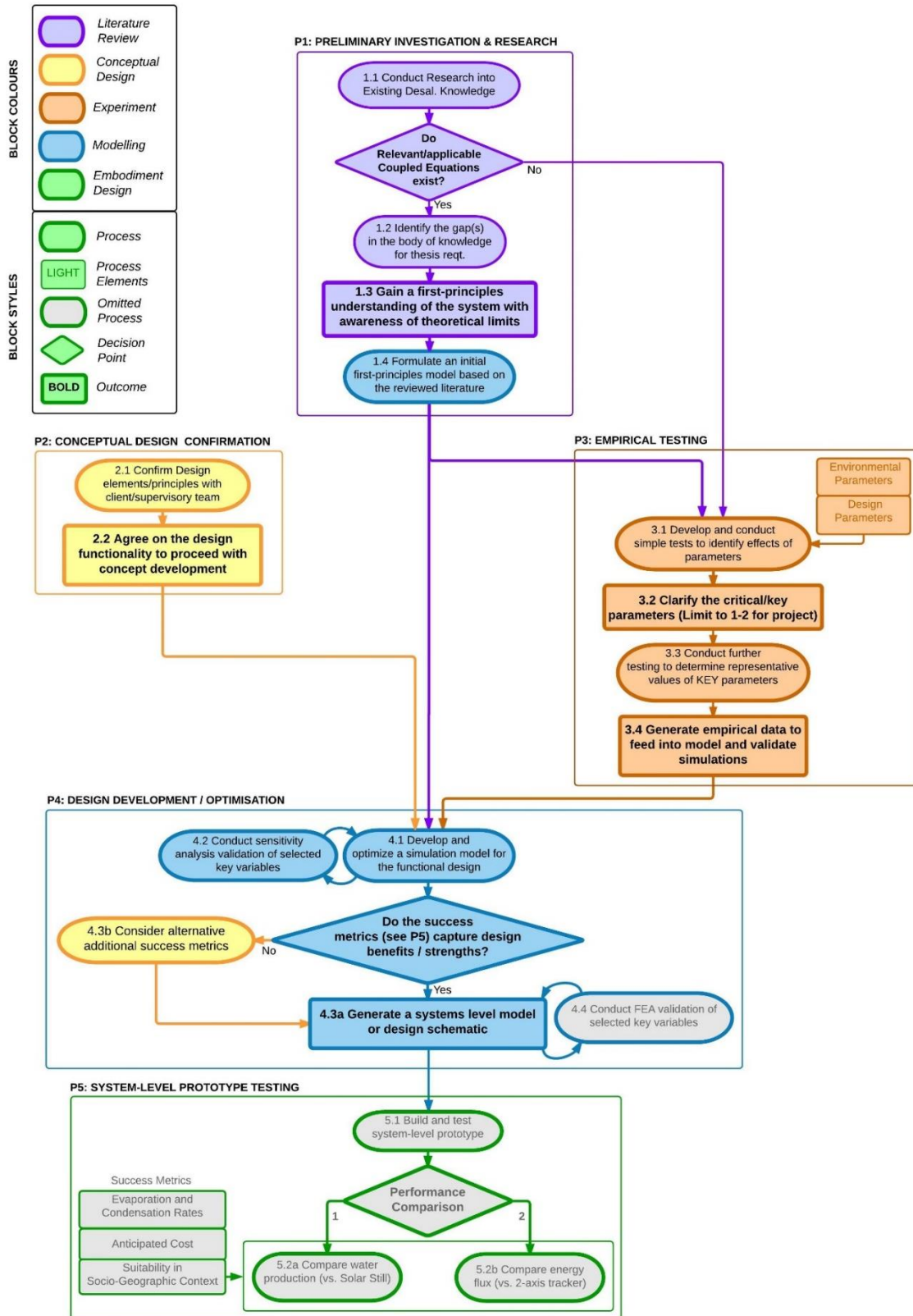
Figure 3.3: Project Plan Schematic Detailing Main Phases P1 – P5.

4 Experimental Phase and Results

This chapter details the rig design and build stages as well as the data collection procedure with sufficient detail for the testing to be replicable in the future.

4.1 Assumptions and Simplifications

The desalination process involves several environmental factors which interrelate and all have significant influence on still productivity. An *in vitro* test phase was designed and implemented which allowed these factors to be controlled to a greater extent and limited the extra, unmeasurable effects on system dynamics. This action meant the data collected did not require compensation for day-to-day variations in weather. The system was reduced to a state where relationships between productivity and identified design or environmental factors could be observed more explicitly and extracted more easily. The specific modifications of certain environmental conditions and design parameters employed to simplify the testing are detailed in Chapters 4.1.1 − 4.1.6.

4.1.1 Ambient Temperature

The test rig was installed at the University of Canterbury workshop and laboratory facility. The mean temperature during testing was 20.6 ± 1.7 *°C* whereas in Tonga this mean is 24.0 ± 1.7 *°C* [6]. This discrepancy could not practically be compensated for without additional energy input and containing the rig in a microclimate. As such, the results correlate to an Aotearoa (New Zealand) temperature profile. The ambient thermal variations during testing were effectively the same as expected in Tonga which is useful for extrapolating expected performance.

4.1.2 Humidity

Over the course of testing, the mean initial relative humidity was 59 ± 1 *%*, which differed significantly from the 76 ± 3 *%* [5] mean humidity typical of Tonga. As with the ambient temperature, the humidity discrepancy could not practically compensated without more sophisticated climatic control or *in situ* testing.

---

[6] Data obtained from the NASA Langley Research Center Atmospheric Science Data Center (see Appendix 02)

4.1.3 Water Characteristics

The colouration map presented in the World Ocean Atlas 2009 indicated that ocean salinity around Tonga is approximately 35 practical salt units (PSU). This measurement corresponds to 35 grams of dissolved salts present in every kilogram of water. The dissolved salts are typically composed as shown in Figure 4.1.3.
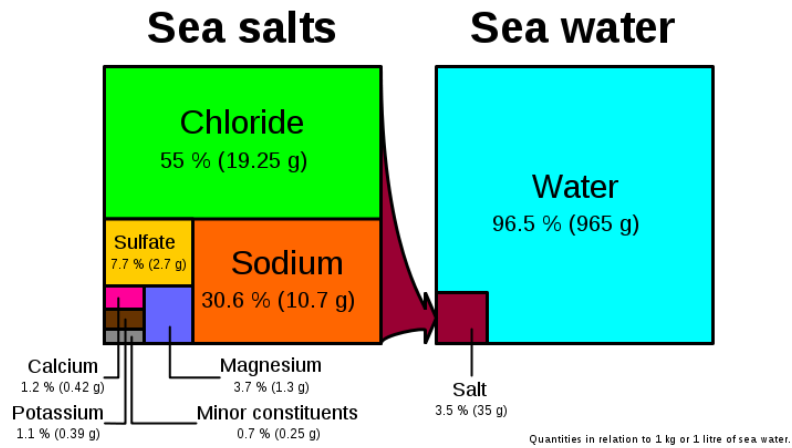
Figure 4.1.3: Salinity of Sea Water (right) and Chemical Composition of Sea Salt. Image: H. Grobe of the Alfred Wegner Institute for Polar and Marine Research, CC BY-SA 2.5, https://en.wikipedia.org/wiki/Seawater#/media/File:Sea_salt-e-dp_hg.svg.

Sodium and chloride account for over 85 *%* of the salt composition. It was deemed sufficient to add appropriate mass of table salt to the tap water to synthesize brine water. Impurities and chemical additions in the tap water were considered negligible. The assumption to ignore the impurities and chemical additions in the tap water was justified through electrical conductivity testing of several desalinated water samples. These samples were compared to tap water and water of known salt concentration, refer to Chapter 4.3.4 for details.

4.1.4 Insolation

Insolation is the intensity of incident solar radiation striking the ground. This quantity depends on geographical location, weather conditions, time of day and time of year. The variability in insolation had the potential to prolong testing or bias results; therefore nullifying direct comparisons in field test results. The mean annual insolation in Tonga is approximately 23 *%* higher than in Aotearoa (New Zealand), so field testing would not be representative of the intended location.

The *in vitro* testing helped to remove the biases and complexities inherent in field testing. The incident solar radiation was simplified by substituting direct sunlight for a lighting array where both the spectral profile and intensity were constant. The array consisted of 10 dichroic filter halogen bulbs (50 *W* each) and a halogen floodlight (200 *W*) which allowed the 450 *W/m²* intensity typical of Tonga to be replicated[7]. The array was designed to be as spectrally similar to sunlight as possible within the project budget, however the bulb configuration was expected to emit greater IR and lesser UV radiation than the typical sunlight spectrum.

Due to these technical limitations, the pyranometer used to measure incident radiation could not be adjusted to compensate for the halogen energy spectrum used in testing. The LE-CL Pyranometer[8] response was calibrated to solar radiation, not halogen bulb emissions. The *in vitro* distillate production required scaling after the pyranometer response to halogen light was calibrated. The lack of feasible dynamic calibration was deemed acceptable to scale the values post-experiment.

---

[7] Refer to Appendix 03 for analysis
[8] Refer to Appendix 04 for manufacturer provided datasheet

4.1.5 Concept Geometry

The cross-sectional views of the proposed concept geometries are shown in Figure 4.1.5 along with their representations as test rigs. The baseline/reference rig allows all identified design parameter variations except the Open Air variation to be tested. The Open Air rig involves a simple modification of the reference rig, shown in Chapter 4.3.6. The rigs were designed to capture the operating principles and intent communicated by the client while allowing for faster and more modular construction than the actual concepts.

The main changes were substitution of curved geometry features for planar surfaces and the inclusion of a separate brine water basin to make filling and emptying the rig safer and easier. The relationships between the primary design features of the concepts; condensation surface, brine basin, absorption surface; were maintained as closely as possible in the rigs.
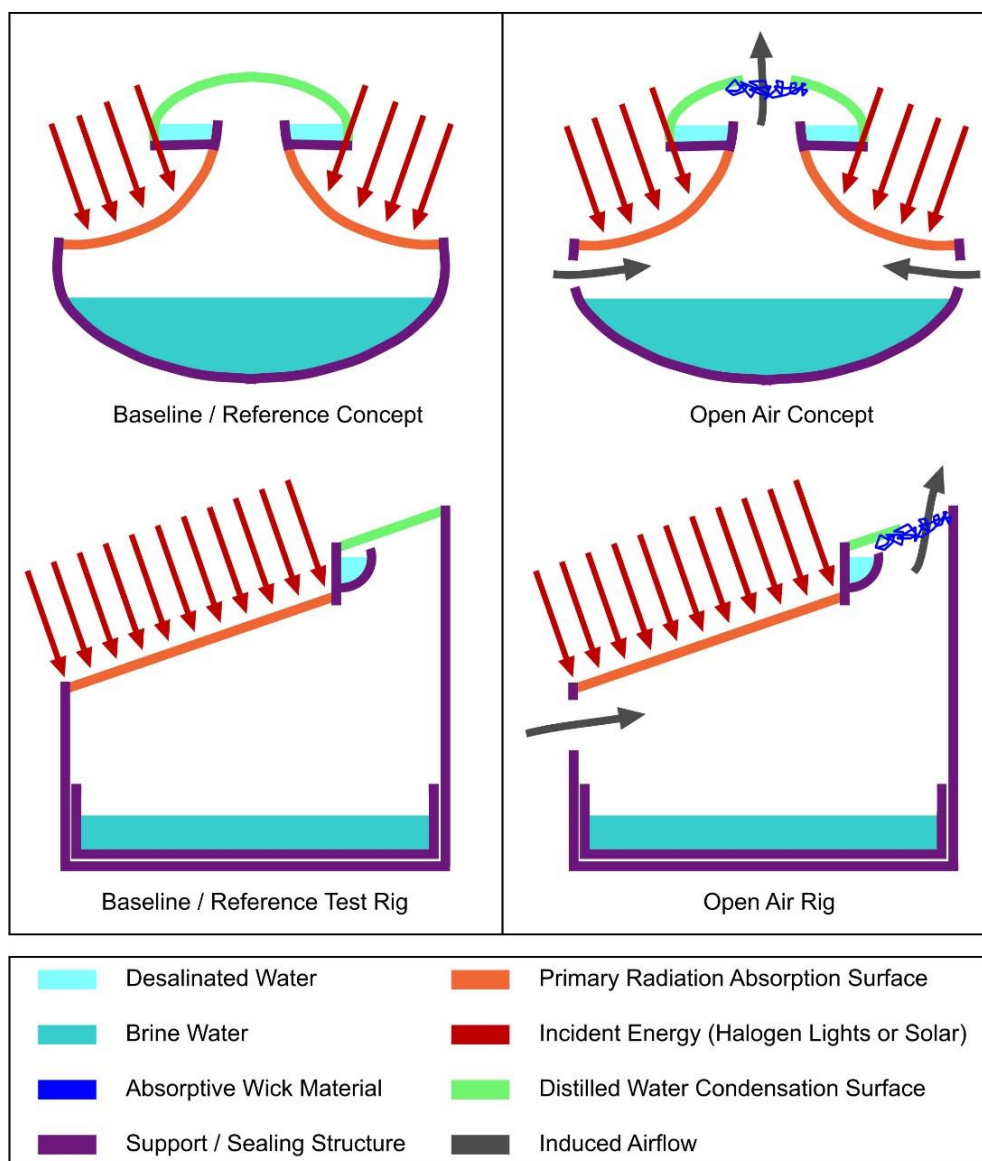
Figure 4.1.5: Functional elements of proposed design concepts and representations as test rigs.

4.1.6 Irreversible System Losses

The internal cavity space of the primary test rig and the removable brine water basin were coated with two coats of Gripset Betta Cemseal and Fix waterproof sealant to minimise the amount of water by each absorbed during operation.

The brine water basin was covered with a single sheet of gloss black polythene (PE) which minimised brine water egress into the basin during operation and provided a better absorption surface for radiative heat transfer than sealed plywood. Rips in the PE were covered with gloss black tape where possible. The average brine water accumulated into the space between the PE and the basin was unaccounted for and was assumed to be negligible due to the undamaged state of the PE.

The internal cavity space of the rig had a layer of aluminium foil pasted all plywood surfaces with the high gloss side visible. This measure minimised the absorptivity of the cavity space and helped to reflect radiant energy to the basin. During the experimental phase, the foil ripped due to movement however appreciable gaps were patched in between tests.

The seals around the removable rear panel of the rig were imperfect. It was therefore assumed that some of the water vapour evaporated would leave the test rig rather than condense for collection. The results showed that this amount was on the order of 17 ± 3 %, based on the discrepancy between initial mass of brine in the basin and the sum of all condensed water and brine remaining in the basin.

4.2 Experimental Configuration

This chapter is concerned with the transition of the rig from a concept; as presented in Chapter 4.1.5, into a functional embodied design assembly. The functional intent, structural elements, necessary instrumentation, contextual considerations, safety measures and devised experimental regime are presented and justified within this chapter.

4.2.1 Development of the Test Rig

The intent was to design a modular rig which allowed different operating configurations to be tested. Functionality of the rig had to reflect the dynamics expected in the concepts. To establish the governing equation set from the testing, the rig required the capacity to isolate all relevant properties enough to distinguish them.

The majority of passive still designs studied in the literature review are of the SSSS variety. The SSSS is the simplest design from a manufacturing perspective as the absorption surface and the condensation surface are one and the same. For testing, data collection and optimisation purposes, it was judged to be advantageous to physically separate the important phenomena; namely the transferral of energy into the absorption surface and out of the condensation surface. This separation provided the means to create independence between the variables, rather than having the effects indistinguishably coupled. The use of a single surface for both heat entry and condensation causes the glass temperature to affect both of these processes. By decoupling the variables, it becomes possible to impose different conditions; such as forced cooling only at the condensation surface. Consequently a decision was made to physically separate the absorption and condensation surfaces which created scope for more optimal system configuration.

4.2.1.1 Detailed Design

Engineering drawings were produced with sufficient detail to replicate the apparatus if necessary, which are provided in Appendix 05. These drawings allowed the transition from the conceptual to embodiment design to occur. The rig geometry presented in Figure 4.1.5 was embodied into a CAD assembly as shown in Figure 4.2.1., with the major dimensions included to give a sense of scale.

ISOMETRIC PROJECTION (FRONT + LHS)   LHS ELEVATION   FRONT ELEVATION
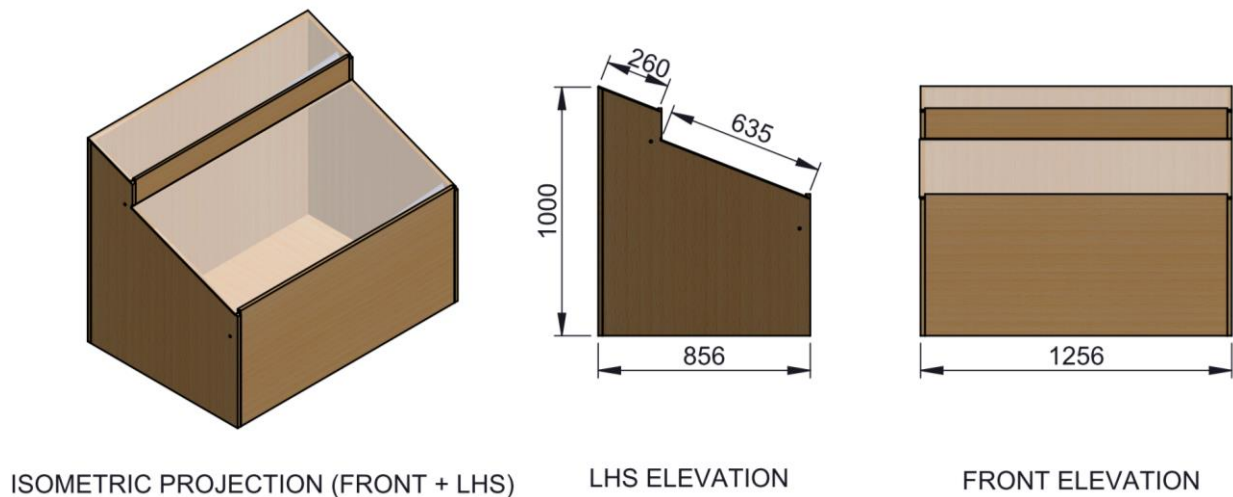
Figure 4.2.1: Projection and elevations of rig assembly without insulation including major dimensions (mm).

The measures taken to minimise irreversible system losses are fully detailed in Chapter 4.1.6. The halogen lighting array that fulfilled the role of the energy source was designed to be representative of the average solar energy flux present in Tonga, as detailed in Chapter 4.1.4.

4.2.1.2   Main Design Features

The rig was designed with a strong focus on ease of fabrication, transport and as-needed modification and on lean manufacturing processes. The final rig is shown in Figure 4.2.2, with functional components highlighted.
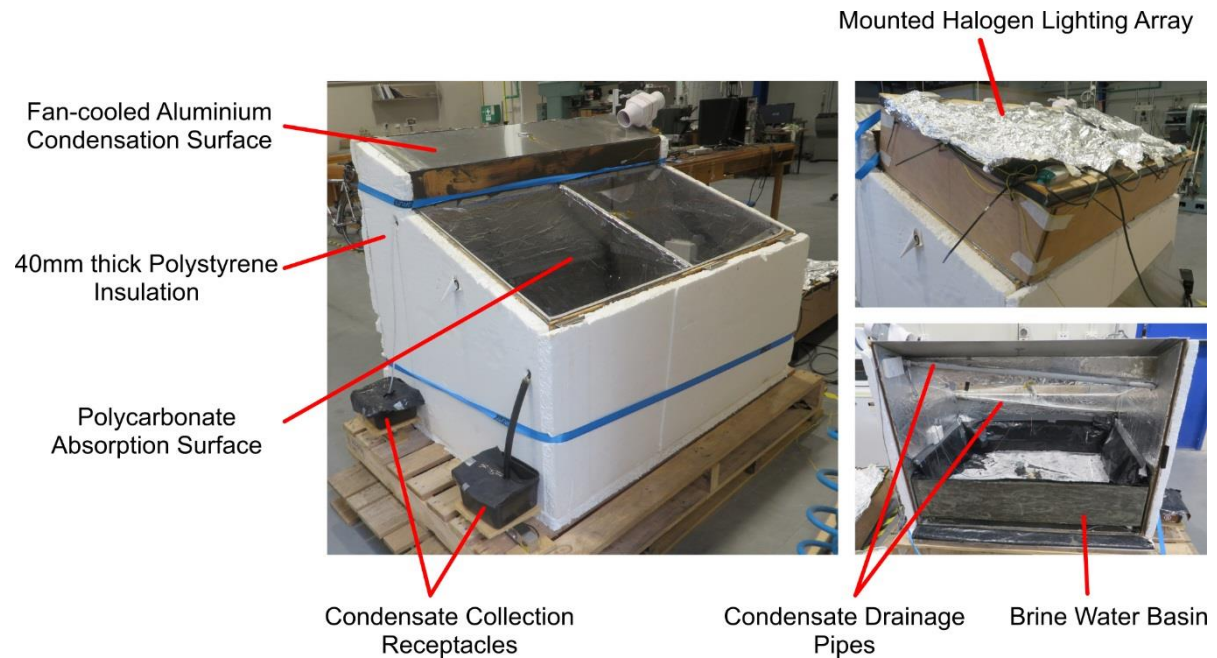
Figure 4.2.2: Annotated functional elements of reference test rig built for *in vitro* experimentation phase.

The plan area of the brine water basin was approximately 1.00 $m^2 \pm 0.04$ m^2, which allowed a unit area energy flux to be considered through testing. Additional unwanted effects were considered to add complexity if the plan area was made significantly smaller. These effects were primarily caused by the directionality of the spotlights in the halogen array. The potential for internal thermal disparity was judged to be higher for a smaller rig. Uniformity in the incident energy was the driving factor to maintain a relatively large rig size with respect to the beam size of the spotlight.

The plan area also allowed it to be mounted on pallets so the entire structural assembly and the instrumentation could be taken outside quickly with the department forklift. The total assembly volume was the largest possible that could easily fit into the back of a standard van.

The assembly size was also driven by the consideration that internal work was required on the rig after the main structural components were complete. The 1.22 m^2 back panel was removable and provided easy access for the preparation of internal surfaces, the integration of sensors and the insertion and removal of the brine water basin once testing had commenced.

The rig was designed with lean manufacturing in mind and required only two sheets of both marine grade plywood and polystyrene insulation for the main assembly structure. The initial design utilised 95 % of these materials and much of the remainder was utilised for ad hoc modifications.

Surface cooling using an electric fan was integrated as a rudimentary simulation of the convective cooling effects of wind on the unit. This project was focussed to a greater extent on exploring the solution space rather than necessarily defining how these conditions would be achieved in context. This focus justified the use of an active component, despite the intention for a passive design.

It has been assumed that the assembly was not hermetically sealed, and that some degree of vapour loss is inevitable during operation. Compressible rubber seals were run along the access surface and at the interface between the assembly and the absorption surface. The absorption surface was in close proximity to multiple, high energy light and heat sources. To limit thermally induced stress damage, tolerance for thermal expansion was integrated into the design absorption surface mount. The absorption surface was required to be as well sealed as possible while still allowing for thermal expansion.

The halogen lighting array weighted down the absorption surface and a pair of ratchet tie-down straps secured the rear access panel. These measures provided additional pressure along the interfaces where leakage was anticipated to be greatest while not compromising the ease with which the absorption surface and the rear panel could be removed if necessary.

4.2.1.3 Hazard Assessment and Commissioning

In conjunction with the practical aspects of the design and build phase, emphasis was maintained on producing a product that was inherently safe to operate during the subsequent testing. The foreseeable hazards associated with operation of the rig were mapped onto consequence-likelihood space during the embodiment design phase. A risk assessment was conducted based on the identified hazards and practical control measures were proposed and implemented to mitigate the potential for damage. The identified highest risk elements of the rig were the potential for electric shock and for fire, the risk mitigation measures have been included below.

Measures to address risk of electric shock:

- Integration of Residual Current Devices (RCD) on all electronics
- Thorough silicon sealing of the cavity to minimise leak potential onto DAQ hardware
- Approval of all wiring and connections by the electronics technician at commissioning and at all electrical changes during testing

Measures to address risk of fire:

- Inclusion of a thermal shutoff circuit to disengage the lighting array if a threshold temperature (90 °C) was exceeded
- Access to a fire extinguisher nearby
- Supervision of the rig during initial testing to monitor the temperatures realised during operation
- Appropriate material selection around the foreseeable hot areas during the embodiment design phase

The risk assessment and corresponding control measures are as presented in their entirety in Appendix 06. The rig was commissioned by the laboratory technicians for electrical safety and overall hazards.

4.2.2 Instrumentation

The main issue in selecting the sensors to capture system behaviour was that the DAQ had a finite number of terminals, which limited what data could be collected about the system. There was a need to evaluate what sensors were most crucial in providing quality data to address the research question as well as where these sensors were placed within and around the rig. The sensor allocation and is shown schematically in Figure 4.2.3 and the individual specifications are shown in Table 4.2.2.1.

An understanding of which quantities were most important in describing the system was gained through the literature. As a thermodynamic basis was proposed for the subsequent model building, numerous temperature measurements were deemed necessary, informed through both the literature and consideration of the most thermally significant aspects of the system.

Energy and mass balances are critical for describing thermodynamic and heat transfer systems, so to address these elements, a pyranometer was incorporated to measure the rate of energy incident on the rig and separate load cell arrangements were incorporated to capture the all relevant liquid water quantities.

The evaporation and condensation processes occurring meant that the moisture content in the internal air had dynamic behaviour which was missing from all empirical studies considered. As such, humidity probes were judged necessary to insert at both the evaporation and condensation interfaces to elucidate the vapour behaviour.

The Low Pressure design configuration proposed by the client necessitated evaluation of the pressure-evaporation relationship so a pressure transducer was fitted to measure the internal-external pressure differential of the rig during operation.

Figure 4.2.3: Schematic representation of sensor designation and placement on test rig.

Table 4.2.2.1: Sensor Specifications				
Measurement	Sensor	Output	Working Range	Data Acquisition Module
M_1	4 x TAL201 Parallel Beam Load Cells	1.0 mV / V	0 - 10 kg per Cell (50 % ultimate overload)	NI 9237
M_2	60k–2 Parallel Beam Load Cell (No. 113895)	*Unspecified on sensor datasheet*	0 - 60 kg	
M_3	PT4000 S-Beam Load Cell	3.0 mV / V	0 - 50 kg	
H_{1-2}	Carel DPWC11000 Humidity Probe	4 - 20 mA	10 - 90 %	NI 9203
P_1	MPX5100 DP Differential Pressure Transducer	0 - 20 mA	0 - 100 kPa	
I_1	LE-CL Pyranometer	4 - 20 mA	0 - 1500 W/m^2	
T_{1-8}	T-type Thermocouple	NI 9219 direct	-200 – 200 °C	NI 9219

The sensor modules were connected to a single National Instruments DAQ-9172 chassis which was run through National Instruments LabVIEW 2012 software for data acquisition. A decision was used to use LabVIEW as the DAQ based on the instrumentation and technical support available at UC. The LabVIEW block diagram built for the data acquisition has been included in Appendix 07.

In order to most reliably capture the brine water mass, one parallel-beam load cell was placed in each corner of the cavity for the brine basin to rest upon. The reading from each sensor was summed within the LabVIEW program to provide a single mass value. This operation was the only processing that occurred internally within LabVIEW. All other data manipulations were conducted using MATLAB R2012b.

4.2.3   Optimisation for Socio-Technical Deployment

The alterations presented in Chapter 4.1 were informed partly by further literature studied, and partly through the experiences gained by the first author while conducting engineering work in Northern India, within a developing, rural context midway through the project. The '*Socio-Technical Deployment Principles*' cited in this chapter are referenced to elements of the New Product Development for Developing Countries study in Chapter 4.3.8. This study is furthermore referenced as the Developing Country (DC) study for conciseness.

4.2.3.1   Glass replaced with Aluminium for Condensation Surface

The majority of passive still designs studied in the literature review are of the Single Slope variety. The Single Slope is the simplest still design from a manufacturing perspective as the absorption surface and the condensation surface are one and the same. As such, a single material; typically glass; makes up the surface. The intended unit design involved absorption and condensation surfaces which were distinct from one another. This configuration offers scope for more optimal material selection than a single dual-purpose surface. Aluminium has been chosen to replace the glass on the holistic basis considered below.

Mechanical Basis

Considering Deployment Principle 1.3, glass is much more susceptible to failure during transit or operation than a metal sheet comparable thickness. The structural qualities of glass are highly undesirable to transport to the remote locations where the desalination unit is to be installed.

Thermodynamic Basis

The thermal conductivities of some materials of interest are included in Table 4.2.3.1. For optimal condensation to occur, heat must be removed out of the system as rapidly as possible. If utilised correctly, a metal condensation surface could be much more efficient at removing energy from the humid air within the space than a comparable sheet of glass.

Table 4.2.3.1: Thermal Conductivities of selected Condenser Surface materials			
Material	Aluminium	Copper	Glass
Thermal Conductivity (*W/mK*)	205	385	0.8

Socioeconomic Basis

Considering Deployment Principle 2.3 glass is too brittle to be reliable in the intended rural context. Brittle failure is much more of a concern under unfavourable weather conditions or interactions with users than with metal. Eliminating the use of glass helps improve the robustness of design and ensures a longer unit lifetime. Copper exhibits the highest thermal conductivity and corrosion resistance out of the condensation materials considered however it is also the most costly and susceptible to theft. For these reasons, the preliminary testing was conducted with aluminium.

4.2.3.2 Glass replaced with Polycarbonate for Absorption Surface

Mechanical Basis

Considering Deployment Principle 1.3, glass is much more susceptible to failure during transit or operation than a polycarbonate (PC) sheet of comparable thickness. As mentioned, the structural qualities of glass are highly undesirable to transport to the remote locations where the desalination unit is to be installed.

Thermodynamic Basis

The thermal conductivities of the relevant materials are shown in Table 4.2.3.2. It was postulated that maximum evaporation would occur when heat was transferred to the brine as rapidly as possible. The system efficiency is dependent on how much energy is actually absorbed by the brine to heat it. The data in Table 4.2.3.2 show that relative to PC, glass is a thermal conductor. Using a thermodynamic basis, glass is the more favourable material choice for the absorption surface.

Table 4.2.3.2: Thermal Conductivities of selected Absorption Surface materials		
Material	Polycarbonate	Glass
Thermal Conductivity (W/mK)	0.19	0.8

Socioeconomic Basis

Polycarbonate sheet was utilised as the heater absorber for the solar cookers built in rural villages in Northern India as part of the work performed there. The locals were aware of the structural limitations of using glass in a place where replacing broken sheets could take several weeks. A viewpoint was conveyed by the locals that any performance benefits possible through the superior thermodynamic qualities of glass were nullified by the replacement time and cost, lost productivity and high likelihood of failure of the material. The choice to use PC was taken on board readily, irrespective of the diminished heat transfer efficiency.

Considering Deployment Principle 2.3, glass is too brittle to be reliable in the intended context, as mentioned in previously. Brittle failure of glass poses a higher risk than PC under unfavourable weather conditions or interactions with users. Eliminating the need to use glass helps improve the robustness of design and ensure a longer product lifetime. There is also potential to use a thicker glass sheet, however the energy transfer is inhibited as the absorption surface gets thicker. For a *given thickness* of absorption surface, PC will have a greater reliability than glass.

4.2.4   Experimental Procedure

The entire experimental procedure involved two levels of process design. The entire overarching process that captured necessary information on all of the identified parameters of interest was designed first to fit within the project timeframe. A systematic test procedure was also designed to ensure that tests were conducted under the same conditions and were therefore comparable.

4.2.4.1   Overall Test Regime

The experimental regime was designed to capture as much information about the independent effects of each identified parameter as possible. The timeframe available for testing was limited, and it was evaluated that each system variable could have, at most, three possible permutations or *states*. A schematic detailing the reference state of the system (*S1*) and the nine tested state variations of this system (*S2-S10*) provided in Figure 4.2.4.
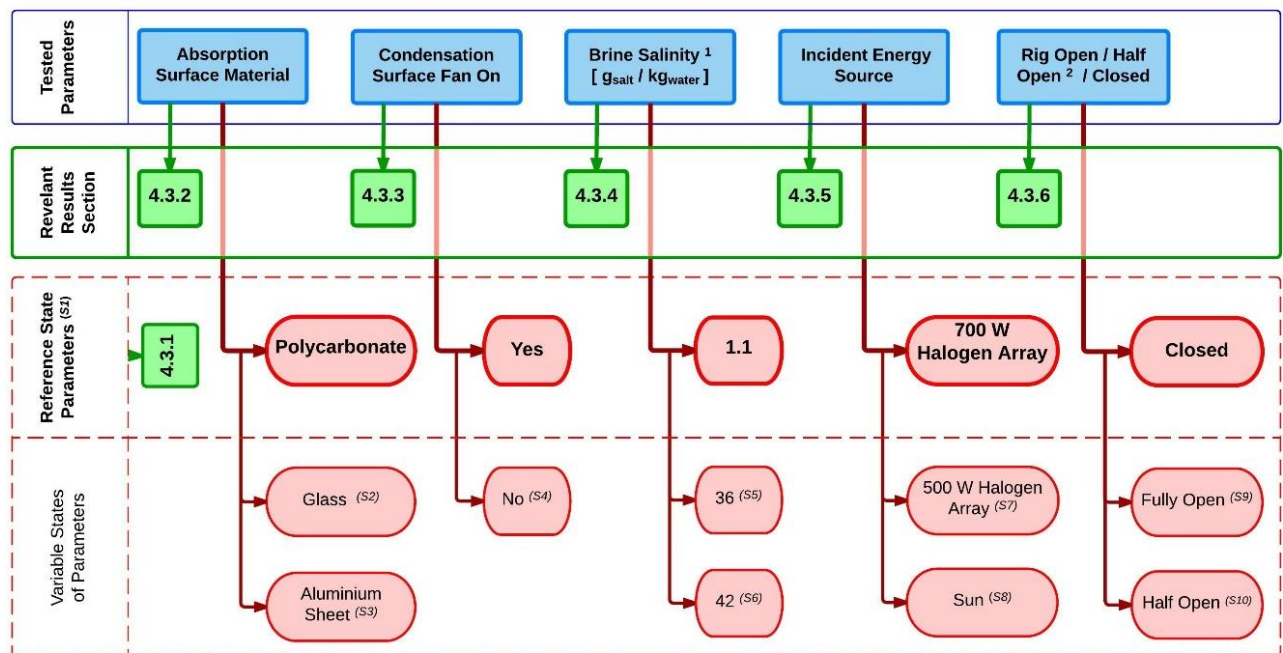
Figure 4.2.4: Reference state of system and states of varied parameters explored during testing.

[1] The reference state value of 1.1 *g* is the salinity of tap water as inferred from the electrical conductivity analysis, see Chapter 4.3.4

[2] See Chapter 4.3.6

To isolate the effect of varying the state of each parameter, only a single parameter was varied during any one test. All other parameters were maintained at their reference state value. This approach helped in decoupling effects from one another, which was judged as the most suitable way to explore the solution space within project scope. The experimental regime was designed with specific aims for the testing of each parameter. The regime has been represented schematically in Appendix 08 and includes a comprehensive matrix detailing the state of each parameter in each test conducted.

4.2.4.2   Individual Test Procedure

A systematic process was developed for using the rig and DAQ apparatus, which considered both safety implications quality data collection. The main steps for running a test are detailed below:

1.   INITIALISATION OF APPARATUS:

A test begun by activating the LabVIEW data acquisition program to check that all of the sensor readouts were sensible and that no connections were loose. It took five to ten minutes for the pressure transducer to reach operational state, after which time the system would be zeroed with the brine water basin placed inside the rig. This zeroing procedure applied only to the load cells and pressure transducer as the pyranometer, hygrometers and thermocouples were not given this capacity within the program.

2.   PLACEMENT OF WATER BASINS:

It was important that the brine water basin was placed in a position that avoided contact with the side walls during testing. Any side wall contact had the potential to skew the load cell readings due to frictional effects inhibiting free motion of the basin. The same precaution had to be taken with the condensate collection receptacles.

3.   INPUT OF WATER CHARGE:

Once zeroed, the chosen water mass was added to the rig and the open face was closed and secured with tie down straps at the top and bottom. The straps provided extra pressure along the opening surface to help sustain a better seal.

4.   ACTIVATION OF LIGHTING ARRAY:

The data collection was then initiated followed by activation of the halogen lighting array a few seconds afterwards. For the solar tests, the rig was in position outside before the sunlight was directly striking the absorption surface. The data collection was initiated prior to direct energy incidence in order to maximise capture of the heat-up dynamics.

5.   DURATION OF TEST:

The period of each test was governed by either performance for the *in vitro* cases or adverse weather conditions for the solar cases. *In vitro* tests were aborted if no condensation occurred in the first three hours. Solar tests were aborted as necessary to avoid the instrumentation and DAQ getting wet. The *in vitro* tests were generally run until all of the water initially placed into the basin had evaporated in order to capture as much of the system dynamics as possible. It was acknowledged during the data processing phase that these dynamics would change as the water evaporated, most notably when the basin area was no longer completely wetted and the water was congregating into puddles. The data processing and modelling stage was therefore only applicable while more than 0.5 *kg* was in the basin. This amount was the approximate minimum that would exist while the basin was entirely wetted.

4.3 Experimental Results

The result sets presented in Chapter 4.3 show how the system evaporation and condensation characteristics compare to the reference case for each of the design variations tested. The typical distillate volume produced varied between $0.30 - 2.0$ L/m^2 over a test period depending on the state of the system. The charts presented contain a dense amount of information and several points have been presented to assist in interpretation as listed below.

Interpretive notes for charts:

Systematic Chart Layout

- The first chart presented in each sub-chapter shows the distilled water mass collected as this is the overall system performance metric
- The second chart in each sub-chapter shows the time profile of water evaporating from the brine basin
- The mass of water evaporated always starts at zero for a clear comparison of how the evaporation rates differ
- Subsequent charts show response profiles of other parameters relating to internal system dynamics rather than system performance, for clarity of explanations
- The charts have been truncated to the lowest comparable time period between the tests presented
- The reference test is always plotted in red for quick identification

Evaporation and Condensation Response Profiles

- The most effective condensation configuration reaches the highest magnitude positive number by the end of the test period.
- The most effective evaporation configuration reaches the highest magnitude negative number by the end of the test period
- Steeper gradients in the condensation and evaporation profiles indicate better productivity
- Flat lines in condensation or evaporation profiles indicate nil productivity

4.3.1   Repeatability Testing

Purpose: This testing was intended to clarify whether all results were directly comparable, or whether the system response to a 'reference test' initial condition varied over the experimentation phase.

Outcome: Results between the first two reference tests show a 0.15 % difference in the amount of water condensed at the end of the comparable time period, indicating that the system response displays the effectively same behaviour to a given set of initial conditions. The third reference test displayed a 26 % reduction in water condensed from the next closest test, indicating a discrete change in measured system response. This disparity was assessed to be caused by degradation of the load cells after prolonged elevated temperature operation.

Over the course of the test phase, the reference test was repeated periodically to ensure that the results were comparable with one another. The brine water evaporated and distilled water condensed are overall system performance metrics and have been plotted in Figure 4.3.1.1 to describe the similarity of system performance during each reference test. Note that Test 08 is obscured behind Test 17 for the condensation profiles, indicating a high degree of uniformity.
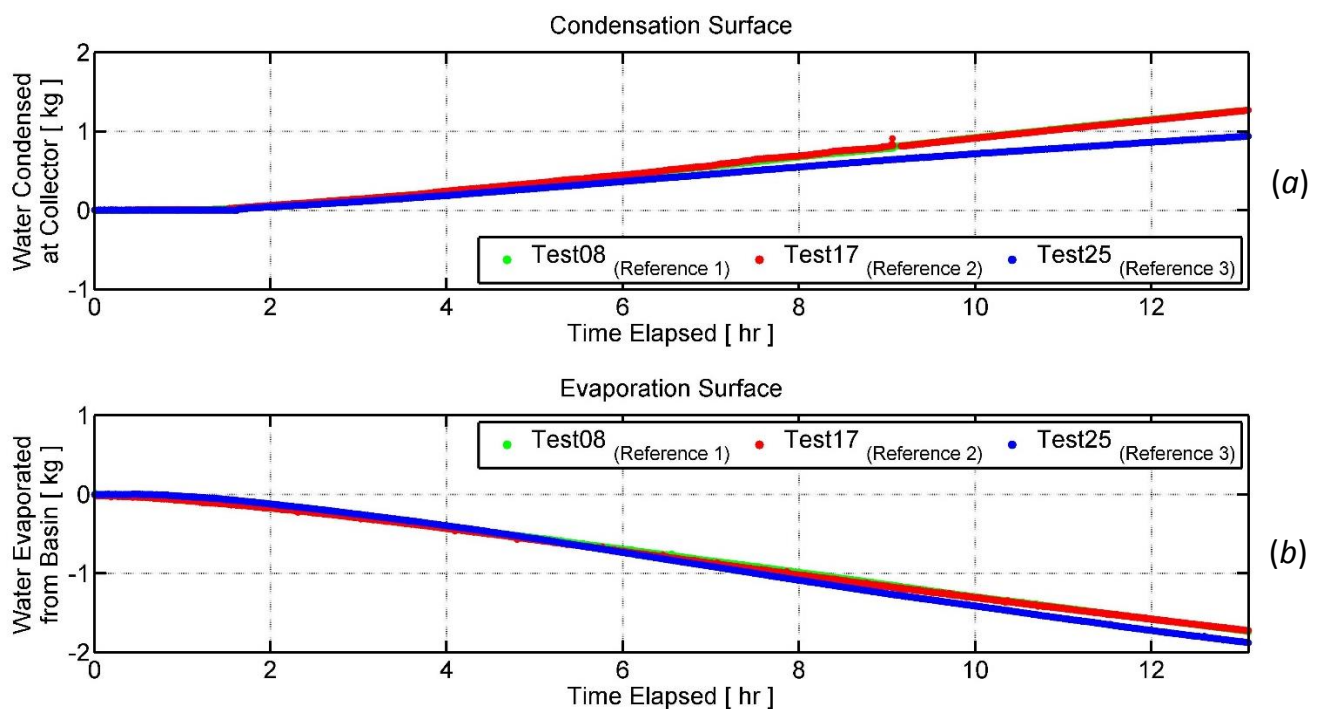
Figure 4.3.1.1: Repeatability of water mass condensed (*a*) and evaporated (*b*) during reference tests.

The relative humidity values at the evaporation and condensation surfaces are system dynamics and have been plotted in Figure 4.3.1.2 to describe the similarity of the internal system behaviour during each reference test. The discrete changes observable in humidity at the condensation surface are assumed to be the result of unwanted drip-back of the condensed water at this surface. The humidity sensor was placed in a position that made it susceptible to being influenced by drip-back. However, this outcome did not dramatically skew the data trends. The observed behaviour was evaluated to be within limits of acceptable perturbation to the system to continue testing without modification of the humidity sensor.
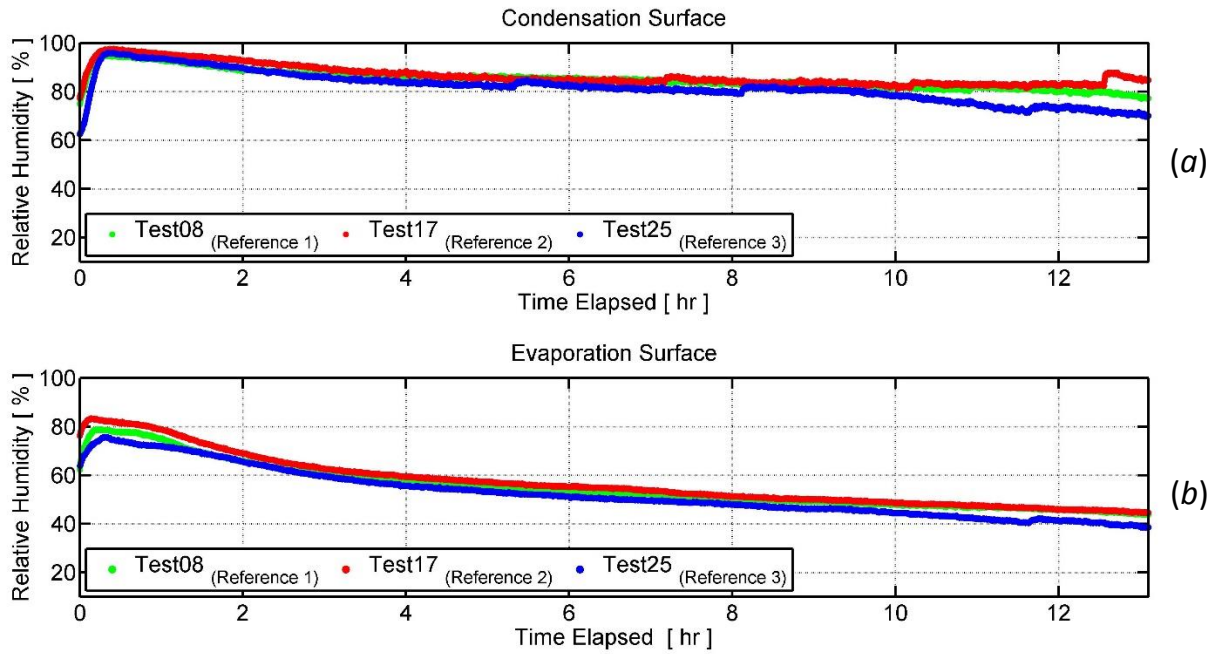
Figure 4.3.1.2: Repeatability of relative humidity conditions during reference tests at condensation surface (*a*) and evaporation surface (*b*)

All three reference tests (Tests 08, 17, 25) were highly concordant with respect to the internal system behaviour (relative humidity). However, the third reference test showed a large discrepancy in the performance metric (distilled water collected) compared to the first two. This phenomenon was investigated to verify the quality of data.

The reference tests were comparable for just over 13 hours, at which point, the lighting array was switched off in Test 08. Initial tests had limited durations due to available laboratory access, although this constraint was remediated prior to Test 17. Test 17 has a longer uninterrupted data collection period so has been used as the reference standard for all other rig variations. Between the first two reference tests, the distilled water mass collected differs on average by 0.0019 *kg* during the comparable 13 hour period. This discrepancy represents 0.15 *%* of the final condensate mass collected

Test 25 differs substantially from the first two tests. This difference is most pronounced with measurements taken at the condensation surface where approximately 26 *%* less condensate was collected compared to the other two reference tests. The amount of water that was measured compared to that which had evaporated after the same time period had increased by 9 *%*.

The test regime involved periodic reference tests, to validate continued uniformity of the system behaviour. The third reference test was scheduled for Test 26, however the observation was made during Test 24 that the total amount of water measured by the load cells was decreasing steadily over the test duration. Approximately 50 *%* of the initial water mass was unaccounted for by the end of Test 24. This behaviour had not been apparent for all prior tests.

It was judged necessary to immediately conduct the third reference test after having observed this step change in system response. This change was investigated and detailed further in Appendix 09. The total water mass in the system as measured by the load cells in the brine basin and at the condensation surface is shown in Figure 4.3.1.3 for the three reference tests.
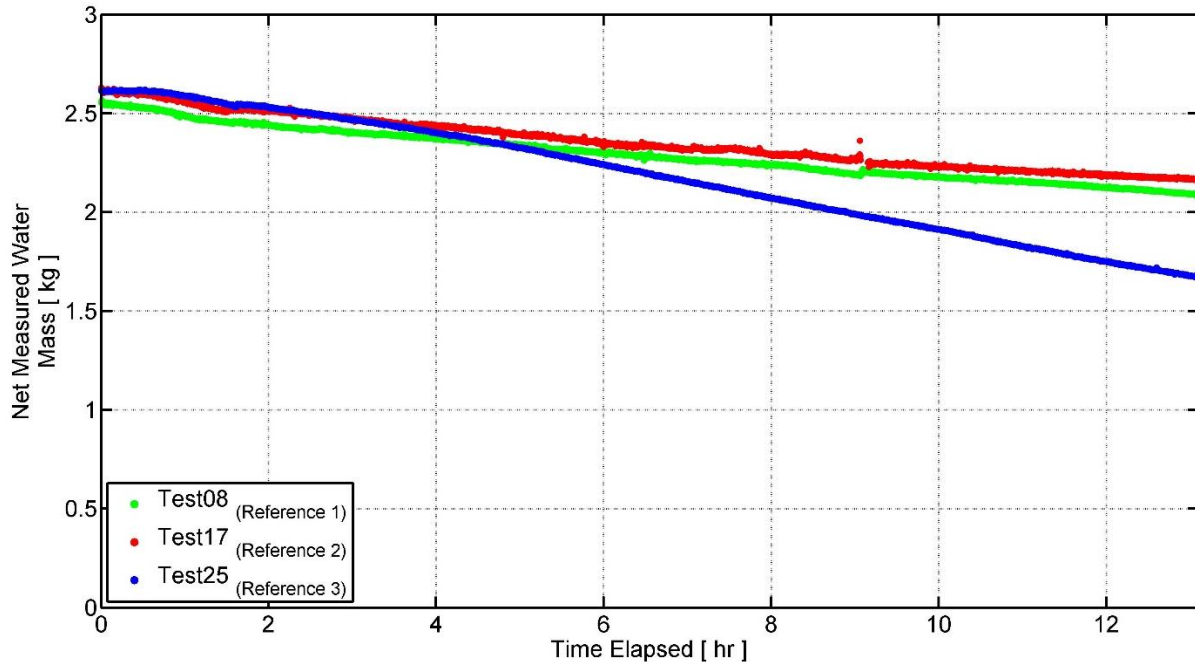
Figure 4.3.1.3: Total water mass in system as measured by load cells during reference tests

It is clear from Figure 4.3.1.3 that the system behaviour in Test 25 is not the same as Tests 08 and 17. The sensors failed to account for more than 50 % of the initial water mass by the end of the test. It must also be noted that the basin was completely dry at the conclusion of Test 25. Test 25 was truncated for comparative purposes. Subsequent testing was conducted to find the source of the discrepancy and it was concluded that the load cells had degraded after prolonged exposure to temperatures at the upper limit of their rated operating range. The testing was suspended after Test 25 and the data collected between the second and third reference tests was judged to be sufficient for direct comparison.

4.3.2   Absorption Surface Material Testing

Purpose: This testing was intended to investigate the effect that the absorption surface material had on still productivity. Polycarbonate, glass and aluminium sheet (no surface treatment applied after purchase) absorption surfaces were considered.

Outcome: Results show glass is thermodynamically more efficient than PC of comparable thickness, achieving 33 % more condensation mass than glass over the comparable test period. The glass shattered under the controlled in vitro *test conditions which was indicative that the material choice is insufficient in context. For the rig geometry tested, aluminium sheet metal is non-functional as an absorption surface.*

The initial system commissioning, instrument calibration and first two tests were conducted using a sheet of 3 *mm* float glass as the absorption surface to transfer the heat into the unit. Thermal stress due to localised heating from the bulbs caused the glass to shatter at the end of the second test, wherein the lighting array was increased from the initial 500 W value to 700 W to accelerate the evaporation rate and account for radiation losses from the rear of the lighting array.

The replacement absorption surface was PC, as described in Chapter 4.2.3.2. A small degree of thermally-induced curvature occurred in the PC as a result of the close proximity halogen bulb, although this was deemed negligible to system performance. A comparison of the aforementioned glass absorber and an aluminium absorber against the PC reference case is shown in Figure 4.3.2.1.
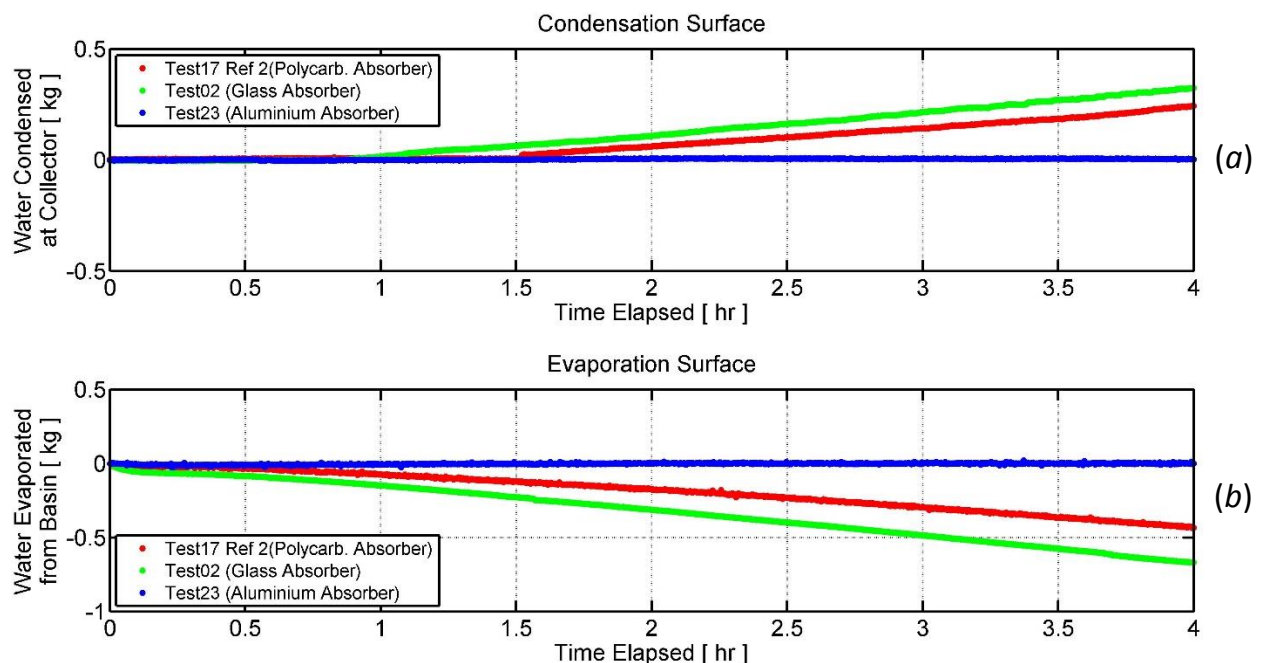
Figure 4.3.2.1: Effect of Absorption Surface Material on water condensation rate (*a*) and evaporation rate (*b*).

The glass absorber test case was subject to the same time limitation as was mentioned in Chapter 4.3.1. The datasets are therefore only comparable until four hours had elapsed, at which point the lighting array was switched off for Test 02.

As expected, the glass absorber case began collecting condensate faster than the PC absorption surface. The PC lagged behind the glass by approximately half an hour for the same energy input from the lighting array. At the end of the comparable test period, the glass surface had condensed 33 *%* more water than the PC.

As shown in Figure 4.3.2.1, the condensate collection rates are effectively linear through the comparable test period. None of the other tests produced a noticeably non-linear relationship for the condensate collection rate. There is no evidence from the testing to justify that this relationship alters as more of the brine water evaporates and it has been judged accordingly that the PC is approximately 33 *%* less efficient than the glass in terms of projected productivity.

The client was interested in testing the using an aluminium absorption surface. This surface did not produce any condensate nor did it initiate any evaporation of the brine water. It can be concluded that for the rig geometry tested, an aluminium absorption surface is ineffective at transferring heat to the internal space. This conclusion is quantified through the data presented in Table 4.3.2.1.

Table 4.3.2.1: Quasi-steady temperatures and final condensate mass based on absorption surface				
		Absorption Surface		
		Polycarbonate (3 *mm*)	Glass (3 *mm*)	Aluminium (2 *mm*)
Internal Absorption Surface Temperature	[$^{\circ}C$]	97	67	61
Internal Air Cavity Temperature	[$^{\circ}C$]	48	56	27
Water Surface Temperature	[$^{\circ}C$]	49	55	24
Water Condensed	[*kg*]	0.24	0.33	0.00

The aluminium surface had the slowest temperature response of the three absorber materials tested and reached the lowest quasi-steady temperature. The same trend in response was observed with the internal air temperature characteristics also, although difference between aluminium and the other cases was even more pronounced. The brine water in basin exhibited a negligible temperature rise from ambient in this instance.

Further work regarding an aluminium absorption surface could involve altering the surface condition to make it less reflective. It was observed that the aluminium bounced a qualitatively larger amount of light back into the lighting array than did the other absorption surface materials. Making the surface matt black or dark blue may be an avenue worth exploring to help increase the energy absorption properties. The use of aluminium to absorb and transfer incident energy appears to be of no value according to the *in vitro* testing conducted for this type of test rig. The geometry requires complete redesign to validate further aluminium tests.

The glass shattered under *in vitro* test conditions which indicated a lack of suitability for application in a developing or rural context where the degree of environmental control is significantly lesser. Further optimisation of the glass surface is limited by overall size and sheet thickness. The heat transfer capability of the glass decreases with increased sheet thickness. Design scalability was found to be poor based on a secondary project conducted in conjunction with the main body of work[9], and the unit productivity decreased exponentially with reduced size. The means to optimise system reliability and performance aspects act antagonistically to one another, which puts significant bounds on the potential of a feasible glass absorption surface.

Although PC is considerably less efficient than glass as the absorption surface material, the use of glass in the intended socio-economic context may not be justifiable. Further work could involve an in-depth investigation of plastics that have more optically similar properties to glass, but which do not pose the same liability for brittle failure. The testing, in conjunction with Deployment Principles 1.3 and 2.3 from the DC study presented in Chapter 4.3.8 has informed future design work to a more focussed exploration of plastic absorption surfaces. The PC exhibited no appreciable scratching or discolouration during the course of the work.

---

[9] A series of small rigs were built and tested by Lap Kei (Michael) Leung with assistance from the first author, see Chapter 6.1.4 for more detail

4.3.3   Condensation Surface Modification Testing

Purpose: This testing was intended to investigate the effect that cooling of the condensation surface played on still productivity. The cooling was achieved using an electric fan, although focus was on achieving high productivity rather than the specific mechanism required. The mechanism was of secondary importance as this project served as a preliminary exploration of the design space, rather than embodiment design work.

Outcome: Results show that disengaging the fan and thereby raising the condensation surface temperature by 20 °C causes a 60 % decreases in condensate productivity over the comparable test period. This testing has quantified the crucial importance of maintaining the lowest condensation temperature possible.

The effect of condensation surface temperature on system performance was evaluated by conducting tests with the cooling fan switched off. For all other tests, the cooling fan was blowing air along the condensation surface at 12 *m/s* (130 *ft³/min*). The evaporation and condensation characteristics without the cooling fan are compared to the reference test performance in Figure 4.3.3.1. Note: Tests 23 and 18 have almost identical condensation characteristics.
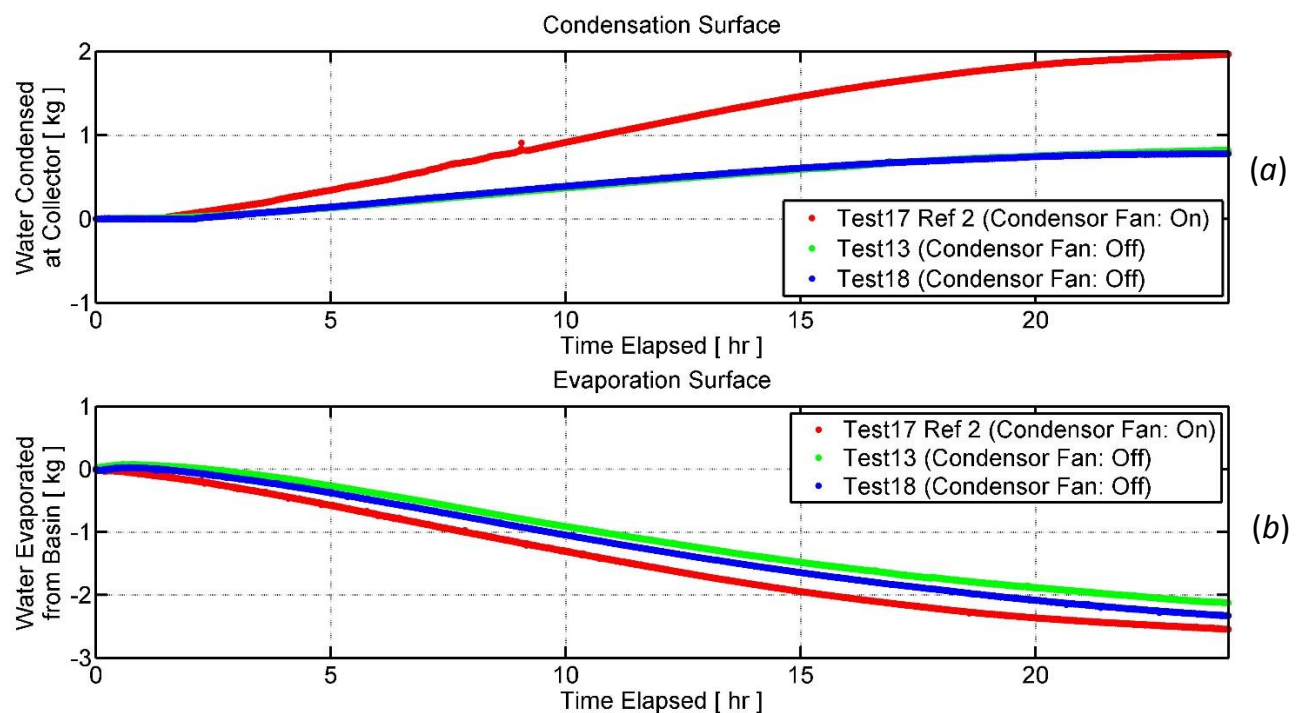
Figure 4.3.3.1: Effect of condensation surface condition on water condensation rate (*a*) and evaporation rate (*b*)

Note: Tests 23 and 18 have almost identical condensation characteristics so the blue line obscures the green line

There is a 1.1 *kg* reduction in the amount of condensate collected over the comparable time period when the cooling fan was switched off, which translates to a 60 *%* performance decrease. Removal of the fan caused an approximate 12 *%* reduction in the mass of water evaporated at the water surface, so the effect here was much less pronounced than at the condensation surface, but still appreciable.
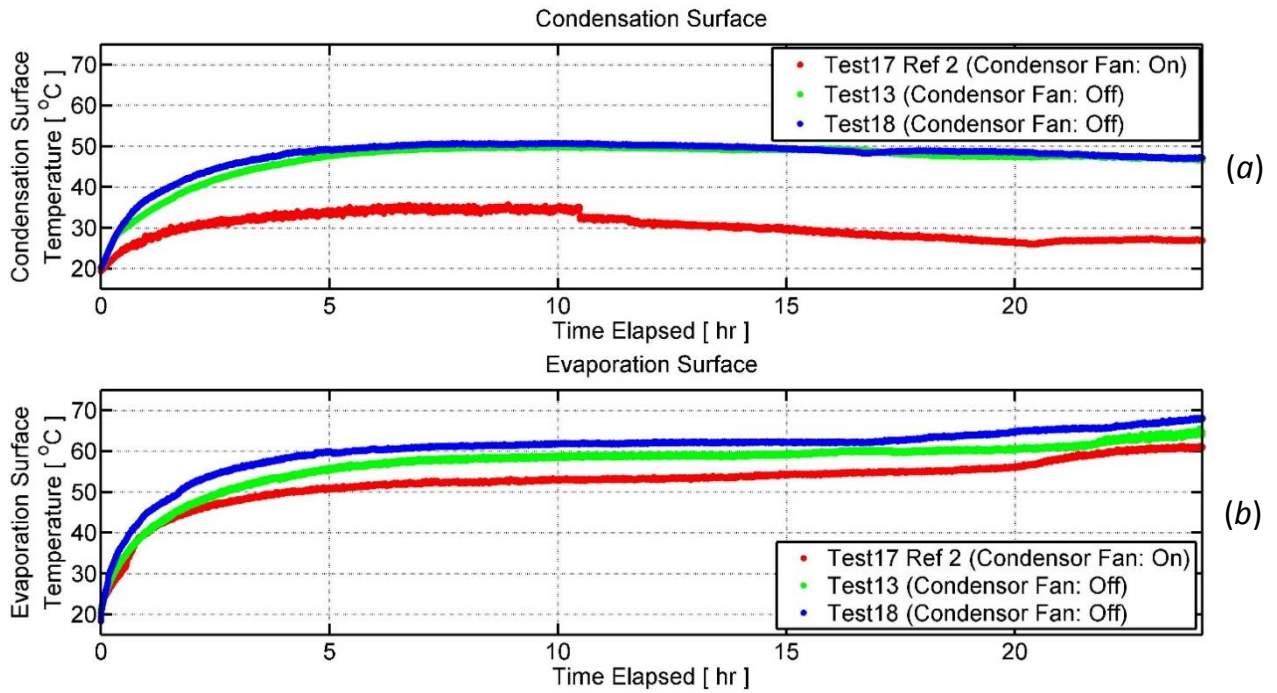
Figure 4.3.3.2: Effect of Condensation Surface Condition on temperatures at evaporation surface (*a*) and condensation surface *(b)*

Figure 4.3.3.2 shows the condensation surface temperature increased on average by 20 *°C* (a 74 *%* increase), while the water surface increased on average by only 5.3 *°C* (an 8 *%* increase). The temperature difference between the condensation and evaporation surfaces was observed to decrease by approximately 15 *°C* on average (a 43 *%* decrease in magnitude). A reduced temperature difference between these surfaces is less favourable for the desirable heat transfer modes to occur. Convection, conduction and radiation are all dependent on the temperature difference and reduction of this differential reduces the potential for heat transfer. It was clear from the *in vitro* test results that maintaining the lowest possible condensation surface temperature is one of the major factors influencing solar still productivity.

The semi-empirical dew point temperature has been overlaid onto each condensation surface temperature profile in Figure 4.3.3.3. This overlay is indicative of when condensation was expected to occur based on current psychrometric theory. While the condensation surface is below the dew point temperature, water vapour in the air is expected to condense onto the surface.
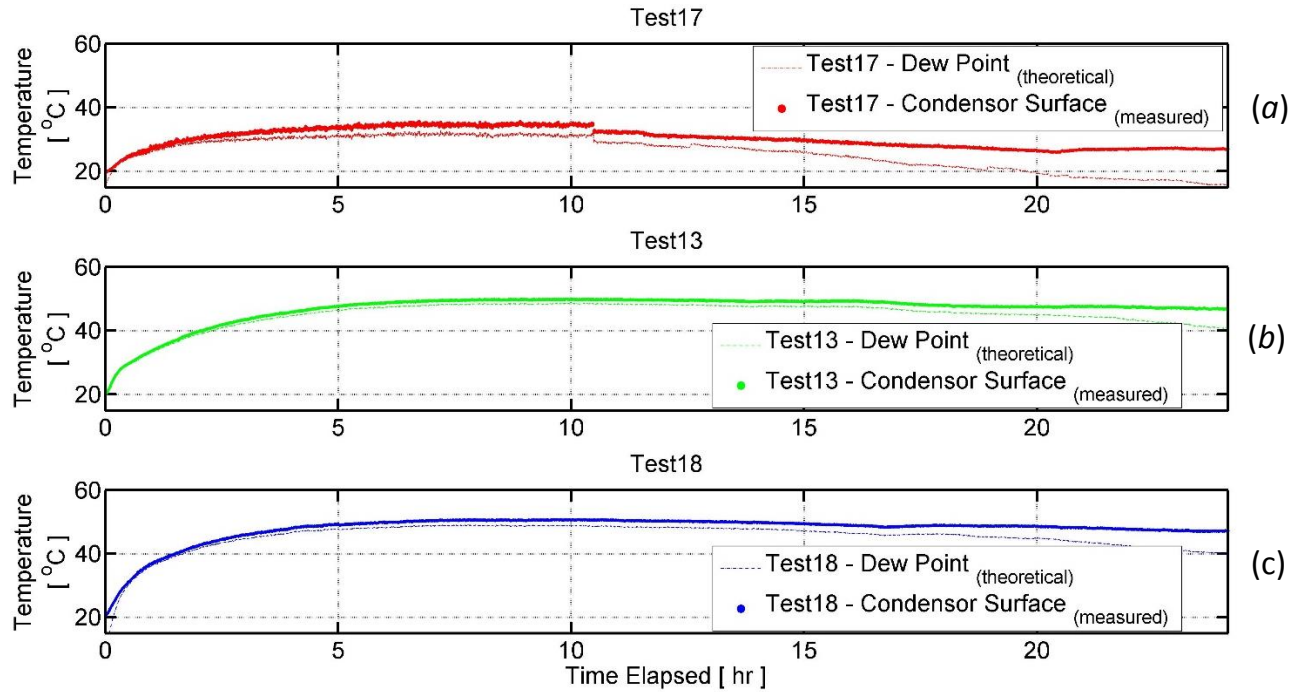
Figure 4.3.3.3: Individual dew point and condensation surface temperatures for Test 17 (a), Test 13 (b) and Test 18 (c)

The dew point temperature (T_{DP}) was calculated using the Magnus Equation, reproduced in equations (4.3.3.1-4.3.3.2). Nomenclature has been maintained from Figure 4.2.3.

$$\gamma(T_3, H_2) = \ln\left(\frac{H_2}{100}\right) + \frac{b_1 T_3}{c_1 + T_3}$$
(4.3.3.1)

$$T_{DP} = \frac{c_1 \gamma}{b_1 - \gamma}$$
(4.3.3.2)

where experimental data from condensation surface temperature (T_3) and relative humidity (H_2) are used to define the intermediate parameter (γ) which is then used to define T_{DP}. The calibration parameters (b_1, c_1) used in the equations were obtained from work conducted by Sonntag [57] and were relevant for test conditions; specifically situations where $1\ \% < H_2 < 100\ \%$ and $0\ °C < T_3 < 60\ °C$.

Condensation was not predicted, for even Reference Test 17, based on the thermocouple measurements. The relevant thermocouple was placed in direct contact with the condensation surface at the geometric centre. However, the surface was not expected to have a uniform temperature during operation due to both internal airflow dynamics and the forced convective cooling of the fan. The fan was placed at one side of the rig as shown in Figure 4.2.2. Based on the power and placement of the fan, a bulk thermal gradient was judged to exist along the condensation surface as a result. It was assumed that at least some of the surface was below the dew point temperature to account for the condensation that was measured. The temperature was expected to be locally much cooler around the fan than elsewhere.

The practical implications of modifying the condensation surface condition were also investigated in Tests 21 and 22, conducted under sunshine conditions as detailed in Chapter 4.3.5. The *in vitro* test setup represented an idealised case where the incident energy was only transferred through the desired surface. In reality, all surfaces are subjected to the incident energy flux and this may have a detrimental effect on performance.

4.3.3.1 Implications for possible future research and development

Allocating more thermocouples on the condensation surface would provide a more detailed spatial temperature characteristic for different operating conditions. No further thermocouple terminals were available in the DAQ hardware chassis, and thermal mapping of the condensation surface has been proposed as an area for future investigation. This additional research would help determine the optimal length of the solar still to ensure benefit from the surface cooling effects of the fan.

No permanent measure has been thus far designed to shade and cool the condensation surface, although the effects of an additional reflective surface atop the condensation surface are detailed in Chapter 4.3.5. It was observed that the distillate production increased by approximately 25 *%* under sunshine test conditions when this second surface, identical to the first, was included for shading. The fan remained free to operate between these two surfaces.

The condensation surface was observed to be a highly sensitive design parameter based on the 60 *%* performance decrease that resulted from a 20 *℃* decrease in the condensation surface to water temperature difference. Unlike the discrete parameters tested such as the choice of absorption surface material or Open Air configuration, the possible permutations of the condensation surface condition are much more numerous.

4.3.4   Water Salinity Testing

Purpose: This testing was intended to provide a calibration factor to convert the condensate mass obtained using tap water in the basin to an equivalent expected condensate mass using saline water.

Outcome: Results show that for the halogen array energy input, there is an insignificant difference in productivity if saline water at the concentration of Tongan seawater is used instead of tap water. Increasing the salinity concentration beyond this was observed to cause a significantly non-linear response. The mechanism of this non-linearity is discussed, although it was beyond the scope of the project to fully elucidate.

The reference tests were conducted using tap water rather than saline water as the project was focused on ascertaining the mathematical relationships between evaporation and condensation. It was, however, still necessary to investigate the extent to which saline water affected the evaporation rate. This investigation allowed tap water performance of the *in vitro* rig to be correlated to expected seawater performance in context. The literature studied indicated that increased salinity corresponded to decreased performance [16-18], but the underlying mechanisms and governing physics behind this were not addressed in these papers. The saline water solution used had approximately the same salt concentration as the seawater typical of Tonga (36 g_{salt} / kg_{water}). The evaporation and condensation characteristics of saline water are compared to the reference test in Figure 4.3.4.1.
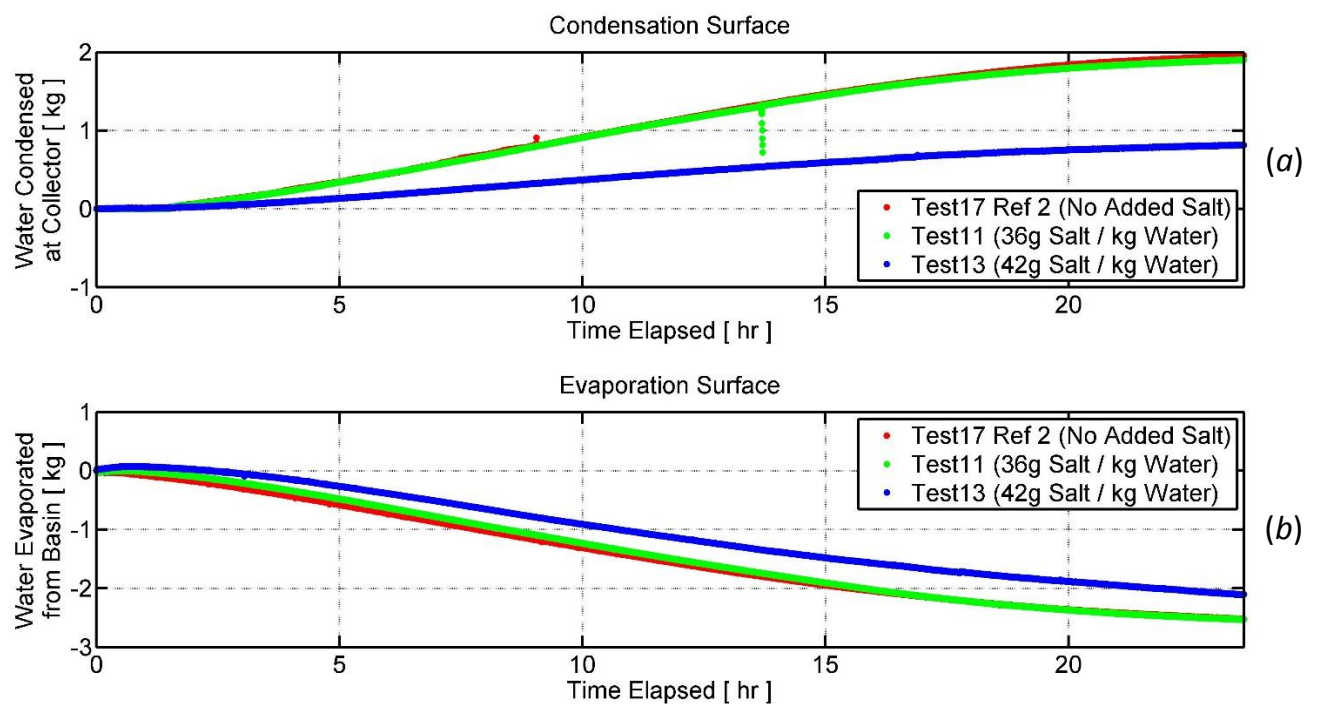
Figure 4.3.4.1: Effect of water salinity on condensation rate (*a*) and evaporation rate (*b*)

The testing indicated that for the *in vitro* reference energy input, saline water at the concentration expected in Tonga caused no appreciable performance difference compared to tap water in the basin. This result was particularly useful as it indicates that evaporation behaviour of the *in vitro* rig is representative of actual performance in context.

The data exhibits an appreciable non-linearity as salinity is increased from 36 to 42 g_{salt} / kg_{water} as shown in Figure 4.3.4.1. It has been proposed that a dynamic equilibrium exists with the saline concentration that shifts depending on the incident energy intensity. This proposed behaviour may be a contributing factor to the global differences in ocean salinity. Further testing is necessary to clarify the mechanism behind this change, as it was outside the scope of this project to pursue this salinity relationship.

In order to quantify the desalination efficacy of the unit, samples of the condensed water collected from the saline tests (Test 11 and Test 13) were measured using an electrical conductivity meter. The results of this test are shown in Table 4.3.4.1. A conductivity meter was used to measure salt concentrations of water samples before and after tests. Three samples of known salt concentration were used to calibrate the conductivity meter, which allowed effective salt concentrations of the distilled water samples collected at the condensation surface to be inferred. The conductivity of tap water has been tabulated as this was used for all tests except 11 and 13. The calibration values used relate to the Tongan seawater salt concentration, half seawater salt concentration and one tenth seawater salt concentration.

Table 4.3.4.1: Electrical conductivity and salt concentration of water samples relevant to testing							
Sample	-	Tap Water	Test 11	Test 13	Calibration 1	Calibration 2	Calibration 3
Electrical Conductivity	$[\mu S]$	**145**	**35.8**	**58.6**	**25500**	**13500**	**1340**
Inferred Salt Concentration	$[g / kg]$	1.3	1.1	1.2	36	18	3.5

The desalinated water samples were found to be between 20 *%* and 40 *%* as conductive as the tap water that was put into the unit for testing. Compared to the original 36 g/*kg* salt concentration, the desalinated water samples reflect a 97 *%* reduction in salt concentration. The World Health Organisation guidelines for drinking-water quality indicate that the threshold sodium chloride salt concentration in drinking water is 1.50 g/*kg*, and the desalinated sample results are below this. The desalinated samples indicated that electrically conductive impurities are not readily transported to the condensation surface through the water vapour movement.

4.3.5   Incident Energy Testing

Purpose: This testing was primarily intended to clarify that the system dynamics for the halogen bulb lighting array were comparable to those under solar radiation. The secondary intention was to investigate how performance changed using a lower power halogen array, representative of poorer weather conditions. As a continuation from the testing conduction in Chapter 4.3.3, the effect on productivity of shading the condensation surface under solar conditions was also investigated.

Outcome: The conditions present for the in vitro *testing were considerably more favourable than real solar conditions. The* in vitro *operation was deemed to represent an ideal case that potential future design development could benchmark solar performance against. Passive cooling through shading of the condensation surface was found to increase productivity by approximately 25 %.*

The effect of incident radiation on system performance was investigated by reducing the total electrical power rating of the halogen array through removal of one of the floodlights. This distinctly different energy input provided another case to further the parameter identification for the energy input term in the proposed system model. Several tests were also conducted with the sun as the energy source to provide values to compare performance against the halogen bulb array. The evaporation and condensation characteristics for all solar tests and the reduced electrical power test are compared to the reference test performance in Figure 4.3.5.1.
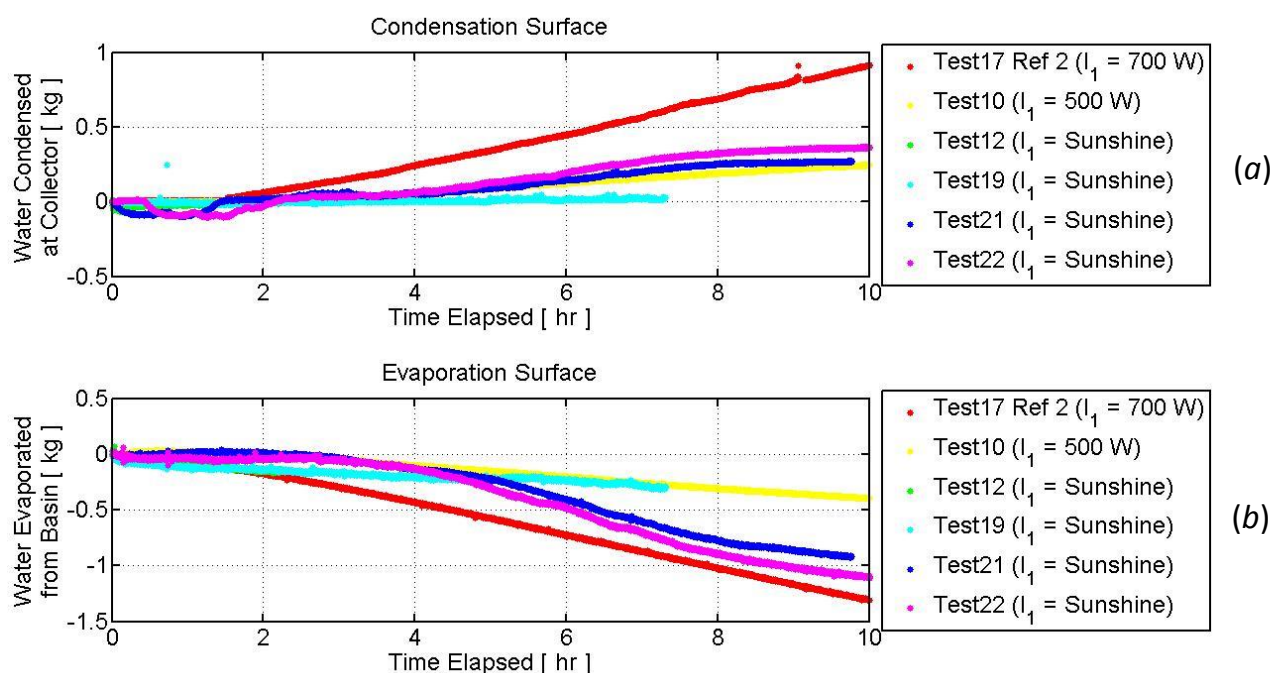
Figure 4.3.5.1: Effect of incident energy source and intensity on condensation rate (*a*) and evaporation rate (*b*)

High winds were present during Test 19 and the condensate drainage pipe was repeatedly blown out of the collection receptacle attached to the mass sensor. The load cell registered only negligible amounts of condensate as a result. Compared to the other sunshine tests, Test 19 exhibited the lowest rate of evaporation, so loss of the condensation data is not of paramount importance in performance evaluation.

None of the literature studied addressed scaling *in vitro* test results to provide expected performance values under sunlight conditions. The pyranometer used for the entirety of testing was internally calibrated to give an accurate response to sunlight. The halogen array used for *in vitro* testing was aimed to replicate sunlight as best as was practicably possible. The sunlight spectral distribution differs from that of halogen bulbs and no means of validating the sensitivity of the pyranometer to the latter spectrum were possible during the project. The data shown in Figure 4.3.5.1 indicates that the halogen array had the highest intensity, however this result conflicts with the pyranometer readings shown in Figure 4.3.5.2. Both the instantanous power intensity and the cumulative energy flux incidenting the basin have been plotted. The cumulative energy was attained by integrating the power measurement with respect to time and provides a clearer representation of the total energy measured by the sensor.
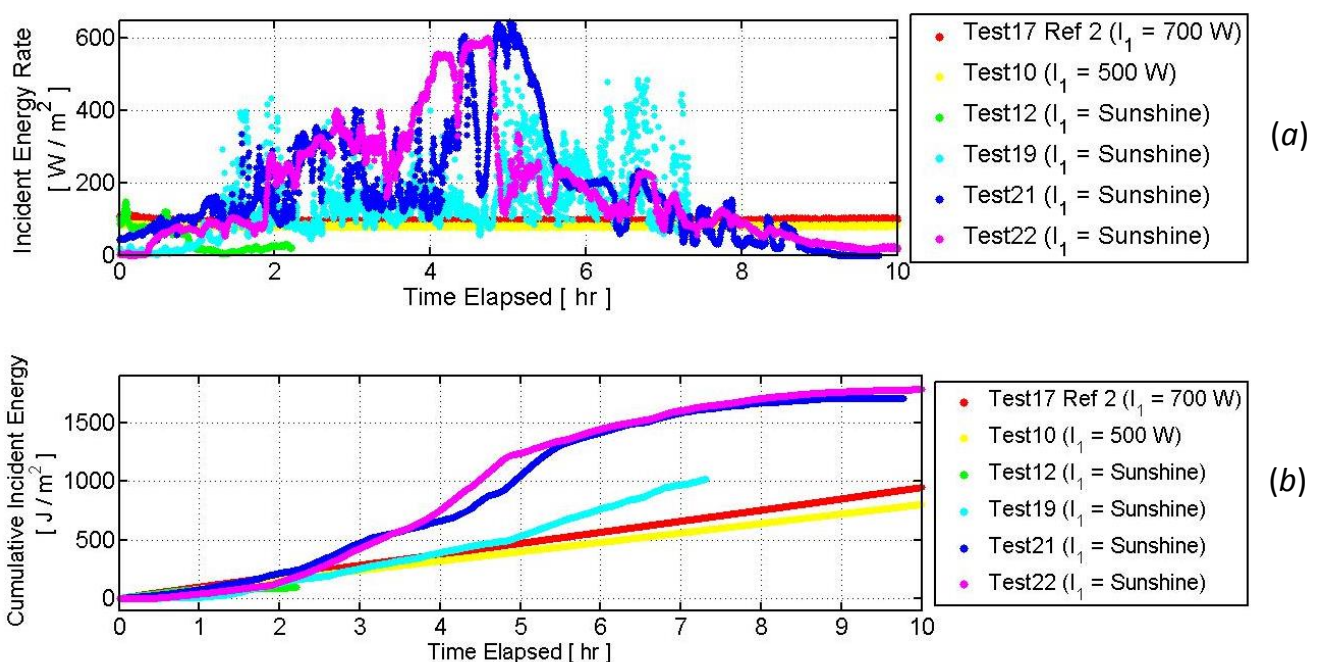
Figure 4.3.5.2: Instantaneous power (*a*) and accumulated energy (*b*) incidenting rig during testing.

The sunshine tests were typically commenced between 8:00 and 8:30 am on clear sky days, or days with little cloud during February and early March in Ōtautahi, Aotearoa (Christchurch, New Zealand). The rig was positioned to be north-facing and in direct sunlight for the duration of the sunlight hours. Where possible, the testing was continued after sunset in order to gauge the heat retention capacity of the system. Test 12 was aborted early to preserve the data acquisition equipment as the weather became overcast then wet in the two hours after testing commenced. Insufficient data were acquired to justify processing this test. The efficacy of the crow totem was relatively unknown under these conditions.

During a comparable timeframe the *in vitro* reference test collected a greater amount of condensate than any of the sunshine tests, indicating that the energy input for these tests was greater than what was measured by the pyranometer. A secondary analysis has been conducted on the basis of equating thermal changes in the rig to energy input. This analysis was an attempt to correct values of the incident energy measurements under halogen lights to an equivalent sunshine intensity. The provisional scaling factor to convert the halogen measurements to solar measurements was provisonally assessed to be 2.91. The method employed has been detailed in Appendix 10.

During the subsequent model building stage of the project, a parameter identification process was employed. This analysis method accounted for the different sensitivities of the pyranometer to halogen and solar spectrums. This parameter identifaction method is more robust than the approach mentioned here and is detailed in Chapter 5.

4.3.5.1　Informed design development

One variation was made to the rig under sunshine conditions during Test 22. An aluminium sheet, identical to the condensation surface, was located approximately 80 *mm* above the original condensation surface. This second surface provided shading from the sunlight without restricting the airflow generated by the fan.

The relevant evaporation and condensation characteristics and the accumulated incident energy are shown in Figure 4.3.5.3. These profiles are simply replotted from Figures 4.3.5.1 and 4.3.5.2 to compare the relevant data sets more clearly.
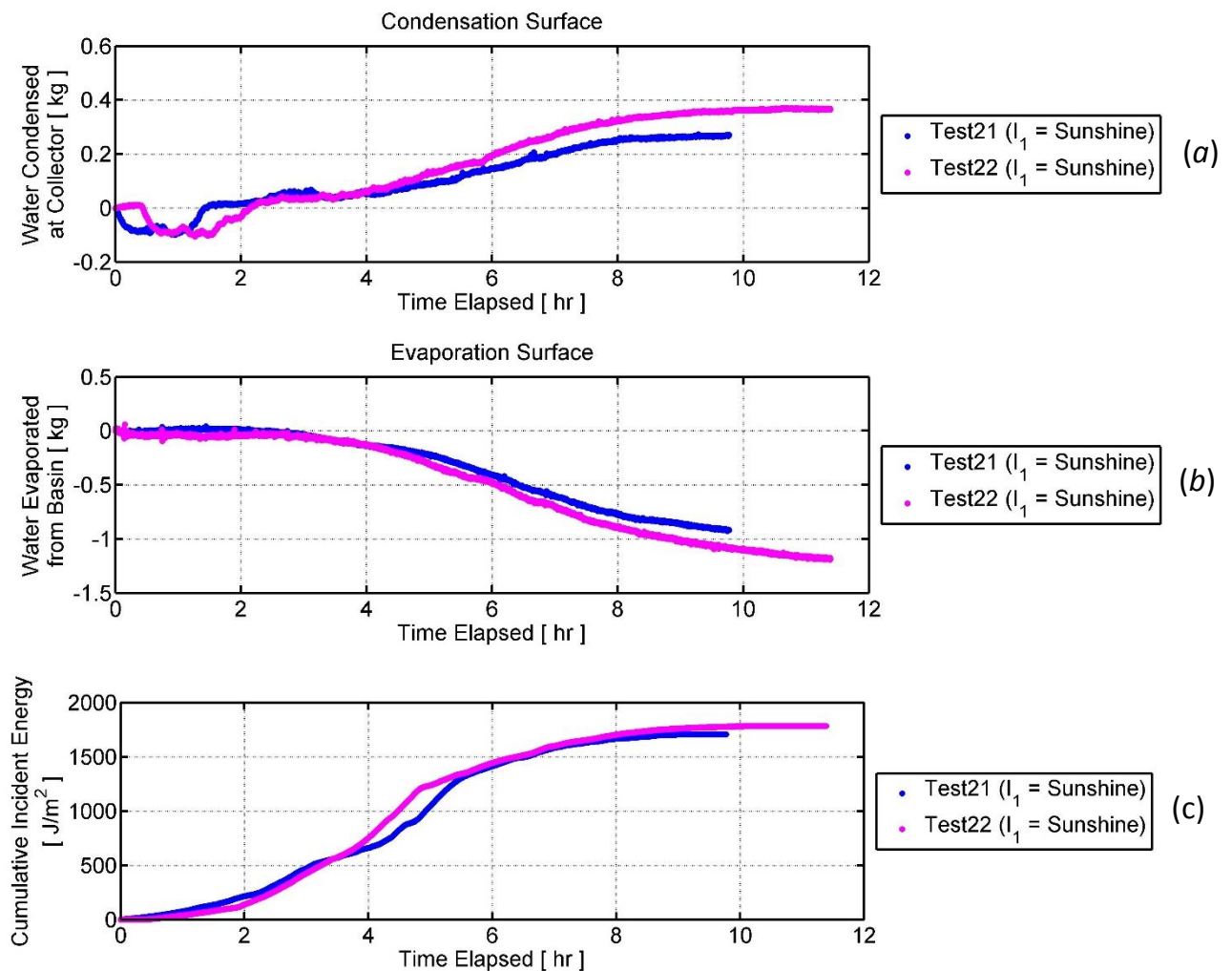
Figure 4.3.5.3: Condensation profile (*a*), evaporation profile (*b*) and corresponding incident energy accumulation (*c*) for solar tests comparing the effect of shading the condensation surface

At the end of the comparable test period, Test 22 had produced approximately 25 % (85 g) more distilled water at the output with only 96 % of the accumulated incident energy of Test 21, as measured by the sensor. Tests 21 and 22 were conducted on consecutive days which helped ensure uniformity in the solar radiation flux between tests and Figure 4.3.5.3 highlights the similarity in accumulated energy. The average difference in ambient temperatures on these days was 0.5 ℃ with Test 21 being conducted on the hotter day. This temperature variation was deemed acceptable for the results of these tests to be directly compared to one another. The performance of the added shade cover in Test 22 helps to quantify the usefulness of passively reducing the condensation surface temperature in a manner feasible to the implement in the intended context.

Figure 4.3.5.3 (*a*) shows negative condensation readings for a period directly after the tests were commenced. None of the other sunshine tests displayed this behaviour and the same magnitude of negative offset is apparent in both Test 21 and Test 22. The cause has been assumed to be a combination of wind deflecting the collection receptacle prior to water condensation and the sensor being in direct sunshine during the first few hours. This effect was judged to be of secondary importance to the overall test outcomes and has been assumed safe to ignore for this analysis.

The condensation surface temperature and cumulative solar radiation profiles from these tests are shown in Figure 4.3.5.4. As expected, Test 22 exhibited a markedly lower temperature at the condensation surface. Over the comparable time period, the mean temperatures were 4.2 ℃ lower and 2.3 ℃ lower at the internal and external faces respectively.
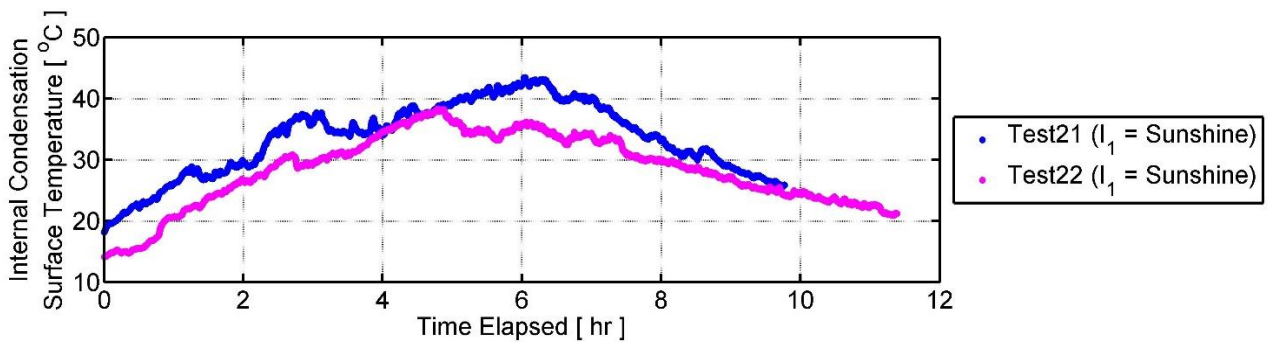
Figure 4.3.5.4: Internal Condensation Surface Temperature during relevant solar tests

The condenser temperature in Test 21 begins to converge toward the same temperature as in Test 22 after 8 hours, which was expected as the sun had set at this point and the rig was approaching a steady night time temperature. The sustained lower temperature in Test 22 ensured higher distillate productivity over the duration of the day-long test. For approximately 10 minutes of the 10 hour comparable test duration, the condensation surface temperature in Test 22 exceeded the same temperature in Test 21, but this never by more than 0.6 ℃.

4.3.6   Client-proposed Design Testing: Open Air Configuration

Purpose: The client was determined to investigate performance of a design configuration with openings at both the absorption and condensation surfaces that were intended to enhance convective heat transfer and therefore evaporation through the unit. The research team were sceptical as they expected that such a system would exhibit a reduction in productivity due to accelerated water vapour egress through the openings. A specific set of tests were conducted to determine which perspective was more accurate.

Outcome: The results confirmed that the open configuration failed to produce condensate, and was not a viable design option to take forward.

The modular test rig allowed the Open Air design to be realistically represented and trialled. The client-proposed design was intended to increase condensate productivity through increased convective airflow through the unit. Rig variations with respect to the reference rig are shown in Figures 4.3.6.1 and 4.3.6.2.

Reference Rig [*Sealed*]   Open Air Rig [*Aperture (1) highlighted in red*]

Figure 4.3.6.1: Structural differences in energy absorption surfaces for reference and open rigs.
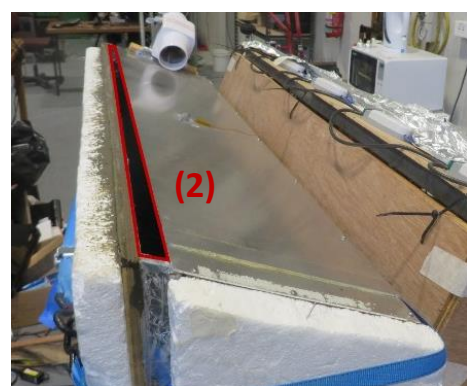
Reference Rig [*Sealed*]   Open Air Rig [*Aperture (2) highlighted in red*]

Figure 4.3.6.2: Structural differences between condensations surfaces for reference and open rigs.

The only difference between the Open Air and reference rigs were the two apertures as shown in Figures 4.3.6.1 and 4.3.6.2. The first aperture, (1) was located just beneath the absorption surface in very close proximity to the lights. This aperture allowed air to enter the rig to replace the heated air leaving through the

condensation surface aperture. This second aperture, (2) was located along the uppermost edge of the condensation surface. Spacers were placed along the base and sides of the unit to restrict heat and vapour loss through these surfaces. This aperture had a double layer of jute wick cloth (not pictured for clarity) attached to it to collect vapour from the outward bound air. The purpose of aperture (2) was to direct the warm humid air evaporated from the basin out of the rig. It was assumed that the only appreciable mass transfer occurred through the highlighted aperture areas. The evaporation and condensation performance characteristics for two Open Air rig variations are compared to the reference test in Figure 4.3.6.3.
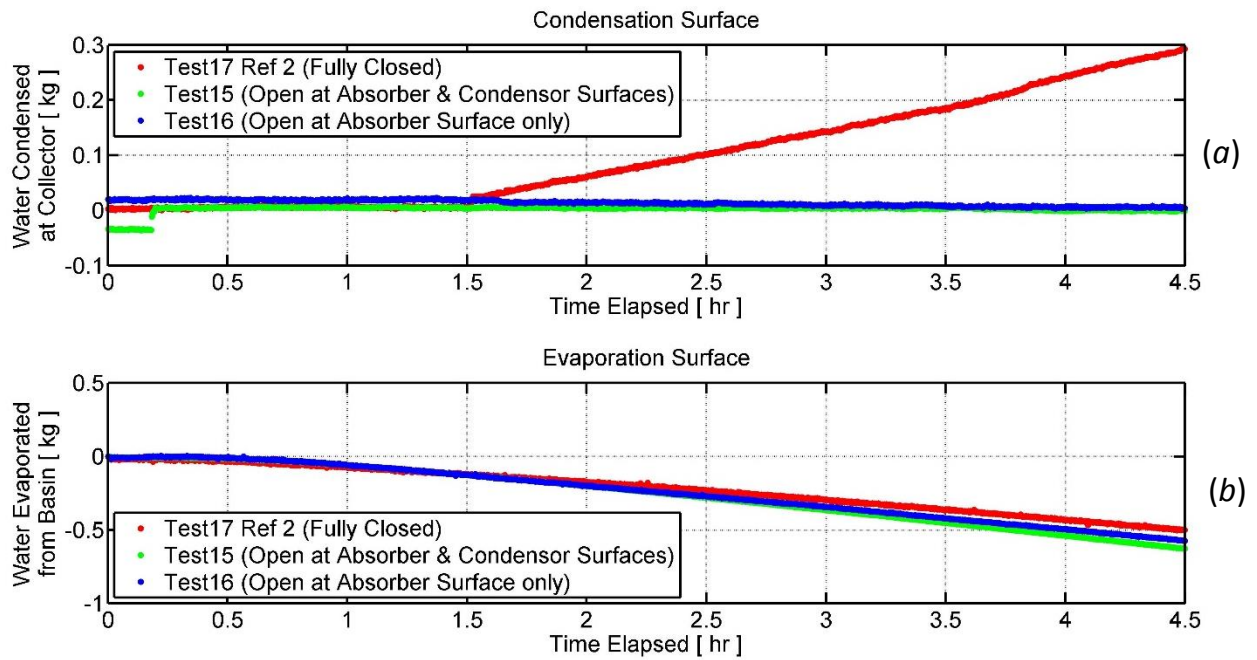
Figure 4.3.6.3: Profiles of water condensed (*a*) and evaporated (*b*) during Open Air Rig operation

The configuration with both apertures open was been defined as the Fully Open rig, which was trialled in Test 15. This test exhibited a similar evaporation profile to the reference case (Figure 4.3.6.3(*b*)) although no condensate was collected (*a*). The lighting array was shut off after four and a half hours due to the lack of condensate after this time period, which marks the end of the comparable test results.

A second open rig modulation was introduced in Test 16 with only aperture (1) open. This configuration has been defined as the Half Open rig. This modulation helped to isolate the condensation and evaporation dynamics wick efficacy. However, sealing aperture (2) prohibited the airflows that were the intended Open Air design benefit. This half-open case also exhibited a similar evaporation to the reference test (Figure 4.3.6.3(*b*)), however no condensate was collected (*a*).

Aperture (1) was substantially closer to the evaporation surface than the condensation surface. This aperture also provided a relatively large area for any evaporated water vapour to escape the system. The temperature and humidity of the external, ambient air were both lower than at the condensation surface. Therefore it was a thermodynamically more favourable for vapour to leave the system rather than to move to the condensation surface. The Open Air operating principle was only tested under *in vitro* conditions where wind is negligible.

4.3.7   Client-proposed Design Testing: Low Pressure Configuration

Purpose: This testing was intended to investigate the performance capability and deployment practicality of the Low Pressure operating mechanism proposed by the client.

Outcome: This design analysis required both empirical and theoretical components to explore the solution space within the project scope. The results indicate that the Low Pressure system has the potential to be up to 19 % more productive than the basic reference system. This figure represents ideal operational characteristics and is only applicable under the strict proviso that probabilities of failure after one year for the concertina tube and the seals (employed to maintain the low pressure region) are no more than 10 % and 5 % respectively. The practicalities of recharging water into such a system were not evaluated. The empirical test results were used to develop a reliability model to represent the practical limitations of the solution. This proposed framework considered implications of implementing a novel technology into a rural or DC context. Further development of this concept should be approached with caution as analysis has indicated that six basic system units could perform with the same efficacy as five passive Low Pressure units. The basic units would be expected to have lower maintenance requirements over their design life than the Low Pressure units which makes them the more preferable option.

4.3.7.1   Background and Proposed Strategy

One of the identified knowledge gaps was investigation of a system that operated at low pressure while aligning with the socio-geographic scope of the project. The low pressure systems presented in the literature all operated using active componentry, which conflicted with the design intent the client had for this project. For clarification, 'active' componentry is defined here as those requiring fuel or electricity to operate; pumps, motors, instrumentation, sensors and servos are included in the definition.

According to the Clausius-Clapeyron relationship, the boiling temperature of water decreases with decreased pressure. This decreased pressure means surface molecules are less tightly bound to the bulk liquid at a given temperature and therefore are more easily liberated into the vapour state.

Several studies have focussed on employing low pressure processes into desalination systems as a means to increase performance as detailed in Chapter 2.2.8. To summarise, prior studies concerned with passive vacuum applications have typically involved using a pair of approximately 10 *m* water columns connected at the top to create a Torricelli Vacuum. To maintain the desired conditions, active componentry such as pumps and heat exchangers are typically necessary [41, 44, 48]. The point of difference with the current study is that the focus is on establishing the vacuum through volume change rather than using the fluid weight.

The proposed Low Pressure design involves pulling a negative pressure inside the sealed desalination unit by increasing the volume using a concertina tube or similar volume expansion mechanism. The Low Pressure design is focussed solely on increasing the rate of evaporation to increase the unit productivity, no modification

to the rate of condensation has been integrated into the analysis. The condensation rate has been assumed to have linear dependence on the evaporation rate as a starting point for the analysis. In reality, this consideration is optimistic and negates the effect that drawing a vacuum will have at the condensation surface

The volume change component has provisionally been proposed as UV Flex flexible ducting, which has the capacity to act like a concertina or bellows. The UV Flex is fabricated from Thermoplastic Elastomer (TPE) coated polyester and supported with a spring steel wire helix. This model was recommended by a representative from the New Zealand Duct and Flex Company as having the best UV durability and saline corrosion resistance of available flexible ducting. The datasheet is provided in Appendix 11.

The primary test rig allowed several different design configurations to be investigated. However it was unable to be modulated to cater for the Low Pressure configuration with the available resources and instrumentation. The proposed modifications to achieve low pressure operation all involved active componentry and it was deemed insufficient to address problem using these means. The use of active componentry was not representative of the original design intent. The literature has shown that active systems allow low pressure operation to be reached, so testing an active experimental rig would only confirm these results, not verify the design mechanism conceptualised by the client.

4.3.7.1.1 Empirical Analysis

An empirical test phase was carried out as an initial exploration of the solution space to gauge the extent to which low pressure operation was a feasible option. A purpose-built, small scale test rig was commissioned and utilised for pressure testing. The objectives of this test phase were to quantify the magnitude and temporal characteristic of the pressure drop that could be achieved.

4.3.7.1.2 Theoretical Analysis

In parallel to the experimental work, a design strategy was implemented that harnessed the concepts of reliability engineering. Solution reliability is of paramount importance in any context where availability of repair and maintenance resources or personnel are severely limited. The Low Pressure design feasibility was evaluated on the consideration of trading-off the increased system productivity with the reduced system reliability as a result of the added complexity.

The basis for the analysis is that in the remote rural context, a failure means no water produced until the system is fixed. In the field, repair may take anywhere between a few days and a few weeks. Therefore, any modifications to the basic system, especially active components, add failure modes and effectively decrease the water output. The basic system also has a probability of failure, however for the purposes of the analysis it has been used as the reference which the Low Pressure designs are compared against.

The system has been decomposed into a series block diagram, each component of which has an associated probability of success after a year of operation. It has been assumed that a failure downs the system and that the failure occurrence regime can be modelled with an exponential distribution.

4.3.7.2   Proof of Concept: Empirical Testing

The theoretical analysis required justification with a physical basis to ensure that the assumptions and simplifications along the process were sound. A small low pressure rig was designed and built to test the vacuum capacity of a candidate material. This rig is shown in Figure 4.3.7.1, and has been constructed primarily from a 250 *mm* length of 82 *mm* diameter UV Flex flexible ducting. This ducting was the only product readily available for testing purposes. No other alternatives were assured by their suppliers to be suitable for UV and salt water and moist air exposure.

(*a*)   (*b*)   (c)
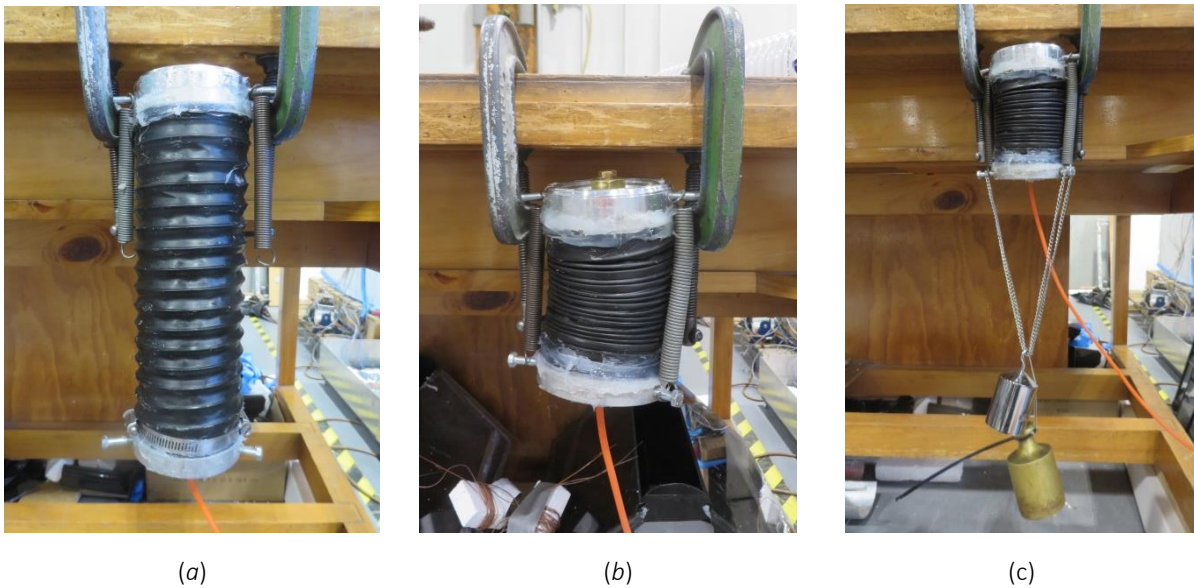
Figure 4.3.7.1: Low Pressure Test Rig fully extended (*a*), compressed (*b*) and externally weighted (*c*).

A pair of aluminium end caps were machined to seal the ends of the Flex and secured in place using a combination of silicon glue and hose clips to provide both the seal and the mechanical strength necessary. External compression springs helped distribute the load-bearing away from the silicon glue.

This testing phase was for proof of concept only and was therefore concerned only with the vacuum capabilities of the flex ducting. The only measurement of interest was the pressure differential between the rig internal cavity and the ambient air. No water was placed inside the rig for evaporation. The same transducer was used as for the primary rig testing.

A test run involved suspending the rig from the two upper mount points (*a*) and compressing it to minimum internal volume (*b*). The outlet hose was connected to the low pressure tap of the pressure transducer. A test mass of 2.40 *kg* was suspended from the two lower mount points (c) to passively engage the volume expansion. Data was recorded using the same LabVIEW software and hardware as prior tests until the pressure difference reduced to less than 1.0 *kPa*. This limit was set to a value slightly below the typical 1.3 *kPa* lower threshold of vacuum pressure testing in the literature [44]. The data recording rate was increased to 1 *Hz* while all other data acquisition settings remained the same.

Assuming the calculated seal reliability and the volume change are realistic in context, the vacuum potential of the ducting reduces with increased diameter. A compromise exists here between the evaporative free surface area of water in the unit and the expected increased productivity obtained by lowering the pressure operation. The more frequently the unit has to be opened, refilled and closed, the more productive it has to be in the remaining time for the additional operating mechanism to provide a net benefit.

4.3.7.3   Proposed Solutions for Theoretical Analysis

The main functional components of the basic system and two Low Pressure system options have been identified as well as the operational mechanism of each Low Pressure system, as shown in Table 4.3.7.1. The proposed operational procedure for the Low Pressure systems involve filling in the morning and leaving sealed until after sunset so that the vacuum-induced evaporation benefit is not lost. The water collected is intended for the evening or the subsequent day.

Table 4.3.7.1: Functional components of systems considered for Low Pressure Operation feasibility analysis			
System Label	*Operation*	*Description of partial vacuum mechanism*	*Functional Components*
Basic	Passive	Not applicable	Basic System Components comprising: - Absorption Surface - Condensation Surface - Brine Basin - Cavity Structure - Collectors
Low Pressure Option 1	Passive	Water is placed in the still cavity and the input valve is sealed. A steel helix reinforced polyester tube is manually extended to increase the still cavity volume, thereby reducing the internal pressure	- Basic System Components - Concertina/ Volume Increase Element - Manual Actuator to provide Volume Increase - Additional Frame to support Volume Increase - Valves and Seals
Low Pressure Option 2	Active	Water is placed in the still cavity and the input valve is sealed. The same polyester tube as in Option 1 is autonomously extended to increase the still cavity volume, thereby reducing the internal pressure. A mechanical actuator, powered by a small PV panel provides the extension. Both the panel and actuator are signalled by electronic controllers.	- Basic System Components - Concertina/ Volume Increase Element - Actuator to provide Volume Increase - Additional Frame to support Volume Increase - Valves and Seals - Electrical Controller Units - Flat Plate PV panel to power electronics

4.3.7.4   Results

The evaporation model presented in the relevant literature [58] informed the experimental work which then validated continuing on with the reliability analysis to obtain the quantifying the expected performance benefit.

4.3.7.4.1   Predictive Modelling of Pressure Effect on Evaporation

The relationship between vapour pressure difference and evaporation rate for pools of different characteristic length was explored computationally in a study by Vinnichenko *et al*. [58]. The most applicable outcome of the study has been reproduced as Figure 4.3.7.2.

The Vapour Pressure Difference (ΔP_{S-V}) was defined in the study as the differential between saturation pressure at the water surface (P_S) and vapour pressure far from this surface (P_V). The results show a strong linear dependence of evaporation rate for a given characteristic length (L) over the pressure range explored. This dependence becomes more pronounced as the tube diameter decreases, which is indicative that at least one energy transferral mechanism has greater effect at smaller scales over the range of lengths considered.

The author was unable to find further studies that dealt with relating evaporation rate and pressure difference. The study did not explicitly refer to whether the pressure differential was free or forced. There was a lack of relevant data available concerning evaporation rate – pressure difference relationships. Therefore the assumption was made that the relationships presented by Vinnichenko *et al* also describe the current situation and are valid to apply.
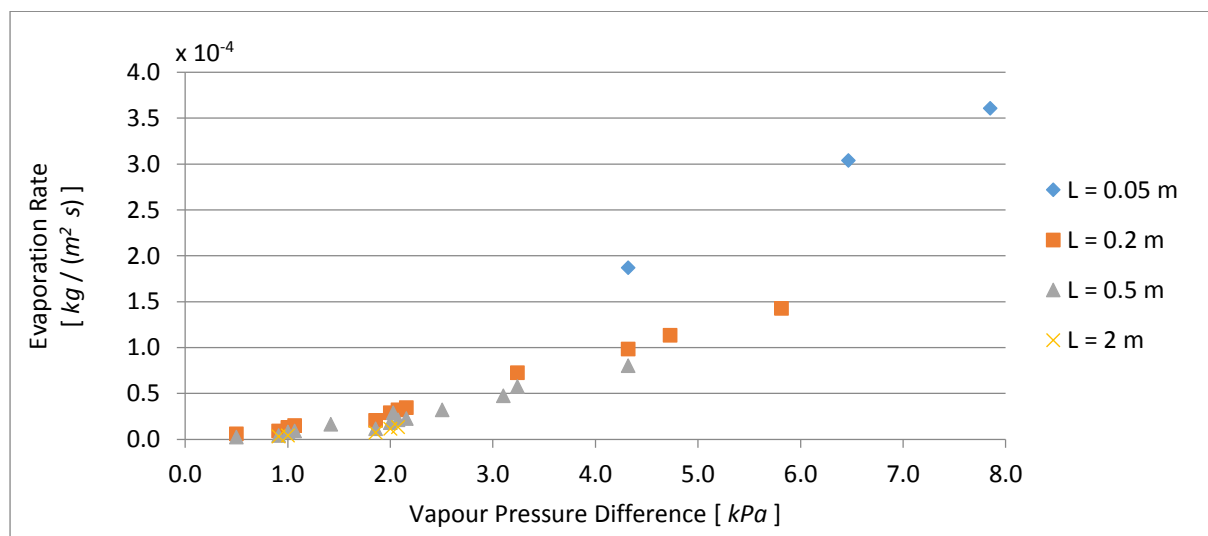
Figure 4.3.7.2: Results for relationship between pressure differential and evaporation rate as a function of characteristic length.

The relationship between sensitivity of evaporation rate on vapour pressure difference and characteristic length was obtained by processing the data and has been included in Appendix 12. This derived relationship allowed the evaporation-pressure sensitivity to be inferred for characteristic lengths other than those investigated in the previous study.

The concertina tubes considered for the volume change component are available in several diameters and each has a maximum achievable negative pressure associated. Larger tubes are limited to pulling smaller magnitude negative pressures. Results indicate that a smaller unit size makes low pressure operation most viable. For practical purposes only the two largest tubes have been considered. The smallest tube is 50 *mm* in diameter, and this would limit the water mass that could be input into the unit to an impractically low volume. The potential exists for multiple small diameter tubes to be utilised in parallel, but this action has been anticipated to exponentially decrease the system reliability.

4.3.7.4.2   Empirical Test Outcomes

The maximum vacuum pressure obtainable inside this diameter Flex ducting was rated at 6.0 *kPa*. In practice it was found that this pressure could not be passively maintained due to imperfect sealing. Under self-weight, the rig converged to maintaining a steady state internal pressure of 1.7 *kPa* after 2 hours, with an average vacuum pressure of 2.2 *kPa* over the nine hour duration. The pressure variation after the system had reached steady state was found to be 0.20 *kPa*.

The addition of external weight significantly changed the achievable vacuum pressure. The vacuum magnitude ranged between 5.8 – 6.8 *kPa* but the 1.0 *kPa* threshold marking test termination occurred at just over 45 minutes. The potential for water evaporation within this time period is severely limited.

For the purpose of the analysis, the average vacuum pressure of 2.2 *kPa* has been assumed to be the relevant achievable pressure. This is a conservative value with respect to the datasheet rating, but optimistic with respect to what was actually achieved during the empirical test phase under external loading conditions.

Several practical limitations of the concept became apparent during this build and test phase. The original client-proposed design involved using tidal action to obtain the sealed volume expansion. A qualitative analysis of the 80 *mm* diameter test rig indicated that extension under sealed conditions required an applied force beyond what could be exerted by a single person. At such a small scale of test rig, the surface area available meant that tidal suction could not be relied upon to provide the volume change and either a manual or automated actuator must be integrated to facilitate the expansion. This consideration deviated from the original design intent, as a degree of complexity is added to the system through the actuator.

Some form of mechanical advantage is required for practical use and a compromise exists between the force necessary to expand the volume, and the force that will tear the ducting or break the seals. The unit prototype is expected to be several times larger than this rig, and the required force to do work on a significantly large surface area would increase proportionally from what was required at the small scale. No failure tests were conducted on the maximum tensile stress of the ducting due to limited availability of the component.

Data obtained during primary rig testing was used in conjunction with psychrometric and thermodynamic relations to calculate the pressure terms relevant to this analysis. These pressure terms allowed the evaporation rate to be evaluated using the framework presented in the relevant literature and are shown in Table 4.3.7.3. The psychrometric and thermodynamic analysis employed to solve for the relevant pressure terms is detailed comprehensively in Appendix 13.

Table 4.3.7.3: Semi-empirical Pressure terms relevant to the reliability analysis			
Description	*Term*	*Units*	*Value*
Saturation Pressure (Evaporation Surface)	$P_{S\,(evap)}$	[*kPa*]	12.0 ± 0.7
Partial Vapour Pressure (Condensation Surface)	$P_{V\,(cnds)}$	[*kPa*]	3.2 ± 1.2
Vapour Pressure Difference	ΔP_{S-V}	[*kPa*]	8.8 ± 1.4

The values presented in Table 4.3.7.3 corresponded to the operating conditions of the basic system. No forced low pressure condition was imposed to obtain these data. This basic operating condition was processed according to the predictive modelling analysis presented prior to obtain the corresponding rate of evaporation from the water surface. The processed empirical data is shown in Figure 4.3.7.3 for the basic system operating condition and also the expected condition under low pressure operation. The Low Pressure design modification was assessed to contribute an increase of 2.2 *kPa* to the vapour pressure differential as mentioned above.
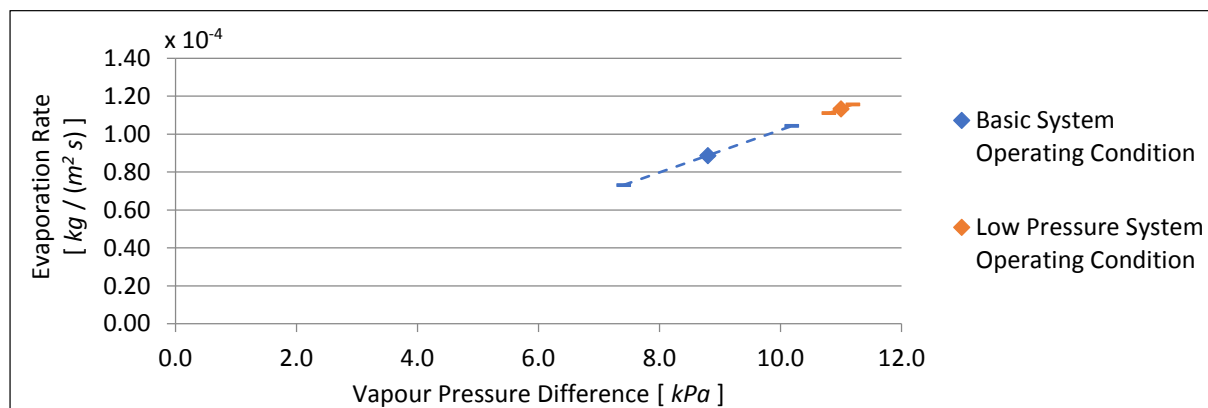
Figure 4.3.7.3: Processed empirical data relationship between evaporation rate and vapour pressure difference for both basic and Low Pressure system operation

The plotted Low Pressure operating condition is with respect to the mean basic operating condition. The magnitude of the expected evaporation rate is a relative indicator only. The difference between basic and Low Pressure operation states was of greater interest for this study. Extrapolation of the pressure-evaporation relationship was necessary to capture the operating conditions of both the basic and Low Pressure systems and therefore must be approached with a degree of caution. The data provided in Figure 4.3.7.2 only extends to vapour pressures of 7.8 *kPa*, whereas the relevant empirical data applied to the region between $7.4 - 11.2$ *kPa*.

A brief analysis has assessed the validity of data extrapolation given the test conditions present. As pressure decreases, the boiling point of water occurs at lower temperatures according to the Clausius-Clapeyron equation. The mean air temperature in the primary rig during *in vitro* testing was found to be 52 *°C*, which has been assumed to be representative of operational conditions in context. As a result, volume changes causing a pressure drop of greater than 88 *kPa* will induce flash boiling. A pressure drop of this magnitude would be impractical and almost impossible to achieve in context based on seal efficacy and material strength. However this consideration presents a theoretical absolute limit to where the pressure - evaporation relation can be justifiably linear. The range of pressure differentials in the literature do not exceed 10 *kPa*, and it has been assumed that the model cannot be accurately relied upon to predict evaporation rates for pressure differentials more than 100 *%* beyond this range without further empirical data justifying the relationship. The empirical data points all lie within 44 *%* of the previously acquired data, so have been evaluated as useable and valid for the current analysis.

The expected evaporation increase obtained by modifying the basic system to the Low Pressure system has been quantified in Appendix 14 as 27.8 ±2.5 *%*. This value is the same for both the active and passive Low Pressure systems as it represents the increased evaporation capacity irrespective of the mechanism.

4.3.7.5 Reliability Analysis of System Components

The specific situation under consideration involved filling up the system and actuating the volume increase-decrease cycle on a daily basis. A one-year operational timeframe has been considered for the analysis and the failure probability for the corresponding number of cycles have been considered. The effects of infant mortality and wear out have both been neglected. The analysis has been focussed towards reliability during the constant wear phase of each component. A conservative approach has been taken when considering the values of each parameter. As a result, the worst case scenario for reliability has been calculated.

The mechanical components (actuator, valves and seals) were evaluated using the Handbook of Reliability Prediction Procedures for Mechanical Equipment [59]. The PV specific components (solar panel and controller) were evaluated using product data made available through the client, consultation with an electrical engineer who has installed panels in Tonga [60] and a publication from the International Energy Agency Photovoltaic Power Systems Programme [61]. The remaining components were estimated. Failure of any one component was assumed to be independent of the rest, so the overall reliability of the design (Rel_{sys}) after time t, was obtained using a series system model as shown in equation 4.3.7.2, exemplified for an N component system. The entirety of the reliability analysis has been compiled in .

$$Rel(t)_{sys} = \prod_i^N (Rel(t)_i) = e^{-\lambda t} \tag{4.3.7.2}$$

The reliability measures the probability that the sub-system or component has remained functional up until time t. For this analysis, t has been set as one year. The assumption has been made that the repaired component operates to an as-good-as-new standard, implying that both the subsequent reliability and performance is unchanged. As the reliability has been assumed to follow an exponential distribution, the second equality in equation (4.3.7.2) is valid. In the exponential form, λ represents the decay constant. This expression can be used to obtain the Mean Time to Failure ($MTTF$) through equation (4.3.7.3). It must be acknowledged that the units for λ are dependent on what timescale is used for the preceding analysis. The component and overall system reliability values and the $MTTF$ for each system are presented in Table 4.3.7.4.

$$MTTF = \int_0^\infty e^{-\lambda t} dt \tag{4.3.7.3}$$

Table 4.3.7.4: System Reliability Analysis and MTTF				
	System Components	*Component Reliability*	*System Series Reliability[1] (t = 1 yr)*	*Mean Time to Failure*
Configuration	-	$Rel(t)_i$	$Rel(t)_{sys}$	MTTF
	-	%	%	Years
Basic System		100.0	100	-
Low Pressure Passive System	PE Concertina Tube	90.0	62.5	2.1
	Manual Actuator	99.3		
	Support Frame	90.0		
	Actuator Seal	94.7		
	Unit Seals	84.9		
	Valve	96.7		
Low Pressure Active System	PE Concertina Tube	90.0	45.6	1.3
	Automated Actuator	99.3		
	Controller Unit - Actuator	90.0		
	Controller Unit - Panel	90.0		
	Power Source (PV Panel)	90.0		
	Support Frame	90.0		
	Actuator Seal	94.7		
	Unit Seals	84.9		
	Valve	96.7		

[1] Probability of system success after one year

The intended design life of the overall system has been set at 10 years. The number of failure events (*NoF*) is obtained through equation (4.3.7.4)

$$NoF = \frac{D\ (yr)}{MTTF\ (yr)}$$
(4.3.7.4)

where the design life (*D*) and the *MTTF* are expressed in the same time units. Each failure event has an associated Mean Time to Repair (*MTTR*) before the system is operational again. The concept of Lost Utility (*LU*) has been introduced as a measure of how the reliability of the system affects the ability of the system to serve the needs of the people for whom it is intended. *LU* over the design life of the system has been defined as a function of the *MTTR* and the *NoF* according to equation (4.3.7.5).

$$LU = NoF \times MTTR$$
(4.3.7.5)

For this analysis, the *MTTR* has been assumed to be 14 days, regardless of the failure mode. Many South Pacific nations comprise of multiple islands which are most commonly journeyed between by boat. It has been assumed that communication networks in the more remote islands are insufficient to provide inhabitants with continuous connection to the more central islands. Therefore the boat provides the most direction line of communication to central islands. The frequency of boat stopovers is assumed to be twice daily on the basis of workers commuting to more central islands. The message that a component has failed is therefore expected to

take two days to reach the more central islands once it is realised. It is expected that the delay time in diagnosing the nature of the failure, scheduling the necessary human resources and sourcing the necessary material resources for repair could not occur in less than one week. Between one and three days are expected for the technician to perform the repair. In total the assumed *MTTR* is two working weeks, although the unit will still cease to function during weekend periods. This timeframe reflects an optimistic assumption; especially for poorer socio-geographic communities and may need to be revisited when better data are available. The provisional *NoF* and *LU* for the system are presented in Table 4.3.7.5.

Table 4.3.7.5: Expected System Failures and Total Lost Utility over Design Life				
	Number of Failure events per 10 year Design Life	*Mean Time to Repair*	*Total Lost Utility over Design Life*	
Configuration	*(NoF)*	*(MTTR)*	*(LU)*	
	-	*Days*	*Days*	*%*
Basic System	-	-	-	-
Low Pressure Passive System	4.70	14	66	**-3.6**
Low Pressure Active System	7.86	14	110	**-6.0**

The Active System is expected to failure approximately twice as often as the Passive System over the design life based on the series reliability considerations. For either Low Pressure system to be of greater benefit than the basic system to the people it serves, a productivity increase is necessary to recover the *LU*. For this analysis, it has been proposed that the Low Pressure system is only successful if the productivity increase exceeds 20 *%* of breaking even with the basic system.

If the systems have indistinguishable performance characteristics, the basic system is preferable as it has less failure modes than either Low Pressure system. It has been judged that for a productivity increase to be considered significant, it must be exceed 10 *%* beyond the expected margin of error in the preceding analysis. The error margin is assumed to be between 5 – 10 *%* due to limited data availability for several components. As such, the Low Pressure system must display a net performance increase at least 20 *%* greater than the basic system to be considered successful. This margin helps account for both error propagation through to *LU* and unforeseeable factors that contribute to additional costs to system performance.

This reliability analysis assumed that the concertina tube has probability of successful operation of 90 *%*. This quantity is based on the design standard for reliability of engineering components. A further phase of testing is necessary to validate this reliability of this tube, specifically considering the intended application. A more detailed materials selection process would inform the most suitable option for a concertina tube, however this was beyond the current project scope. The selected component must withstand exposure to salt and UV radiation and also cyclic expansion cycles under considerable applied force without failure of the seals.

The reliability analysis has dealt thus far with the technical factors that influence performance. As mentioned in the DC study presented in Chapter 4.3.8, there are also socio-cultural factors which must be considered accordingly when assessing design suitability and operation in rural contexts. The most relevant consideration at this stage of analysis is related to Deployment Principle 2.7 of the DC study in Chapter 4.3.8 which relates to adhering to operational procedures. A more complex operating procedure means greater potential for user error. The human-interaction based reliability risk has been integrated into the analysis in the form of a Correct Operational Procedure Factor. This factor is representative of the percentage time that the low pressure systems are correctly sealed and left to operate without premature removal of the condensed water (meaning loss of the vacuum). The provisional analysis indicated that correct operation would be realised for 8 out of every 10 days on average. The system is assumed to function with the same efficiency as the basic system for remainder of the time.

4.3.7.6   Net Effect on System

The action of reducing the operating pressure was proposed to increase the evaporation rate only. This analysis has assumed that the condensation rate is unaffected by the change and therefore the performance increase of the system is directly proportional to the evaporation rate. This assumption will require experimental grounding to justify completely. The system performance results are presented in Table 4.3.7.6.

Table 4.3.7.6: Net effect of Low Pressure Operation on the system				
System	LU (%)	Expected Increased Productivity[1] (%)	Correct Operational Procedure Factor	Net Productivity Gain[2] (%)
Basic	0	0	1.00	**0**
Low Pressure Passive	-3.6	+ 27.8	0.80	**+ 19.3**
Low Pressure Active	-6.0	+ 27.8	0.80	**+ 17.4**

1 Based on theoretical relationship presented by Vinnichenko *et al* [58] which is irrespective of the mechanism behind the pressure differential

2 Compared to basic System

The net performance increases of 19.3 and 17.4 *%* accounts for the *LU* and operational reliability of both the Low Pressure systems considered. The *LU* equates to a relatively small proportion of the total design life according to the analysis conducted. The magnitude of the performance gain indicates that further development of the Low Pressure concept should be approached with caution as is not likely to be a viable design pathway. The observed productivity increases for each Low Pressure system are based on the assumption of 100 *%* conversion efficiency between additional water evaporated and additional water condensed. This assumption requires empirical validation. However, the liquid-vapour dynamic equilibrium behaviour resulting from pressure changes were unable to be measured with the available instrumentation.

The necessity for sealed operation means elimination of the system drainage potential. This condition has been proposed to have adverse effects on the amount of condensate collection rate due to the unmoderated increase in water vapour in the system. Therefore all performance increase values presented are associated with the ideal case, and are expected in reality to be slightly lower than what the analysis indicated.

The main limitations of this analysis are the lack of available empirical data relating evaporation rate of water with pressure differential and the assumptions regarding Mean Time to Repair within the rural or developing context.

The derived relationships have indicated that if the system operated using the 2.2 *kPa* negative pressure increase obtainable with integration of a low pressure operating system, the evaporation rate would be expected to increase by 19 *%* as a best case scenario. Neither proposed Low Pressure system has not met the performance threshold imposed to justify further development of the concept. Effectively six basic units would have the same performance as five Low Pressure units, but with added complexity and maintenance requirements.

4.3.8 New Product Development Process for Developing Countries

Purpose: This study was focussed on formalising the technical and socio-cultural elements and implications for developing and implementing a successful design within the context of a developing country (DC). The body of work was informed through a solar cooker design and build project undertaken by the first author during the thesis

Outcomes: This chapter presents a novel framework for the New Product Development process targeted toward applications in DCs. A series of Deployment Principles were extracted as the context-specific requirements for successful design. These principles dealt with both technical and the socio-cultural factors relevant to the process which are unnecessary in the more conventional context of a developed country market.[10]

4.3.8.1 Introduction: Engineering in Developing Country contexts

The most suitable path for an engineering design depends heavily on the intended context. This consideration is the premise for the current paper. Converse to the majority of other literature in the field, the focus of this paper is not toward overcoming market constraints for commercialising products in DC. The concern is on successfully deploying products that service a need identified in the immediate community. These community needs may be around increasing local water or food security or sanitation levels.

4.3.8.2 Background Literature

Countries are commonly classified as having either a Developed Economy, an Economy in Transition or a Developing/Emerging Economy [62-64]. Countries classified as the former tend to have greater economic security and growth compared to the latter. The conventional process for new product development (NPD) is heavily premised on the notion of creating products for consumption in developed economies.

The perspective towards NPD within a firm is therefore focussed on gaining the best competitive advantage to capitalise on the target market and ultimately make the most profitable returns [65]. The general performance metric for R&D and manufacturing firms is the success of the products and services provided using profitability as the bottom line [66]. Several frameworks are commonly used for NPD which largely contain the same functional elements. The NPD framework has been formalised several times through a Stage-Gate Process as

---

[10] This content has been submitted for journal publication.

used by Cooper *et al* [67, 68]. An assimilation of several versions of the framework have been reproduced as Figure 4.3.8.1 to highlight the market focus of the process.
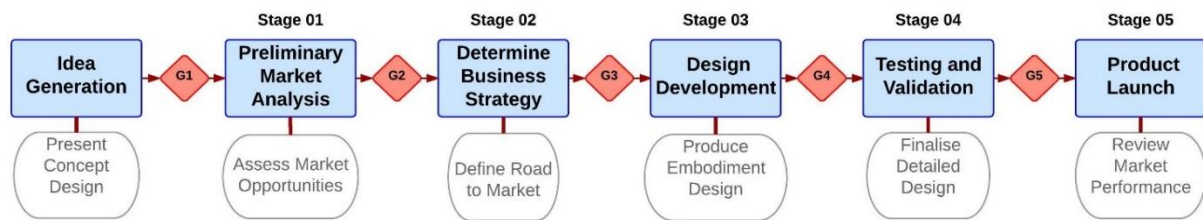
Figure 4.3.8.1: Adapted Stage-Gate framework for NPD process. *Subsequent design stages are separated by Gates (G) which act as screening elements to remove unsuitable options*.

It has been acknowledged that technological knowledge and market intelligence are two of the most important factors underpinning the profitability focus [69]. The conventional NPD perspective tends to regard the marketing aspects of the process as pivotal [70] and tightly interrelated to the research and development (R&D) aspects [71]. The NPD process was not found to have been formalised for application in areas where the focus deviates from marketing and commercialisation opportunities, such as providing basic necessity items to DC.

There is, however, a considerable amount of literature addressing the issues that come from implementing new technologies into DC contexts. A recent article (2016) has reviewed the findings of more than 350 papers published in the last two decades, all of which address the topic of off-grid rural electrification systems in developing countries [72]. The literature appears to pivot around the significance of providing electrical power systems and the problem statements are often posed around the necessity of electricity [73, 74]. There is relatively little focus on the broader perspective of providing systems that fulfil a basic human need, the bulk focus is on providing functional electrical systems.

Solution suitability in a rural DC context does not depend on financial and technical feasibility alone, but must also account for local environmental and socio-cultural dynamics. It has been observed that many rural electrification projects have failed as a result of underestimating the importance of considering these latter factors [73]. Several major enablers to the success of a project have been identified as community involvement, anti-corruption measures, standardisation of practices and the banning of bargaining agents [74]. These factors are often unnecessary considerations for applications in more developed countries where the operational infrastructure of a firm is more regulated and standardised.

The literature concerned with rural DC context NPD was found to be very limited. The only attempts at providing a framework to the rural DC NPD process were a reproduction of the process formulated by Cooper *et al* presented in Figure 4.3.8.1 [75] and a set of guidelines orientated around the concept of Design for Micro-Enterprise [76]. Both studies were concerned with obtaining market intelligence on DC consumers.

The most prevalent gap in the collective body of knowledge is the lack of a DC specific framework for augmenting the conventional NPD approach that is applied within commercial sectors of developed countries. This paper presents a translation of the classic NPD process as applied to a rural DC context, considering the issues observed first hand implementing a solar cooking technology into rural India.

4.3.8.3   Approach

Case Study: Research Question

There is a need to identify the both the barriers and the enablers to applying a design process within a rural DC context, and to modify the existing NPD framework to account for these context dependent factors. The knowledge capturing process associated with this paper involved the first author assuming the role of an embedded participant managing a rural DC design project. This project involved a period of volunteer work undertaken in the Spiti Valley in Himachal Pradesh, India, and encompassed designing, building and refining passive solar cookers. These cookers were targeted toward the available resources and needs of the local people.

Case Study: Context and Background

There are many small villages in the valley, all of which depend primarily on agriculture for livelihoods. Few trees exist in Spiti and connection with the outside world is via a single road running through the central village, Kaza. Natural resources are scarce and availability of materials and expertise is limited. The Spiti Valley was opened up to the western world a little over two decades ago and is still early on in the process of adopting more western educational and technology systems.

One reality faced by the Spitian locals is the lack of reliable electricity, hence a reliance on dung fires or Liquid Petroleum Gas (LPG) for cooking and heating. Dung is foraged from the high pasturelands during the summer and bottled LPG is transported approximately 580 km by road from Ambala. Known health and environmental implications exist around burning dung [77]. The transported LPG poses a high emission cost and renders the locals vulnerable to supply reliability.

The need to develop a locally available cooking alternative was apparent. This alternative was focussed on being less damaging to the environment and the health of the user, as well provide greater independence from external suppliers than the current options. Factors of influence particular to this context became apparent during the volunteering period and directed the solar cooker development significantly. The passive cooker developed and refined during the project is shown in Figure 4.3.8.2. This project had several similarities with the desalination unit investigated during the thesis.

(*a*)   (*b*)

Figure 4.3.8.2: Initial (*a*) and final (*b*) passive solar cookers implemented in Spiti Valley

The researchers applied engineering product development skills and knowledge to the task of developing a solar cooker. It was noted where locals struggled to comprehend the process, and the elements at which they excelled. The outcomes were compared against the orthodox NPD process and the key factors were extracted.

4.3.8.4   Results

These factors have been classified into categories of Technical and Sociocultural Influences. These two areas were the most natural expressions of the factors observed, and were also aligned with classifications found in the literature [73]. Each identified factor has been given at least one accompanying 'Deployment Principle' (*DP*). These principles offer insight from the perspective of an embedded participant to best address contextually specific problems and forward the design process to successful deployment of the unit.

4.3.8.4.1   Technical Factors

Technical factors relate to aspects of the design and build process that are explicitly involved with fabrication and/or transportation of components of the assembly.

Global Connectivity

Kaza received only several hours of electricity every few days due to poorly set up and maintained electrical infrastructure in the valley. As a result, internet access was severely limited. This constraint meant that the majority of the project was carried out without external information. As such, optimising the solar cooker performance based on prior work was limited. The technological limitations meant that the solution was guided by the path of least resistance, rather than necessarily highest performance.

Deployment Principle 1.1: Finalise projects through prior communication or assume resource and technical knowledge availability is limited to what the embedded participant comes in with

Finalising the desired projects prior to arrival in the remote area gives time for potential problems to be remediated or at least considered. If projects are decided upon after arrival, the pool of accessible knowledge is considerably lesser. The availability of and convenience with which knowledge can be accessed in a more developed country is easy to take for granted. The projects should be chosen based on the strengths and competency of the person undertaking them. It cannot be assumed that all of the physical and digital resources will be available in context.

Local Connectivity

Kaza was approximately one day of driving away from the next economic centre in either direction. Several delays were incurred waiting for suppliers to respond to resource requests. In one instance the requested part (PC sheet) arrived after two weeks of waiting but was unusably damaged during transport. The materials used in the design solution should account for the infrastructure required for them to reach destination as safe transport of delicate or brittle materials is not assured.

Plans were made ad hoc, and did not extend more than a day or two into the future. Lack of communication infrastructure between villages meant that plans could not always be changed remotely. Several stone masons requisitioned to help with one of the cooker builds waited for four hours at the gate to a satellite village due to unforeseeable delays and there was no way to contact them. No animosity was shown, the cultural viewpoint appreciates that plans do not always go as expected. Village life is not regimented in terms of minutes and hours. Seasonal changes which are important for harvesting crops or moving stock help dictate workloads. The native vocabulary lacks words to describe relatively short time periods (minutes, hours). Sometimes a supplier would indicate they would reach Kaza four or five days earlier than they did. Delays were inevitable with the poor infrastructure connecting centres and the access road was often blocked with rock falls.

Deployment Principle 1.2: Plan for project delays when working in remote contexts by integrating parallel work-streams

Parallel work streams are useful to add value to the waiting time and reduce the impact of delays in a project. Deadlines should include weekly or fortnightly allowance periods to account for extraneous factors that cause delays. Acknowledgement that the culture may have developed without the concept of a regimented, precise western system of ordering time is an important consideration. Patience is a very useful skill. The acknowledgement that local people will not have the same sense of urgency or need for efficient time use as the embedded participant is important to maintain a positive working relationship.

Deployment Principle 1.3: Consider the reliability of transporting materials in from external suppliers

Transportation of delicate materials must be considered in the feasibility of their use in a project. Labelling of fragile goods may not be heeded or even provided at all. The infrastructure to reach remote communities is considerably less forgiving than urban infrastructure. This issue was circumvented in the embodiment design phase by limiting suitable materials to those that had the least potential to be damaged in transit.

In Kaza, there were few existing braces or frames to hold objects that needed to be nailed together or sawn apart. The concept of using a saw horse for working was completely novel. The nails available were generally too soft to remain straight while being hammered. Plywood quality was varied and unreliable and substantial gaps existed in the laminate layers. Mud was the primary building resource. Timber was scarce and expensive. Sheet metal was limited in both size and variety.

Deployment Principle 1.4: Acknowledge that material or component quality in a rural DC context will be variable and generally limited and make design decisions accordingly

Knowledge of what materials are locally available and feasible to get reliable results with should be assimilated during the conceptual design phase of a project. The option to import materials in may also exist, although it is important to be aware that locals will have the most complete knowledge of how to work with the materials familiar to them. The design process should pivot around what is possible in the context. This consideration generally reduces to keeping the solution as simple as possible to minimise failure modes.

Solution Visualisation

The visualization skills of lay people were below expected. When fabricating the drawer frame for the solar cooker, as shown in Figure 4.3.8.3, there was a conceptual block for locals to see how the four pieces of wood fitted together to form a Roman numeral II shape despite numerous 2D and 3D representations of the design.

Figure 4.3.8.3: Detail of wooden frame for solar cooker drawer

In order to convey the relationships between the four pieces of wood, offcut pieces were numbered to match the illustrations then placed roughly in the required shape. Attempts were made to memorize all necessary dimensions to reproduce the assembly, rather than relate the labelled schematic to the design.

The carpenters and metal workers had substantially better visualization skills than other people. The gap between those who could understand a drawing and those who could not was more pronounced than expected. On the whole, representing a physical, precise object using a drawing was a largely underdeveloped and untouched skill.

Deployment Principle 1.5: Appreciate that a visual basis for idea communication may be a learnt skill

The locally manufactured parts and/or assemblies for a project should factor in the potential lack of visualisation skills of local tradespeople. Most engineering degrees develop the capacity of the student to form an image in their mind. This skill of communicating information in directed into predominantly visual formats; hand sketches, CAD models, technical drawings. The western formal education structure largely standardises how information is communicated; part elevations, exploded views, isometric or perspective views, sectioning conventions, dimensioning, use of a particular measurement unit (i.e. millimetres). These concepts become second nature to many designers and engineers but it is incorrect to assume they are universally understood, or that a visual basis can be easily conveyed to everyone.

Deployment Principle 1.6: Trial the broadest possible range of learning styles when communicating the design to people in a rural DC context, then capitalise on the style(s) that are readily understood

Any assemblies that were given to the tradespeople in Spiti were replicated without too much difficulty. Reaching an outcome was much more successful if workers were shown what was required by using either a pre-made version of the final product or actually stepping through the construction process with them. When designing in communities that have not had exposure to western education systems, communication of ideas should be approached as broadly as possible. Technical drawings can generally not be relied upon as the primary communication means. The outcomes were more successful in this particular context when a kinaesthetic approach to communication and learning was taken.

Quality of Manufacture

As mentioned, mud was the primary structural building resource. The required precision for working mud bricks or ramming earth is much less than what is necessary for wood or metal. Mud structures could be reworked at a later date if desired. The mud artisans were particularly skilled and knew how to get the exact consistency required for mud serving a particular purpose. Both structural and aesthetic aspects were considered.

The precision of the solar cooker designed was limited by the mud. Fitting a timber drawer frame and precision sheet metal pieces within a mudbrick cavity required chipping of the mudbrick and subsequent cutting and re-bending of the metal. Although reworking was possible, it was more efficient to force conformity of the mud by using an external frame.

After the first prototype, the mudbrick construction was substituted for a rammed earth construction. Purpose built timber frames were constructed to standardise the mud brick structure of the cooker therefore ensuring compatibility with the internal components. These frames were an integral part of the rammed earth construction process, as shown in Figure 4.3.8.4.

(*a*)　　　　　　　　　　(*b*)　　　　　　　　　　(*c*)
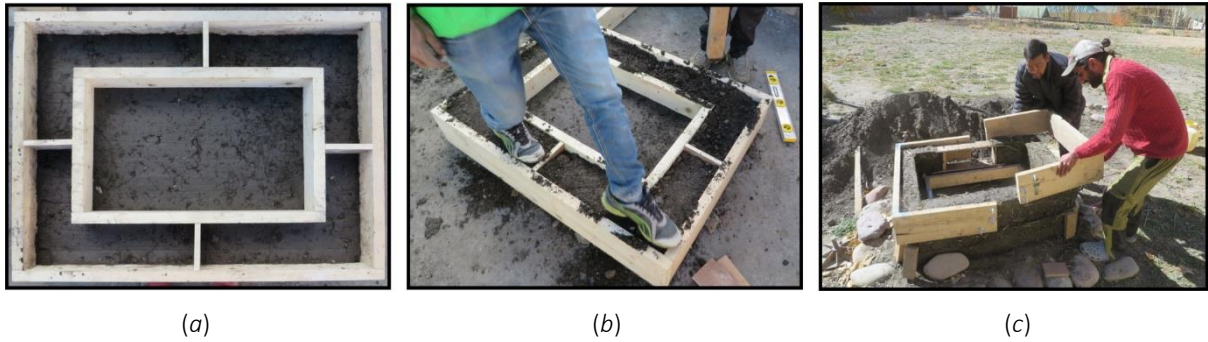
Figure 4.3.8.4: Timber frames to standardise cooker structure and assure reliable quality *(left)*, rammed earth construction process *(b)*, removal of frame after mud has dried *(c)*

Screws were often hammered in just as with nails. This misuse caused serious damage to the timber frames. Part of the problem lay in the lack of electricity to justify purchasing an electric drill and part was assumed to be due to the lack of knowledge of how screw adhesion and nail adhesion worked at a mechanical level.

Deployment Principle 1.7: Design for manufacturability by capitalising on available resources and skills

Designing for (limited) manufacture is of paramount importance. If all manufacturing and fabrication is to be undertaken by the same people (as opposed to delegating specific tasks to specific groups), then it helps to keep design dimensions parametric. The lack of quality assurance in developing country contexts means that specifications such as 'Part A must have external diameter of 12 cm, Part B must have a hole with diameter 12.2 cm' is not a useful way to describe mating parts. It is much easier to specify as 'Part A must fit inside part B snugly' and give the least number of numeric dimensions possible to complete the project.

Deployments Principle 1.8: Provide parametric templates for reproducing complex parts

The solar cooker designed for Spiti required several sheet metal pieces, one of which had unavoidable complexity, shown below in Figure 4.3.8.5 (*b*). This piece was placed on the east and west sides of the cooker cavity. The only way to ensure the side piece could be replicated to reliably fit inside each cooker was to make a master template, Figure 4.3.8.5 (*a*).

(*a*)　　　　　　　　　　　　　　　　　　(*b*)
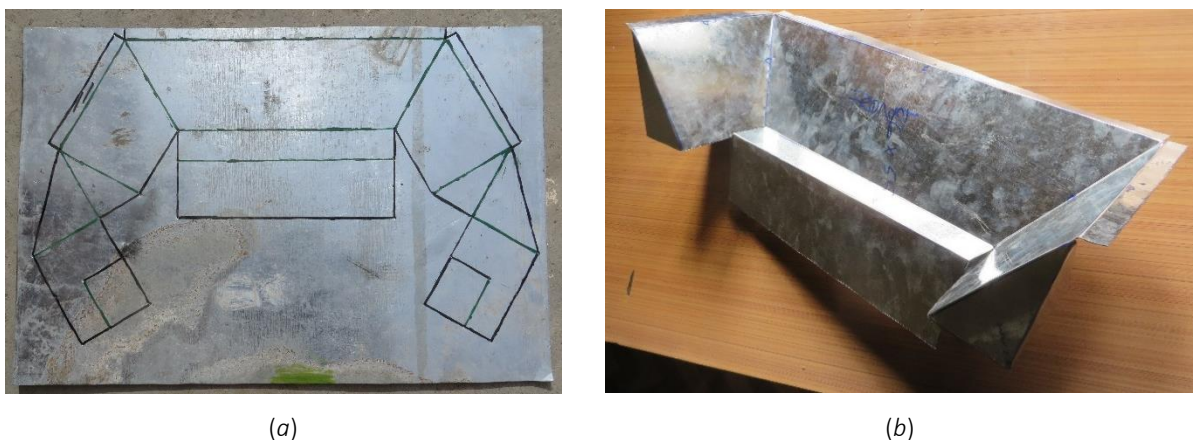
Figure 4.3.8.5: Parametric Sheet Metal Template (*a*) and Finished Piece for Solar Cooker (*b*)

The template was overlaid on a piece of sheet metal and holes were punched at all the corner positions so that fold lines could then be drawn. This template removed the need for any of the 15 linear and angular dimensions to be recorded or memorised and ensured that the piece was always identical. The cutting sequence was refined and standardised to ensure no hazardous ragged edges were present. The bending sequence was refined to a simple eight step process. Both sequences were recorded through photographs and taught to several of the locals for future replication of the part.

4.3.8.4.2 Socio-cultural Influences

Sociocultural factors relate to how local people interact with the finished design or aspects of the build process. The associated DP's have ben numbered with respect to their appearance in the integrated framework schematic (Figure 4.3.8.6), but grouped according to similar categories.

Communicating Ideas

A general apprehension to accept new ideas on the basis of words alone was observed. Little credit was given to the knowledge of someone who was from outside Spiti. Scepticism had to be dispelled by showing the physical product or the process functioning, and the tangible outcome.

Direct address was not the norm for communicating requests. The first author would often be told '*if one were to do this…*' which meant '*I want you to do this*…' It was observed that too direct of an address would often fail to warrant a response.

The whole concept of providing instructions was alien to the locals collaborating on the project. The instruction set developed initially contained drawings and schematics of the build process. To adapt to the context, the graphics were substituted for photographs but they were also shied away from. Those that wished to learn how to make a solar cooker had to see it done and/or do it themselves. Prior to western influence being introduced to Spiti, the society was primarily agricultural. The apprehension toward using instructions may have been linked to relative lack of development of visualisation thinking techniques.

Deployment Principle 2.1: Observe the ways that locals learn best and tailor the knowledge transfer process toward these

Communication of ideas and instructions are highly important in the success of any project. Two-way communication is also paramount. It is obvious that a language barrier will cause hindrance in communication. It is less obvious that some cultures with less exposure to western education systems may not respond positively to written/graphic instructions. The difficulties that arise can most easily be remediated by collaborating with someone who speaks both the local language and your own. A translator can convey the intent of written or diagrammatic instructions, or the purpose of certain actions and how thee relate to the overall goal or outcome.

Just because locals do not understand your own methods of conveying information does not make them ignorant or incapable. In contexts that have not had substantial exposure to western learning systems, learning kinaesthetically may be more a successful approach than providing instructions. It is particularly helpful to have a translator here, as the amount of information that can be communicated purely through gesture is limited.

Deployment Principle 2.7: Assume standard operating practices will not necessarily be adhered to the entirety of the time, so design to the simplest operation principle

As the operational procedure becomes more intricate, a greater degree of explanation is required for the end user to understand how each of the steps relate to the overall functionality. Additional design complexities offer points for the end user to deviate from a standardised operating practice. The approach presented has a high focus on increased solution reliability than increased efficiency. Simplicity of the design and operational procedure introduces as few failure points as possible and helps to keep performance reliability as high as possible.

Community Perceptions of Proposed Design

A social stigma existed around the installation of solar cookers in Spiti as prior models issued by the government were too fragile with large glass panes and mirrors integrated into the design. When the first author proposed using PC for the design it was received well. PC would not be susceptible to breaking when rogue cricket balls struck it; this was the main cause of damage to the government-issued cookers. The glass itself was not the issue, but there was no way to replace broken panes.

These cookers units were provided as a large scale government operation to provide a healthier and less energy intense option for cooking in rural contexts. The purpose of the cookers not been adequately communicated to the Spitians and therefore they were perceived as somewhat superfluous to their needs. The reliability of the units and ease of replacing broken components was not considered by the government and therefore they tended to remain broken. The reflector component was more valuable as a mirror than the unit was as a cooker.

Deployment Principle 2.2: Involve the end user(s) as much as possible so they feel a sense of ownership for the solution

Providing the recipient with a sense of ownership is important for the success of an implemented design. The government-issued solar cookers were not widely used despite their functionality because the people of Spiti had no attachment with them. It is critical that the solution addresses a user identified need or else the relevance of providing the solution is clearly communicated and understood by the intended user.

Involving the user during the construction phase is critical for helping them to understand the functionality of and relationships between different components, to understand how to perform repairs and to also gain a sense of pride and attachment to the design.

Deployment Principle 2.8: Community acceptance of the solution is a crucial factor in successful design

The solar cookers designed and built by the first author were completed with assistance from different groups who all voiced particular modifications they wanted to employ from the standard design; an extra base layer of stones to stop water ingress from snow melt, an adjustable reflector to increase energy input, a particular finish to match the aesthetic of the house it was built for. It was important to keep the design flexible enough to facilitate these changes as they allowed *user-identified needs* to be accounted for. The result was that users had a higher degree of commitment and affiliation with the design than if the final product was simply provided without their input. The local knowledge of the environment also helped refine the design beyond what the first author was capable of foreseeing.

Repair and Maintenance

'Jugaad' (*dew-gard*) solutions were the most common fixes to problems that arose. These solutions are typically patch-ups by people the locals refer to as 'barefoot engineers'. The solutions are innovative and tend to satisfy the bare minimum for functional requirements only. One such example was using a hacksaw blade (with no handle) to tap a thread into a PVC pipe used for a water heating system. The thread lacked the required precision to fit in the fixture and subsequent shaving using a shard of window glass was undertaken. The shaving attempt also failed, at which point the PVC was heated using a candle and forced into the fixture. Water was run through the piping and no leaking occurred. When breakages in a system occurred, it was more feasible to solve the problem using what was readily available than to get expert advice or waiting for the appropriate tools.

When working with mud, nothing is an irreversible problem. Any defects or damage done can be fixed with application of more mud. Cracks can be joined. Extra width can be added, excess can be removed. The same frugal mentality was extended to working with other materials to make use of everything. Examples are detailed below:

- Wood that snapped was reinforced at the break so it could be reused
- A threaded PVC pipe that broke at a connection was given a jugaad thread using a hacksaw blade, then heated and rammed back into the connector. This was watertight.
- Metal that was damaged or scrapped by someone else was bashed into shape for continued use. No edge was deemed too rough to be unusable
- Shirts and blankets that were worn out beyond repair were used with rocks as valves for the canals to provide water control for field irrigation

Deployment Principle 2.3: Design for lifespan reliability rather than optimal efficiency

Robust materials should be used wherever the option exists. It is more useful in this context to provide a long-lasting design with reduced efficiency than an increased efficiency design that is more susceptible to severe damage. If material selection influences both lifespan and efficiency, design for life span. The one study that

detailed new product failure in rural DC markets identified lack of local service network and robust design features as the most important factor preventing successful implementation [76].

Deployment Principle 2.6: Acknowledge the local perception towards repurposing materials to fix system failure points

The most probable failure points of a system should be identified to give some idea of how these will be fixed by the locals. Designing for ease of cleaning and for non-destructive replacement of parts is critical. The less moving parts in a design, the better, as these add extra degrees of complexity that will be harder to reproduce with limited resources.

It has to be assumed that any repair work on a damaged system will be carried out without adequate tools. Failure points of a design should be considered on the basis of how they are likely to be repaired. The path of least resistance is generally the repair pathway. If repairs occur during the build phase, it is interesting and informative to leave the locals to their own devices and see how they tackle the problem using their own skillset and resources. This can help to expand the options open to the external designer, and also to gauge how the locals will cope with keeping the system functional.

Workplace Safety

The concept of worker and bystander health and safety was unapparent in Kaza. The vast majority of labour observed could be termed 'unskilled'. The more skilled trades such as metal working or carpentry had no regulatory framework to make sure that both workers and passers-by were safe in and around the site. Some of the practices observed within workplaces are detailed below:

- The dangers of inhaling either LPG from leaky canisters or enamel paint fumes while painting were unknown.
- The carpenters and metal workers wore sandals or very occasionally leather shoes. None of the workshops or job sites provided gloves, ear protection, eye protection or hard hats to workers.
- The metalworkers doing welding had tinted sunglasses, although bare faces and arms were exposed to the radiation. No shields or screens were used to protect others close proximity.
- Many workers were intoxicated at the metal workshop on the day of a festival. Machines were still operating amidst the inebriety.
- Electrical safety was minimal and a supervisor gave himself a mild electric shock while replacing a photovoltaic cell battery when touching both terminals while holding conductive tools.

Deployment Principle 2.4: Maximise the unskilled, hand fabrication or repair processes required by the end user(s) to limit risk exposure

Considering the perspective of workplace safety, maximising the fabrication that can be done by hand or without heavy machinery minimises unnecessary risk exposure for those involved with this phase of the design.

The availability of more sophisticated tools also tends to be limited and for ease of ad hoc repair or replacement of components, the solution will be more reliable if the end user is capable of repairing as much as possible without external aid.

Sanitation and Hygiene

The sanitation and hygiene knowledge held by those in rural DC contexts is not necessarily aligned with what is accepted in developed countries. The idea of cause and effect relating to health issues was observed to be marginal in Kaza. Gastric flu cases were put down to the patient getting too cold, rather than the possibility of eating bad food or drinking bad water. No second thought was given to mouth-siphoning stagnant brown water from an irrigation catchment tank that contained several years of fertiliser runoff and general organic debris. Children scooped water from the communal drinking water barrels using their hands or returned backwashed water back into the barrels. The causality of health issues was observed to be strongly ingrained, and conflicting ideas were not given any credit.

Deployment Principle 2.5: Assume sanitation practices common in developed countries will not be adhered to and design precautions accordingly

From a hygiene perspective, systems dealing with food and/or water should have precautions inbuilt into the design to help minimise germ spread or contamination. Such precautions will depend on whether the design is to be used by a single person, a family unit or a whole community.

4.3.8.5 Discussion

4.3.8.5.1 Proposed NPD Framework

The identified implications specific to NPD in the rural DC context have been classified as deployment principles in the results above. The framework for developing a general NPD process within this context was initially based on the temporal Stage-Gate methodology proposed by Cooper *et al*. It was found that the proposed NPD framework had very little overlap with this conventional model and am alternative methodology was constructed to define the process more realistically. The bottom line for the conventional NPD framework is profitable returns through extensive market intelligence. In contrast, the proposed framework is driven by fulfilling the needs of the community for whom the end product is intended. The former framework involves a highly directive approach to obtaining the final product where the end users are typically excluded from the development process. Conversely, the proposed framework takes a co-determinative approach where decisions are influenced and informed directly by the end users throughout. The proposed framework is shown in Figure 4.3.8.6 and the Deployment Principles are summarised in Table 4.3.8.1
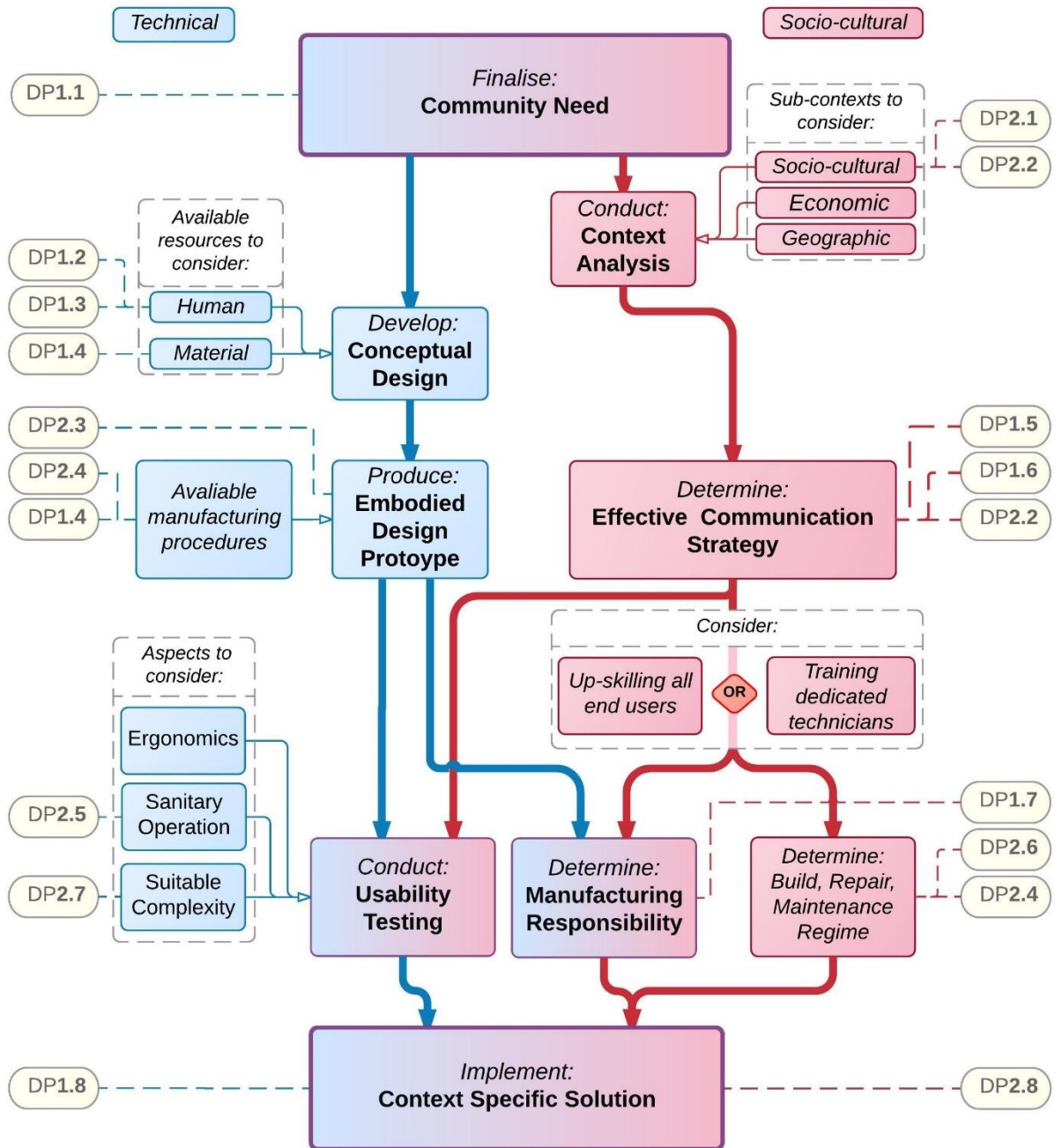
Figure 4.3.8.6: Proposed framework for new product development process in rural developing country contexts.

Table 4.3.8.1: Summary of Deployment Principles (DP)	
Technical Deployment Principles (DP1)	*Socio-cultural Deployment Principles (DP2)*
DP 1.1: Finalise projects through prior communication or assume resource and technical knowledge availability is limited to what the embedded participant comes in with	*DP 2.1: Observe the ways that locals learn best and tailor the knowledge transfer process toward these*
DP 1.2: Plan for project delays by integrating parallel work streams	*DP 2.2: Involve the end user(s) as much as possible so they feel a sense of ownership for the solution*
DP 1.3: Consider the reliability of transporting materials in from external suppliers	*DP 2.3: Design for lifespan reliability rather than optimal efficiency*
DP 1.4: Acknowledge that material or component quality will be variable and limited, make design decisions accordingly	*DP 2.4: Maximise the unskilled, hand fabrication/repair processes required by the end user(s) to limit risk exposure*
DP 1.5: Appreciate that visual communication may be a learnt skill	*DP 2.5: Assume sanitation practices common in developed countries or standard operating practices will not necessarily be adhered to*
DP 1.6: Trial the broadest possible range of learning styles and capitalise on the style(s) that are most readily understood	*DP 2.6: Acknowledge the local perception towards repurposing materials to fix system failure points*
DP 1.7: Design for manufacturability by capitalising on available resources and skills	*DP 2.7: Assume standard operating practices will not necessarily be adhered to the entirety of the time*
DP 1.8: Provide parametric templates for reproducing complex parts	*DP 2.8 Appreciate that community acceptance of the solution is a crucial factor in successful design*

Whereas the conventional NPD process involves technological innovation or novelty, the present framework is constructed around implementing functional technology in a novel context. The design development and validation aspects are not intended to encompass proof of concept work, rather the implementation of a proven concept in a new context.

The framework has been split into dual pathways that influence each other, but have a distinctly differently focus from one another. The technical pathway, coloured blue, detail considerations that ensure the design functionality based on the specific contextual constraints. The socio-cultural pathway, coloured red, details considerations that ensure the end user integration and comprehension of the process elements. Several deployment principles could not be realistically isolated to one pathway and appear in both

4.3.8.5.2   Implications for Solar Desalination Units

The deployment principles informing the framework are generalised enough for direct application to the context of rural DC salt water desalination. This study has highlighted the following considerations which are of crucial importance to a successful design in a rural DC context:

- Direct the solution toward a user-identified need rather than an externally identified need for optimal appeal and acceptance by the user
- Involve community members as early and as often as possible to help building their understanding and pride for the solution
- Focus design effort toward increasing unit reliability rather than efficiency
- Gather knowledge on how the locals learn best, what areas they excel at and which materials they are competent using if on-site fabrication is selected
- Assimilate the knowledge of local skills and learning styles into the design and build process to ensure contextual suitability

4.3.8.6   Conclusions

The purpose of this work was to identify the factors affecting the NPD in a rural DC context. The findings have been highlighted and summarised as the technical and socio-cultural Deployment Principles for successful design as detailed in Table 4.3.8.1. These Principles have been integrated into the proposed NPD framework.

The originality of this work is the formalisation of this NPD framework. Special attention has been given to the rural DC context, as opposed to the conventional application of the NPD process in developed country consumer markets. The work provides insights into elements that embedded participants must consider when implementing designs within rural communities in developing countries.

4.4 Implications

The experimental phase highlighted aspects for possible future development through subsequent testing and also facilitated the data collection necessary to begin the construction and analysis of a theoretical systems level model describing system behaviour.

4.4.1 Client proposed designs

The client-proposed Open Air design did not establish the intended system dynamics and did not produce any condensate under realistic *in vitro* test conditions. The initial test phase has indicated that it would not be viable to put further development focus into this option due to its lack of productivity.

The client-proposed Low Pressure design involves establishing a partial vacuum using a volume change. The vacuum was intended to promote more rapid evaporation. A theoretical analysis was employed in conjunction with experimental testing and a reliability analysis. Results (detailed in Chapter 4.3.7) show that performance could be enhanced by up to 19 *%* through Low Pressure means, but there are significant issues with reliability and practical implementation.

4.4.2 Possible Directions for Future Research

The experimental scope for this project was to ascertain what parameters were worth investigating further and to quantify and qualify the expected performance of the two client-proposed designs. The results obtained during the test phase provided an initial indication of what areas of the solution space offer viable options for further development. To summarise the above findings, the key variables in optimising water productivity are closely related to the condition of the condensation surface. Although unrelated explicitly to further desalination unit development, the highly non-linear salinity relationship observed offers potential for further investigation of whether an equilibrium condition exists between seawater salinity and solar radiation incidence at a given location.

4.4.2.1 Condensation Surface Condition

The next phase of research could be focussed on narrowing down the optimal condensation surface condition that can be practically achieved within the intended context. The initial test phase showed that a 25 *%* increase in performance was observed under solar conditions when the condensation surface was shaded as opposed to being directly lit by the sun. Conversely, a 60 *%* performance decrease was observed when the fan providing forced cooling on the condensation surface was disabled. These results highlight the critical importance of the temperature of the condensation surface. The corresponding observed change in evaporation dynamics during

these cases was much less pronounced, and for this reason it was proposed that the condensation surface offered more potential to optimise and should be the attention of subsequent design work. The key areas identified for further condensation surface research are presented in Chapter 6.1.3 and have been summarised below.

Aspects of further research for the condensation surface:

- Integration of active componentry to maintain the necessary temperature difference
- Addition of a passive surface shading to limit the amount of solar energy incident on the surface
- Addition of fins to increase the available area for more optimal heat loss

4.4.2.2   Effect of Brine Water Salinity on Performance

This test phase highlighted that the system response was insensitive to water salinity changes for saline concentrations between tap water and what is expected for seawater in Tonga. If the salinity was increased by 15 % above the Tongan seawater concentration, a significant non-linearity was observed in the response. This outcome has particular implications for relating the salinity of seawater at a given location to the solar energy incident there. It has been postulated that a dynamic equilibrium between these two geographically dependent variables which affects the evaporation rate to moderate changes in the salinity of the water. Investigation of this proposed relationship was beyond the scope of this project.

4.4.3   Implications for Model Building

At the conclusion of the experimental test phase, the quality and quantity of data obtained was judged to be sufficient to inform the building of a theoretical systems-level model. The current data acquisition process involved greater variety, quantity and sampling frequency of properties (detailed in Chapter 4.2.2) was greater than what was documented in the prior experimental literature studied.

5 Condensation and Evaporation Modelling

The aim of this component of the project was to create a first principles model to capture evaporation and condensation of various brine concentrations. This modelling was a complex undertaking due to the multiple prior and concurrent thermodynamic processes occurring (temperature, humidity and brine water mass changes). In contrast to the majority of relevant literature, which typically takes a curve fitting approach [5-7, 16-18, 35, 40], the current study demonstrated the possibility of constructing a model based on heat transfer and that the results have excellent fit to the data.

5.1 Approach

The modelling approach involved identifying critical dynamics between the light source and the condensation of water at the collection surface. Modelling was concurrent with the experimentation and informed iteration on experimental rig design. Relevant thermodynamic laws were extracted from literature and synthesised with further considerations pertaining specifically to the experimental apparatus. These laws defined the distinct, critical properties of the condensation process which formed the system level framework for model building. The condensation process used is shown schematically in Figure 5.1.
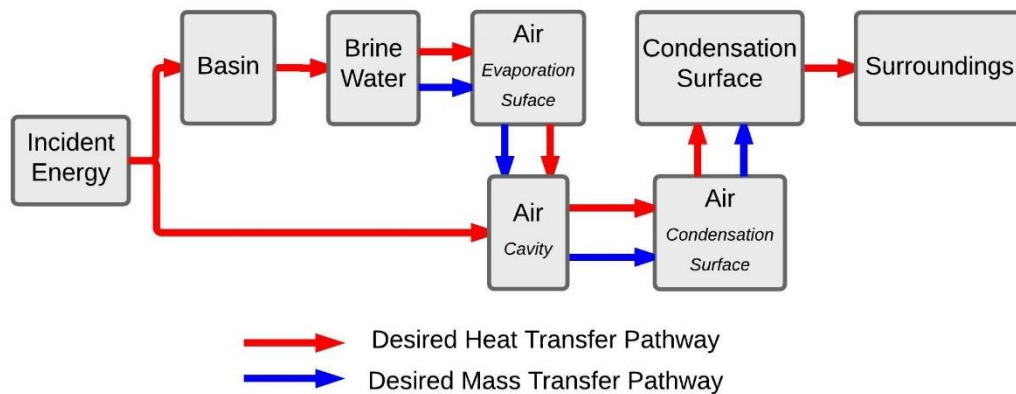
Figure 5.1: Initial heat transfer framework proposed to inform model building process.

The critical properties have been defined as:

- brine water temperature
- evaporation of brine water
- humidity of air at the evaporation surface
- humidity of air at the condensation surface
- condensation of distilled water at the condensation surface

This model was constructed using concepts presented in a recent review paper (2013) by Xiao *et al* [4]. The paper included a representation of heat transfer processes are typically presented in literature ([Figure 2.1](#)). The

model in this study has a similar structure, but extends on this widely accepted process with a more complex description of the heat and mass transfer dynamics between the brine water and condensation surface. This adaptation integrated relative humidity as a system variable as this has been considered an important missing property in previous system models [5].

This preliminary work indicated that embodying the model required quantitative data about the identified critical properties. This directed the sensor and instrumentation requirements for the experimental phase, as detailed prior in Chapter 4.2.2.

The equations were based on known physical laws of thermodynamics and mass conservation. This contrasts to existing curve fitting approaches found in literature. While curve fitting has provided some close empirical fits to data, the insight from such approaches is generally deficient and applicability of the conclusions beyond the explicit experimental setup is limited. A first principles approach does not appear to have been achieved in the literature. Such a first principles approach has the potential to quantify underlying physical behaviour and thus, allows extrapolation of the model to predict the outcomes of conditions proximal to the experimental setup.

The raw data displayed trends indicative of first-order differential equations. Hence, ordinary differential equations (ODE) were assumed as the basis for the model. These equations each defined certain mass or volume balances and allowed identification of variables that quantified the observed behaviour. The model variables were modulated such that dynamics between relevant experimental input/output data was captured. The model efficacy was defined by its ability to closely capture the experimental output data. The specific operational coefficients for each property of interest were obtained through parameter identification methods using MATLAB. These methods are employed to find the optimal values of parameters that fit a proposed model to measured data [78].

5.2 Theoretical Framework

The basis for the physical system model is shown diagrammatically in Figure 5.2.1 as a systems-level representation. The framework presented above was condensed as a result of the experimental phase into a more concise functional representation. Only the critical properties have been included, as these were considered a minimal level of complexity that captured the key dynamics of the system. The nomenclature is maintained from Figure 4.2.3 and is expanded upon in Table 5.2.1. The property equations represent the virtual partitioning of the system.
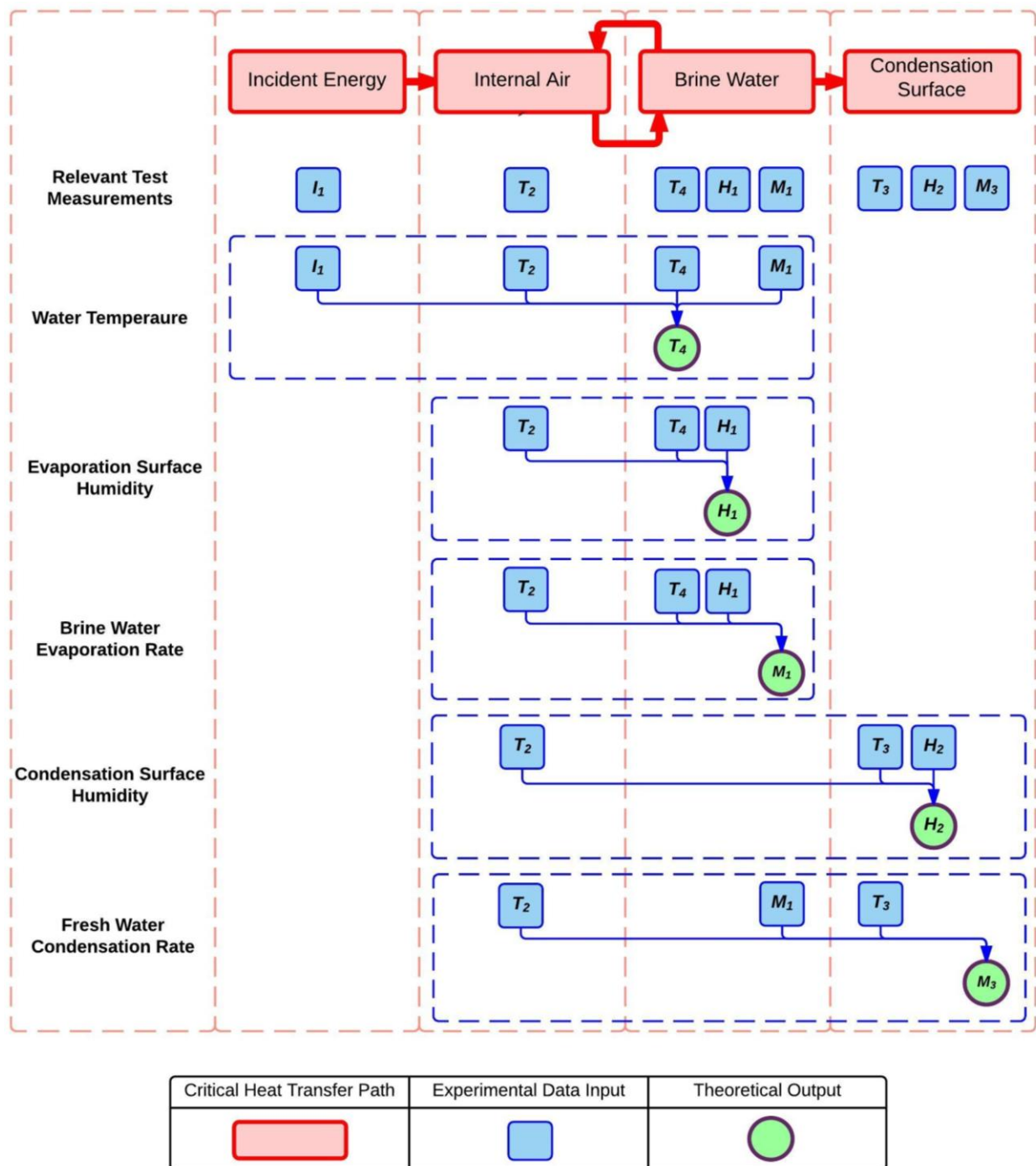
Figure 5.2.1: Initial block diagram representation of equations governing system.

Table 5.2.1: Parameter nomenclature for equation formulation (as per Figure 4.2.3)			
A_e	Effective Area of energy input	$[m^2]$	*a priori*
H_1	Relative Humidity at Evaporation Surface	$[\%]$	Measured Modelled (Eq 5.2.2)
H_2	Relative Humidity at Condensation Surface	$[\%]$	Measured Modelled (Eq 5.2.4)
I_1	Incident Energy Flux	$[W/m^2]$	Measured
k_i	Heat and mass transfer coefficients	[*see Table 5.4.1*]	Identified
M_1	Brine Water Mass in Basin	$[kg]$	Measured Modelled (Eq 5.2.3)
$M_1(0)$	Initial Brine Water Mass in Basin	$[kg]$	Measured
M_3	Distilled Water Mass at Condensation Surface	$[kg]$	Measured Modelled (Eq 5.2.5)
P_1	Internal to External Pressure Difference	$[Pa]$	Measured
T_2	Internal Air Cavity Temperature	$[°C]$	Measured
T_3	Internal Condensation Surface Temperature	$[°C]$	Measured
T_4	Evaporation Surface Temperature	$[°C]$	Measured Modelled (Eq 5.2.1)
ψ	Residual error between Data and Model	[*model dependent*]	Calculated

The energy transfer between the internal air and the brine water has not been expressed as unidirectional (Figure 5.2.1). This energy balance is represented mathematically through the appearance of the internal air temperature (T_2) in each identified equation. The prevalence of T_2 was based on the assumed system dynamics occurring at the interface between the internal air and brine.

Equation (5.2.1) models the heat transfer from the energy source through the air to the brine. Equation (5.2.2) relates heat and mass transfer from the brine to relative humidity near the evaporation surface (H_1). Equation (5.2.3) relates the brine to air heat and mass transfer and the evaporation surface humidity to the brine evaporation rate ($\dot{M}_1$). Equation (5.2.4) relates heat and mass transfer between the air and the condensation surface to the relative humidity at the condensation surface. Equation (5.2.5) models the rate of condensate collection ($\dot{M}_3$) according to the air to condensation surface heat trasnfer and the brine mass evaporating from the basin. The relationships identified for each property are expressed below. Note: the effective area term (A_e) is equal to 1 m^2 for the experimental setup as the lit area of the rig is 1.0 m^2.

$$\dot{T}_4 = -k_1 \frac{A_e I_1}{C_p M_1} - k_2(T_4 - T_2) \tag{5.2.1}$$

$$\dot{H}_1 = -k_3 H_1 - k_4(T_4 - T_2) \tag{5.2.2}$$

$$\dot{M}_1 = -k_5(T_4 - T_2) - k_6(100\% - H_1) \tag{5.2.3}$$

$$\dot{H}_2 = -k_7 H_2 - k_8(T_3 - T_2) \tag{5.2.4}$$

$$\dot{M}_3 = -k_9(T_3 - T_2) - k_{10}(M_1(0) - M_1) \tag{5.2.5}$$

5.3 Formulation of Model Components

The heat and mass transfer coefficients are identified parameters that were initially identified using a Levenberg-Marquardt non-linear least squares algorithm in MATLAB (lsqnonlin.m, MATLAB 2012b). The algorithm uses first and second order gradient descent to determine the parameter values that minimise the norm of the residual error between model and data ($\|\psi\|_2$). The linear regression coefficient (R^2) was calculated as a more accessible metric describing how well the model fits the data.

5.3.1 Water Temperature Equation (5.2.1)

As the brine mass decreases, the energy required for a particular change in temperature rise decreases. The temperature difference term ($T_4 - T_2$) accounts for heat transfer between water and air. The identified k_1 parameter is related to the energy input and implicitly contains the scaling factor that corrects for the pyranometer response to halogen lights as mentioned in Chapter 4.3.5. The brine temperature model has been superposed on an *in vitro* data set in Figure 5.3.1.1, the residual error has also been presented. The same system property and residual error are plotted in Figure 5.3.1.2 for a solar data set to indicate model response to more realistic energy inputs. The solar test parameters (k_{1-2}) differ from the *in vitro* test parameters.
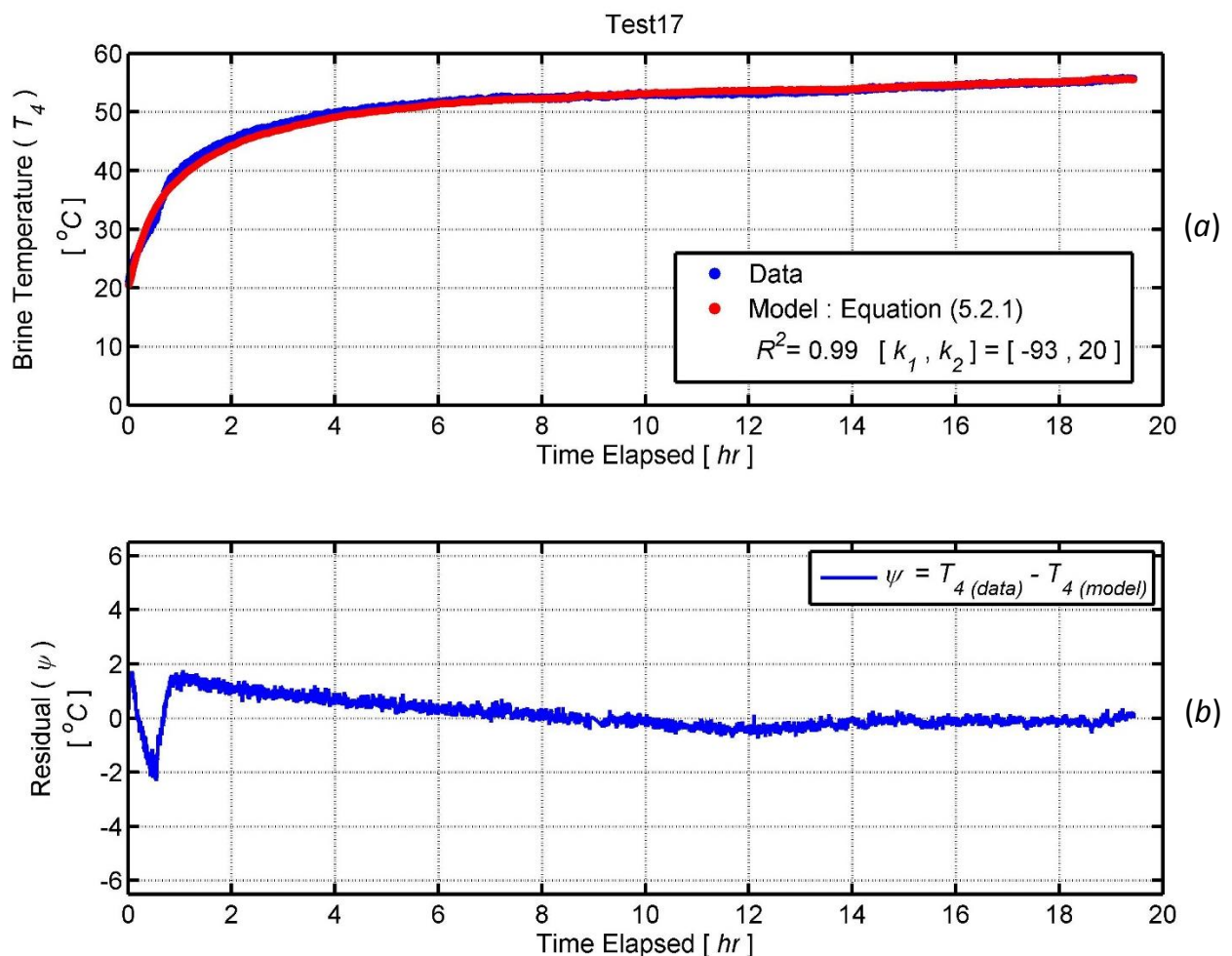
Figure 5.3.1.1: Identified brine temperature model (equation 5.2.1) and *in vitro* data (*a*), residual error (*b*)
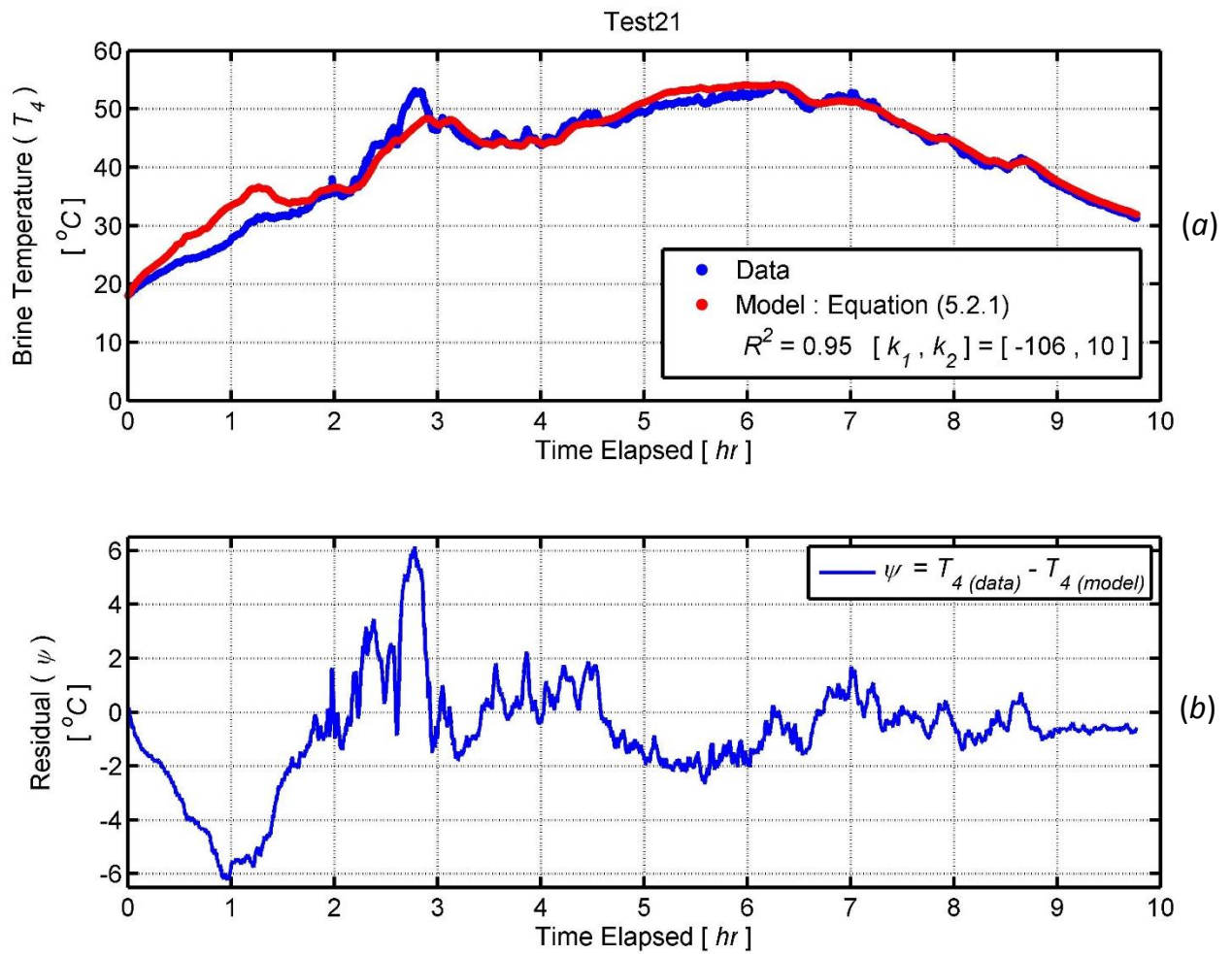
Figure 5.3.1.2: Identified brine temperature model (equation 5.2.1) and solar data (*a*), residual error (*b*)

5.3.2   Evaporation Surface Humidity Equation (5.2.2)

Equation (5.2.2) was constructed using the thermodynamic principles that affect the water vapour mass in the air. Lower air temperatures have a lower dew point temperature and thus the holding capacity of water vapour mass is lower. A higher brine water temperature means that more water vapour molecules were expected to have sufficient energy to evaporate to airborne vapour. The relative humidity term described the amount of water vapour in the air and contains information on the mass of water in the air. Equation (5.2.2) is a linear approximation of more complex dynamics that require transfer functions from the psychometric map to properly capture the energy and mass balances that define the dynamics of the system. However, this model was chosen as a sensible, identifiable and robust approach to capturing the key dynamics of the system. The model defining humidity at the evaporation surface has been superposed on an *in vitro* data set in Figure 5.3.2.1, also plotted is the instantaneous residual error.
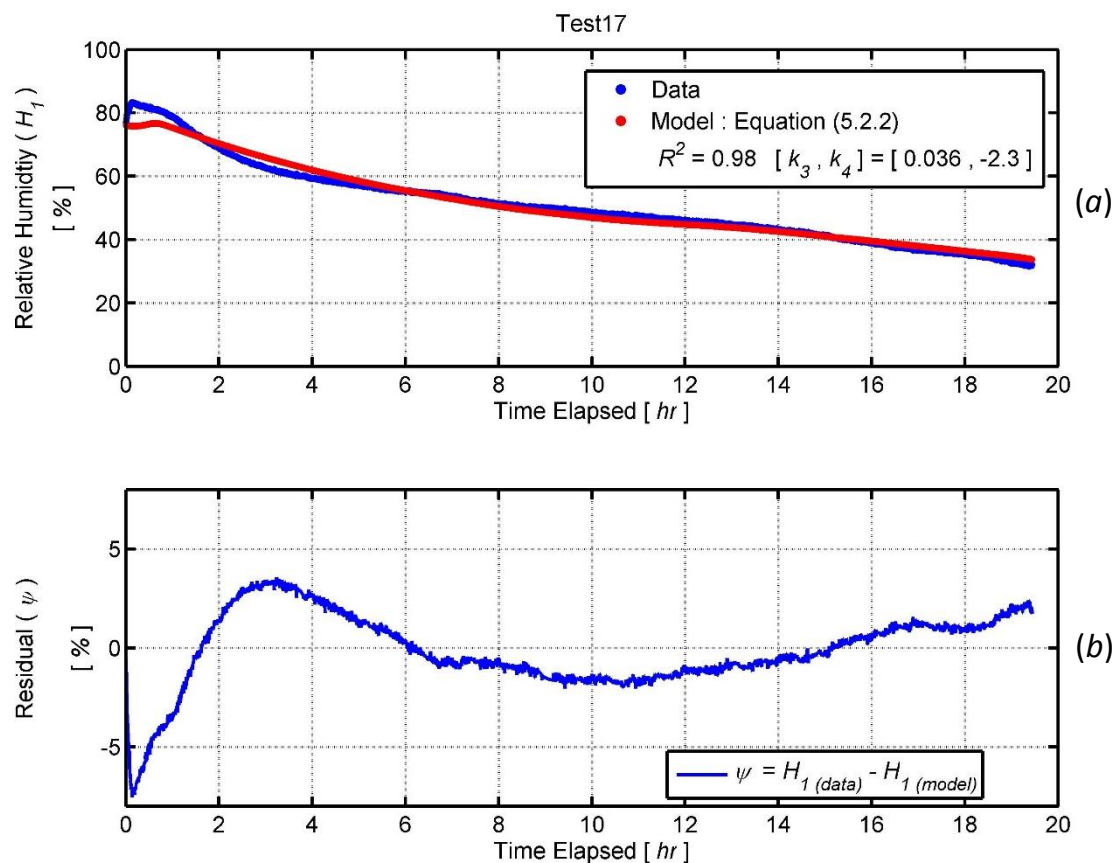
Figure 5.3.2.1: Identified evaporation surface humidity model (equation 5.2.2) and *in vitro* data (*a*), residual error (*b*)

5.3.3 Evaporation Rate Equation (5.2.3)

Equation (5.2.3) contains a temperature difference dependent heat exchange and relative humidity to determine the brine mass. It was postulated that as the air reaches saturation (H_1 approaches 100 %), the evaporation rate would tend toward an asymptote of zero. Hence, the coefficient of evaporation was $1-H_1$. The brine water mass change is implicitly contained in the parameters k_5 and k_6. Higher temperature differences were expected to accelerate the evaporation of brine water in a similar manner to equation (5.2.2). The brine water evaporation model is compared with an *in vitro* data set in Figure 5.3.3.1, the instantaneous residual error is also plotted.
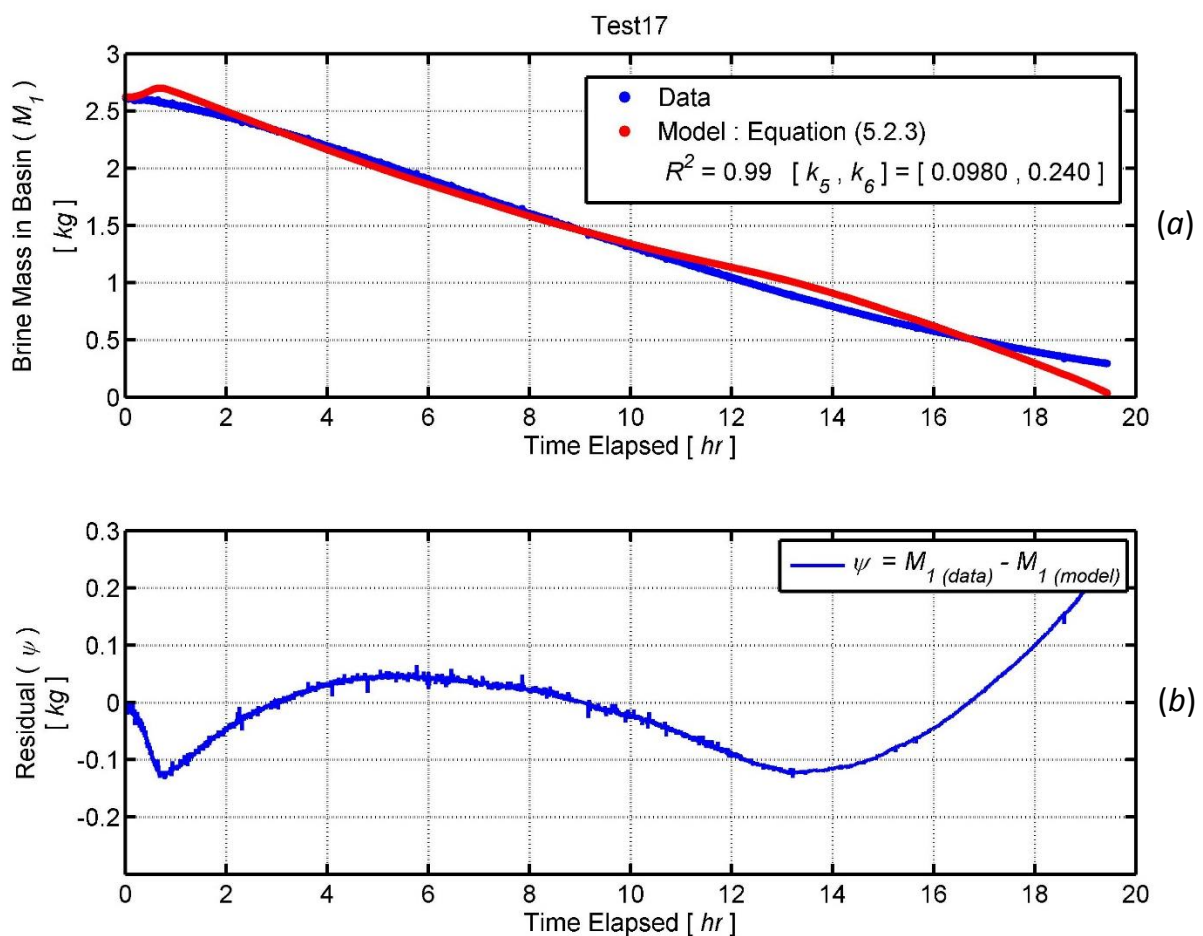
Figure 5.3.3.1: Identified evaporation rate model (equation 5.2.3) and *in vitro* data (*a*), residual error (*b*)

5.3.4 Condensation Surface Humidity Equation (5.2.4)

The equation formulation used to model condensation was similar to the formulation applied to the evaporation surface. Since mass and heat transfer at the condenser was vapour to liquid, and not liquid to vapour like the evaporator surface, the sign of the parameters k_7 and k_8 were reversed form the equivalent terms in equation 5.2.2. The model describing humidity at the condensation surface has been plotted in Figure 5.3.4.1 along with an *in vitro* data set for this property. The instantaneous residual error between the two is also plotted.
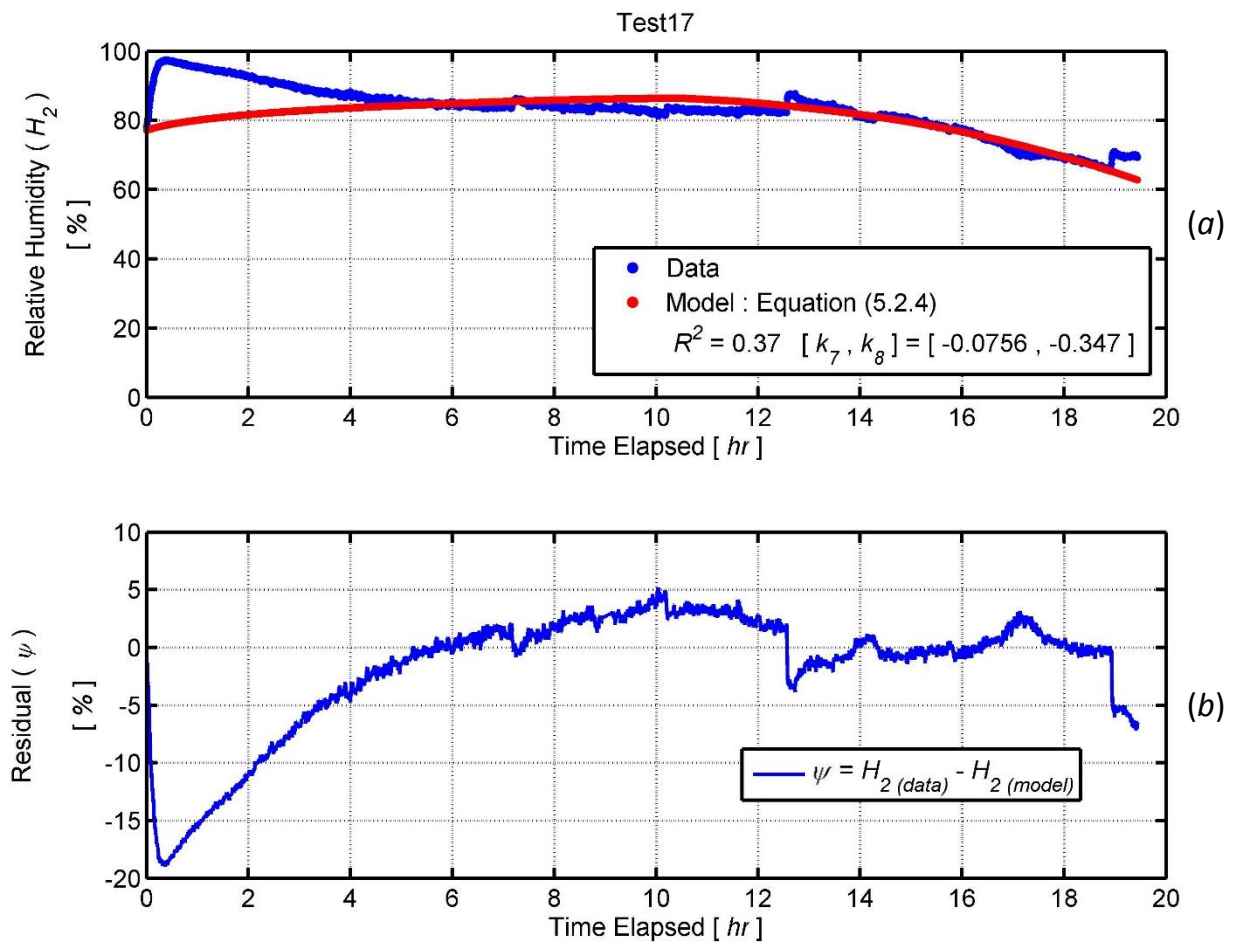
Figure 5.3.4.1: Identified condensation surface humidity model (equation 5.2.4) and *in vitro* data (*a*), residual error (*b*)

5.3.5 Condensation Rate Equation (5.2.5)

Equation 5.3.5 defines the condensation rate as a function of the ΔM_1 term, which was included to link condensation to changes in brine mass. While using the vapour mass may seem a more reasonable strategy, the change in brine mass was determined to be more accurate as it is a directly measured property. Dependence on energy transfer out of the system also exists and is accounted for by the temperature difference term. The humid air had to lose energy though the condensation surface in order for the water vapour to condense out to the liquid phase. This loss was assumed to be driven by the temperatures of the bulk air volume and the temperature of the condensation surface. The parameter k_9 accounts for the particular heat transfer mechanisms occurring. The distilled water condensation equation has been overlaid onto an *in vitro* dataset in Figure 5.3.5.1. The instantaneous residual error between the data and model has been plotted.
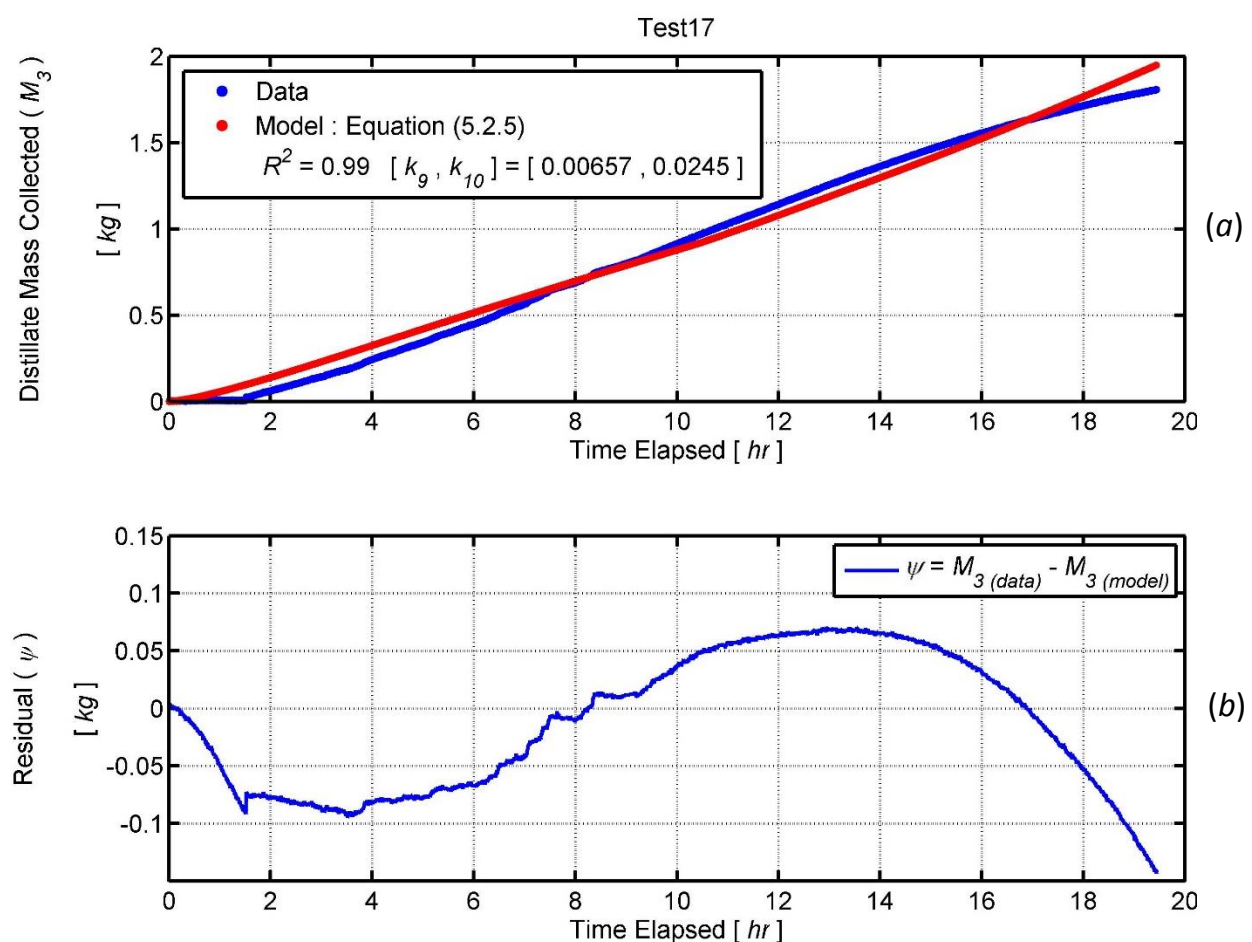
Figure 5.3.5.1: Identified evaporation surface humidity model (equation 5.2.5) and *in vitro* data (*a*), residual error (*b*)

5.4 Combination of Component Models

The sequential nature of each component equation was employed so that the system dynamics could ultimately be combined into a single, overarching model detailing the transfer from brine water temperature rise to condensate collection. The similarity between air and brine temperature meant that it was arbitrary to select either property as the initial model input. The water temperature was selected as this variable had a more explicit and direct link to the brine water evaporation rate than the air temperature. The analytical solutions to equations 5.2.1 – 5 have been combined into equation 5.4.5, which is presents a preliminary system model for the desalination unit. The evaporation surface temperature, T_4, has been expressed as a singular term in the combined system model for readability purposes. The initial value of a quantity is denoted by the ($t = 0$) notation.

$$T_4 = e^{-k_1 t}\left[T_4(t = 0) + \int_0^t e^{k_2 t}\left(k_2 T_2 + k_1 \frac{A_e I_1}{C_p M_1}\right) dt\right] \tag{5.4.1}$$

$$H_1 = e^{-k_3 t}\left[H_1(t = 0) + \int_0^t e^{k_3 t}\left(k_4(T_4 - T_2)\right) dt\right] \tag{5.4.2}$$

$$M_1 = M_1(t = 0) + \left[\int_0^t\left(-k_5(T_4 - T_2) - k_6(100\,[\%] - H_1)\right) dt\right] \tag{5.4.3}$$

$$M_3 = \left[\int_0^t\left(-k_9(T_3 - T_2) - k_{10}(M_1(t = 0) - M_1)\right) dt\right] \tag{5.4.4}$$

When equations 5.4.1 – 5.4.4 are combined, the condensate mass is represented as:

$$M_3 = \left[\int_0^t\left(-k_9(T_3 - T_2) + k_{10}\left(\int_0^t\left(-k_5(T_4 - T_2) - k_6\left(100 - e^{-k_3 t}\left[H_1(0) + \int_0^t e^{k_3 t}\left(k_4(T_4 - T_2)\right) dt\right]\right)\right) dt\right)\right) dt\right]$$

$$\tag{5.4.5}$$

This relationship represents the equation of state for the desalination unit approximated by the test rig. The implications are that if the internal air temperature, initial values of the brine water mass, water temperature and internal humidity at the evaporation surface are known then it is possible to evaluate the condensation mass at a given time. The coefficients obtained for the rig under different test conditions are presented in Table 5.4.1.

	Test Condition	Reference (*in vitro*)	Glass Absorption Surface	No Condensation Surface Cooling	Saline Water	Solar Energy Input	Open Air Rig
	[*Section in Results*]	[4.3.1]	[4.3.2]	[4.3.3]	[4.3.4]	[4.3.5]	[4.3.6]
Parameter [*units*]							
k_1	[s^{-1}]	-92.7	433	-108	638	-106	115
k_2	[s^{-1}]	20.2	36.1	9.63	16.9	10.4	4.35
k_3	[s^{-1}]	0.0424	-0.0184	-0.0106	-0.163	-0.17	-0.00145
k_4	[% .$(s\ °C)^{-1}$]	-1.52	-11.6	-13.2	-14.3	-5.02	2.3
k_5	[kg .$(s\ °C)^{-1}$]	0.0342	-0.138	0.0315	0.0639	0.0384	-0.0353
k_6	[kg .$(s\ \%)^{-1}$]	0.241	0.0555	0.33	0.532	0.267	0.114
k_9	[kg .$(s\ °C)^{-1}$]	0.00535	0.00401	0.00383	0.00036	0.00363	0
k_{10}	[s^{-1}]	0.019	0.00876	0.00254	-0.26	-0.0204	0

Table 5.4.1: Identified parameter values for each test state

The model complexity was necessary due to the multiple candidate properties that could be modelled and the numerous quantifiable pathways of energy transfer between states. In particular, since multiple identified model parameters were required to capture the observed mass and heat transfer, the robustness of the parameters was reduced. However, the variable parameter set defined in equations (5.2.1 – 5) were deemed the minimum set to capture all of the behaviours and properties desired inform the development of prototype brine condensers. However, shifting the model role of some parameters from variables to *a priori* estimates would reduce parameter variability.

5.5 Evaluation: Comparison with Other Theories in Literature

Several different methods of analysis have been utilised in the relevant literature. These methods provided a benchmark for comparing the theory presented in the current study. A brief summary of the methods used, a quantified error comparison and the overall originality in the current study are presented below.

5.5.1 Basis in Fundamental Thermodynamics

Models based on experimental data [5-7, 16-18, 35, 40] have achieved a reasonable fit, but at the cost of having a weak or non-existent basis in first principles thermodynamics. Such curve fitting models generally used polynomials or power laws. In one case, the polynomial was extended to sixth order [35] for the sake of maximizing the regression coefficient, R^2. Several studies initially introduced a heat transfer basis to the work but failed to explicitly link back to this with the experimental results and findings [32, 41, 44]. Further studies built their work upon a mixture of empirical relations obtained from prior studies and first principle heat transfer relations [21, 40].

Only a small number of experimental studies [12, 55, 79] proposed that a first order differential equation defined the behaviour of the brine water temperature. The same equation was applied in each study, reproduced as equation 5.5.1 below.

$$\dot{T}_w + a_1 T_w = f(t) \tag{5.5.1}$$

The function, $f(t)$, was assumed to be effectively constant over small time scales in each case to solve the equation. The coefficient (a_1) was an aggregated term containing the effective area, the heat transfer coefficient, the brine water mass and the specific heat capacity. However this approach does not account for the heat loss due to evaporation. In contrast, the current work is grounded in fundamental thermodynamics. This gives it the ability to capture the evaporative process (Figure 5.3.3.1).

5.5.2 Comparison with Model Presented by Dimri *et al*

The study conducted by Dimri *et al* [12] had a particularly strong thermodynamic basis and related the brine temperature to hourly output through a series of heat transfer equations. The equations proposed in this study display a relatively good fit to the data, and are validated using a cumulative residual method. This was the only experimental study that declared an error analysis method. The overall residual error for property X (ψ_X) has been defined as a scaled two-norm in equations (5.5.2 – 3).

$$\psi_i = \frac{X_{mod,i} - X_{expt,i}}{X_{mod,i}} \tag{5.5.3}$$

$$\psi_X = \sqrt{\frac{\sum_i^N (\psi_i)^2}{N}} = \frac{1}{\sqrt{N}} \|\boldsymbol{\psi}\|_2 \tag{5.5.2}$$

The instantaneous residual (ψ_i) is the relative difference between the model prediction ($X_{mod,\,i}$), and the experimental data ($X_{expt,\,i}$). N is the number of data points and $i = \{1, 2\dots N\}$. The error values have been presented by Dimri *et al* for the brine water temperature (T_4) and distillate productivity (M_3) only, as per Table 5.5.1. The errors on corresponding properties have been included for comparative purposes.

Table 5.5.1: Comparable residual error values between current and prior studies		
Study	Brine Temperature Error, ψ_{T_4}	Distillate Productivity Error, ψ_{M_3}
Dimri *et al*.	11.5 %	37.0 %
Current work	0.01 %	3.1 %

None of the literature studied has provided an accompanying sensitivity study into the robustness of the equations or identified parameters therein. The curve-fitting equations have no physical basis to justify predicting how the coefficients would be expected to change as a result of changing the operating conditions.

5.5.3 Originality

The current study has shown that it is possible to construct a model with a heat transfer basis, and that the results have excellent fit to data. None of the other experimental studies have considered the effect of internal relative humidity as a system variable. The measurement of this variable in the experimental phases and the subsequent inclusion in the subsequent model building was a point of difference between the current study and prior studies. Prior models have assumed that the state of the internal air is saturated. An observation that the internal humidity was considerably below saturation was made by Ahsan *et al* [5]. However that study lacked sufficient resources to integrate this observation into the analysis and saturation was assumed. None of the other literature was found to explicitly consider sub-saturated air humidity as a variable in system models.

The current study has put a greater focus on obtaining humidity profile data than the other experimental studies reviewed. The utilisation of a hygrometer at both the evaporation surface and the condensation surface helped quantitatively evaluate the system dynamics and shed light on the state of humidity within the system as shown in Figure 4.3.1.2. The system never reached saturation during the experimental phase, and the humidity profile at the evaporation surface was substantially different from the condensation surface. This outcome, although implicit in prior studies, was not found to be directly quantified. The integration of relative humidity factored into both the component equations and the overall combined system equation.

The collection of humidity data in particular offered a novel view of the system dynamics and directed the model development process. The distinct differences in measured humidity and temperature helped to formulate the concept of compartmentalising the internal rig cavity into virtual volumes based on the local conditions, as proposed in Figure 5.7.1. This measure adds a necessary degree of complexity to the analysis, but the benefit is that the system is more realistically described than if a singular internal condition is used.

5.6   Critique of Model

The model of Equations 5.2.1-5.2.5 represents the culmination of exploratory work into a solution space that has not previously been described with the same degree of instrumentation. As such, some elements of this model had a low numerical robustness and measurement error had a significant effect on the identified parameter variance. This low robustness is detailed along with proposed causes and courses of action in Chapters 5.6.1 – 5.6.3.

5.6.1   Areas of Weaker Representation

This initial analysis captured the brine temperature and evaporation rate dynamics. However, the condensation characteristic was not captured as well as evaporation and failed to describe the data for some of the test cases. The condensation rate is the overall system performance metric of the solar still and was therefore considered more important than the others metrics in terms of the overall project.

The long data segments caused issues with simple forward simulation methods and thus novel methods were required to enable the inbuilt MATLAB Levenberg-Marquardt algorithm to perform satisfactorily on all of the data sets. This novel forward simulation method analysed the test period in a piecewise fashion rather than processing the entirety at once. The algorithm was complex to code and was slightly more computationally intense, but allowed for better modelling of the more rapid dynamics. A Picard iteration as the basis for the novel forward simulation method to simulate the model responses. The forward simulation script and a detailed description of the strategy are provided in Appendix 16.

5.6.2 Tests of Sensitivity and Model Non-Identifiability

A sensitivity analysis was conducted to investigate the effect of perturbing the parameters through an arbitrary range of values. The regression coefficient and norm of the residual error were mapped onto parameter space to give a visual representation of how changing the parameters altered the fit between the data and the model. The mapping is shown for equation (5.2.1) in Figure 5.6.2.1 for an *in vitro* test (Test 17) and Figure 5.6.2.2 for a solar test (Test 21).

(*a*)

(*b*)
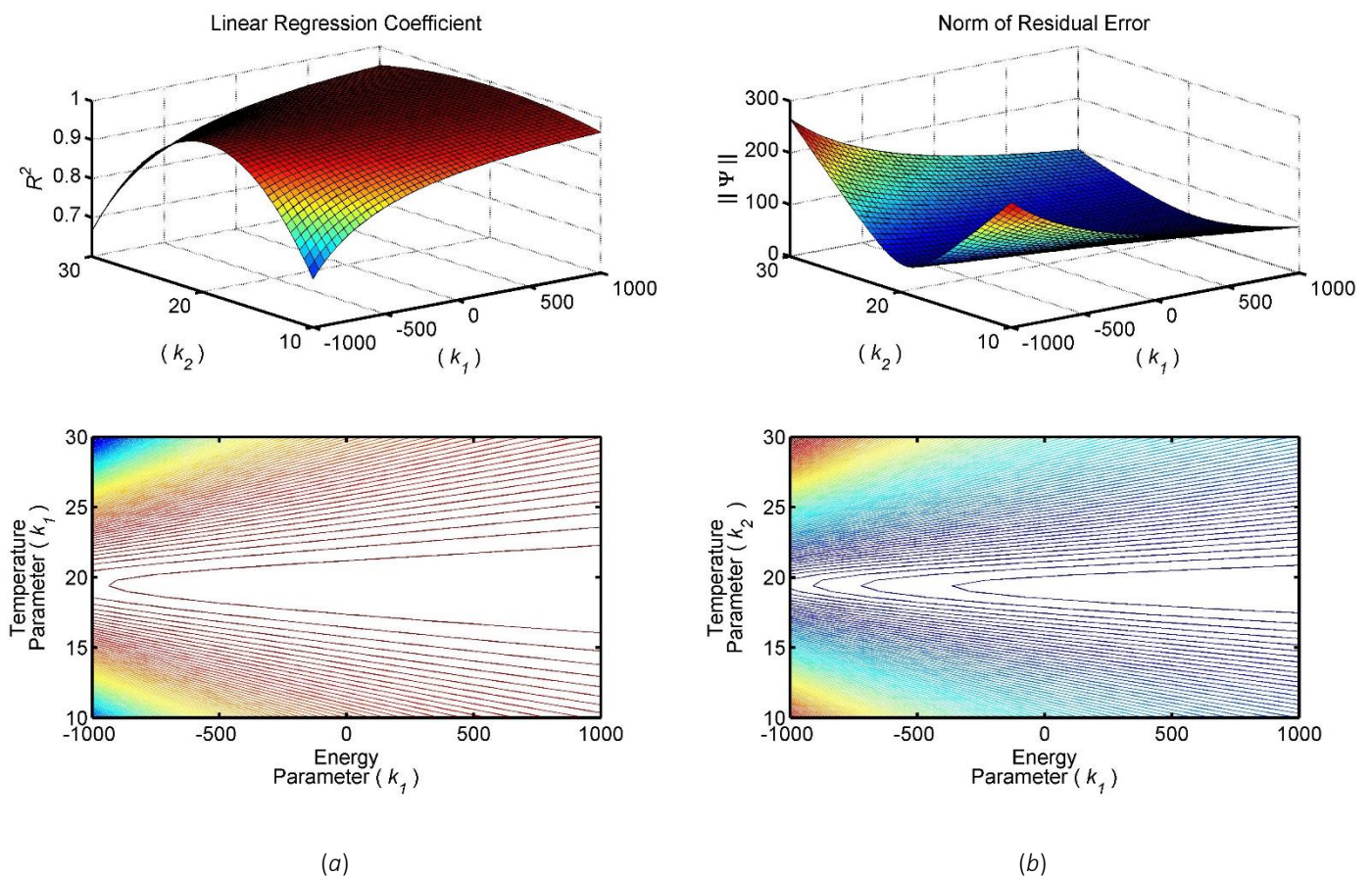
Figure 5.6.2.1: Effect of identified parameter values on regression coefficient (*a*) and residual error (*b*) on for equation (5.2.1), *in vitro* test
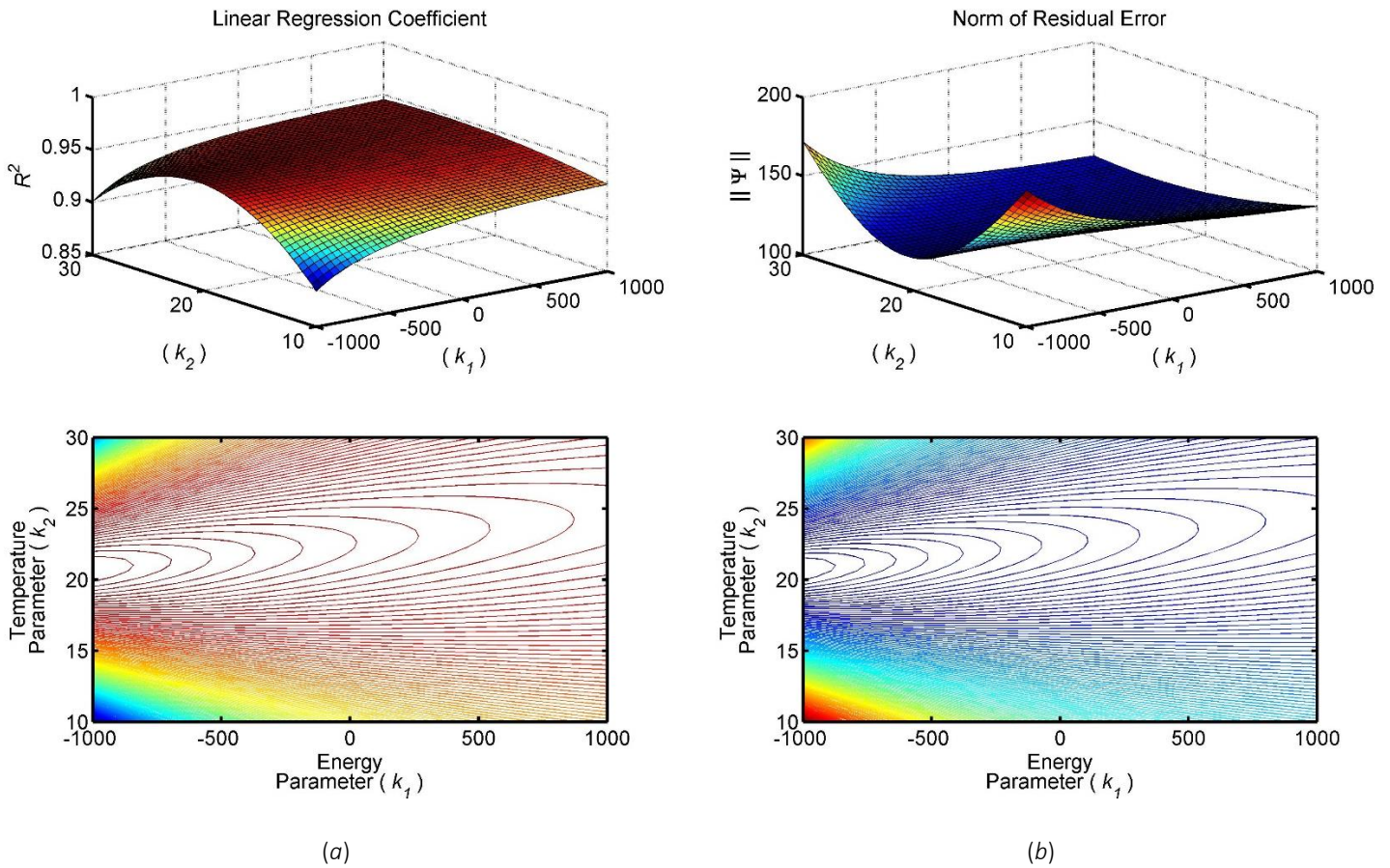
Figure 5.6.2.2: Effect of identified parameter values on regression coefficient (*a*) and residual error (*b*) for equation (5.2.1), solar test

The number of model variables required (10) made the system model susceptible to practical non-identifiability [80, 81]. The behaviours described by some of the parameters encompassed a lot of information. This problem was most obvious in equations (5.2.2) and (5.2.4) where the parameters implicitly contain information regarding the brine water mass in the basin.

This analysis yielded concerning results about the identifiability of the system using the methods implemented. Inspection of the equations did not suggest structural non-identifiability however a rigorous identifiability analysis was not undertaken to guarantee this outcome. A system may have either structural or practical identifiability.

This analysis yielded concerning results about the practical identifiability of the system model. Structural identifiability is related to the mathematical formulation of the equations involved. A system is structurally non-identifiable if the modelled behaviour of a system can be described by the variance in more than one parameter [80]. The result is a non-unique set of model parameters.

Practical identifiability is related to the quantity and quality of data used to construct the model. A study conducted by Raue *et al* [81] describes a practical non-identifiability as a relatively flat valley in the residual map. The model is practically non-identifiable if the objective function is insensitive to changes in a particular

parameter when other model parameters can perform similar (but not identical) modelled behaviours. In particular, if the objective function sensitivity is much lower along any particular vector of the parameter space than the objective sensitivity on other directions, then the model is at risk of practical non-identifiability. When a model is practically non-identifiable, the measurement accuracy or experimental design does not allow precise identification of model parameters due to a lack of observation of the disparate model roles. While it seems most likely that the system was structurally identifiable, its practical identifiability seemed weak in a number of cases.

The red region of the regression coefficient contour map on Figures 5.6.2.1 – 2 correspond to an R^2 fit greater than 90 %. The flatness of this region indicates that any choice of the energy parameter k_1 between -900 and +1000 will give a satisfactory fit between the model and the data. This result is also apparent in the residual map, where only k_2 greater than 22 affects the norm of the residual. The contour map highlights a very weak dependence between the choice of k_1 and the norm of the residual. As appropriate, the component models have been based on thermodynamic first principles. However, this does not guarantee that the experimental data will yield unique parameters.

5.6.3 Non-identifiability of the Thermodynamic Model

The thermodynamic model was built on the assumption that the air temperature T_2 is distinctly different from the brine water temperature T_4. No prior literature indicated that this was an unreasonable assumption. However, this analysis indicates that this was an unacceptable assumption for this experimental setup. Results show that the two temperatures show similar trends (Figure 5.6.3.1). This shows up clearly with the chosen sampling rate of 0.1 *Hz*. In comparison other studies have tended to involve widely spaced data collection focussed on the end-state rather than intermediate stages, and may have missed this phenomenon [18, 35, 82].
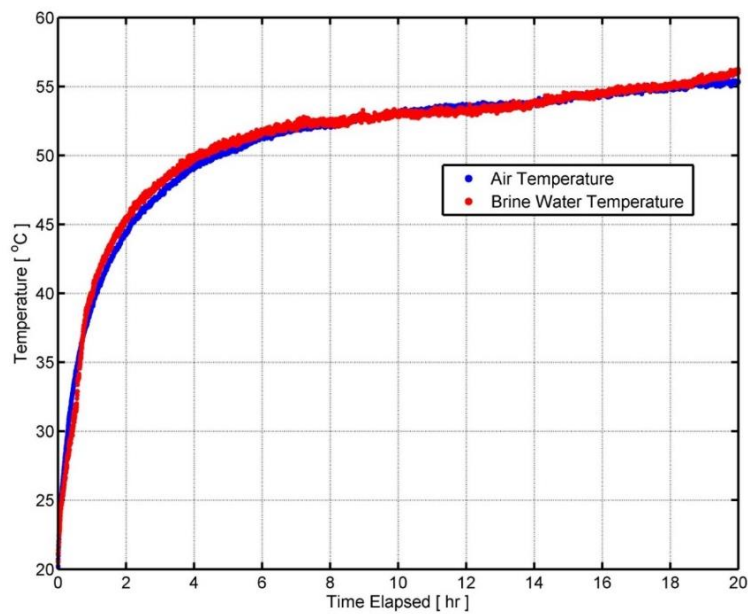
Figure 5.6.3.1: Comparison of internal air and brine water temperatures for *in vitro* test (Test 17)

The consequence of this is that a wide range of k_1 and k_2 parameter values yield good model fits, per Figure 5.6.2.1. The implication is that the sign of k_1 makes no substantial difference to the residual or regression coefficient. The sign of k_1 dictates which way heat is transferred in equation (5.2.1). A negative value of k_1 means T_4 increases with increased incident energy, whereas a positive value contradicts heat transfer laws.

The data obtained through testing show that the thermocouples measuring both air temperature, T_2 and brine water temperature, T_4 were heating up at about the same rate. The following interpretations and causes have been offered:

- This behaviour might be a sensor artefact as both thermocouples were exposed to the same heat flux, (moderating effects of the air and brine may have been negligible. If so, this would bring into doubt the common assumption that sensor temperature is representative of of the surrounding fluid).
- Assuming the sensors were correctly representing their respective fluid compartments, then the implication is that the air and brine temperatures equilibrated rapidly. Rapid equilibration may possibly be caused by turbulent internal flows – which in other areas are known to accelerate heat transfer. In turn turbulent flow might arise from the asymmetrical heating (shadowed regions, directionality of lights, plumes of rising air, geometry of the rig, internal circulation). This consideration implies that to better understand the phenomenon it may be necessary in future to study the internal flow dynamics too. No prior studies deal with internal fluid flow.

Formal practical identifiability methods are relatively new and appeared in literature in 2009 [81]. No prior papers were found to have coupled practical identifiability with checking the robustness of a proposed model.

5.7 Implications for Future Research

The temperature uniformity mentioned prior indicates that possibly another quantity could form the basis of the equation formulation. Specifically, it has been proposed that a more explicit mass balance perspective would enable more robust modelling of the overall system behaviour. Future iterations of the project could focus more on implementation of an accurate vapour mass measurement system. This system would allow for greater modulation of the mass values which are directly obtainable rather than simply providing sufficient data to calculate mass values using a thermodynamic or psychrometric first principles analysis.

The testing clarified that operating conditions at the evaporation and condensation surfaces were significantly different from one another and it was necessary to virtually partition the internal space to account for this. A primary spatial partition was suggested that involved splitting the rig cavity evenly into two internal volumes. The air and vapour properties of each volume were then aggregated into mean internal rig properties. This partition was oversimplified but provided the necessary developmental process to view the single cavity in terms of distinct volumes.

A more sophisticated model was proposed with the internal space partitioned into three virtual volumes, shown in Figure 5.7.1, according to the sensor placement. The first volume (V_{H1}) encompassed the space twice the height from the brine water surface to the humidity sensor. The second volume (V_{H2}) encompassed the space below the condensation surface out of direct exposure to the light source. The third volume (V_{INT}) was the remaining intermediate space between the evaporation and condensation volumes. These volumes were defined by the region that could be assumed to have the properties of the relevant humidity sensor, and have been subscripted accordingly.
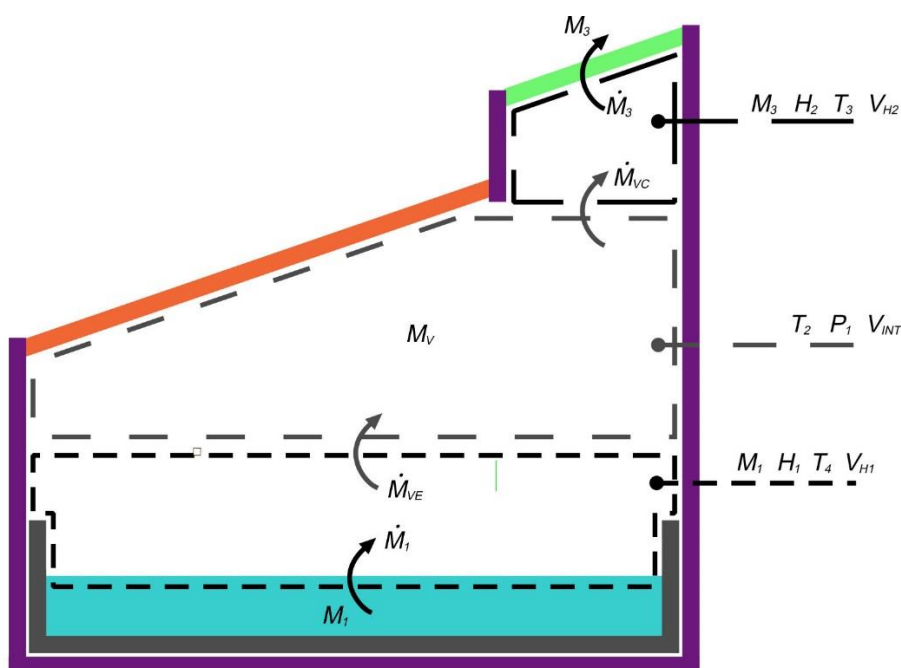
Figure 5.7.1: Virtual partitioning of rig for equation formulation.

This approach reduces the number of explicit equations needed to describe the system, and reduces the overall number of variables required as a result. The trade-off is that intermediate, semi-empirical values are required to fully define the mass balances. The vapour mass quantities (M_V) are introduced as functions of the psychrometric conditions present in the relevant virtual volume. A proposed refined systems-level architecture underpinning the heat transfer process is shown diagrammatically in Figure 5.7.2, based on the prior formulation. As with the initial analysis, each equation is again a first order differential equation.
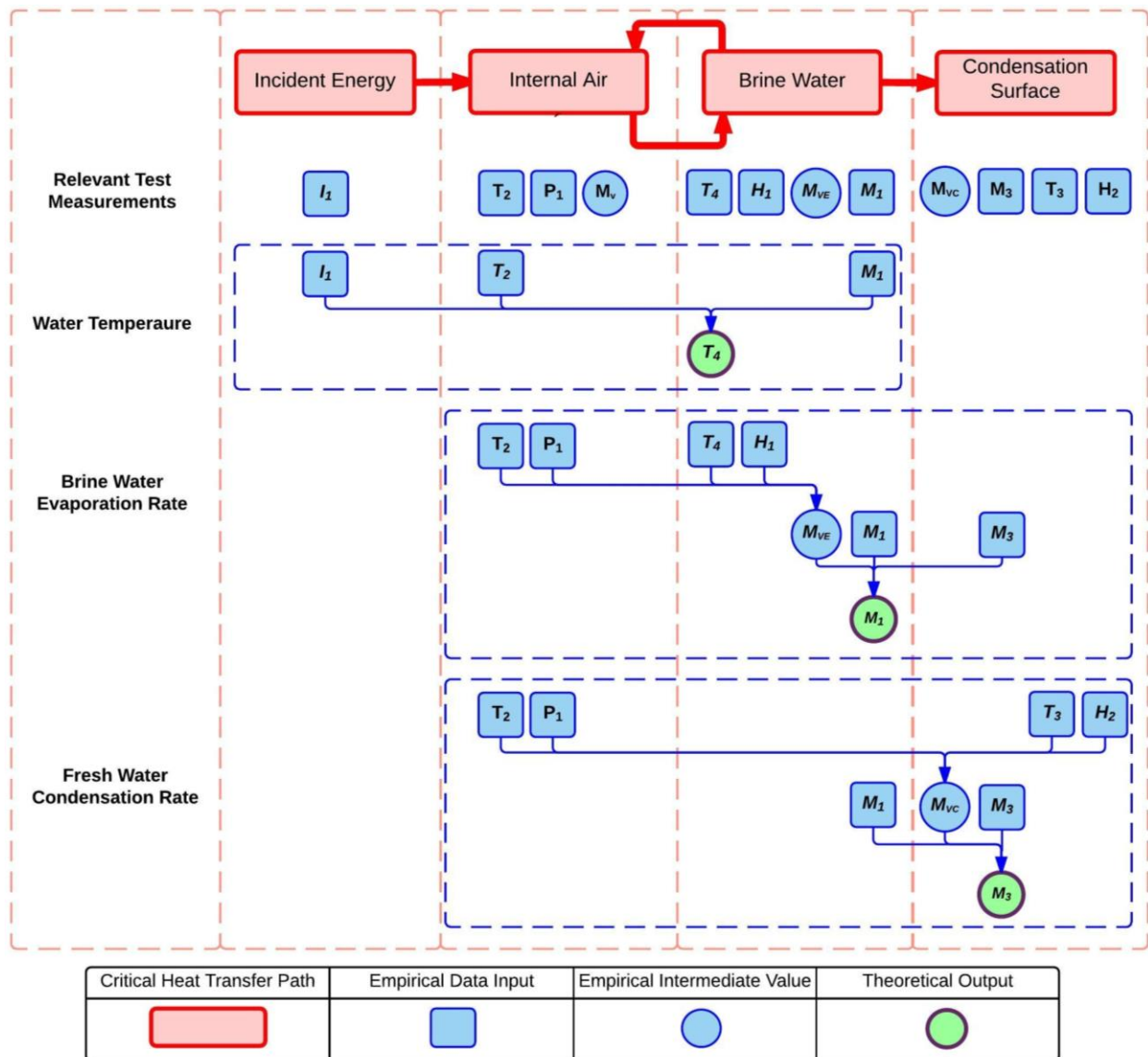
Figure 5.7.2: Refined block diagram representation of equations governing system.

The relationships proposed for each stage are expressed in equations (5.7.1 − 3). The formulation of these equations focussed on mass and energy conservation principles more stringently than the prior equation set presented in Chapter 5.2. There are fewer distinct equations in this proposed model as the emphasis is on output performance metrics rather than the internal system dynamics. Consequently, the detail in each equation is greater than before. These equations require a greater number of input property measurements than the initial formulation.

$$T_4 = \int \left(-k_2 \frac{A_e \, I_1}{C_p \, M_1} - k_1 (T_4 - T_2) \right) dt - \frac{(M_1 - M_1(0)) \, \Delta H_{vap}}{M_1 Cp} \qquad (5.7.1)$$

$$\dot{M}_{VE} = \dot{M}_1 - k_3 M_{VE} + k_4 M_{VC} \qquad (5.7.2)$$

$$\dot{M}_{VC} = k_3 M_{VE} - k_4 M_{VC} - \dot{M}_3 \qquad (5.7.3)$$

The formulation of the brine temperature equation is much the same as before. Energy is transferred into the system at a rate of I_1 and the manifestation of this as a temperature rise is mediated by the brine mass M_1. The temperature difference term accounts for heat transfer between the brine water and air. During *in vitro* testing, this differential was of relatively small in magnitude and thus, precluded robust identification of k_2. Therefore a different strategy for defining the convective energy transfer from brine water to air was implemented. This third term represents the energy lost due to the latent heat of evaporation the brine mass when liberating water from the liquid phase into the vapour phase through evaporation. This accounts for the transfer of energy without a primary dependence on the negligible temperature difference.

Adequate representation of the vapour mass quantities was beyond what was possible with the data collected in this project. A greater number and completely revised configuration of load cell sensors would have to be employed for the proposed equations to be properly validated. The existing DAQ hardware was not capable of these additional measurements and an auxiliary chassis would be required to facilitate extra mass measurements. The initial hardware configuration was considered sufficient to capture all of the information required. It was only identified during the data processing phase that some measurements were redundant while others, previously unidentified in the literature, were of greater importance. Distilled water mass and temperatures at the absorption surface were redundant for the main test phase. A greater number of thermocouples at different points inside the rig air cavity and a more direct means of accurately determining the vapour mass would help with the equation formulation.

The revised method therefore has potential to yield a more robust model. However it would require a new project: new experimental procedures, more sophisticated mass-flow measurements, and a new regime of empirical data collection.

5.8 Summary

This project served as an exploratory investigation into the dynamics of a passive solar desalination system from a theoretical and experimental perspective. The approach was based on first-principles thermodynamics. The model has been constructed from a temperature perspective. An excellent model-fit was obtained to the dynamic behaviours of the system. These parameters may be given a qualitative interpretation as modifying factors for the geometry and implicit unit conversions. The benefit of this approach is that none of the first principles quantities are lost from the equations with inclusion of these parameters. The first attempt at the model included some assumptions that grouped a number of dynamics into single linear terms. Further investigation may elucidate the full value of the identified parameters.

The model exhibited practical non-identifiability in some cases. This is attributed primarily to the small temperature difference between the internal air and the brine water surface, which prevent robust parameter identification from occurring. This differential has been a pivotal element in the equation formulation for prior studies, and the uniformity of temperature may be due a combination of the particular geometry and the *in vitro* lighting array. This problem was not anticipated with the test rig setup and was not described in prior literature. However, the exploratory test phase was sufficient to inform the next phase of design development independent of the model building process. A greater understanding of which elements in the solution space are worth further investigation has been obtained. The subsequent implications for practitioners have been evaluated and summarised in Chapter 6.

6 Implications for Further Product Development and Design

The experimental scope for this project was to ascertain what parameters were worth investigating further and to quantify and qualify the expected performance of the two client-proposed designs. These designs are summarised in Chapters 4.4.1 and 4.4.2. The outcomes and conclusions obtained during the test phase provided an indication as to which areas of the solution space offer viable options for further development. These results have been directed toward providing practitioners with commercially viable, practical and context-relevant way to enhance still performance.

6.1 Design Implications for Practitioners

In this context practitioners are those who are designing and manufacturing solar stills, whether in developed or developing countries. Important functional considerations for further development are summarised visually in Figure 6.1.
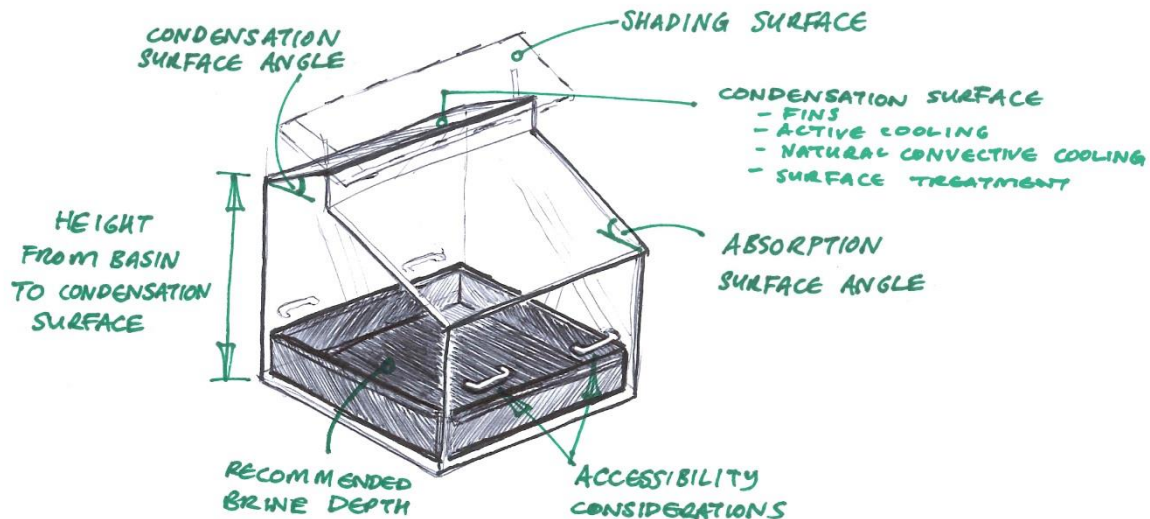
Figure 6.1: Considerations for further concept development based on testing and modelling conducted.

6.1.1 Optimisation of Condensation Surface Cooling

The design intent for this project was focussed on a fully passive design. However, it is important for practitioners to consider the extent to which productivity can be increased using active components. The rig had a 12 W axial flow fan (shown in Figure 4.2.2), operating on a constant duty cycle during the test regime. Performance decreased by 60 $\%$ when this fan was disengaged (Chapter 4.3.3). The fan was originally incorporated as a rudimentary wind representation, and was not intended to be design feature. Therefore fully characterising the forced cooling effect and mechanism was beyond project scope. Future work could involve a detailed investigation of operational states beyond the 'fan on' or 'fan off' options tested to optimise the surface condition. Alternatively, the focus could be shifted to investigating passive means of achieving the desired surface condition.

6.1.1.1 Natural Convective Cooling

The constant air flow effects achieved through active componentry are highly desirable based on the testing results. A fully passive system is desirable for reliability and maintenance reasons. If the convective effects can be replicated without active componentry, this would be a more contextually appropriate solution.

It has been proposed that an extended cover could be integrated to promote desirable convective air movement along the condensation surface in lieu of the fan option. The cover would be intended to concentrate heat onto a small region to initiate natural air flow using the established temperature difference. The less dense air would be directed over the condensation surface using the geometry of the cover, thereby increasing convective heat transfer across the surface. A cover concept has been included in Figure 6.1.1 to exemplify the intended dynamics.
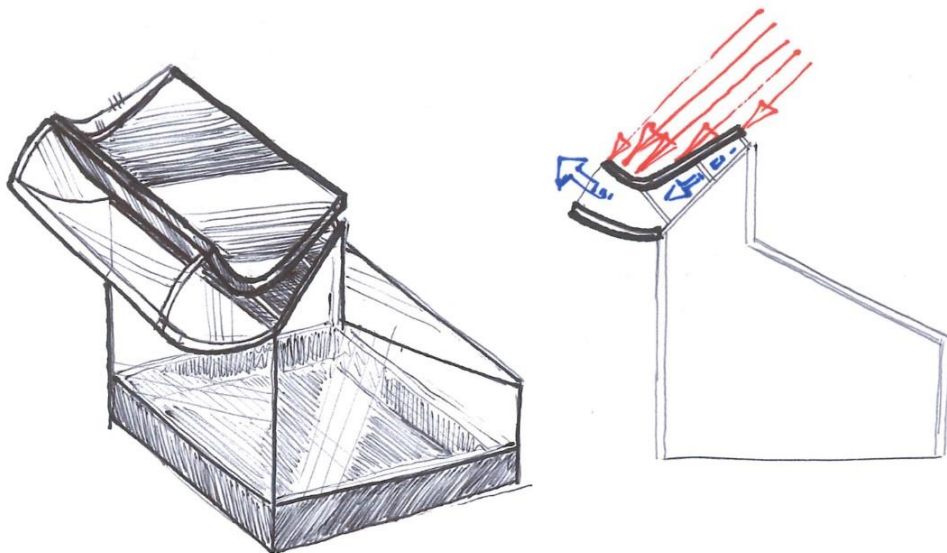
Figure 6.1.1: Conceptual design for passively increasing convective heat transfer over condensation surface. Red arrows represent incident solar radiation.

Testing is required to validate that this configuration would not risk heating the condensation surface. The efficacy of the modification would be dependent on the temperature gradient that could be established between the heat concentration region and the ambient air above the condensation surface.

A 20 °C temperature rise at the condensation surface was observed after disengaging the fan. This led to the assumption that the fan provided thermodynamic benefit (surface cooling that enhanced condensation) rather than mechanical benefit (surface vibration that enhanced distillate movement to the collector). These two dynamics were unable to be decoupled with the current rig apparatus. Further work should consider isolating the vibration and cooling dynamics, to see the relative impact of each. If vibration is identified to be a significant factor, this offers scope for easier passive means to achieve the desirable condensation than using a cooling fan. This vibrational element may be a rod or wire connected to the surface that oscillates in the wind.

6.1.1.2   Active System Cooling

Forced cooling of the condensation surface was not foreseen as a crucial element as the majority of experimental studies in the literature review [1, 7, 16-18, 20-23, 27, 30, 33, 36, 39, 40, 56]. These studies were concerned with purely passive systems and none mentioned use of a cooling fan. However, the system performance reduction without the fan was so dramatic that it was judged necessary to give some consideration to active options. This outcome has highlighted that some form of cooling mechanism is necessary for system functionality. In reality, the wind behaviour cannot be reasonably assumed to be match the consistency of a fan, so the intention to provide this cooling with wind alone is insufficient.

The fan used during the test phase required a 12 *W* power input which could be provided by a relatively small PV solar panel in context. Connection to grid electricity is not necessary. The panel may also provide shading for the condensation surface as a multiple-effect addition to the unit. This option could be assessed under the reliability engineering framework (Chapter 4.3.7.5) to quantify whether the added complexity was justified through the productivity increase. This active option needs to be compared to whether the PV panel would be better utilised boiling brine water directly with a kettle.

The fan geometry and placement need to be considered in greater detail. A conceptual representation of possible fan and PV panel configurations is shown in Figure 6.1.2. Optimal air flow may be realised through use a series of axial computer fans (*a*) or single centrifugal fan (*b-c*). Both options would direct air movement along the gradient of the slope rather than perpendicular to it. The perpendicular fan arrangement was used during the test phase (Figure 4.2.2), and results in an asymmetric thermal distribution across the length of the condensation surface. Alternative fan placement to more effectively cool a greater area of this surface would be expected to increase performance.

| (*a*) | (*b*) | (*c*) |
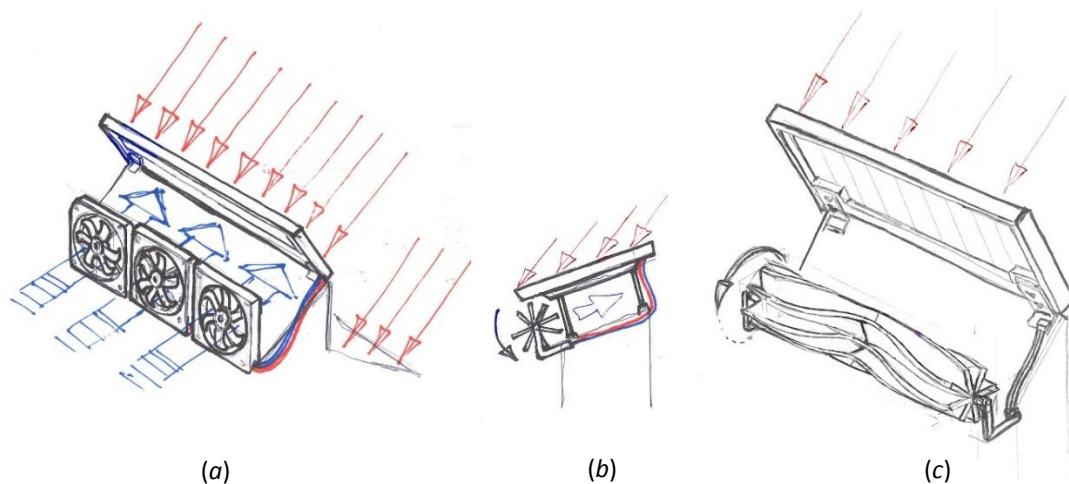
Figure 6.1.2: Conceptual fan configurations for further development of actively cooling condensation surface; forced airflow shown in blue. (*a*) An array of three axial fans (*b-c*): Single centrifugal fan. Red arrows represent incident radiation striking PV panel.

6.1.1.3   Mapping of Temperature Distribution

The next testing iteration would involve more comprehensive sensor placement on the condensation surface. Sensor and DAQ availability meant that only a single thermocouple was allocated to measure this surface, precluding a spatial temperature profile to be established. As a result, the region of influence of the fan was unknown. Clarification of this region would provide definite boundaries on the optimal unit size that could be cooled by a similar fan. It would be beneficial for active systems optimisation to devote multiple thermocouples to mapping the thermal profile of the condensation surface, and potentially include tuft wands to facilitate flow regime visualisation. Possible thermal measurement and flow visualisation arrangements are shown in Figure 6.1.3.

(*a*)   (*b*)
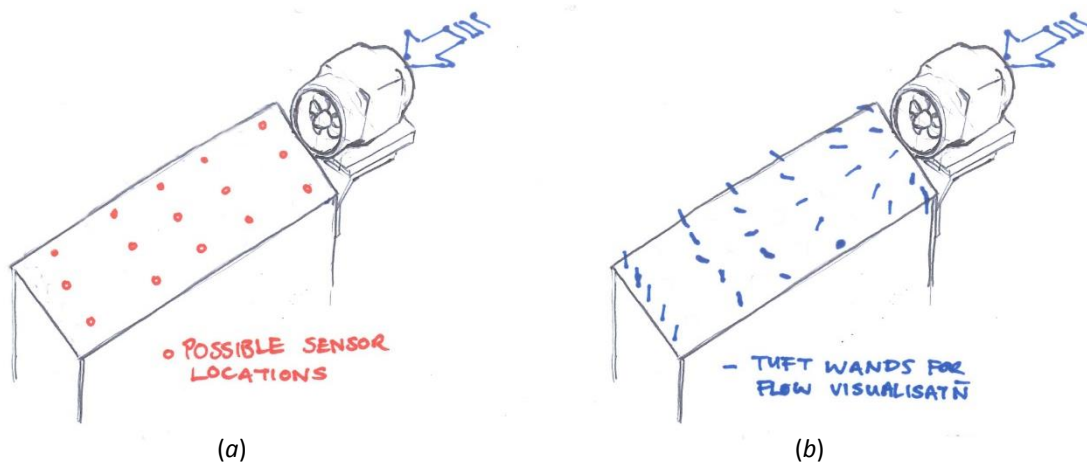
Figure 6.1.3: Proposed sensor positions to comprehensively map thermal profile on condensation surface (*a*) and tuft wand positions as means to visualise flow dynamics (*b*).

6.1.2 Optimisation of Desired Heat Transfer Regimes

The initial testing has emphasised the critical importance of cooling the condensation surface (60 *%* performance decrease occurring from 20 *°C* rise in surface temperature). The original design intent was for develop of a fully passive design to suit the DC context and so options aligned with this are more favourable.

The brine can be heated by means of a solar concentrator or pre-heater unit to promote more rapid evaporation. However, if the condensation surface is not cool enough to liqueify the vapour, then the system fails to perform. There is an abundance of heat in the Pacific, so the evaporation-surface heat transfer dynamics are easily realised. However, transferring heat away and maintaining a cool space is not so readily established and maintained.

6.1.2.1 Addition of Heat Fins

The condensation surface tested was an untreated, flat sheet of aluminium. It has been proposed that the heat transfer capacity of the sheet may be increased with the addition of cooling fins. Fins would provide a greater contact area for convective heat transfer between the surface and ambient air. Trialling different fin designs to optimise heat dispersion has been judged an important next step in the development process. The effects of both rod and plate type fins could be compared against one another and against a non-finned surface to extend the work conducted during the current study. Possible fin configurations are represented in Figure 6.1.4.
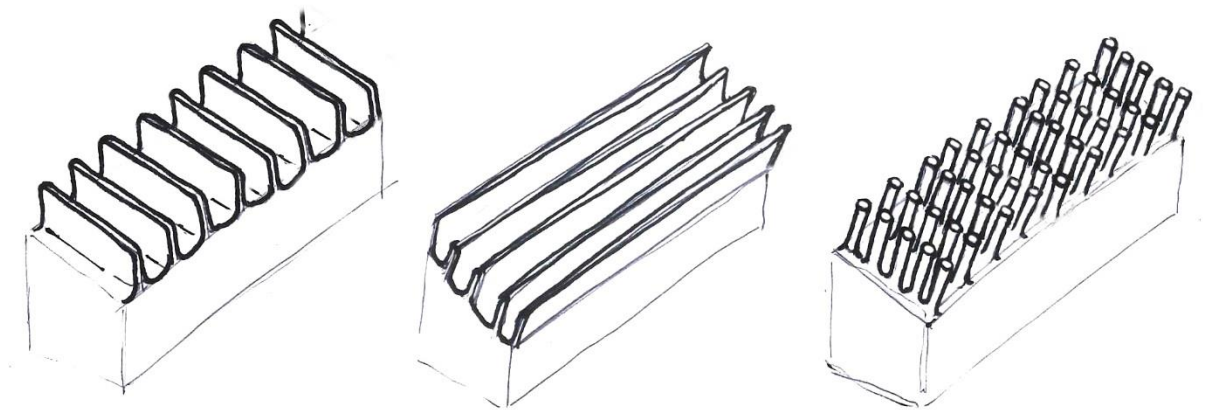
Figure 6.1.4: Possible fin configurations to increase convective heat transfer at condensation surface.

6.1.2.2 Addition of Shading Surface

A single shade surface configuration was tested as part of the regime of the current study, which was shown to increase condensation by 25 %. A conceptual representation of possible shading surface configurations is shown in Figure 6.1.5. Relevant shade surface parameters have been identified as pitch (P), overhang (O) and offset (T) as labelled in Figure 6.1.5 (*c*). Further modulation of these parameters under solar conditions would provide a more comprehensive understanding of how to optimise passive surface cooling. The choice of surface material, treatment and finish are anticipated to the cooling performance of the shade surface.
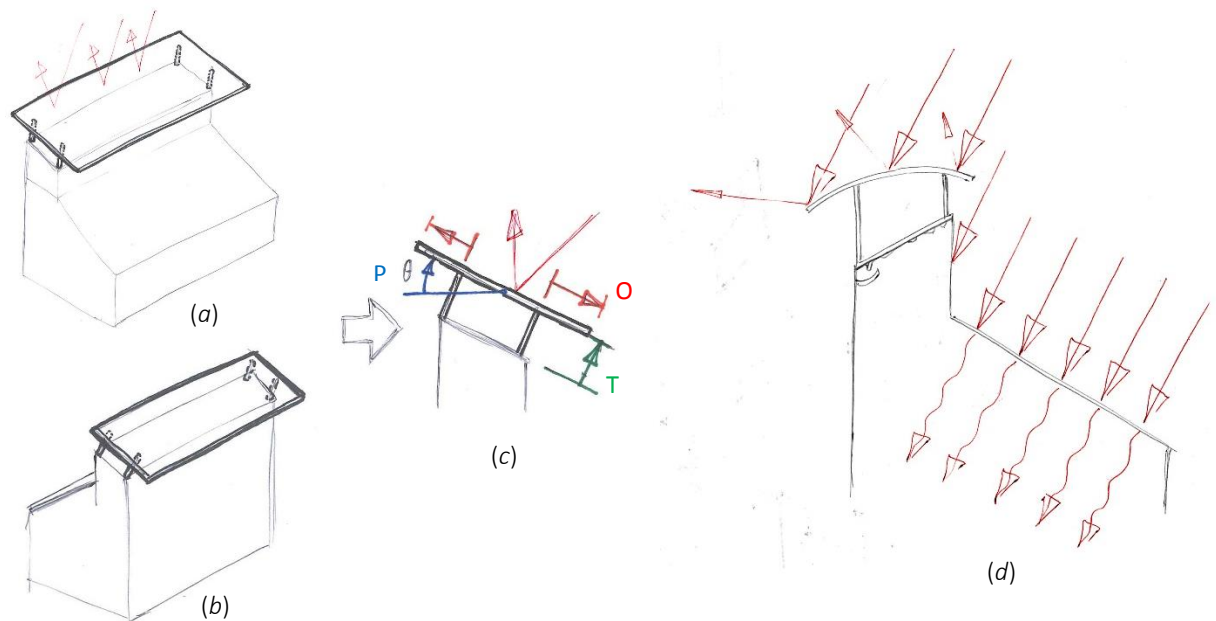
Figure 6.1.5: Possible passive shading configurations to decrease direct solar energy (red arrows) incident onto condensation surface. Planar shade surfaces parallel (*a*), and oblique (*b*) to absorption surface. Identified shade surface parameters (*c*), curved shade surface deflecting direct solar energy (*d*).

The rig used for the current study had a dedicated PC absorption surface. The lighting array for *in vitro* testing was constructed so only the absorption surface was heated. This feature had adverse effects when the rig was tested under solar conditions as the plywood sides shaded the basin during early morning and late evening periods. As a result, it was judged advantageous to investigate constructing the entire unit; except for the condensation surface, from PC or another non-opaque structural material. This choice offers the potential to increase the incident energy absorbed by the basin and brine water over a day. The majority of the unit has the potential to become an absorption surface. Therefore precise positioning to maximise energy absorption is not as crucial as the unit has a greater degree of omnidirectional functionality.

6.1.3 Optimisation of Condensation Surface Geometry and Surface Treatment

A large portion of the literature studied was concerned with variations of the SSSS [1-3, 20, 21, 23, 39, 83]. An inherent weakness in this design was elucidated during testing. Optimal conditions for water condensation and energy absorption act antagonistically to one another, which act to limit performance.

An optimal absorption surface should have exposure to the maximum amount of solar radiation to ensure the brine is heated as much as possible. Conversely, the condensation surface should be maintained at the lowest temperature available to promote the distilled water vapour to liquefy and collect upon it. A single surface designed to facilitate both dynamics will inherently compromise on one. This dual functionality justified the design choice to maintain two distinct surfaces, despite the increased manufacturing complexity. There is scope for further optimisation of the condensation surface dynamics, which was beyond the modular capacity of the current rig.

6.1.3.1 Optimisation of Inclination Angles

The absorption surface must collect as much energy from the sun as possible so the optimal angle depends on geographic conditions and latitude [21]. The condensation surface, however, must be optimised toward condensing as much water vapour and transporting this to the collection receptacle as possible, with minimum drip-back into brine water basin. This inclination angle is independent of the geographic conditions, but benefits from facing away from the direction of incident solar energy. A steeper inclination of the condensation surface will promote more rapid transport of the condensate to a receptacle. However, this dynamic is limited by the greater potential for drip-back due to the self-weight of the droplets. The optimal angle will be dependent on the material selected for the condensation surface, as this has been shown to influence droplet formation and transport [22]. The surface will get also progressively hotter surface as it approaches the brine basin, so will contribute less to additional condensation potential. The scope of future work could involve designing a test rig that allows modulation of the condensation angle through the widest range possible, as conceptualised in Figure 6.1.6. This range may even consider allocating the entire back surface to be the condensation surface as a limiting case (*i.e.* vertical condensation surface).
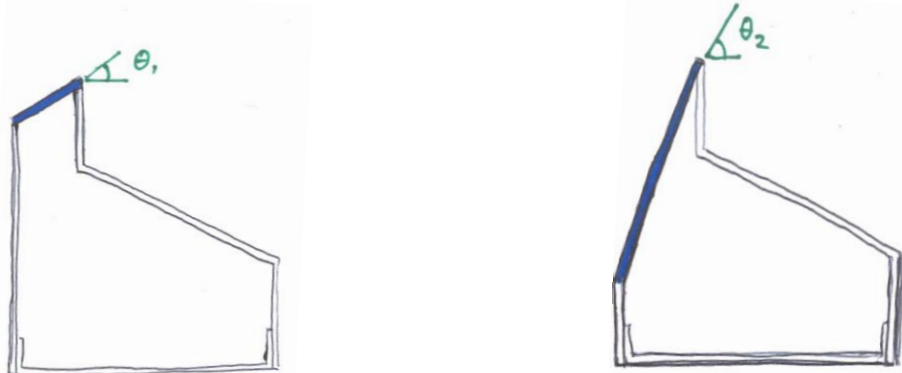
Figure 6.1.6: Variation of condensation surface angle to optimise distillate collection

6.1.3.2   Drip-back Catchment Tray

The extent to which drip-back occurred was unable to be measured or observed with the current test rig configuration. It has been proposed that a secondary catchment surface be added to the rear surface, as shown in Figure 6.1.7, to indicate the extent to which drip back is occurring. The vertical location of the surface would place it in a hot enough region that condensation on the bottom would be inhibited.
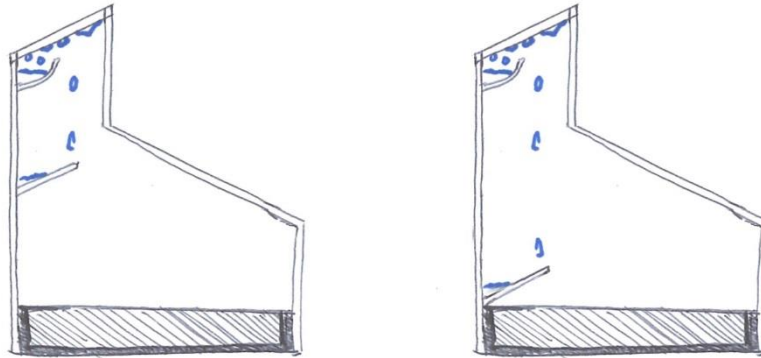
Figure 6.1.7: Secondary catchment tray to decrease distilled water lost through drip-back.

The vertical location of this secondary surface would be informed by subsequent testing. To limit shading the brine water or inhibiting vapour motion to the condensation surface, the secondary surface may be a wick material that allows both light and water vapour through, but captures distilled water droplets as they fall.

A secondary surface adds complexity to the fabrication process and this may be avoided through further research into the condensation surface finish; explicitly roughness and coating. The optimisation here would be focussed on promotion of film-wise rather than drop-wise condensation regimes if drip-back is an appreciable concern.

6.1.4   Design Scalability

A series of small scale rigs with approximately one sixth of the plan area of the primary test rig were investigated as a secondary project during the primary test phase. This work was undertaken by Lap Kei (Michael) Leung with assistance from the current author. These smaller rigs produced proportionally much less condensate than the primary rig despite a variety of modified operating parameters. Only provisional data has been presented in the current study as comprehensive results from the secondary work were unavailable at the time of writing. The distillate collected in these small rigs averaged 0.5 *%* of the initial 1 *kg* water input. This quantity was significantly lower than the reference conditions for the primary rig. This result is indicative that the same system dynamics do not apply at differential length scales. The rigs have been represented graphically in Figure 6.1.8.

$A \simeq 1.0 m^2$ (*a*) $A \simeq 0.16 m^2$ (*b*)
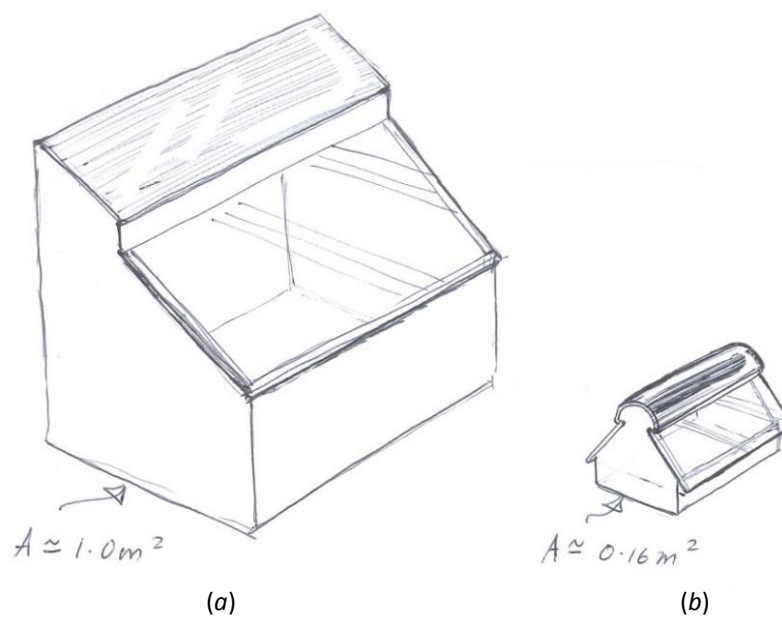
Figure 6.1.8: Primary rig (*a*) and translation as secondary rig (*b*) indicative of relative size.

Results established that unit size influences the ease with which a particular temperature difference can be realised under particular energy input. For a given energy source and cooling apparatus, one effect will dominate if the two are in closer proximity. The regions of direct influence overlap to a much greater extent at smaller length scales. This overlap directly inhibits the magnitude of the temperature difference that may be established. The first testing phase has indicated that a unit with a 1.0 *m²* plan area is significantly more effective than a unit with a 0.16 *m²* plan area.

In terms of deploying the units to nations in the Pacific, all components must fit easily in a shipping container. It is also critical that the components are compatible with the on-land transport available to get them to the intended location. These end user considerations put a practical upper bound on the unit size that is more important than bounding the size based on thermodynamic considerations. The primary test rig represented the maximum size that can be easily transported in a standard van.

6.1.5 Thermal Storage Mechanisms and Brine Mass in Basin

A thermodynamic analysis considering typical ambient conditions prevalent in Pacific nations was conducted to evaluate the efficacy of integrating thermal storage mechanisms into the design. The benefits of thermal storage in a design are realised more fully as the day-night temperature difference becomes greater. As the external ambient temperature drops after sunset, the thermodynamic driver for heat transfer out of the unit increases.

When the internal condensation surface has cooled to a temperature below the dew point temperature, vapour in the air will continue to condense. This process aided by the heat loss to ambient air. If a thermal storafe mechanism maintains the brine water at an elevated temperature, then the unit has the potential to continue distillate production for a period after sunset. The thermal storage acts as on overnight heat source for the system and increases the evaporative heat transfer coefficient between the brine and condensation surface [28]. The day-night temperature variation in is typically on the order of 2 $°C$ in Tonga [11], which is indicative that there is limited benefit to incorporating thermal storage in this context. The relevant literature conducted tests in locations where the day-night temperature range was typically between $13 - 16$ $°C$ [28, 29]. This temperature difference was greater than what is possible in the context of this study.

The exclusion of thermal storage influences the optimal brine depth for the unit. With an assumed negligible capacity for overnight production, the unit is suited to inputting the smallest mass of brine water possible that does not require refilling over the course of a day. A smaller brine water mass has less thermal inertia than a larger mass and will therefore reach a high enough temperature to begin accelerated evaporation in a shorter time period.

The salinity testing (Chapter 4.3.4) indicated that typical Tongan seawater concentrations did not influence the productivity rate. No appreciable drop off in evaporation rate was observed even as the brine water in the basin approached zero. It was observed through the testing that the current configuration evaporated approximately 1.8 kg of brine water in a 12 hour period under energy input conditions typical of what is expected in Tonga. Evaluating the current unit capability and the expected potential of incorporating thermal storage, a daily input of approximately 2.0 L would be expected to be optimal as the unit would not have to be refilled during sunlight hours.

---

[11] Data obtained from the NASA Langley Research Center Atmospheric Science Data Center (see Appendix 02)

6.1.6 Optimisation of Unit Height

In moving from polar to equatorial locations, the path of the sun tracks closer to directly overhead. As a result, the potential for the side walls to cause undesirable shading of the brine water surface decreases closer to the equator. In context, there is less emphasis on reducing the unit height to limit undesirable shading of the brine water surface than if the unit was intended for more polar regions. As such, the unit can have greater height to maximise the evaporation side – condensation side temperature difference without compromising the flux of direct energy.

The performance was found to have poor scalability at smaller sizes. Two distinct conditions are required for the system to produce distilled water; a hot evaporation surface and a cool condensation surface. In order to achieve both of these conditions, it has been assessed that the distance between surfaces plays an important role in distillate productivity.

Further testing of the overall unit height would inform design development as to the minimum distance required between the evaporation and condensation surfaces. This minimum distance would ensure the least amount of material is required, while maintaining surfaces that are effectively thermally independent of one another. The optimisation for this process involves maximising the temperature difference (assuming the evaporation surface is effectively constant) while using the least amount of material to keep costs low and transportation easy. The solution space is represented schematically in Figure 6.1.9.
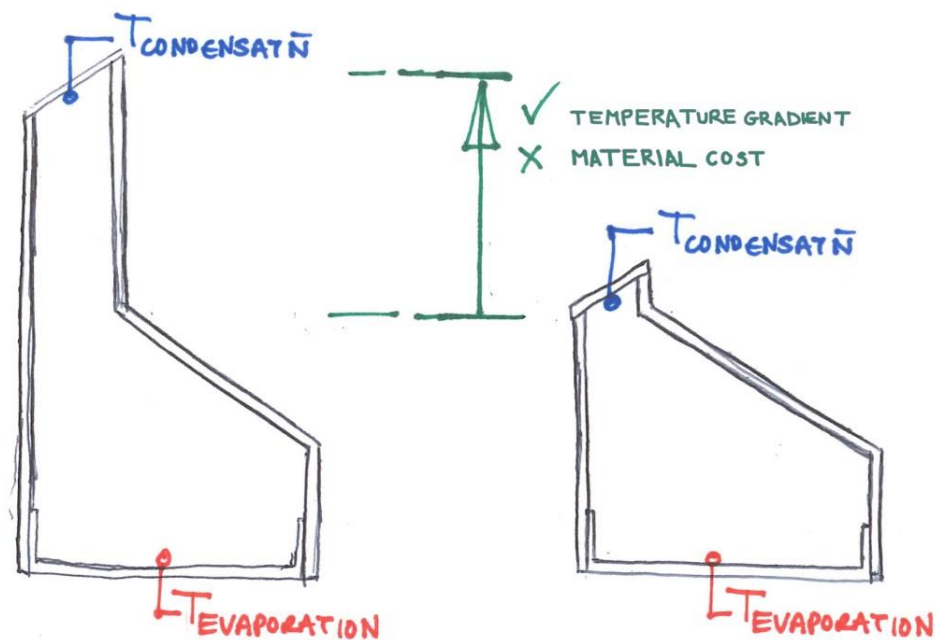
Figure 6.1.9: Conceptual representation of most important aspects of height optimisation.

6.1.7 Unit Ownership

Considering Deployment Principles 2.2 and 2.8 from the DC study (Chapter 4.3.8), the concept of instilling pride, affiliation and attachment to an implemented design is critical for its success. The needs of the user must form the basis for the project. The solution must either address a concern identified by the intended users or communicate effectively why their current practice needs adjustment. The first option is preferable. With this basis, the relevance of design and the benefits it offers is ingrained into the end user from the start.

Utilising Deployment Principle 2.2, it has been proposed that the desalination units be transported to location and then constructed to maximise their integration with the community they service. If local people are involved with the construction process they will have a greater propensity and competency for repairing the unit themselves. The implementation of a novel technology has to be viewed as a desirable addition to the community it services. The people must feel that it is their solar desalination unit and that they will benefit from its continued operation for it to remain in an operable state. The major design features and structure should be determined prior to deployment, but the process should be fluid enough to incorporate informal changes if they add value to the end users. Such changes have the potential to utilise local knowledge on expected situational conditions (people, weather, animals) that may be overlooked by an outsider.

6.1.8 Optimisation of Unit Accessibility

The unit requires at least one opening or separation point for filling and emptying. The larger the opening, the easier the unit will be to clean but this comes at the expense of increased potential for sealing failure. The water collection system is intended to produce potable water, which prioritises the ease of cleaning and inherent measures inhibiting contamination highly.

In the Pacific context, the growth and spread of contaminants is of high concern. In accordance with Deployment Principle 2.5 from the DC study (Chapter 4.3.8), it cannot be assumed that the intended cleaning cycle will be maintained once the unit is deployed. The design needs health and safety precautions built in to the functionality, not as an optional alternative.

Hygiene, structural integrity and simplicity are key aspects of the solution space when considering how the unit can be accessed in between cycles. The test rig had a removable rear panel as shown in Figure 4.2.2, although this required additional securing measures to keep it in position.

It has been proposed that the entire unit; with the exception of the condensation surface, could be made from PC sheet. This choice has been based on the relatively high brittle failure potential of glass compared to PC, both of which are viable solar still materials. Additional structural components are required to make a glass unit and the choice of glass precludes maximising the absorption surface. The community perceptions of the proposed design will influence the material choice. Community aversion toward using glass may be an issue (Chapter 4.3.8.4.2) that requires consideration of. The brine basin would be a separate PC structure which would act as the male part of the assembly, as represented conceptually in Figure 6.1.10 (*a*).
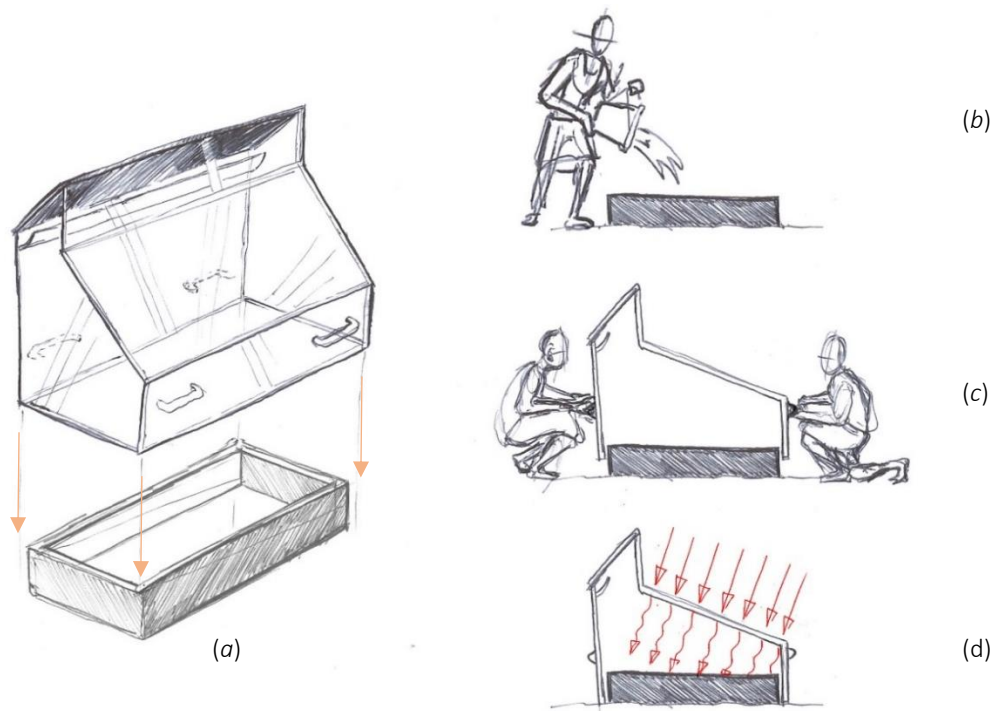
Figure 6.1.10: Conceptual representations of hygienic and easily accessible rig geometry. Basin and cover assembly (a), filling of basin (*b*), insertion of cover piece (*c*) and operation (*d*).

The relatively lightweight external PC structure would be designed with an ergonomic focus so two people could easily lift it from the brine basin and place it back on. The basin could either sit flush with the edges of the structure (utilising a rubber seal around the perimeter) or there could be a small gap between the two functional elements. The PC component would touch the ground and therefore may pick up soil or organic matter depending on location. For sanitation purposes, a small gap between the brine basin and external structure would help to mitigate direct contact between the brine water and organic matter on the ground.

The necessity of hermetically sealing the unit needs to be the primary focus of further project iterations. This design concept would be significantly easier to fabricate, maintain and repair if imperfect sealing did not prove to be detrimental to distillate productivity. The ergonomics and sanitation of the design would be evaluated with a regime of usability tests once an easily fabricated design has been decided and this would feed back into further design development. Future work should involve exploring the PC material choice in terms of surface degradation due to either UV or abrasive particle exposure (salt, sand). These phenomena were was not observed over the time scale of the current project.

6.1.9   Brine Basin Modifications

For hygiene purposes and ease of use it is advantageous to have a separate brine basin. The mobility of the basin will help to both moderate the salt accumulation and facilitate ease of cleaning. The testing for this project involved using only a simple basin design with a single compartment. Potential exists to increase the available evaporative surface area with a wick or a baffle arrangement, or a combination of the two. The baffle would minimise the occurrence of water slop during transportation if it is easier to fill the basin at the shore then transport it to the intended location.
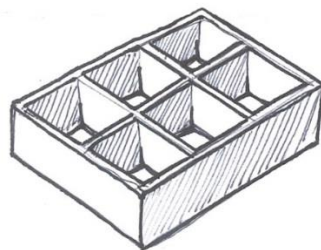
Figure 6.1.11: Concept for baffle arrangement to increase evaporative surface area.

It has been proposed that design solutions in DC contexts are more readily accepted if they are designed with multiple functionalities [76]. With this concept in mind, the practicality of retrieving the salt for further use should be investigated. The crystallised salt was easily removed from the basin during the test regime and no permanent scaling evolved on the PE basin liner. Further work in this area could investigate the commercial potential of integrating salt production as a secondary function of the unit. If this option is unviable, the basin will still require scale removal. Further embodiment design work will involve a materials selection process to isolate a thermally conductive material which is as resistant to UV degradation and scale build-up as possible.

6.2 Summary

A design strategy has been proposed that outlines implementing a solar still in a Pacific nation context, based on the results of the current study. This strategy has considered the relevant social and technical factors that are anticipated to influence solution suitability in such a context.

In application, a future development of a passive solar still would establish the community need, decide on the physical envelop (sizes) of the product, perform the detailed design of functional geometry, and conduct tests with users in the field to validate product suitability. It will also be necessary to decide on whether or not to include electrical power, e.g. by PV panels. The manufacturing will need to be considered, especially if local peoples are to be involved. There is also the matter of reliability and maintenance to consider at design time. This strategy is represented in Figure 6.2.1 as a sequential flow chart covering the systems-level elements of the process.
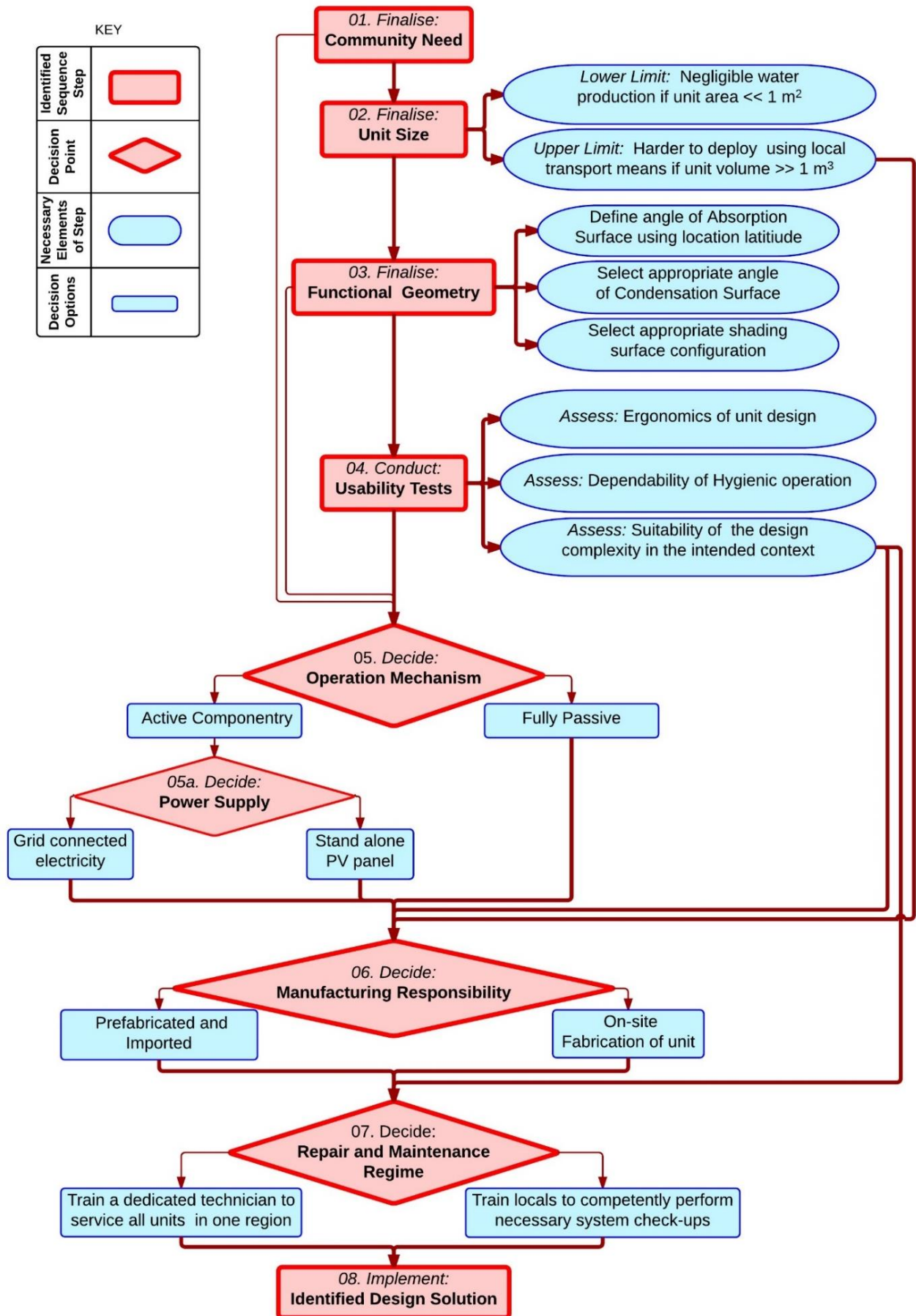
Figure 6.2.1: Systems-level design strategy for implementing solar still.

7 Conclusions

Orginality

This work makes several original contributions. The first is the explicit identification of relative humidity and quantification of the effect.

Fundamental gaps were found to exist in the body of knowledge pertaining to passive solar desalination as outlined in Chapter 2.4. The decision was made to focus the experimental regime on internal relative humidity as the acknowledgement of this parameter had been ignored in all of the studies reviewed with the exception of one conducted by Ahsan *et al* [5]: they had acknowledged that the measured internal relative humidity was substantially below saturated, but still assumed saturated operating conditions for convenience. The testing conducted by Ahsan *et al* was in Malaysia [5], where the ambient relative humidity is typically between 84 - 88 *%.* The current project was conducted in Ōtautahi, Aotearoa (Christchurch, New Zealand) where the ambient relative humidity during the period was found to be, on average, 59 *%*. Based on this consideration it was assumed that the internal relative humidity during testing was below saturated.

The current study has foccused on obtaining relative humidity data and integrating this into the subsequent thermodynamic model-building phase. This focus was in response to the lack of acknowledgement of this quantity as a system variable in the literature studied.

The results showed a general decrease in humidity over the course of a single test. The system humidity only rarely approached saturation levels at the condensation surface. The inclusion of relative humidity in the governing equations meant that the proposed models fitted the data particularly closely and the residual errors were smaller than the only other study that disclosed their error calculation methods [12].

A second contribution is the development of a dynamic model of system behaviour, including the temporal production rate of condensed water over the day. The system behaviour was described using a set of five differential equations which were combined into a single equation, as shown in Chapter 5.4. These equations had a basis in first-principles thermodynamics. At most, only two experimental coefficients were associated with each equation and these were relatable to physcial quantities of the system. This majority of literature reviewed presented system equations in a curve-fit form that did not relate specifically to the underlying physics of the desalination processes occuring. The predictive power of the model was weaker than desired, however it produced excellent fit to the data acquired. An alternative system architecture has been propoed to increase robustness of the parameter identification and therefore the predictive power of the model. This architecture would require a new experimental regime and instrumentation arrangement and offers a starting point for future work.

The third contribution of the work is the identification of development principles for NPD in the context of developing countries. A process has been identified and principles established. The NPD literature is otherwise focussed almost exclusively on the commercial process for developed countries.

A fourth contribution has been the evaluation of two innovations proposed by the client. These were the Open Air and Low Pressure design concepts. Both have been shown to have poor viability.

A fifth contribution is the introduction of the concept of 'Lost Utility' to compare the functional benefits of greater technical complexity against the reliability issues that arise in developing countries. The anticipated performance increases must be compared to the decreased operational reliability during design life. A generalisable framework was constructed that allows the modified unit to be compared to a basic system.

A sixth contribution was the identification of the key importance of the condensation surface. The most influential factor to system performance was found to be the condition of the condensation surface. A 20 $°C$ change in temperature of this surface induced by disengaging the cooling fan reduced performance by 60 $\%$. Testing highlighted the crucial importance of keeping this surface cool. The brine can be heated by means of a solar concentrator or active pre-heater to promote more rapid evaporation. However, if the condensation surface is not cool enough to liquify the vapour, the system fails to function. There is an abundance of heat in the intended Pacific context, however maintaining a cool space is not so readily available. Several measures have been proposed to optimise the condensation surface properties and therefore maximise productivity, (see Chapter 6.1).

Outcomes

The purpose of this work was to obtain quantitative knowledge of which climatic, operational and design parameters have the greatest influence on maximising productivity for the chosen geometry of solar still, the relationships between those parameters, and the implications for design.

The results as determined from a purpose-built experimental apparatus have identified that the key parameters are: cover material for absorption surface, cooling of condensation surface, geometric scalability, internal temperatures, and humidity.

The work resulted in a set of governing equations that described the dynamic response of the system over a representative day. The knowldege extracted through the analysis was applied toward assessing the suitability of several still designs. Implications were identified for further design.

References

1. Kalidasa Murugavel, K., K.K.S.K. Chockalingam, and K. Srithar, *Progresses in improving the effectiveness of the single basin passive solar still.* Desalination, 2008. **220**(1–3): p. 677-686 DOI: http://dx.doi.org/10.1016/j.desal.2007.01.062.

2. Muthu Manokar, A., K. Kalidasa Murugavel, and G. Esakkimuthu, *Different parameters affecting the rate of evaporation and condensation on passive solar still – A review.* Renewable and Sustainable Energy Reviews, 2014. **38**: p. 309-322 DOI: http://dx.doi.org/10.1016/j.rser.2014.05.092.

3. Muftah, A.F., et al., *Factors affecting basin type solar still productivity: A detailed review.* Renewable and Sustainable Energy Reviews, 2014. **32**: p. 430-447 DOI: http://dx.doi.org/10.1016/j.rser.2013.12.052.

4. Xiao, G., et al., *A review on solar stills for brine desalination.* Applied Energy, 2013. **103**: p. 642-652 DOI: http://dx.doi.org/10.1016/j.apenergy.2012.10.029.

5. Ahsan, A., et al., *Parameters affecting the performance of a low cost solar still.* Applied Energy, 2014. **114**: p. 924-930 DOI: http://dx.doi.org/10.1016/j.apenergy.2013.08.066.

6. Khalifa, A.J.N. and A.M. Hamood, *Performance correlations for basin type solar stills.* Desalination, 2009. **249**(1): p. 24-28 DOI: http://dx.doi.org/10.1016/j.desal.2009.06.011.

7. Nafey, A.S., et al., *Parameters affecting solar still productivity.* Energy Conversion and Management, 2000. **41**(16): p. 1797-1809 DOI: http://dx.doi.org/10.1016/S0196-8904(99)00188-0.

8. Kamal, W.A., *A theoretical and experimental study of the basin-type solar still under the arabian gulf climatic conditions.* Solar & Wind Technology, 1988. **5**(2): p. 147-157 DOI: http://dx.doi.org/10.1016/0741-983X(88)90074-4.

9. Al-Hinai, H., M.S. Al-Nassri, and B.A. Jubran, *Effect of climatic, design and operational parameters on the yield of a simple solar still.* Energy Conversion and Management, 2002. **43**(13): p. 1639-1650 DOI: http://dx.doi.org/10.1016/S0196-8904(01)00120-0.

10. Tiwari, G.N. and Madhuri, *Effect of water depth on daily yield of the still.* Desalination, 1987. **61**(1): p. 67-75 DOI: http://dx.doi.org/10.1016/0011-9164(87)80007-3.

11. Soliman, S.H., *Effect of wind on solar distillation.* Solar Energy, 1972. **13**(4): p. 403-415 DOI: http://dx.doi.org/10.1016/0038-092X(72)90006-0.

12. Dimri, V., et al., *Effect of condensing cover material on yield of an active solar still: an experimental validation.* Desalination, 2008. **227**(1–3): p. 178-189 DOI: http://dx.doi.org/10.1016/j.desal.2007.06.024.

13. El-Sebaii, A.A., *Effect of wind speed on active and passive solar stills.* Energy Conversion and Management, 2004. **45**(7-8): p. 1187-1204 DOI: http://dx.doi.org/10.1016/j.enconman.2003.09.036.

14. El-Sebaii, A.A., *Effect of wind speed on some designs of solar stills.* Energy Conversion and Management, 2000. **41**(6): p. 523-538 DOI: http://dx.doi.org/10.1016/S0196-8904(99)00119-3.

15. Castillo-Téllez, M., et al., *Experimental study on the air velocity effect on the efficiency and fresh water production in a forced convective double slope solar still.* Applied Thermal Engineering, 2015. **75**(0): p. 1192-1200 DOI: http://dx.doi.org/10.1016/j.applthermaleng.2014.10.032.

16. Akash, B.A., M.S. Mohsen, and W. Nayfeh, *Experimental study of the basin type solar still under local climate conditions.* Energy Conversion and Management, 2000. **41**(9): p. 883-890 DOI: http://dx.doi.org/10.1016/S0196-8904(99)00158-2.

17. Abu-Hijleh, B.A.K. and H.M. Rababa'h, *Experimental study of a solar still with sponge cubes in basin.* Energy Conversion and Management, 2003. **44**(9): p. 1411-1418 DOI: http://dx.doi.org/10.1016/S0196-8904(02)00162-0.

18. Mahdi, J.T., B.E. Smith, and A.O. Sharif, *An experimental wick-type solar still system: Design and construction.* Desalination, 2011. **267**(2–3): p. 233-238 DOI: http://dx.doi.org/10.1016/j.desal.2010.09.032.

19. Medugu, D.W. and D.I. Malgwi, *Design and development of solar still for effectiveness in eliminating microbial contamination and salt in Mubi, Adamawa State, Nigeria.* Nigerian Journal of Physics, 2006. **18**(2): p. 203-210 DOI: http://dx.doi.org/10.4314/njphy.v18i2.38104.

20. Tiwari, A.K. and G.N. Tiwari, *Effect of water depths on heat and mass transfer in a passive solar still: in summer climatic condition.* Desalination, 2006. **195**(1–3): p. 78-94 DOI: http://dx.doi.org/10.1016/j.desal.2005.11.014.

21. Khalifa, A.J.N., *On the effect of cover tilt angle of the simple solar still on its productivity in different seasons and latitudes.* Energy Conversion and Management, 2011. **52**(1): p. 431-436 DOI: http://dx.doi.org/10.1016/j.enconman.2010.07.018.

22. Bhardwaj, R., M.V. ten Kortenaar, and R.F. Mudde, *Influence of condensation surface on solar distillation.* Desalination, 2013. **326**: p. 37-45 DOI: http://dx.doi.org/10.1016/j.desal.2013.07.006.

23. Zurigat, Y.H. and M.K. Abu-Arabi, *Modelling and performance analysis of a regenerative solar desalination unit.* Applied Thermal Engineering, 2004. **24**(7): p. 1061-1072 DOI: http://dx.doi.org/10.1016/j.applthermaleng.2003.11.010.

24. Abu-Hijleh, B.A.K., *Enhanced solar still performance using water film cooling of the glass cover.* Desalination, 1996. **107**(3): p. 235-244 DOI: http://dx.doi.org/10.1016/S0011-9164(96)00165-8.

25. Sivakumar, V. and E. Ganapathy Sundaram, *Improvement techniques of solar still efficiency: A review.* Renewable and Sustainable Energy Reviews, 2013. **28**: p. 246-264 DOI: http://dx.doi.org/10.1016/j.rser.2013.07.037.

26. El-Sebaii, A.A., S. Aboul-Enein, and E. El-Bialy, *Single basin solar still with baffle suspended absorber.* Energy Conversion and Management, 2000. **41**(7): p. 661-675 DOI: http://dx.doi.org/10.1016/S0196-8904(99)00141-7.

27. Abdallah, S., M.M. Abu-Khader, and O. Badran, *Effect of various absorbing materials on the thermal performance of solar stills.* Desalination, 2009. **242**(1–3): p. 128-137 DOI: http://dx.doi.org/10.1016/j.desal.2008.03.036.

28. El-Sebaii, A.A., et al., *Thermal performance of a single basin solar still with PCM as a storage medium.* Applied Energy, 2009. **86**(7–8): p. 1187-1195 DOI: http://dx.doi.org/10.1016/j.apenergy.2008.10.014.

29. Ansari, O., et al., *Desalination of the brackish water using a passive solar still with a heat energy storage system.* Desalination, 2013. **324**: p. 10-20 DOI: http://dx.doi.org/10.1016/j.desal.2013.05.017.

30. Ismail, B.I., *Design and performance of a transportable hemispherical solar still.* Renewable Energy, 2009. **34**(1): p. 145-150 DOI: http://dx.doi.org/10.1016/j.renene.2008.03.013.

31. Gorjian, S., et al., *Experimental performance evaluation of a stand-alone point-focus parabolic solar still.* Desalination, 2014. **352**: p. 1-17 DOI: http://dx.doi.org/10.1016/j.desal.2014.08.005.

32.   Zhang, L., et al., *An experimental investigation of a natural circulation heat pipe system applied to a parabolic trough solar collector steam generation system.* Solar Energy, 2012. **86**(3): p. 911-919 DOI: http://dx.doi.org/10.1016/j.solener.2011.11.020.

33.   Yadav, Y.P., et al., *An asymmetric line-axis compound parabolic concentrating single basin solar still.* Renewable Energy, 1996. **9**(1–4): p. 737-740 DOI: http://dx.doi.org/10.1016/0960-1481(96)88389-3.

34.   Kothdiwala, A.F., P.C. Eames, and B. Norton, *Optical performance of an asymmetric inverted absorber compound parabolic concentrating solar collector.* Renewable Energy, 1996. **9**(1–4): p. 576-579 DOI: http://dx.doi.org/10.1016/0960-1481(96)88355-8.

35.   Ayoub, G.M., L. Malaeb, and P.E. Saikaly, *Critical variables in the performance of a productivity-enhanced solar still.* Solar Energy, 2013. **98**: p. 472-484 DOI: http://dx.doi.org/10.1016/j.solener.2013.09.030.

36.   Rajamanickam, M.R. and A. Ragupathy, *Influence of Water Depth on Internal Heat and Mass Transfer in a Double Slope Solar Still.* Energy Procedia, 2012. **14**: p. 1701-1708 DOI: http://dx.doi.org/10.1016/j.egypro.2011.12.1155.

37.   Cooper, P.I. and W.R.W. Read, *Design philosophy and operating experience for Australian solar stills.* Solar Energy, 1974. **16**(1): p. 1-8 DOI: http://dx.doi.org/10.1016/0038-092X(74)90037-1.

38.   *Solar distillation: M. A. S. Malik, G. N. Tiwari, A. Kumar and M. S. Sodha. Pergamon Press, Oxford, 1982, 130 pp: Cost £12.50 STG; $25.00.* Solar Energy, 1984. **33**(6): p. 643-644 DOI: http://dx.doi.org/10.1016/0038-092X(84)90035-5.

39.   Al-Karaghouli, A.A. and A.N. Minasian, *A floating-wick type solar still.* Renewable Energy, 1995. **6**(1): p. 77-79 DOI: http://dx.doi.org/10.1016/0960-1481(94)00047-A.

40.   Kalidasa Murugavel, K. and K. Srithar, *Performance study on basin type double slope solar still with different wick materials and minimum mass of water.* Renewable Energy, 2011. **36**(2): p. 612-620 DOI: http://dx.doi.org/10.1016/j.renene.2010.08.009.

41.   Gude, V.G. and N. Nirmalakhandan, *Desalination at low temperatures and low pressures.* Desalination, 2009. **244**(1–3): p. 239-247 DOI: http://dx.doi.org/10.1016/j.desal.2008.06.005.

42.   Shah, M.M., *Improved method for calculating evaporation from indoor water pools.* Energy and Buildings, 2012. **49**: p. 306-309 DOI: http://dx.doi.org/10.1016/j.enbuild.2012.02.026.

43.   Lorenzini, G., A. Conti, and D. De Wrachien, *Computational Fluid Dynamics (CFD) Picture of Water Droplet Evaporation in Air.* Irrigation & Drainage Systems Engineering, 2012. **1**(1): p. 1-12 DOI: http://dx.doi.org/10.4172/2168-9768.1000101.

44.   Muthunayagam, A.E., K. Ramamurthi, and J.R. Paden, *Low temperature flash vaporization for desalination.* Desalination, 2005. **180**(1–3): p. 25-32 DOI: http://dx.doi.org/10.1016/j.desal.2004.12.028.

45.   Augusto, C.M., et al., *A mathematical model describing the two stages of low-pressure-vaporization of free water.* Journal of Food Engineering, 2012. **112**(4): p. 274-281 DOI: http://dx.doi.org/10.1016/j.jfoodeng.2012.05.013.

46.   Hosseini Araghi, A., et al., *Performance analysis of a low pressure discharge thermal energy combined desalination unit.* Applied Thermal Engineering, 2015. **76**: p. 116-122 DOI: http://dx.doi.org/10.1016/j.applthermaleng.2014.10.092.

47.   Valladares Linares, R., et al., *Life cycle cost of a hybrid forward osmosis – low pressure reverse osmosis system for seawater desalination and wastewater recovery.* Water Research, 2016. **88**: p. 225-234 DOI: http://dx.doi.org/10.1016/j.watres.2015.10.017.

48.   Al-Kharabsheh, S. and D.Y. Goswami, *Experimental study of an innovative solar water desalination system utilizing a passive vacuum technique.* Solar Energy, 2003. **75**(5): p. 395-401 DOI: http://dx.doi.org/10.1016/j.solener.2003.08.031.

49.   Orfi, J., N. Galanis, and M. Laplante, *Air humidification–dehumidification for a water desalination system using solar energy.* Desalination, 2007. **203**(1–3): p. 471-481 DOI: http://dx.doi.org/10.1016/j.desal.2006.04.022.

50.   Mohamed, A.M.I. and N.A. El-Minshawy, *Theoretical investigation of solar humidification–dehumidification desalination system using parabolic trough concentrators.* Energy Conversion and Management, 2011. **52**(10): p. 3112-3119 DOI: http://dx.doi.org/10.1016/j.enconman.2011.04.026.

51.   Parekh, S., et al., *Solar desalination with a humidification-dehumidification technique — a comprehensive technical review.* Desalination, 2004. **160**(2): p. 167-186 DOI: http://dx.doi.org/10.1016/S0011-9164(04)90007-0.

52.   Arjunan, T.V., H.S. Aybar, and N. Nedunchezhian, *Status of solar desalination in India.* Renewable and Sustainable Energy Reviews, 2009. **13**(9): p. 2408-2418 DOI: http://dx.doi.org/10.1016/j.rser.2009.03.006.

53.   Kwatra, H.S., *Performance of a solar still: Predicted effect of enhanced evaporation area on yield and evaporation temperature.* Solar Energy, 1996. **56**(3): p. 261-266 DOI: http://dx.doi.org/10.1016/0038-092X(95)00101-V.

54.   Velmurugan, V. and K. Srithar, *Performance analysis of solar stills based on various factors affecting the productivity—A review.* Renewable and Sustainable Energy Reviews, 2011. **15**(2): p. 1294-1304 DOI: http://dx.doi.org/10.1016/j.rser.2010.10.012.

55.   Dev, R., S.A. Abdul-Wahab, and G.N. Tiwari, *Performance study of the inverted absorber solar still with water depth and total dissolved solid.* Applied Energy, 2011. **88**(1): p. 252-264 DOI: http://dx.doi.org/10.1016/j.apenergy.2010.08.001.

56.   Veroustraete, F. *Which bulb closely replicates the sunlight spectrum on earth?* 2015 [cited 2016 July 15]; Available from: https://www.researchgate.net/post/Which_bulb_closely_replicates_the_sunlight_spectrum_on_earth

57.   Sonntag, D., *Important new values of the physical constants of 1986, vapour pressure formulations based on the ITS-90 psychrometer formulae.* Zeitschrift fur Meteorologie, 1990. **40**(5): p. 340-343.

58.   Vinnichenko, N.A., *Direct Computation of Evaporation Rate at the Surface of Swimming Pool.* Recent Researches in Mechanics, 2014: p. 120-124.

59.   Anon, *Handbook of Reliability Prediction Procedures for Mechanical Equipment*. 2011, West Bethesda, Maryland: Naval Surface Warfare Center Carderock Division ISBN.

60.   Bodger, P., *Tongan Schools PV Project*, A.W.T. Gorrie. 9-10/05/2016, Personal communication.

61.   Köntges, M., et al., *Performance and Reliability of Photovoltaic Systems, Subtask 3.2: Review of Failures of Photovoltaic Modules*. 2014, International Energy Agency. p. 1-140.

62.   Choudhary, M.A., et al., *Price setting and price stickiness: A developing economy perspective.* Journal of Macroeconomics, 2016. **48**: p. 44-61 DOI: http://dx.doi.org/10.1016/j.jmacro.2016.01.003.

63.	Danis, W.M., D. De Clercq, and O. Petricevic, *Are social networks more important for new business activity in emerging than developed economies? An empirical extension.* International Business Review, 2011. **20**(4): p. 394-408 DOI: http://dx.doi.org/10.1016/j.ibusrev.2010.08.005.

64.	WESP *World Economic Situation and Prospects 2016*. 2016. 1-25 DOI: www.un.org/en/development/desa/policy/wesp/wesp.../2016wesp_ch1_en.pdf.

65.	Grunert, K.G. and H.C.M. van Trijp, *Consumer-Oriented New Product Development A2 - Alfen, Neal K. Van*, in *Encyclopedia of Agriculture and Food Systems*. 2014, Academic Press: Oxford. p. 375-386.

66.	Suharyanti, Y., et al., *The Scheme of Product Development Process as a Trigger to Product Success: A Theoretical Framework.* Industrial Engineering and Service Science 2015, 2015. **4** DOI: https://doi.org/10.1016/j.promfg.2015.11.013

67.	Cooper, R.G., C.M. Crawford, and T.P. Hustad, *Winning at New Products, by R. G. Cooper1.* Journal of Product Innovation Management, 1986. **3**(4): p. 307-308 DOI: http://dx.doi.org/10.1111/1540-5885.340307.

68.	Cooper, R.G. and S.J. Edgett, *Generating Breakthrough New Product Ideas: Feeding the Innovation Funnel*. First ed. 2007, Canada: Product Development Institute ISBN: 978-0-9732927-2-6.

69.	Rakthin, S., R.J. Calantone, and J.F. Wang, *Managing market intelligence: The comparative role of absorptive capacity and market orientation.* Journal of Business Research, 2016. **Article in Press** DOI: http://dx.doi.org/10.1016/j.jbusres.2016.03.064.

70.	Olson, E.M., O.C. Walker Jr, and R.W. Ruekert, *Organizing for Effective New Product Development: The Moderating Role of Product Innovativeness* Journal of Marketing, 1995. **59**(1): p. 15 DOI: http://dx.doi.org/10.2307/1252014

71.	Olson, E.M., et al., *Patterns of cooperation during new product development among marketing, operations and R&D: Implications for project performance.* Journal of Product Innovation Management, 2001. **18**(4): p. 258-271 DOI: http://dx.doi.org/10.1016/S0737-6782(01)00091-1.

72.	Mandelli, S., et al., *Off-grid systems for rural electrification in developing countries: Definitions, classification and a comprehensive literature review.* Renewable and Sustainable Energy Reviews, 2016. **58**: p. 1621-1646 DOI: http://dx.doi.org/10.1016/j.rser.2015.12.338.

73.	Rahman, M.M., J.V. Paatero, and R. Lahdelma, *Evaluation of choices for sustainable rural electrification in developing countries: A multicriteria approach.* Energy Policy, 2013. **59**: p. 589-599 DOI: http://dx.doi.org/10.1016/j.enpol.2013.04.017.

74.	Rahman, M.M., et al., *Driving and hindering factors for rural electrification in developing countries: Lessons from Bangladesh.* Energy Policy, 2013. **61**: p. 840-851 DOI: http://dx.doi.org/10.1016/j.enpol.2013.06.100.

75.	Mahesh, C. and P.N. James, *Product development and innovation for developing countries: Potential and challenges.* Journal of Management Development, 2008. **27**(10): p. 1017-1025 DOI: http://dx.doi.org/10.1108/02621710810916277.

76.	Austin-Breneman, J. and M. Yang, *Design for Micro-Enterprise: An Approach to Product Design for Emerging Markets*, in *ASME 2013 International Design Engineering Technical Conferences and Computers and Information in Engineering Conference, IDETC/CIE 2013 - Portland, OR, United States*. 2013, American Society of Mechanical Engineers: Portland, OR, USA DOI: http://dx.doi.org/10.1115/DETC2013-12677.

77.	Xiao, Q., et al., *Indoor air pollution from burning yak dung as a household fuel in Tibet.* Atmospheric Environment, 2015. **102**: p. 406-412 DOI: http://dx.doi.org/10.1016/j.atmosenv.2014.11.060.

78. Docherty, P.D., J.G. Chase, and T. David, *Characterisation of the iterative integral parameter identification method.* Medical & Biological Engineering & Computing, 2012. **50**(2): p. 127-134 DOI: http://dx.doi.org/10.1007/s11517-011-0851-y.

79. Omara, Z.M., M.A. Eltawil, and E.A. ElNashar, *A new hybrid desalination system using wicks/solar still and evacuated solar water heater.* Desalination, 2013. **325**: p. 56-64 DOI: http://dx.doi.org/10.1016/j.desal.2013.06.024.

80. Docherty, P., Chase, J.G., Lotz, T., Desaive, T., *A graphical method for practical and informative identifiability analyses of physiological models: A case study of insulin kinetics and sensitivity. .* Biomedical Engineering Online, 2011. **10**(39): p. 1-33.

81. Raue, A., et al., *Structural and practical identifiability analysis of partially observed dynamical models by exploiting the profile likelihood.* Bioinformatics/computer Applications in The Biosciences, 2009. **25**(15): p. 1923-1929 DOI: http://dx.doi.org/10.1093/bioinformatics/btp358.

82. Veza, J. and V. Ruiz, *Solar distillation in forced convection. Simulation and experience.* Renewable Energy, 1993. **3**(6–7): p. 691-699 DOI: http://dx.doi.org/10.1016/0960-1481(93)90076-S.

83. Bhattacharyya, A., *Solar Stills for Desalination of Water in Rural Households.* International Journal Of Environment And Sustainability (IJES), 2013. **2** (1): p. 21-31.

Appendices

Appendix 01: Licensing of Figures for reproduction in current study
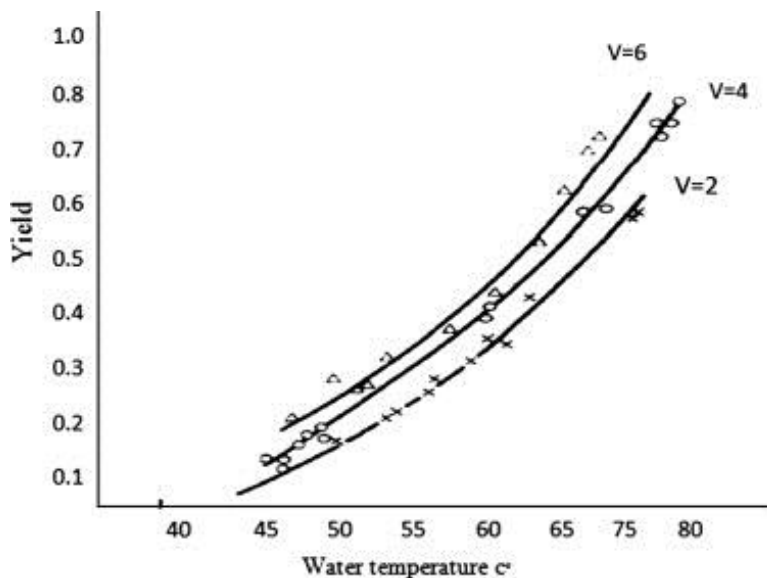
Figure 4: Variation in water productivity (yield) based on wind velocity and water temperature

Type of Use	reuse in a thesis/dissertation
Portion	figures/tables/illustrations
Number of figures/tables/illustrations	1
Format	both print and electronic
Are you the author of this Elsevier article?	No
Will you be translating?	No
Order reference number	
Original figure numbers	Figure 4
Title of your thesis/dissertation	Optimisation of Solar Desalination Process
Expected completion date	Aug 2016
Estimated size (number of pages)	130
Elsevier VAT number	GB 494 6272 12
	Alexander Gorrie
	University of Canterbury
Requestor Location	
	Christchurch, 9011
	New Zealand
	Attn: Alexander Gorrie
Customer VAT ID	NZ15
Total	0.00 USD
Terms and Conditions	

INTRODUCTION

1. The publisher for this copyrighted material is Elsevier. By clicking "accept" in connection with completing this licensing transaction, you agree that the following terms and conditions apply to this transaction (along with the Billing and Payment terms and conditions established by Copyright Clearance Center, Inc. ("CCC"), at the time that you opened your Rightslink account and that are available at any time at http://myaccount.copyright.com).

GENERAL TERMS

2. Elsevier hereby grants you permission to reproduce the aforementioned material subject to the terms and conditions indicated.

3. Acknowledgement: If any part of the material to be used (for example, figures) has appeared in our publication with credit or acknowledgement to another source, permission must also be sought from that source. If such permission is not obtained then that material may not be included in your publication/copies. Suitable acknowledgement to the source must be made, either as a footnote or in a reference list at the end of your publication, as follows:

"Reprinted from Publication title, Vol /edition number, Author(s), Title of article / title of chapter, Pages No., Copyright (Year), with permission from Elsevier [OR APPLICABLE SOCIETY COPYRIGHT OWNER]." Also Lancet special credit - "Reprinted from The Lancet, Vol. number, Author(s), Title of article, Pages No., Copyright (Year), with permission from Elsevier."

4. Reproduction of this material is confined to the purpose and/or media for which permission is hereby given.

5. Altering/Modifying Material: Not Permitted. However figures and illustrations may be altered/adapted minimally to serve your work. Any other abbreviations, additions, deletions and/or any other alterations shall be made only with prior written authorization of Elsevier Ltd. (Please contact Elsevier at

permissions@elsevier.com)

6. If the permission fee for the requested use of our material is waived in this instance, please be advised that your future requests for Elsevier materials may attract a fee.

7. Reservation of Rights: Publisher reserves all rights not specifically granted in the combination of (i) the license details provided by you and accepted in the course of this licensing transaction, (ii) these terms and conditions and (iii) CCC's Billing and Payment terms and conditions.

8. License Contingent Upon Payment: While you may exercise the rights licensed immediately upon issuance of the license at the end of the licensing process for the transaction, provided that you have disclosed complete and accurate details of your proposed use, no license is finally effective unless and until full payment is received from you (either by publisher or by CCC) as provided in CCC's Billing and Payment terms and conditions. If full payment is not received on a timely basis, then any license preliminarily granted shall be deemed automatically revoked and shall be void as if never granted. Further, in the event that you breach any of these terms and conditions or any of CCC's Billing and Payment terms and conditions, the license is automatically revoked and shall be void as if never granted. Use of materials as described in a revoked license, as well as any use of the materials beyond the scope of an unrevoked license, may constitute copyright infringement and publisher reserves the right to take any and all action to protect its copyright in the materials.

9. Warranties: Publisher makes no representations or warranties with respect to the licensed material.

10. Indemnity: You hereby indemnify and agree to hold harmless publisher and CCC, and their respective officers, directors, employees and agents, from and against any and all claims arising out of your use of the licensed material other than as specifically authorized pursuant to this license.

11. No Transfer of License: This license is personal to you and may not be sublicensed, assigned, or transferred by you to any other person without publisher's written permission.

12. No Amendment Except in Writing: This license may not be amended except in a writing signed by both parties (or, in the case of publisher, by CCC on publisher's behalf).

13. Objection to Contrary Terms: Publisher hereby objects to any terms contained in any purchase order, acknowledgment, check endorsement or other writing prepared by you, which terms are inconsistent with these terms and conditions or CCC's Billing and Payment terms and conditions. These terms and conditions, together with CCC's Billing and Payment terms and conditions (which are incorporated herein), comprise the entire agreement between you and publisher (and CCC) concerning this licensing transaction. In the event of any conflict between your obligations established by these terms and conditions and those established by CCC's Billing and Payment terms and conditions, these terms and conditions shall control.

14. Revocation: Elsevier or Copyright Clearance Center may deny the permissions described in this License at their sole discretion, for any reason or no reason, with a full refund payable to you. Notice of such denial will be made using the contact information provided by you. Failure to receive such notice will not alter or invalidate the denial. In no event will Elsevier or Copyright Clearance Center be responsible or liable for any costs, expenses or damage incurred by you as a result of a denial of your permission request, other than a refund of the amount(s) paid by you to Elsevier and/or Copyright Clearance Center for denied permissions.

<div align="center">LIMITED LICENSE</div>

The following terms and conditions apply only to specific license types:

15. **Translation**: This permission is granted for non-exclusive world **English** rights only unless your license was granted for translation rights. If you licensed translation rights you may only translate this content into the languages you requested. A professional translator must perform all translations and reproduce the content

word for word preserving the integrity of the article.

16. **Posting licensed content on any Website**: The following terms and conditions apply as follows: Licensing material from an Elsevier journal: All content posted to the web site must maintain the copyright information line on the bottom of each image; A hyper-text must be included to the Homepage of the journal from which you are licensing at http://www.sciencedirect.com/science/journal/xxxxx or the Elsevier homepage for books at http://www.elsevier.com; Central Storage: This license does not include permission for a scanned version of the material to be stored in a central repository such as that provided by Heron/XanEdu.

Licensing material from an Elsevier book: A hyper-text link must be included to the Elsevier homepage at http://www.elsevier.com . All content posted to the web site must maintain the copyright information line on the bottom of each image.

Posting licensed content on Electronic reserve: In addition to the above the following clauses are applicable: The web site must be password-protected and made available only to bona fide students registered on a relevant course. This permission is granted for 1 year only. You may obtain a new license for future website posting.

17. **For journal authors:** the following clauses are applicable in addition to the above:

Preprints:

A preprint is an author's own write-up of research results and analysis, it has not been peer-reviewed, nor has it had any other value added to it by a publisher (such as formatting, copyright, technical enhancement etc.).

Authors can share their preprints anywhere at any time. Preprints should not be added to or enhanced in any way in order to appear more like, or to substitute for, the final versions of articles however authors can update their preprints on arXiv or RePEc with their Accepted Author Manuscript (see below).

If accepted for publication, we encourage authors to link from the preprint to their formal publication via its DOI. Millions of researchers have access to the formal publications on ScienceDirect, and so links will help users to find, access, cite and use the best available version. Please note that Cell Press, The Lancet and some society-owned have different preprint policies. Information on these policies is available on the journal homepage.

Accepted Author Manuscripts: An accepted author manuscript is the manuscript of an article that has been accepted for publication and which typically includes author-incorporated changes suggested during submission, peer review and editor-author communications.

Authors can share their accepted author manuscript:

- immediately
    - via their non-commercial person homepage or blog
    - by updating a preprint in arXiv or RePEc with the accepted manuscript
    - via their research institute or institutional repository for internal institutional uses or as part of an invitation-only research collaboration work-group
    - directly by providing copies to their students or to research collaborators for their personal use
    - for private scholarly sharing as part of an invitation-only work group on commercial sites with which Elsevier has an agreement
- after the embargo period
    - via non-commercial hosting platforms such as their institutional repository
    - via commercial sites with which Elsevier has an agreement

In all cases accepted manuscripts should:

- link to the formal publication via its DOI
- bear a CC-BY-NC-ND license - this is easy to do
- if aggregated with other manuscripts, for example in a repository or other site, be shared in alignment with our hosting policy not be added to or enhanced in any way to appear more like, or to substitute for, the published journal article.

Published journal article (JPA): A published journal article (PJA) is the definitive final record of published research that appears or will appear in the journal and embodies all value-adding publishing activities including peer review co-ordination, copy-editing, formatting, (if relevant) pagination and online enrichment.

Policies for sharing publishing journal articles differ for subscription and gold open access articles:

Subscription Articles: If you are an author, please share a link to your article rather than the full-text. Millions of researchers have access to the formal publications on ScienceDirect, and so links will help your users to find, access, cite, and use the best available version.

Theses and dissertations which contain embedded PJAs as part of the formal submission can be posted publicly by the awarding institution with DOI links back to the formal publications on ScienceDirect.

If you are affiliated with a library that subscribes to ScienceDirect you have additional private sharing rights for others' research accessed under that agreement. This includes use for classroom teaching and internal training at the institution (including use in course packs and courseware programs), and inclusion of the article for grant funding purposes.

Gold Open Access Articles: May be shared according to the author-selected end-user license and should contain a CrossMark logo, the end user license, and a DOI link to the formal publication on ScienceDirect.

Please refer to Elsevier's posting policy for further information.

18. **For book authors** the following clauses are applicable in addition to the above: Authors are permitted to place a brief summary of their work online only. You are not allowed to download and post the published electronic version of your chapter, nor may you scan the printed edition to create an electronic version.
Posting to a repository: Authors are permitted to post a summary of their chapter only in their institution's repository.

19. **Thesis/Dissertation**: If your license is for use in a thesis/dissertation your thesis may be submitted to your institution in either print or electronic form. Should your thesis be published commercially, please reapply for permission. These requirements include permission for the Library and Archives of Canada to supply single copies, on demand, of the complete thesis and include permission for Proquest/UMI to supply single copies, on demand, of the complete thesis. Should your thesis be published commercially, please reapply for permission. Theses and dissertations which contain embedded PJAs as part of the formal submission can be posted publicly by the awarding institution with DOI links back to the formal publications on ScienceDirect.

 Elsevier Open Access Terms and Conditions

You can publish open access with Elsevier in hundreds of open access journals or in nearly 2000 established subscription journals that support open access publishing. Permitted third party re-use of these open access articles is defined by the author's choice of Creative Commons user license. See our open access license policy for more information.

Terms & Conditions applicable to all Open Access articles published with Elsevier:

Any reuse of the article must not represent the author as endorsing the adaptation of the article nor should the article be modified in such a way as to damage the author's honour or reputation. If any changes have been made, such changes must be clearly indicated.

The author(s) must be appropriately credited and we ask that you include the end user license and a DOI link to the formal publication on ScienceDirect.

If any part of the material to be used (for example, figures) has appeared in our publication with credit or acknowledgement to another source it is the responsibility of the user to ensure their reuse complies with the terms and conditions determined by the rights holder.

Additional Terms & Conditions applicable to each Creative Commons user license:

CC BY: The CC-BY license allows users to copy, to create extracts, abstracts and new works from the Article, to alter and revise the Article and to make commercial use of the Article (including reuse and/or resale of the Article by commercial entities), provided the user gives appropriate credit (with a link to the formal publication through the relevant DOI), provides a link to the license, indicates if changes were made and the licensor is not represented as endorsing the use made of the work. The full details of the license are available at http://creativecommons.org/licenses/by/4.0.

CC BY NC SA: The CC BY-NC-SA license allows users to copy, to create extracts, abstracts and new works from the Article, to alter and revise the Article, provided this is not done for commercial purposes, and that the user gives appropriate credit (with a link to the formal publication through the relevant DOI), provides a link to the license, indicates if changes were made and the licensor is not represented as endorsing the use made of the work. Further, any new works must be made available on the same conditions. The full details of the license are available at http://creativecommons.org/licenses/by-nc-sa/4.0.

CC BY NC ND: The CC BY-NC-ND license allows users to copy and distribute the Article, provided this is not done for commercial purposes and further does not permit distribution of the Article if it is changed or edited in any way, and provided the user gives appropriate credit (with a link to the formal publication through the relevant DOI), provides a link to the license, and that the licensor is not represented as endorsing the use made of the work. The full details of the license are available at http://creativecommons.org/licenses/by-nc-nd/4.0. Any commercial reuse of Open Access articles published with a CC BY NC SA or CC BY NC ND license requires permission from Elsevier and will be subject to a fee.

Commercial reuse includes:

- Associating advertising with the full text of the Article
- Charging fees for document delivery or access
- Article aggregation
- Systematic distribution via e-mail lists or share buttons

Posting or linking by commercial companies for use by customers of those companies.

20. **Other Conditions**:

v1.8

Questions? customercare@copyright.com **or +1-855-239-3415 (toll free in the US) or +1-978-646-2777.**

Figure 6: Effect of salt concentration on distilled water production

Akash, B.A., M.S. Mohsen, and W. Nayfeh, *Experimental study of the basin type solar still under local climate conditions.* Energy Conversion and Management, 2000. **41**(9): p. 883-890.

ELSEVIER LICENSE
TERMS AND CONDITIONS
Jun 14, 2016

This Agreement between Alexander Gorrie ("You") and Elsevier ("Elsevier") consists of your license details and the terms and conditions provided by Elsevier and Copyright Clearance Center.

License Number	3887830135567
License date	Jun 14, 2016
Licensed Content Publisher	Elsevier
Licensed Content Publication	Energy Conversion and Management
Licensed Content Title	Experimental study of the basin type solar still under local climate conditions
Licensed Content Author	Bilal A Akash,Mousa S Mohsen,Waleed Nayfeh
Licensed Content Date	1 June 2000
Licensed Content Volume Number	41
Licensed Content Issue Number	9
Licensed Content Pages	8
Start Page	883
End Page	890
Type of Use	reuse in a thesis/dissertation
Intended publisher of new work	other
Portion	figures/tables/illustrations
Number of figures/tables/illustrations	1
Format	both print and electronic
Are you the author of this Elsevier article?	No

Will you be translating?	No
Order reference number	
Original figure numbers	Figure 6
Title of your thesis/dissertation	Optimisation of Solar Desalination Process
Expected completion date	Aug 2016
Estimated size (number of pages)	130
Elsevier VAT number	GB 494 6272 12
	Alexander Gorrie University of Canterbury
Requestor Location	
	Christchurch, 9011 New Zealand Attn: Alexander Gorrie
Customer VAT ID	NZ15
Total	0.00 USD

Terms and Conditions

INTRODUCTION

1. The publisher for this copyrighted material is Elsevier. By clicking "accept" in connection with completing this licensing transaction, you agree that the following terms and conditions apply to this transaction (along with the Billing and Payment terms and conditions established by Copyright Clearance Center, Inc. ("CCC"), at the time that you opened your Rightslink account and that are available at any time at http://myaccount.copyright.com).

GENERAL TERMS

2. Elsevier hereby grants you permission to reproduce the aforementioned material subject to the terms and conditions indicated.

3. Acknowledgement: If any part of the material to be used (for example, figures) has appeared in our publication with credit or acknowledgement to another source, permission must also be sought from that source. If such permission is not obtained then that material may not be included in your publication/copies. Suitable acknowledgement to the source must be made, either as a footnote or in a reference list at the end of your publication, as follows:

"Reprinted from Publication title, Vol /edition number, Author(s), Title of article / title of chapter, Pages No., Copyright (Year), with permission from Elsevier [OR APPLICABLE SOCIETY COPYRIGHT OWNER]." Also Lancet special credit - "Reprinted from The Lancet, Vol. number, Author(s), Title of article, Pages No., Copyright (Year), with permission from Elsevier."

4. Reproduction of this material is confined to the purpose and/or media for which permission is hereby given.

5. Altering/Modifying Material: Not Permitted. However figures and illustrations may be altered/adapted minimally to serve your work. Any other abbreviations, additions, deletions and/or any other alterations shall be made only with prior written authorization of Elsevier Ltd. (Please contact Elsevier at permissions@elsevier.com)

6. If the permission fee for the requested use of our material is waived in this instance, please be advised that your future requests for Elsevier materials may attract a fee.

7. Reservation of Rights: Publisher reserves all rights not specifically granted in the combination of (i) the license details provided by you and accepted in the course of this licensing transaction, (ii) these terms and conditions and (iii) CCC's Billing and Payment terms and conditions.

8. License Contingent Upon Payment: While you may exercise the rights licensed immediately upon issuance of the license at the end of the licensing process for the transaction, provided that you have disclosed complete and accurate details of your proposed use, no license is finally effective unless and until full payment is received from you (either by publisher or by CCC) as provided in CCC's Billing and Payment terms and conditions. If full payment is not received on a timely basis, then any license preliminarily granted shall be deemed automatically revoked and shall be void as if never granted. Further, in the event that you breach any of these terms and conditions or any of CCC's Billing and Payment terms and conditions, the license is automatically revoked and shall be void as if never granted. Use of materials as described in a revoked license, as well as any use of the materials beyond the scope of an unrevoked license, may constitute copyright infringement and publisher reserves the right to take any and all action to protect its copyright in the materials.

9. Warranties: Publisher makes no representations or warranties with respect to the licensed material.

10. Indemnity: You hereby indemnify and agree to hold harmless publisher and CCC, and their respective officers, directors, employees and agents, from and against any and all claims arising out of your use of the licensed material other than as specifically authorized pursuant to this license.

11. No Transfer of License: This license is personal to you and may not be sublicensed, assigned, or transferred by you to any other person without publisher's written permission.

12. No Amendment Except in Writing: This license may not be amended except in a writing signed by both parties (or, in the case of publisher, by CCC on publisher's behalf).

13. Objection to Contrary Terms: Publisher hereby objects to any terms contained in any purchase order, acknowledgment, check endorsement or other writing prepared by you, which terms are inconsistent with these terms and conditions or CCC's Billing and Payment terms and conditions. These terms and conditions, together with CCC's Billing and Payment terms and conditions (which are incorporated herein), comprise the entire agreement between you and publisher (and CCC) concerning this licensing transaction. In the event of any conflict between your obligations established by these terms and conditions and those established by CCC's Billing and Payment terms and conditions, these terms and conditions shall control.

14. Revocation: Elsevier or Copyright Clearance Center may deny the permissions described in this License at their sole discretion, for any reason or no reason, with a full refund payable to you. Notice of such denial will be made using the contact information provided by you. Failure to receive such notice will not alter or invalidate the denial. In no event will Elsevier or Copyright Clearance Center be responsible or liable for any costs, expenses or damage incurred by you as a result of a denial of your permission request, other than a refund of the amount(s) paid by you to Elsevier and/or Copyright Clearance Center for denied permissions.

<div align="center">LIMITED LICENSE</div>

The following terms and conditions apply only to specific license types:

15. **Translation**: This permission is granted for non-exclusive world **English** rights only unless your license was granted for translation rights. If you licensed translation rights you may only translate this content into the languages you requested. A professional translator must perform all translations and reproduce the content word for word preserving the integrity of the article.

16. **Posting licensed content on any Website**: The following terms and conditions apply as follows: Licensing material from an Elsevier journal: All content posted to the web site must maintain the copyright information line on the bottom of each image; A hyper-text must be included to the Homepage of the journal from which

you are licensing at http://www.sciencedirect.com/science/journal/xxxxx or the Elsevier homepage for books at http://www.elsevier.com; Central Storage: This license does not include permission for a scanned version of the material to be stored in a central repository such as that provided by Heron/XanEdu.

Licensing material from an Elsevier book: A hyper-text link must be included to the Elsevier homepage at http://www.elsevier.com . All content posted to the web site must maintain the copyright information line on the bottom of each image.

Posting licensed content on Electronic reserve: In addition to the above the following clauses are applicable: The web site must be password-protected and made available only to bona fide students registered on a relevant course. This permission is granted for 1 year only. You may obtain a new license for future website posting.

17. **For journal authors:** the following clauses are applicable in addition to the above:

Preprints:

A preprint is an author's own write-up of research results and analysis, it has not been peer-reviewed, nor has it had any other value added to it by a publisher (such as formatting, copyright, technical enhancement etc.).

Authors can share their preprints anywhere at any time. Preprints should not be added to or enhanced in any way in order to appear more like, or to substitute for, the final versions of articles however authors can update their preprints on arXiv or RePEc with their Accepted Author Manuscript (see below).

If accepted for publication, we encourage authors to link from the preprint to their formal publication via its DOI. Millions of researchers have access to the formal publications on ScienceDirect, and so links will help users to find, access, cite and use the best available version. Please note that Cell Press, The Lancet and some society-owned have different preprint policies. Information on these policies is available on the journal homepage.

Accepted Author Manuscripts: An accepted author manuscript is the manuscript of an article that has been accepted for publication and which typically includes author-incorporated changes suggested during submission, peer review and editor-author communications.

Authors can share their accepted author manuscript:

- immediately
    - via their non-commercial person homepage or blog
    - by updating a preprint in arXiv or RePEc with the accepted manuscript
    - via their research institute or institutional repository for internal institutional uses or as part of an invitation-only research collaboration work-group
    - directly by providing copies to their students or to research collaborators for their personal use
    - for private scholarly sharing as part of an invitation-only work group on commercial sites with which Elsevier has an agreement
- after the embargo period
    - via non-commercial hosting platforms such as their institutional repository
    - via commercial sites with which Elsevier has an agreement

In all cases accepted manuscripts should:

- link to the formal publication via its DOI

- bear a CC-BY-NC-ND license - this is easy to do
- if aggregated with other manuscripts, for example in a repository or other site, be shared in alignment with our hosting policy not be added to or enhanced in any way to appear more like, or to substitute for, the published journal article.

Published journal article (JPA): A published journal article (PJA) is the definitive final record of published research that appears or will appear in the journal and embodies all value-adding publishing activities including peer review co-ordination, copy-editing, formatting, (if relevant) pagination and online enrichment.

Policies for sharing publishing journal articles differ for subscription and gold open access articles:

<u>Subscription Articles:</u> If you are an author, please share a link to your article rather than the full-text. Millions of researchers have access to the formal publications on ScienceDirect, and so links will help your users to find, access, cite, and use the best available version.

Theses and dissertations which contain embedded PJAs as part of the formal submission can be posted publicly by the awarding institution with DOI links back to the formal publications on ScienceDirect.

If you are affiliated with a library that subscribes to ScienceDirect you have additional private sharing rights for others' research accessed under that agreement. This includes use for classroom teaching and internal training at the institution (including use in course packs and courseware programs), and inclusion of the article for grant funding purposes.

<u>Gold Open Access Articles:</u> May be shared according to the author-selected end-user license and should contain a [CrossMark logo](), the end user license, and a DOI link to the formal publication on ScienceDirect.

Please refer to Elsevier's [posting policy]() for further information.

18. **For book authors** the following clauses are applicable in addition to the above: Authors are permitted to place a brief summary of their work online only. You are not allowed to download and post the published electronic version of your chapter, nor may you scan the printed edition to create an electronic version. **Posting to a repository:** Authors are permitted to post a summary of their chapter only in their institution's repository.

19. **Thesis/Dissertation**: If your license is for use in a thesis/dissertation your thesis may be submitted to your institution in either print or electronic form. Should your thesis be published commercially, please reapply for permission. These requirements include permission for the Library and Archives of Canada to supply single copies, on demand, of the complete thesis and include permission for Proquest/UMI to supply single copies, on demand, of the complete thesis. Should your thesis be published commercially, please reapply for permission. Theses and dissertations which contain embedded PJAs as part of the formal submission can be posted publicly by the awarding institution with DOI links back to the formal publications on ScienceDirect.

<u>Elsevier Open Access Terms and Conditions</u>

You can publish open access with Elsevier in hundreds of open access journals or in nearly 2000 established subscription journals that support open access publishing. Permitted third party re-use of these open access articles is defined by the author's choice of Creative Commons user license. See our [open access license policy]() for more information.

Terms & Conditions applicable to all Open Access articles published with Elsevier:

Any reuse of the article must not represent the author as endorsing the adaptation of the article nor should

the article be modified in such a way as to damage the author's honour or reputation. If any changes have been made, such changes must be clearly indicated.

The author(s) must be appropriately credited and we ask that you include the end user license and a DOI link to the formal publication on ScienceDirect.

If any part of the material to be used (for example, figures) has appeared in our publication with credit or acknowledgement to another source it is the responsibility of the user to ensure their reuse complies with the terms and conditions determined by the rights holder.

Additional Terms & Conditions applicable to each Creative Commons user license:

CC BY: The CC-BY license allows users to copy, to create extracts, abstracts and new works from the Article, to alter and revise the Article and to make commercial use of the Article (including reuse and/or resale of the Article by commercial entities), provided the user gives appropriate credit (with a link to the formal publication through the relevant DOI), provides a link to the license, indicates if changes were made and the licensor is not represented as endorsing the use made of the work. The full details of the license are available at http://creativecommons.org/licenses/by/4.0.

CC BY NC SA: The CC BY-NC-SA license allows users to copy, to create extracts, abstracts and new works from the Article, to alter and revise the Article, provided this is not done for commercial purposes, and that the user gives appropriate credit (with a link to the formal publication through the relevant DOI), provides a link to the license, indicates if changes were made and the licensor is not represented as endorsing the use made of the work. Further, any new works must be made available on the same conditions. The full details of the license are available at http://creativecommons.org/licenses/by-nc-sa/4.0.

CC BY NC ND: The CC BY-NC-ND license allows users to copy and distribute the Article, provided this is not done for commercial purposes and further does not permit distribution of the Article if it is changed or edited in any way, and provided the user gives appropriate credit (with a link to the formal publication through the relevant DOI), provides a link to the license, and that the licensor is not represented as endorsing the use made of the work. The full details of the license are available at http://creativecommons.org/licenses/by-nc-nd/4.0. Any commercial reuse of Open Access articles published with a CC BY NC SA or CC BY NC ND license requires permission from Elsevier and will be subject to a fee.

Commercial reuse includes:

- Associating advertising with the full text of the Article
- Charging fees for document delivery or access
- Article aggregation
- Systematic distribution via e-mail lists or share buttons

Posting or linking by commercial companies for use by customers of those companies.

20. **Other Conditions**:

v1.8

Questions? customercare@copyright.com **or +1-855-239-3415 (toll free in the US) or +1-978-646-2777.**

Figure 2: Freshwater Production Contours for Constant 1000 *kJ/h* heat input.

Gude, V.G. and N. Nirmalakhandan, *Desalination at low temperatures and low pressures.* Desalination, 2009. **244**(1–3): p. 239-247.

ELSEVIER LICENSE
TERMS AND CONDITIONS
Jun 14, 2016

This Agreement between Alexander Gorrie ("You") and Elsevier ("Elsevier") consists of your license details and the terms and conditions provided by Elsevier and Copyright Clearance Center.

License Number	3887830467846
License date	Jun 14, 2016
Licensed Content Publisher	Elsevier
Licensed Content Publication	Desalination
Licensed Content Title	Desalination at low temperatures and low pressures
Licensed Content Author	Veera Gnaneswar Gude,Nagamany Nirmalakhandan
Licensed Content Date	August 2009
Licensed Content Volume Number	244
Licensed Content Issue Number	1-3
Licensed Content Pages	9
Start Page	239
End Page	247
Type of Use	reuse in a thesis/dissertation
Intended publisher of new work	other
Portion	figures/tables/illustrations
Number of figures/tables/illustrations	1
Format	both print and electronic
Are you the author of this Elsevier article?	No
Will you be translating?	No
Order reference number	
Original figure numbers	Figure 2
Title of your thesis/dissertation	Optimisation of Solar Desalination Process
Expected completion date	Aug 2016

| Estimated size (number of pages) | 130 |
| Elsevier VAT number | GB 494 6272 12 |

Alexander Gorrie
University of Canterbury

Requestor Location

Christchurch, 9011
New Zealand
Attn: Alexander Gorrie

| Customer VAT ID | NZ15 |
| Total | 0.00 USD |

Terms and Conditions

INTRODUCTION

1. The publisher for this copyrighted material is Elsevier. By clicking "accept" in connection with completing this licensing transaction, you agree that the following terms and conditions apply to this transaction (along with the Billing and Payment terms and conditions established by Copyright Clearance Center, Inc. ("CCC"), at the time that you opened your Rightslink account and that are available at any time at http://myaccount.copyright.com).

GENERAL TERMS

2. Elsevier hereby grants you permission to reproduce the aforementioned material subject to the terms and conditions indicated.

3. Acknowledgement: If any part of the material to be used (for example, figures) has appeared in our publication with credit or acknowledgement to another source, permission must also be sought from that source. If such permission is not obtained then that material may not be included in your publication/copies. Suitable acknowledgement to the source must be made, either as a footnote or in a reference list at the end of your publication, as follows:

"Reprinted from Publication title, Vol /edition number, Author(s), Title of article / title of chapter, Pages No., Copyright (Year), with permission from Elsevier [OR APPLICABLE SOCIETY COPYRIGHT OWNER]." Also Lancet special credit - "Reprinted from The Lancet, Vol. number, Author(s), Title of article, Pages No., Copyright (Year), with permission from Elsevier."

4. Reproduction of this material is confined to the purpose and/or media for which permission is hereby given.

5. Altering/Modifying Material: Not Permitted. However figures and illustrations may be altered/adapted minimally to serve your work. Any other abbreviations, additions, deletions and/or any other alterations shall be made only with prior written authorization of Elsevier Ltd. (Please contact Elsevier at permissions@elsevier.com)

6. If the permission fee for the requested use of our material is waived in this instance, please be advised that your future requests for Elsevier materials may attract a fee.

7. Reservation of Rights: Publisher reserves all rights not specifically granted in the combination of (i) the license details provided by you and accepted in the course of this licensing transaction, (ii) these terms and conditions and (iii) CCC's Billing and Payment terms and conditions.

8. License Contingent Upon Payment: While you may exercise the rights licensed immediately upon issuance of the license at the end of the licensing process for the transaction, provided that you have disclosed

complete and accurate details of your proposed use, no license is finally effective unless and until full payment is received from you (either by publisher or by CCC) as provided in CCC's Billing and Payment terms and conditions. If full payment is not received on a timely basis, then any license preliminarily granted shall be deemed automatically revoked and shall be void as if never granted. Further, in the event that you breach any of these terms and conditions or any of CCC's Billing and Payment terms and conditions, the license is automatically revoked and shall be void as if never granted. Use of materials as described in a revoked license, as well as any use of the materials beyond the scope of an unrevoked license, may constitute copyright infringement and publisher reserves the right to take any and all action to protect its copyright in the materials.

9. Warranties: Publisher makes no representations or warranties with respect to the licensed material.

10. Indemnity: You hereby indemnify and agree to hold harmless publisher and CCC, and their respective officers, directors, employees and agents, from and against any and all claims arising out of your use of the licensed material other than as specifically authorized pursuant to this license.

11. No Transfer of License: This license is personal to you and may not be sublicensed, assigned, or transferred by you to any other person without publisher's written permission.

12. No Amendment Except in Writing: This license may not be amended except in a writing signed by both parties (or, in the case of publisher, by CCC on publisher's behalf).

13. Objection to Contrary Terms: Publisher hereby objects to any terms contained in any purchase order, acknowledgment, check endorsement or other writing prepared by you, which terms are inconsistent with these terms and conditions or CCC's Billing and Payment terms and conditions. These terms and conditions, together with CCC's Billing and Payment terms and conditions (which are incorporated herein), comprise the entire agreement between you and publisher (and CCC) concerning this licensing transaction. In the event of any conflict between your obligations established by these terms and conditions and those established by CCC's Billing and Payment terms and conditions, these terms and conditions shall control.

14. Revocation: Elsevier or Copyright Clearance Center may deny the permissions described in this License at their sole discretion, for any reason or no reason, with a full refund payable to you. Notice of such denial will be made using the contact information provided by you. Failure to receive such notice will not alter or invalidate the denial. In no event will Elsevier or Copyright Clearance Center be responsible or liable for any costs, expenses or damage incurred by you as a result of a denial of your permission request, other than a refund of the amount(s) paid by you to Elsevier and/or Copyright Clearance Center for denied permissions.

LIMITED LICENSE

The following terms and conditions apply only to specific license types:

15. **Translation**: This permission is granted for non-exclusive world **English** rights only unless your license was granted for translation rights. If you licensed translation rights you may only translate this content into the languages you requested. A professional translator must perform all translations and reproduce the content word for word preserving the integrity of the article.

16. **Posting licensed content on any Website**: The following terms and conditions apply as follows: Licensing material from an Elsevier journal: All content posted to the web site must maintain the copyright information line on the bottom of each image; A hyper-text must be included to the Homepage of the journal from which you are licensing at http://www.sciencedirect.com/science/journal/xxxxx or the Elsevier homepage for books at http://www.elsevier.com; Central Storage: This license does not include permission for a scanned version of the material to be stored in a central repository such as that provided by Heron/XanEdu.

Licensing material from an Elsevier book: A hyper-text link must be included to the Elsevier homepage at http://www.elsevier.com . All content posted to the web site must maintain the copyright information line on

the bottom of each image.

Posting licensed content on Electronic reserve: In addition to the above the following clauses are applicable: The web site must be password-protected and made available only to bona fide students registered on a relevant course. This permission is granted for 1 year only. You may obtain a new license for future website posting.

17. **For journal authors:** the following clauses are applicable in addition to the above:

Preprints:

A preprint is an author's own write-up of research results and analysis, it has not been peer-reviewed, nor has it had any other value added to it by a publisher (such as formatting, copyright, technical enhancement etc.).

Authors can share their preprints anywhere at any time. Preprints should not be added to or enhanced in any way in order to appear more like, or to substitute for, the final versions of articles however authors can update their preprints on arXiv or RePEc with their Accepted Author Manuscript (see below).

If accepted for publication, we encourage authors to link from the preprint to their formal publication via its DOI. Millions of researchers have access to the formal publications on ScienceDirect, and so links will help users to find, access, cite and use the best available version. Please note that Cell Press, The Lancet and some society-owned have different preprint policies. Information on these policies is available on the journal homepage.

Accepted Author Manuscripts: An accepted author manuscript is the manuscript of an article that has been accepted for publication and which typically includes author-incorporated changes suggested during submission, peer review and editor-author communications.

Authors can share their accepted author manuscript:

- immediately
  - via their non-commercial person homepage or blog
  - by updating a preprint in arXiv or RePEc with the accepted manuscript
  - via their research institute or institutional repository for internal institutional uses or as part of an invitation-only research collaboration work-group
  - directly by providing copies to their students or to research collaborators for their personal use
  - for private scholarly sharing as part of an invitation-only work group on commercial sites with which Elsevier has an agreement
- after the embargo period
  - via non-commercial hosting platforms such as their institutional repository
  - via commercial sites with which Elsevier has an agreement

In all cases accepted manuscripts should:

- link to the formal publication via its DOI
- bear a CC-BY-NC-ND license - this is easy to do
- if aggregated with other manuscripts, for example in a repository or other site, be shared in alignment with our hosting policy not be added to or enhanced in any way to appear more like, or to substitute for, the published journal article.

Published journal article (JPA): A published journal article (PJA) is the definitive final record of published

research that appears or will appear in the journal and embodies all value-adding publishing activities including peer review co-ordination, copy-editing, formatting, (if relevant) pagination and online enrichment.

Policies for sharing publishing journal articles differ for subscription and gold open access articles:

Subscription Articles: If you are an author, please share a link to your article rather than the full-text. Millions of researchers have access to the formal publications on ScienceDirect, and so links will help your users to find, access, cite, and use the best available version.

Theses and dissertations which contain embedded PJAs as part of the formal submission can be posted publicly by the awarding institution with DOI links back to the formal publications on ScienceDirect.

If you are affiliated with a library that subscribes to ScienceDirect you have additional private sharing rights for others' research accessed under that agreement. This includes use for classroom teaching and internal training at the institution (including use in course packs and courseware programs), and inclusion of the article for grant funding purposes.

Gold Open Access Articles: May be shared according to the author-selected end-user license and should contain a CrossMark logo, the end user license, and a DOI link to the formal publication on ScienceDirect.

Please refer to Elsevier's posting policy for further information.

18. **For book authors** the following clauses are applicable in addition to the above: Authors are permitted to place a brief summary of their work online only. You are not allowed to download and post the published electronic version of your chapter, nor may you scan the printed edition to create an electronic version. **Posting to a repository:** Authors are permitted to post a summary of their chapter only in their institution's repository.

19. **Thesis/Dissertation**: If your license is for use in a thesis/dissertation your thesis may be submitted to your institution in either print or electronic form. Should your thesis be published commercially, please reapply for permission. These requirements include permission for the Library and Archives of Canada to supply single copies, on demand, of the complete thesis and include permission for Proquest/UMI to supply single copies, on demand, of the complete thesis. Should your thesis be published commercially, please reapply for permission. Theses and dissertations which contain embedded PJAs as part of the formal submission can be posted publicly by the awarding institution with DOI links back to the formal publications on ScienceDirect.

Elsevier Open Access Terms and Conditions

You can publish open access with Elsevier in hundreds of open access journals or in nearly 2000 established subscription journals that support open access publishing. Permitted third party re-use of these open access articles is defined by the author's choice of Creative Commons user license. See our open access license policy for more information.

Terms & Conditions applicable to all Open Access articles published with Elsevier:

Any reuse of the article must not represent the author as endorsing the adaptation of the article nor should the article be modified in such a way as to damage the author's honour or reputation. If any changes have been made, such changes must be clearly indicated.

The author(s) must be appropriately credited and we ask that you include the end user license and a DOI link to the formal publication on ScienceDirect.

If any part of the material to be used (for example, figures) has appeared in our publication with credit or acknowledgement to another source it is the responsibility of the user to ensure their reuse complies with the terms and conditions determined by the rights holder.

Additional Terms & Conditions applicable to each Creative Commons user license:

CC BY: The CC-BY license allows users to copy, to create extracts, abstracts and new works from the Article, to alter and revise the Article and to make commercial use of the Article (including reuse and/or resale of the Article by commercial entities), provided the user gives appropriate credit (with a link to the formal publication through the relevant DOI), provides a link to the license, indicates if changes were made and the licensor is not represented as endorsing the use made of the work. The full details of the license are available at http://creativecommons.org/licenses/by/4.0.

CC BY NC SA: The CC BY-NC-SA license allows users to copy, to create extracts, abstracts and new works from the Article, to alter and revise the Article, provided this is not done for commercial purposes, and that the user gives appropriate credit (with a link to the formal publication through the relevant DOI), provides a link to the license, indicates if changes were made and the licensor is not represented as endorsing the use made of the work. Further, any new works must be made available on the same conditions. The full details of the license are available at http://creativecommons.org/licenses/by-nc-sa/4.0.

CC BY NC ND: The CC BY-NC-ND license allows users to copy and distribute the Article, provided this is not done for commercial purposes and further does not permit distribution of the Article if it is changed or edited in any way, and provided the user gives appropriate credit (with a link to the formal publication through the relevant DOI), provides a link to the license, and that the licensor is not represented as endorsing the use made of the work. The full details of the license are available at http://creativecommons.org/licenses/by-nc-nd/4.0. Any commercial reuse of Open Access articles published with a CC BY NC SA or CC BY NC ND license requires permission from Elsevier and will be subject to a fee.

Commercial reuse includes:

- Associating advertising with the full text of the Article
- Charging fees for document delivery or access
- Article aggregation
- Systematic distribution via e-mail lists or share buttons

Posting or linking by commercial companies for use by customers of those companies.

20. **Other Conditions**:

v1.8

Questions? customercare@copyright.com or +1-855-239-3415 (toll free in the US) or +1-978-646-2777.

Appendix 02a: Relevant Meteorological Data for Tonga

The following data were obtained from the NASA Langley Research Center Atmospheric Science Data Center

Source : https://eosweb.larc.nasa.gov/cgi-bin/sse/grid.cgi?&num=005069&lat=-21.133&hgt=100&submit=Submit&veg=17&sitelev=&email=skip@larc.nasa.gov&p=grid_id&step=2&lon=-175.2

Table A2.1: Monthly Averaged Relative Humidity (%)

Lat -21.13 Lon -175.2	Jan	Feb	Mar	Apr	May	Jun	Jul	Aug	Sep	Oct	Nov	Dec
22-year Average	78.6	79.7	79.5	75.3	73.6	72.7	72	72	73.6	74.7	77	78
Mean value	**76**											
Std Dev.	**3**											

Table A2.2: Average Daily Temperature Range (℃)

Lat -21.13 Lon -175.2	Jan	Feb	Mar	Apr	May	Jun	Jul	Aug	Sep	Oct	Nov	Dec
22-year Average	1.47	1.43	1.45	1.39	1.38	1.43	1.47	1.47	1.41	1.47	1.42	1.37
Mean value	**1.43**											
Std Dev.	**0.04**											

Table A2.3: Monthly Averaged Air Temperature At 10 m Above The Surface Of The Earth (℃)

Lat -21.13 Lon -175.2	Jan	Feb	Mar	Apr	May	Jun	Jul	Aug	Sep	Oct	Nov	Dec
22-year Average	25.8	26.4	26.2	25.5	24.1	23.1	22.2	21.9	22.1	22.5	23.6	25
Minimum	25	25.7	25.5	24.8	23.4	22.4	21.5	21.2	21.4	21.8	22.9	24.3
Maximum	26.5	27.1	26.9	26.2	24.8	23.9	23	22.7	22.8	23.3	24.3	25.7
Mean value	**24**											
Std Dev.	**2**											

Table A2.4: Monthly Averaged Wind Speed At 10 m Above The Surface Of The Earth For Terrain Similar To Airports (*m/s*)

Lat -21.13 Lon -175.2	Jan	Feb	Mar	Apr	May	Jun	Jul	Aug	Sep	Oct	Nov	Dec
10-year Average	5.42	5.28	5.25	6.41	5.99	5.91	5.91	5.94	5.28	5.76	5.77	6.13
Mean value	**5.75**											

Table A2.5: Monthly Averaged Daylight Cloud Amount (*%*)

Lat -21.13 Lon -175.2	Jan	Feb	Mar	Apr	May	Jun	Jul	Aug	Sep	Oct	Nov	Dec
22-year Average	63.6	62.2	63.9	67.3	65.2	64.5	63.1	61.9	62	60	60.9	62.9
Mean value	**63.1**											

Table A2.6: Monthly Averaged Radiation Incident On An Equator-Pointed Tilted Surface (*kWh/m²/day*)

Lat -21.13 Lon -175.2	Jan	Feb	Mar	Apr	May	Jun	Jul	Aug	Sep	Oct	Nov	Dec	*Mean value*
SSE HRZ	6.69	6.3	5.62	4.65	4.04	3.58	3.78	4.43	5.23	6.28	6.69	6.7	*5.32*
K	0.57	0.56	0.56	0.54	0.56	0.55	0.55	0.56	0.56	0.59	0.58	0.56	*0.56*
Diffuse	2.4	2.23	1.94	1.61	1.28	1.17	1.21	1.44	1.78	2.02	2.29	2.42	*1.81*
Direct Normal	6.14	5.85	5.5	4.95	5.02	4.68	4.84	5.08	5.3	6.17	6.29	6.13	*5.49*
Tilt 0	6.66	6.17	5.54	4.61	4.01	3.47	3.65	4.39	5.17	6.16	6.66	6.67	*5.26*
Tilt 6	6.56	6.17	5.64	4.8	4.28	3.73	3.91	4.62	5.31	6.2	6.58	6.73	*5.37*
Tilt 21	6.1	5.97	5.69	5.1	4.81	4.25	4.41	5.03	5.46	6.08	6.16	6.65	*5.48*
Tilt 36	5.35	5.47	5.46	5.14	5.08	4.55	4.68	5.18	5.34	5.65	5.45	6.25	*5.3*
Tilt 90	1.87	2.08	2.68	3.26	3.83	3.58	3.58	3.55	2.92	2.25	1.87	2.72	*2.85*
OPT	6.66	6.18	5.71	5.16	5.12	4.61	4.72	5.18	5.46	6.2	6.66	6.74	*5.7*
OPT ANG	0	3	16	31	43	46	44	36	22	7	0	10	*21.6*
Ratio of Incident Energy at ' *Tilt 0*' to that at '*Optimal Angle*'													*92%*

For testing, the rig angle has been set at 21 °; equal to the latitude of Tonga.

Monthly Averaged Radiation Incident on an Equator-Pointed Tilted Surface
SSE HRZ
The monthly average amount of the total solar radiation incident on a horizontal surface at the surface of the earth for a given month, averaged for that month over the 22-year period (Jul 1983 - Jun 2005).

Clearness Index (K)
The monthly average amount of the total solar radiation incident on a horizontal surface at the surface of the earth divided by the monthly average incoming top-of-atmosphere insolation for a given month, averaged for that month over the 22-year period.

Diffuse
The monthly average amount of solar radiation for a given month incident on a horizontal surface at the surface of the earth under all-sky conditions with the direct radiation from the sun's beam blocked by a shadow band or tracking disk, averaged for that month over the 22-year period.

Direct Normal
The monthly average amount of direct normal radiation incident on a surface oriented normal to the solar radiation for a given month, averaged for that month over the 22-year period.

Tilt 0, Latitude-15, Latitude, Latitude+15, 90
The monthly average amount of the total solar radiation incident on a surface tilted relative to the horizontal and pointed toward the equator for a given month, averaged for that month over the 22-year period (Jul 1983 - Jun 2005). Note that the differences between the Tilt 0 values and the SSE HRZ values are due to approximations in the inputs and time integration inaccuracies when processing the equations and integrating over the "monthly average day" (SSE Methodology). Total solar radiation for each tilt angle was determined using the RETScreen Isotopic Diffuse Method discussed in SSE Methodology.

OPT
The monthly average amount of total solar radiation incident on a surface tilted at the optimum angle relative to the horizontal and pointed toward the equator.

OPT ANG
The angle relative to the horizontal for which the monthly averaged total solar radiation is a maximum.

Units
- SSE HRZ, Diffuse, Direct Normal, and OPT in *$kWh/m^2/day$*
- Tilt angles and OPT ANG in degrees
- K is dimensionless

Appendix 02b: Ocean Temperature Data for Tonga

The water temperature profile is for Peaking surf break in Vava'u, Tonga. The following data was made available and reproduced by permission of Meteo365 Surf Forecast

(http://www.surf-forecast.com/breaks/Peaking/seatemp)
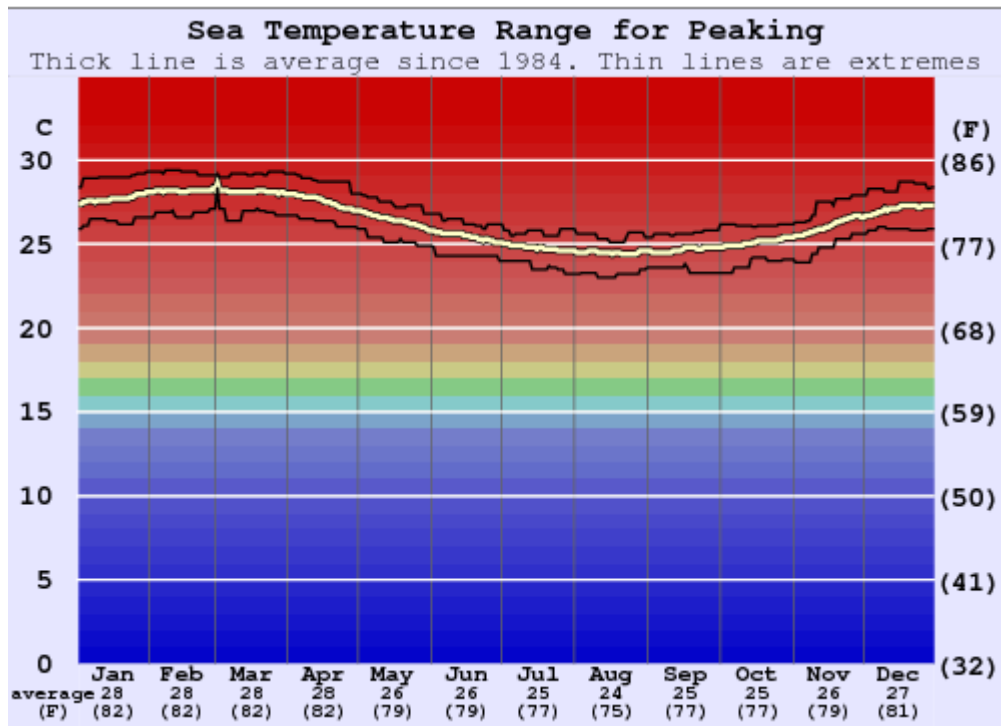
'Actual sea surface water temperatures close to shore at Peaking can vary by several degrees compared with these open water averages. This is especially true after heavy rain, close to river mouths or after long periods of strong offshore winds. Offshore winds cause colder deep water to replace surface water that has been warmed by the sun'

Appendix 02c: Tidal Data for Tonga

The following data was made available and reproduced by permission of Meteo365 Tide Forecast (http://www.tide-forecast.com/locations/Nukualofa-Tonga/tides/latest)
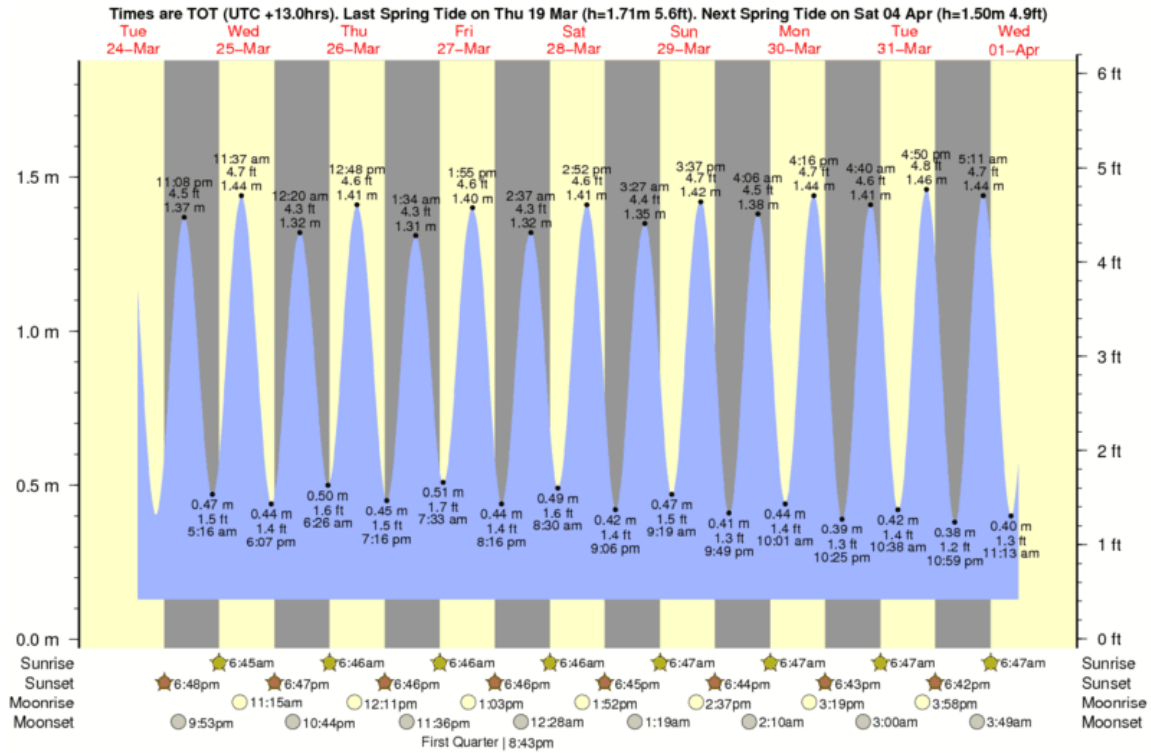
Figure A2.1: Tidal and Solar data from March 24th to April 01st 2016 for Nukualofa, Tonga
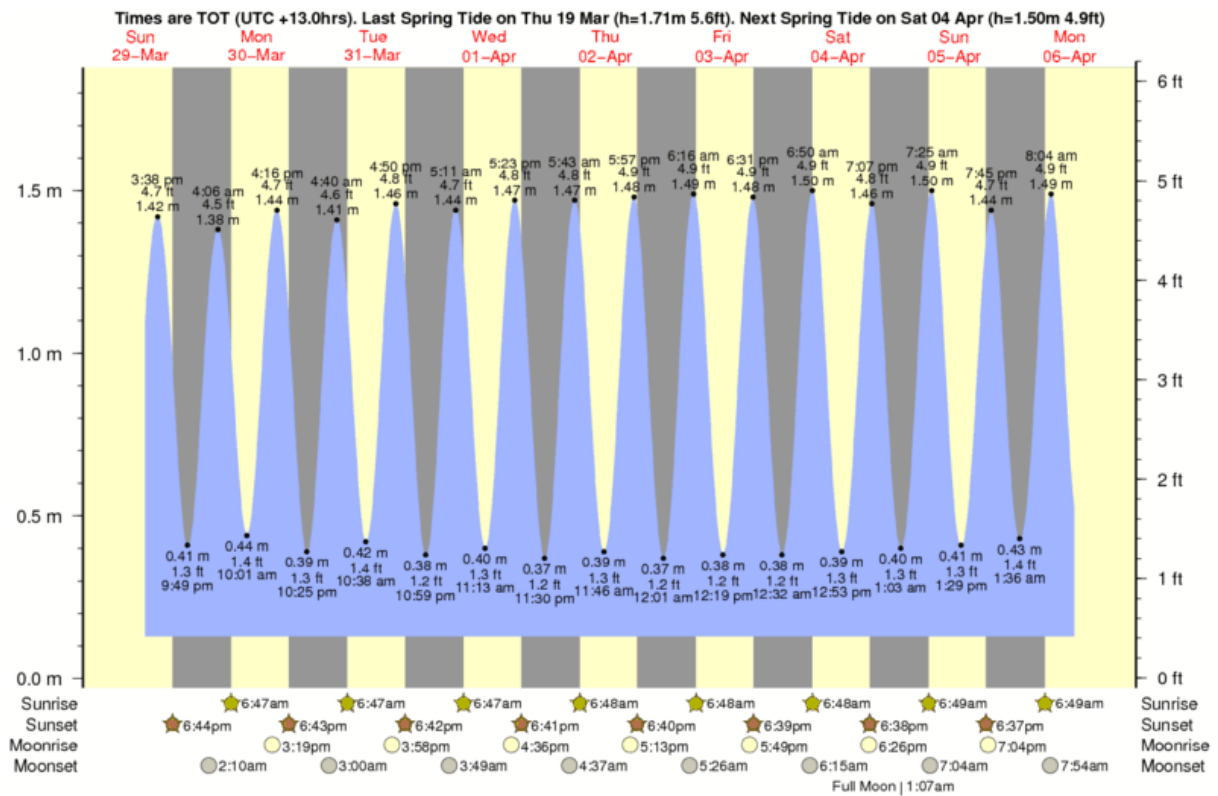
Figure A2.2: Tidal and Solar data from March 29th to April 06st 2016 for Nukualofa, Tonga

Figures A2.1 – 2 show the sunlight hours in Tonga, from the 24th of March until the 6th of April 2015 with tidal heights superimposed over top in blue. The purpose is to illustrate phase difference between solar and tidal patterns. It can be inferred that peak solar radiation occurs after the midpoint of each daylight region, as the midpoint corresponds roughly to the zenith of the sun. On some days, the lagoon-based desalination unit will fill before the midday; in which case a sufficient volume of water will be present for continual evaporation during the day. On other days, the high tide does not occur until much closer to sunset.

To ensure that the volume of water in the unit is regulated, and that the evaporation cycle may be decoupled from the tides, the lagoon-based unit requires a valve system that will let seawater in up to a certain volume. Once filled, the unit will remain at capacity until it starts evaporating off water, at which point the high tide will either fill it back to capacity or there will be no further filling if operating at low tide.

The effect of steadily increasing the salinity must be considered, as this will inhibit evaporation rates, and therefore water production. The easiest way to overcome this issue would be to move the unit to shore and have it manually filled. This task would become a regular part of the user's day, but would completely decouple the unit from tidal patterns and the added complexity of a valve system. The salinity would no longer be an issue as the action of filling it could also include emptying the basin of salt.

The ambient humidity value is approximately 76 *%* +/- 3 *%* over the course of a year based on a 22 year average. The average annual wind speed is 5.75 *m/s* @ 10m elevation. The average annual air temperature range is 1.43 *°C* +/- 0.04, and the average temperature is 24 *°C*

Appendix 03: Solar Flux Energy Calculations

The following calculations have been reproduced from page 49 of the workbook written by the current author as a quick means of finding a representative energy flux indicative of what would be expected in Tonga. The purpose of this analysis was for specification of the lighting array power.

TO ACHIEVE THE SOLAR POWER FOR 1 DAY, THE TOTAL ENERGY MUST BE DIVIDED BY THE NUMBER OF SUNSHINE HOURS.

AVERAGE # SUNSHINE HOURS = 12

REQD. INTENSITY: $5.26\,kWh/m^2/day$ $/12\ hours$ = $.438\,kW/m^2$

FOR A 12 HOUR TEST

→→ COULD LIGHTING INTENSITY BE DOUBLED/QUADRUPLED ETC TO REDUCE TESTING TIME??

SIMILAR ANALYSIS ON PAGE 42 SHOWED THAT THE REQUIRED POWER IS $.450\,kW/m^2$ FOR A 12h DAY/TEST.

SOLAR ENERGY HANDBOOK, 2015 EDITION ⟶ I_{AVG} = $5.41\,kWh/m^2/day$
↳ P_{AVG} = $450W/m^2$

*NASA SURFACE METEOROLOGY + AVAILABLE TABLES → $I_{AVG.}$ = $5.26\,kWh/m^2/day$
↳ P_{AVG} = $438W/m^2$

↳ SOURCES/METHODS DIFFER BY ONLY 2.7%.

Appendix 04: Pyranometer Specifications

Reproduced under fair use: www.**intech**.co.nz/products/weathersensors/weathersensors/LE-Light-Sensor.pdf

Specifications.

Common Specifications:

Accuracy	±5%.
Range	0~1500 w/m².
Cosine error	Typically less than 3% from vertical to 85° in all directions.
Temperature Coefficient	0.15% per 1°C.
EMC Compliances	Emissions EN 55022-A. Immunity EN 50082-1.
Safety Compliances	EN 60950.
Dimensions -Sensor	Ø=38mm, H=45mm.
-Mounting Plate	L=70mm, W=38mm, H=7mm, PCD=5.5mm.

Current Output Specifications:

Output	4~20mA, 2 wire (Loop Powered).
Load Resistance	600Ω @ 24Vdc.

Voltage Output Specifications:

Output	0~5Vdc, 3 Wire (common ground).
Power Supply Required	12Vdc.

USB Output Specifications:

Output	USB (Std Male Type A, 5Vdc Powered).
Baud Rate	9600.
Format	8 Bit, No Parity, 1 Stop Bit (non selectable).
Protocol	MODBUS RTU.

RS485 Output Specifications:

Output	RS485.
Baud Rate	9600.
Format	8 Bit, No Parity, 1 Stop Bit (non selectable).
Protocol	MODBUS RTU.
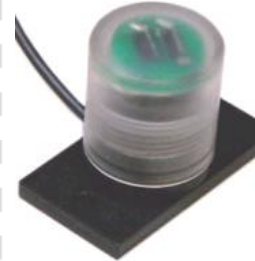
Spectral Response.
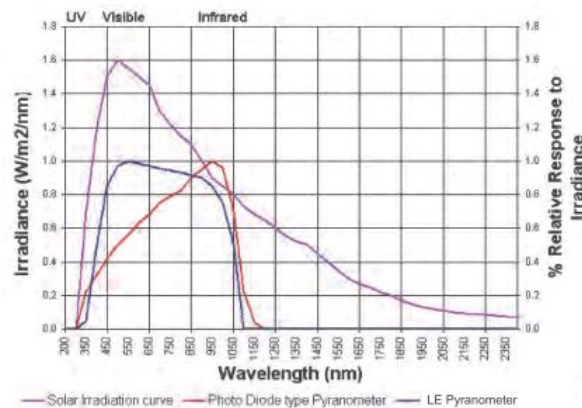
The full terrestrial solar spectrum deposits measurable energy at the earth's surface in the range from 287 nanometers (nm) to beyond 4000 nm. However, as can be seen from the spectral response graph, the pyranometer measures the radiation between 300 and 1100 nanometers. As over 90% of the solar energy is between 300~1100nm, the pyranometer is calibrated so as to estimate the short-wave component of the solar radiation.

Appendix 05a: Rig Dimensions

DETAIL A
SCALE 1 : 2

DETAIL B
SCALE 1 : 2

FRONT ELEVATION

2440

1256

1000

1220

PLAN ELEVATION

855

1260

SIDE ELEVATION

570

635

7

11.4

15.2

5.6

260

5.71

1000

993

D

D

SECTION D-D

7

8.7

557

250

570

5

1220

550

993

115

550

8.44

438

443

115

93

5

5.4

600

550

238

600

838

132

129

137

122

5
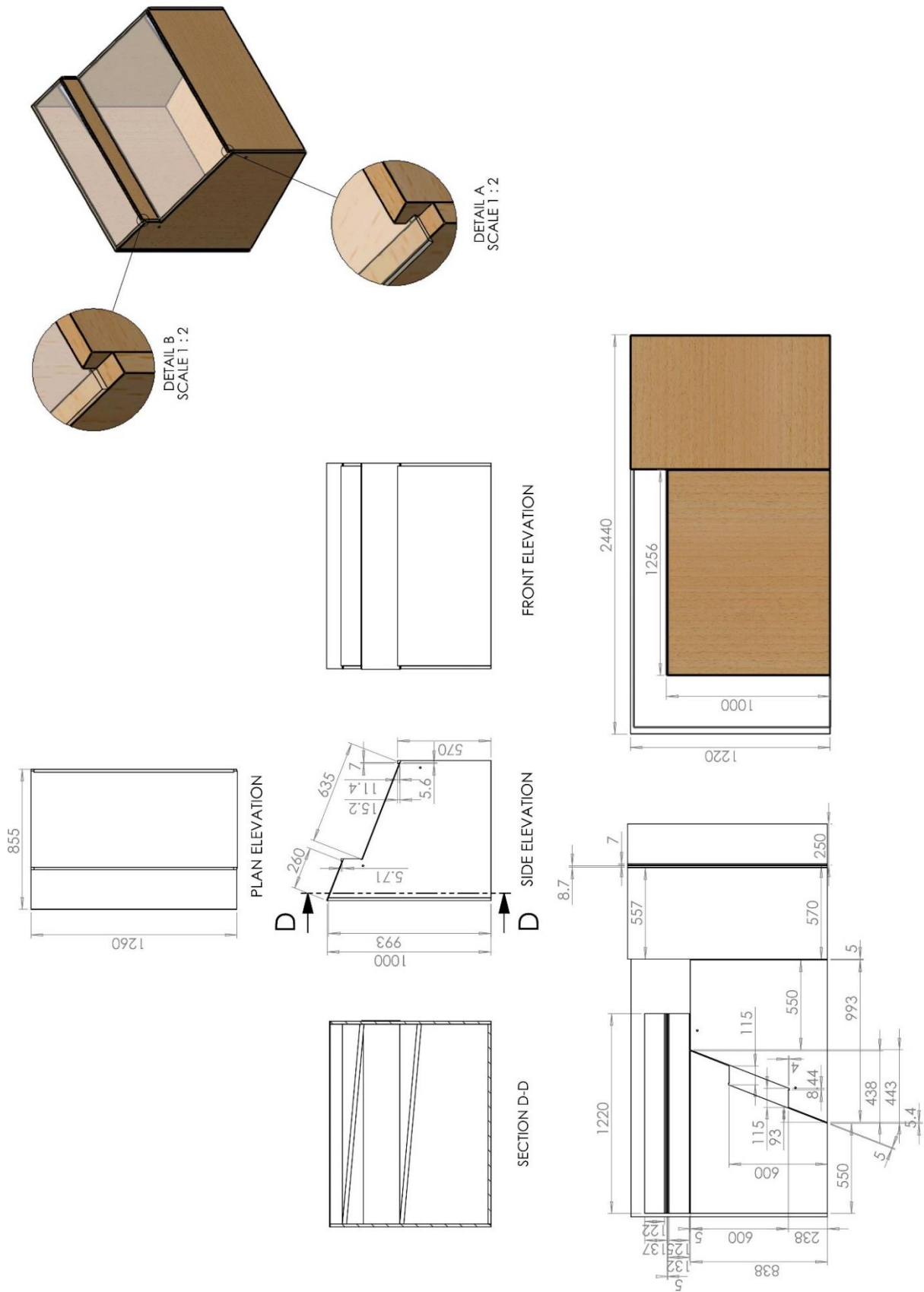
Appendix 05b: Rig Plywood Fabrication

SECTION F-F
SCALE 1 : 30
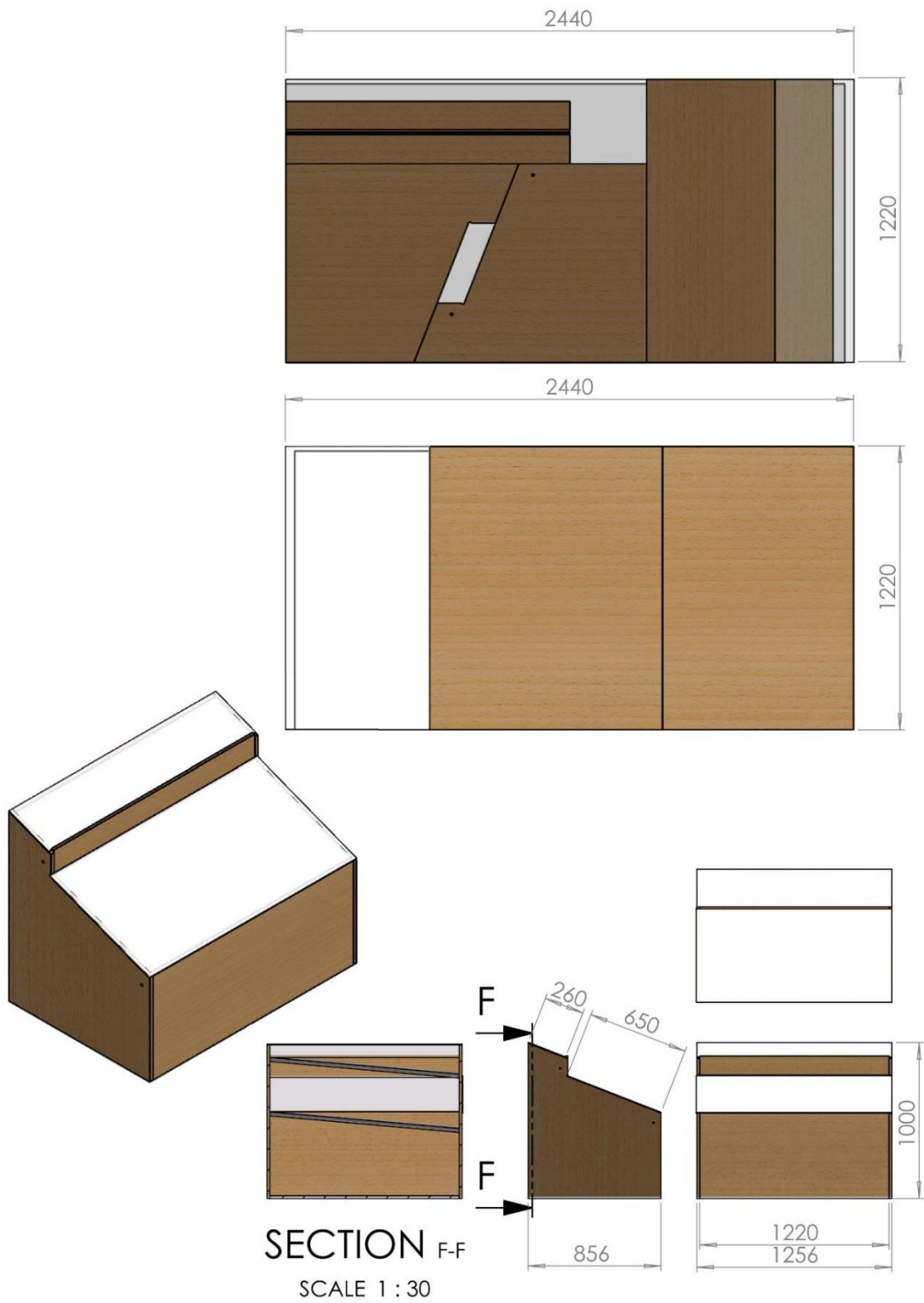
Appendix 06: Risk Assessment for Primary Rig Build Phase

The risks associated with construction and operation of the primary test rig have been mapped onto Consequence – Likelihood space as shown in Figure A6.1. The proposed mitigation and control measures are provided in Table A6.1.

Likelihood	Inconsequential Injury	Minor Injury	Moderate Harm	Severe Harm	Loss of Life
Almost Certain					
Highly Likely	(2): Saline Water Spillage >10 *kg*				
Likely		(3): Rig Implosion			
Possible		(4): Rig Explosion	(6): Fan Blade Injury (7): Burns (9): Heavy Lifting Hazard (> 40 *kg*)	(8): Fire	(1): Electric Shock
Unlikely		(5): Non-Potable Water Hazard			
Highly Unlikely					
Almost Impossible					

Consequence

Figure A6.1: Identified risks pertaining to rig operation mapped onto Consequence – Likelihood Space

Table A6.1: Proposed measures to mitigate and control risks identified with rig during operation	
Numbered Hazard	Proposed Risk Mitigation and Control Measures
(1)	(i) *Implement thorough silicon sealing of the cavity to minimise leak potential onto data acquisition hardware* (ii) *RCD on all electrical devices* (iii) *Check by electrical technician at commissioning and at all major electrical changes during testing*
(2)	(i) Implement thorough silicon sealing of the cavity to minimise leak potential onto data acquisition hardware (ii) *Locate rig in wet space to minimise damage to surrounding equipment* (iii) *Include 'Wet Floor' signage in set up*
(3)	(i) Conduct first principles stress analysis on rig (glass) prior to testing to determine both material fitness for purpose and operable pressure limits (ii) Integrate burst disc or valve to release pressure prior to exceeding the safe limit
(4)	(i) *Integrate pressure release valve to moderate internal pressure during operation* (ii) *Design lighting array to enclose glass surface and therefore eliminate shrapnel hazard*
(5)	(i) *Include 'Do Not Drink' signage*
(6)	(i) *Ensure fan has sufficient guard to minimise risk of injury* (ii) *Include 'Moving Fan Blade Hazard: Do Not Touch' signage*
(7)	(i) *Build sufficient heat dissipation measures into lighting array (fins, thermal insulation, ventilation)* (ii) *Include 'Hot Surface : Do Not Touch' signage* (iii) *Ensure fire extinguisher is nearby*

Table A6.1: ctd	
Numbered Hazard	Proposed Risk Mitigation and Control Measures
(8)	(i) *Build sufficient heat dissipation measures into lighting array (fins, thermal insulation, ventilation)* (ii) *Ensure fire extinguisher is nearby* (iii) *Ensure rig is supervised during initial testing to monitor the temperatures realised during operation* (iv) Select appropriate materials for components around the foreseeable hot areas during the embodiment design phase of rig (v) Include a thermal shutoff circuit to disengage the lighting array if a safe threshold temperature is exceeded

(9)	(i) *Integration of means to lift mechanically (i.e. using pallets to facilitate pallet jack or forklift movement)*

Appendix 07: LABVIEW Block Diagram

The block diagram representation of the LABVIEW script used for recording the acquired sensor data is shown Figure A7.1. This script read all 15 sensor signals from the DAQ chassis and saved the data to a text (.txt) file. The filtering frequency and data save rate were both set up as user defined inputs. The calibration factors for all load cell, hygrometer, pressure transducer and pyranometer measurements were also user defined. The thermocouple calibration factors were inbuilt into the National Instruments software. This generic data acquisition script was built then modified for the purpose of this study by Julian Phillips, the Technical Officer in Electronics Workshop; Mechanical Engineering Department, University of Canterbury.

The four main block elements of the script, as highlighted in Figure A7.1 have been reproduced as detailed images as shown below. The permutations of each block according to the various logical operations relevant to them are also included.
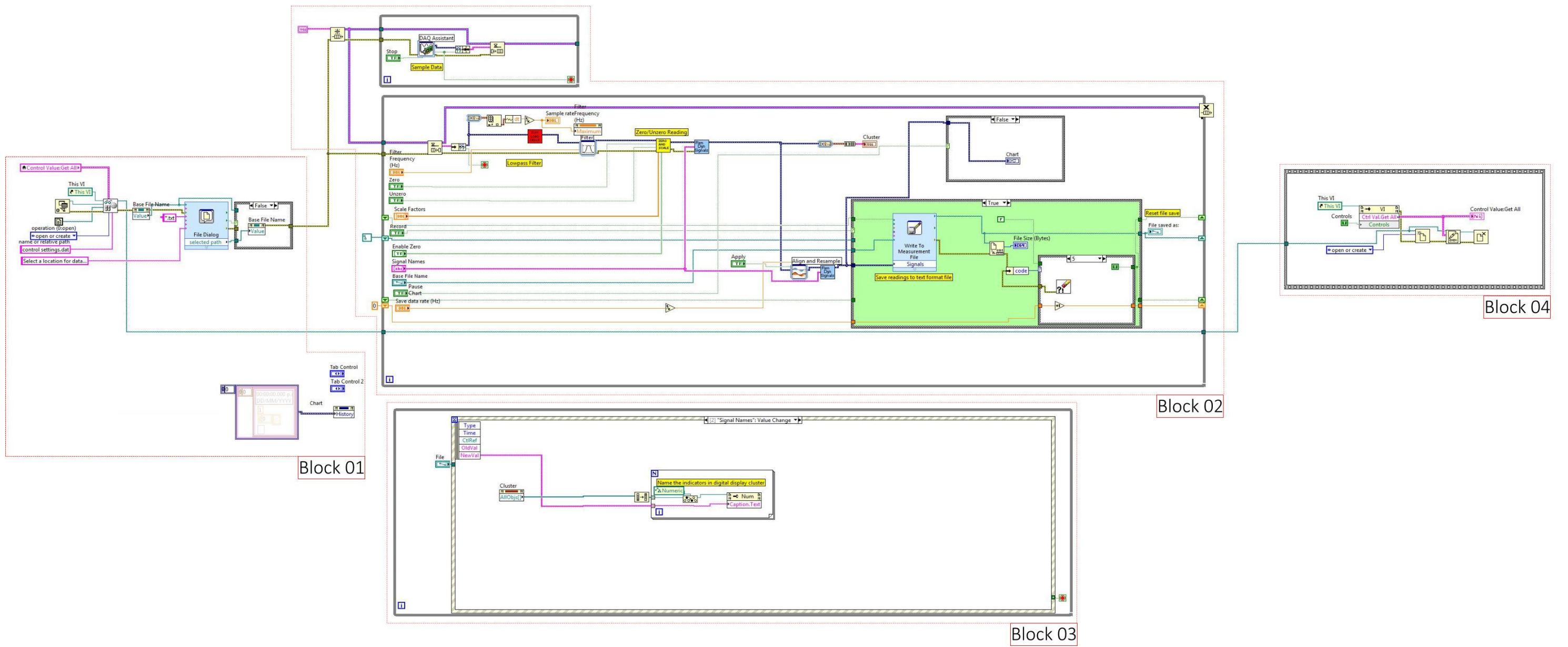
Figure A7.1: LABVIEW block diagram representation of data acquisition script
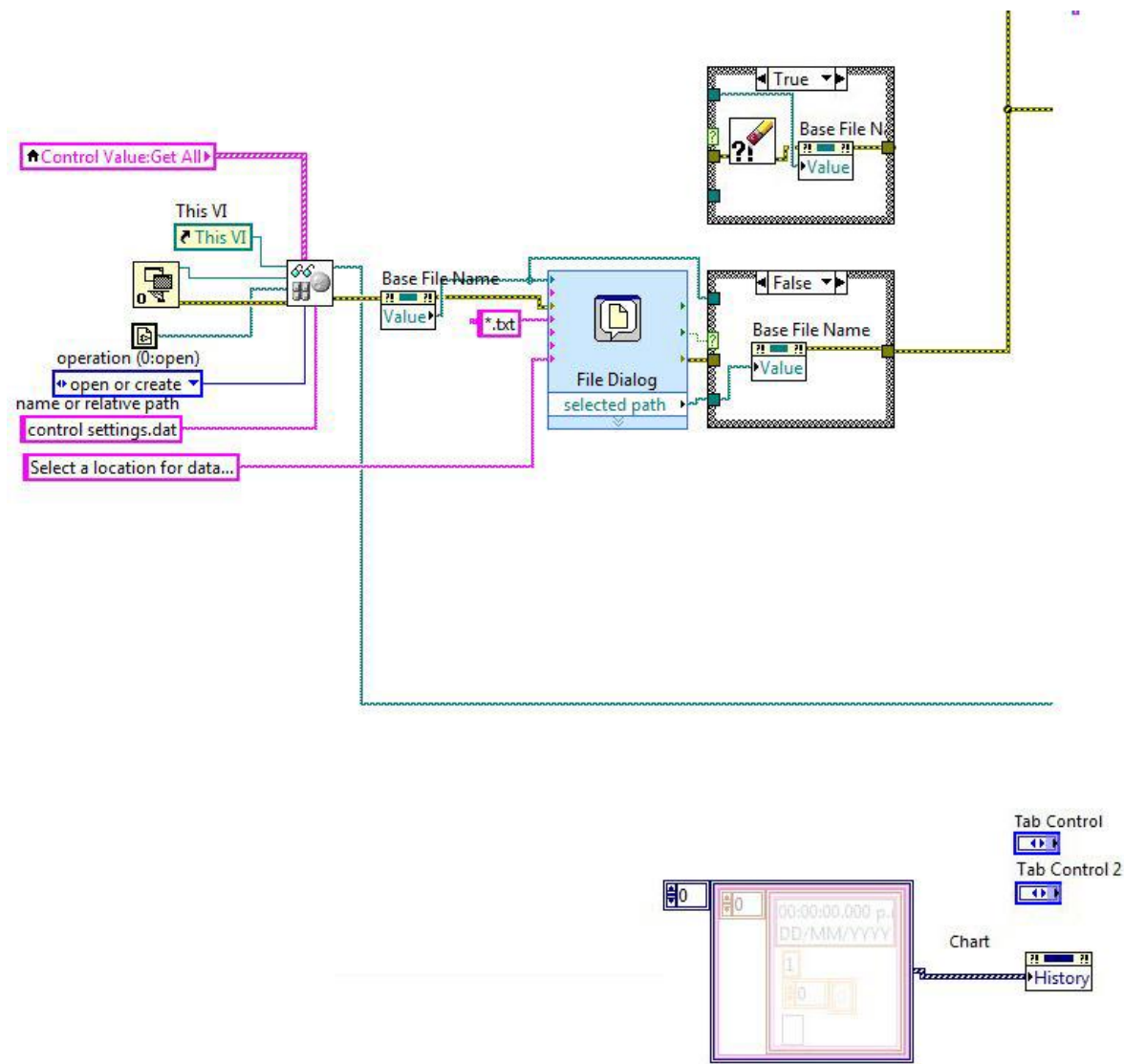
Figure A7.2: Block 01 detailed schematic with True/False Permutation shown
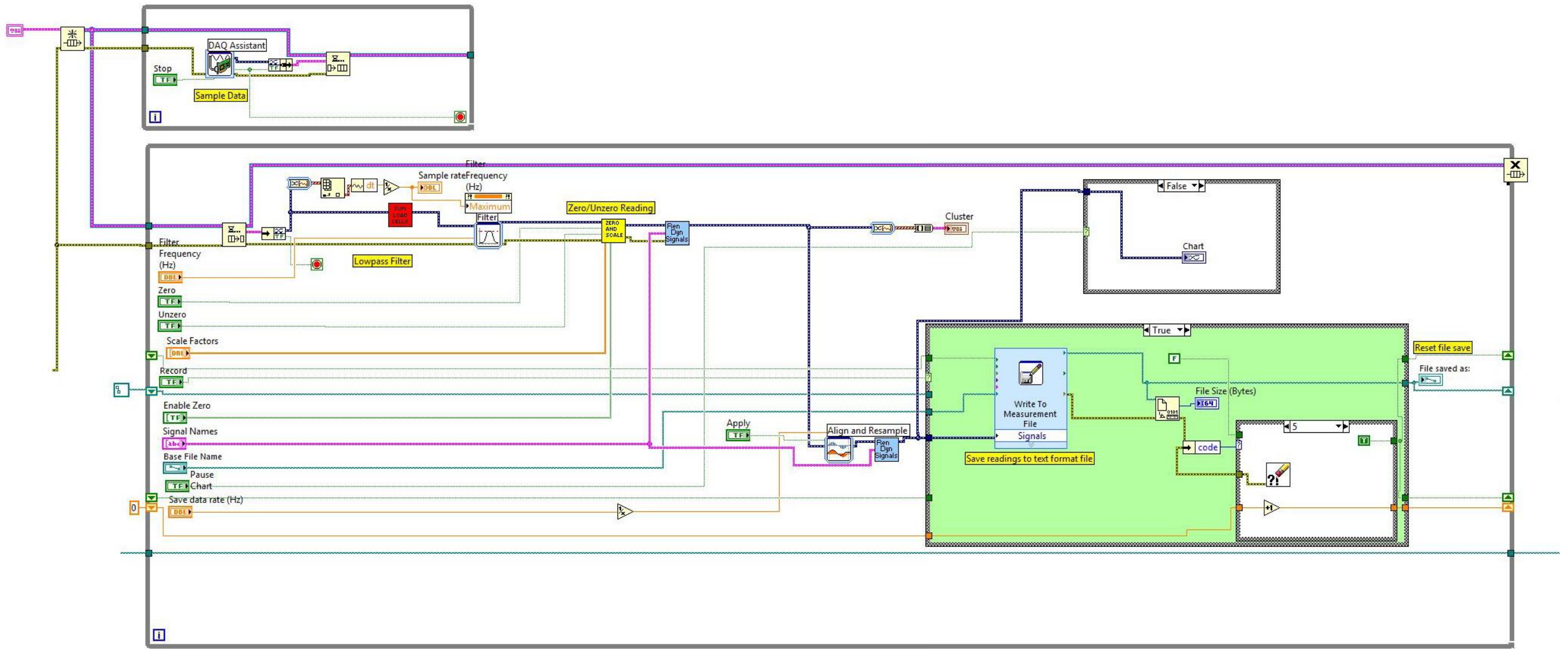
Figure A7.3: Block 02 detailed schematic
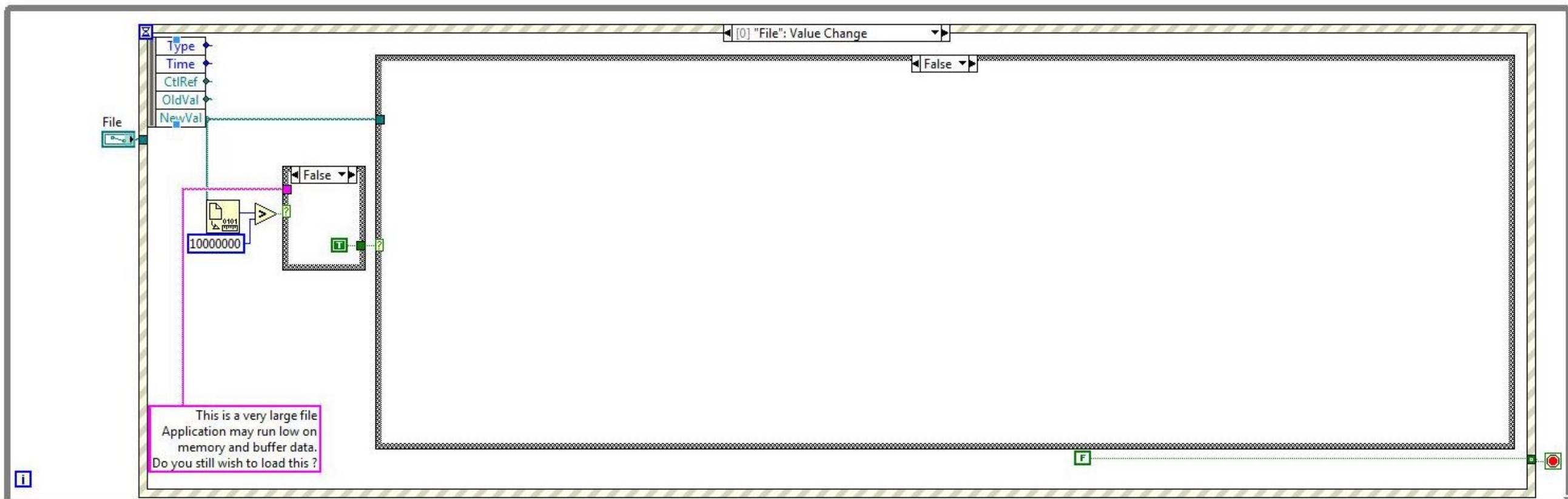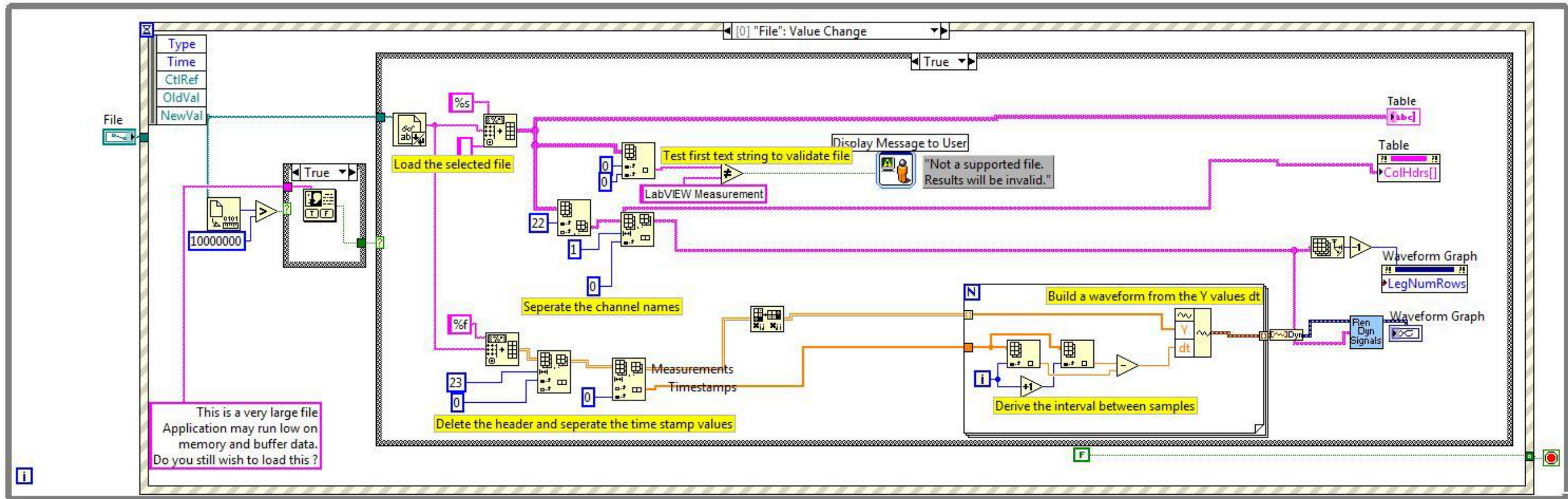
Figure A7.4: Block 03 detailed schematic for System State 0 with True/False Permutation shown
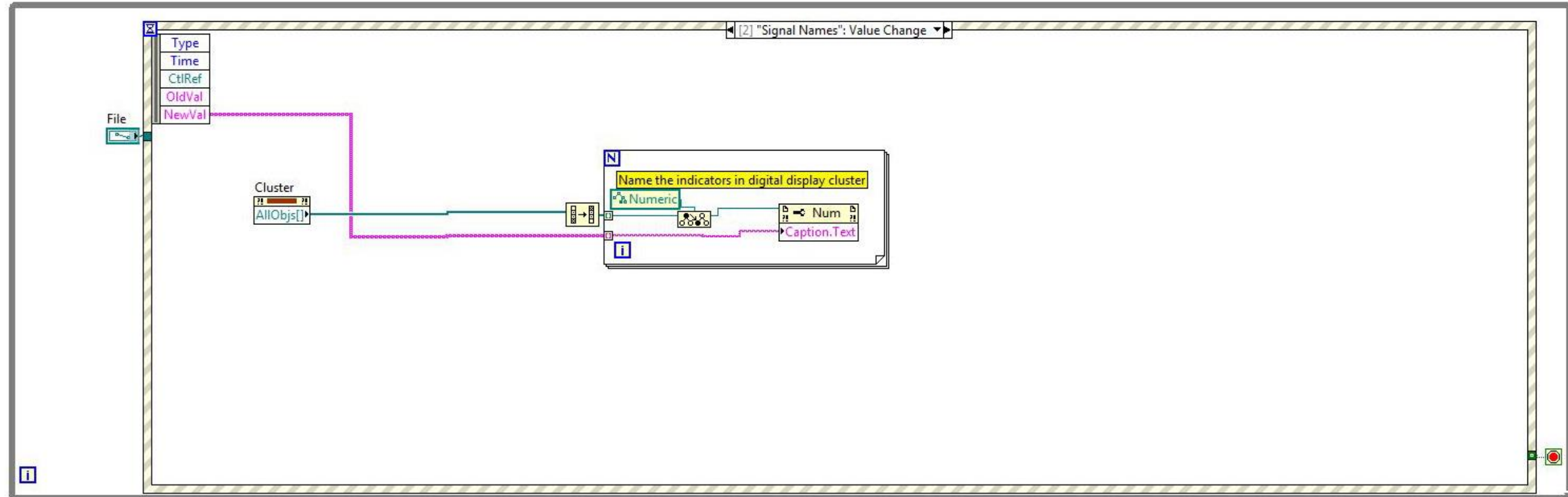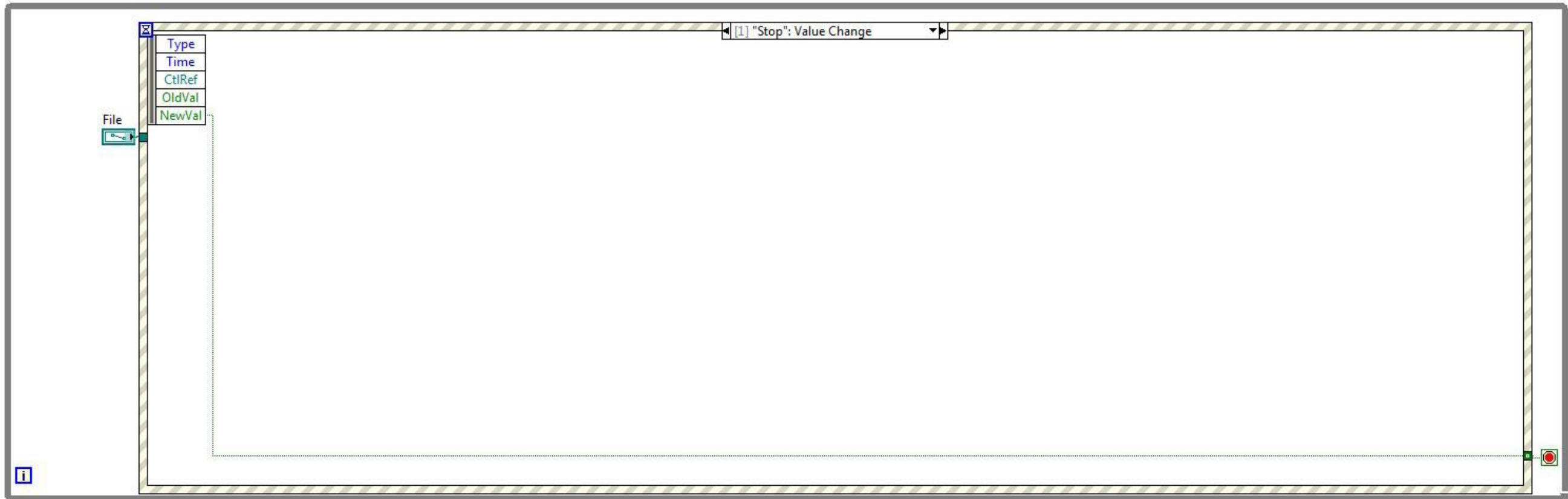
Figure A7.5: Block 03 detailed schematic for System States 1 and 2
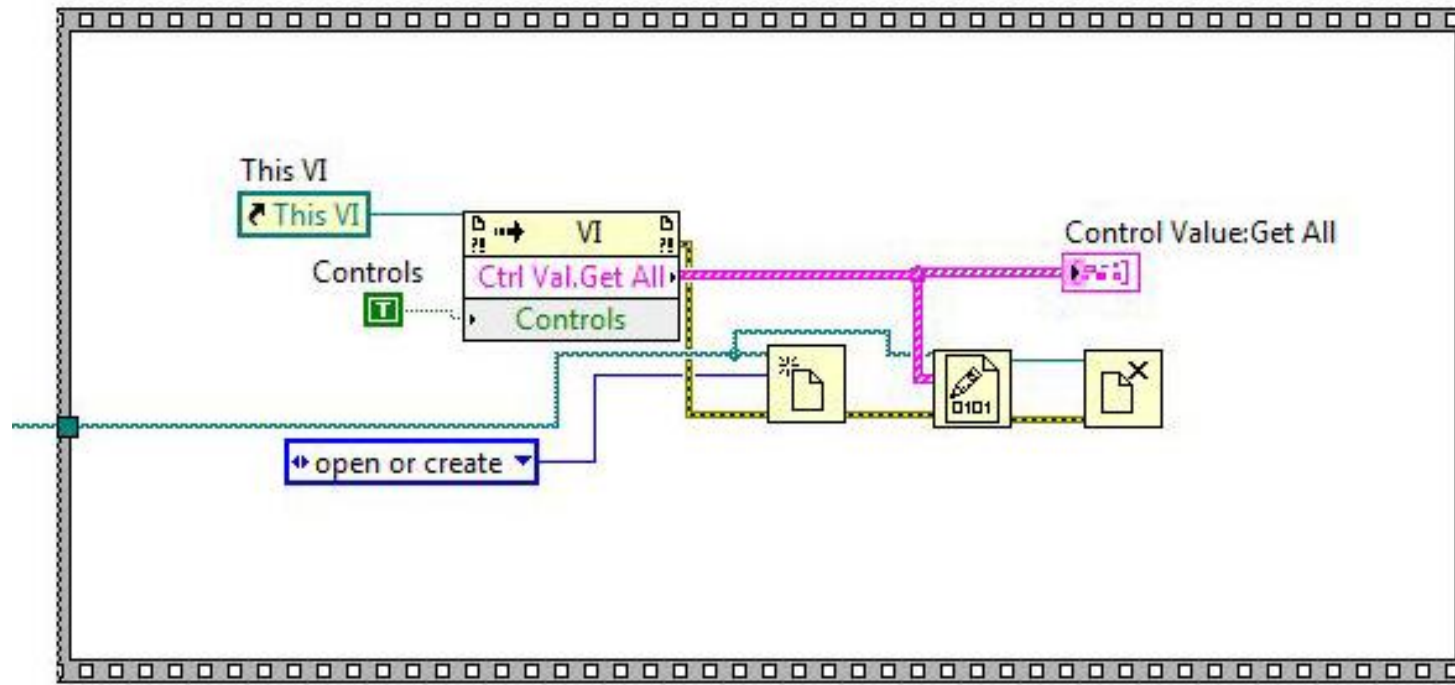
Figure A7.6: Block 04 detailed schematic

Appendix 08a: Design of Experiment

Figure A8.1 (next page) shows the experimental regime that was designed, with specific aims for the testing of each parameter included.

Parameter Tested	Reference Case (default)	State 01 (option)	State 02 (option)	State 03 (option)
Incident Radiation	**Constant 700W Intensity for test duration**	**Constant Intensity for first half of test. No incident energy for second half (typically 12h sunlight in Tonga).**	**Constant 500W Intensity for test duration**	**Sunlight Profile**
	AIM: To achieve baseline productivity of system	*AIM: To test thermal storage of system*	*AIM: To achieve baseline productivity of system*	*AIM: To achieve baseline productivity of system*
Wind Profile	**No 'wind' for test duration**	**Constant 'wind' speed for test duration (5.8 m/s; based on typical wind speeds in area)**	**Pulse wave 'wind' profile (on - off) to assess transient wind effects**	
		AIM: To investigate how forced convection on condensing surface affects productivity	*AIM: To investigate how more realistic wind conditions affect productivity*	
Water Mass	**2.5 kg water mass (Sub Critical)**	**0.6 kg water mass (Sub Critical)**	**4.5 kg water mass (Sub Critical)**	**Critical or Super-critical (>= 45 kg)**
	AIM: To test effect of brine water mass on productivity	*AIM: To test effect of brine water mass on productivity*	*AIM: To test effect of brine water mass on productivity*	**Should give 2.2 - 6 L / day of distillate based on study results**
Lower Operating Presssure	**Atmospheric Pressure**	**Alter Rig into Low Pressure Variant using the extractor fan (for as low a pressure as can be achieved 63.7L/s air flow)**		
		AIMS: To test effect of reduced internal pressure on productivity + to test practicality of reducing pressure		
Absorber Surface Material	**Clear Glass Absorber**	**Glass Absorber with Black Coating**	**Polycarbonate Absorber**	
		AIM: To compare the effect of intended absorber colour with typical clear glass absorber	*AIM: To compare the effect of a PC absorber against typical clear glass absorber*	
Open Air Flow Variation	**Closed Test Rig**	**Alter Rig into Open Air Variant. Test with Free Convection**	**Alter Rig into Open Air Variant. Test with Forced Convection**	
		AIM: To achieve baseline productivity of Open Air Concept	*AIM: To investigate performance difference and inform design direction for forcing airflow*	
Condensor Surface Material	**2mm Aluminium sheet Condensor surface**	**3mm float glass Condensor Surface**		
		AIM: To compare the effect of a thermodynamically superior material to the typically applied material		
Condensor - Evaporator distance	**Standard height of Condensor**	**Reduce air-tunnel height to see if the reduced temperature differential reduces productivity**		
		AIM: To compare the opposite action reducing temperature difference		
Water Salinity	**Standard Tap Water**	**Saline Water at Pacific salinity levels (35g/kg)**		
		AIM: To compare the condensation characteristics with and without salt		

Figure A8.1: Design of Experiment – All tested states of system

Appendix 08b: Test Variable Allocation Matrix

The matrix detailing the specific state of each parameter for each test is provided in Table A8.1

Table A8.1: Test Variable Allocation Matrix										
Date	Test Number	Field Allocation in Code	Initial Water Mass	Lighting Power	Absorber Material[12]	Salinity	Condenser Fan Operating [13]	Evaporation Surface[14]	Rig Open[15]	Cool Down Profile[16]
-	-	-	kg	W	-	g/kg	-	-	-	-
23-Feb	1	1	0	700	GL	0	Y	STD	C	Y
23-Feb	2	2	2.55	700	GL	0	Y	STD	C	Y
24-Feb	3	3	2.55	SUN	GL	0	Y	STD	C	N
25-Feb	4	4	10	SUN	GL	0	Y	STD	C	N
26-Feb	5	5	3	700	PC	0	Y	STD	C	Y
29-Feb	6	6	3	700	PC	0	Y	STD	C	Y
1-Mar	7	7	4	700	PC	0	Y	STD	C	Y
2-Mar	**8**	**8**	**2.55**	**700**	**PC**	**0**	**Y**	**STD**	**C**	**Y**
4-Mar	9	9	0.6	700	PC	0	Y	STD	C	Y
5-Mar	10	10	0.6	500	PC	0	Y	STD	C	N
7-Mar	11	11	2.55	700	PC	36	Y	STD	C	N
8-Mar	12	12	2.55	SUN	PC	36	Y	STD	C	N
8-Mar	13	13	2.12	700	PC	42	N	STD	C	N
10-Mar	14	14	2.21	700	PC	0	Y	RDC	C	N
11-Mar	15	15	2.5	700	PC	0	Y	STD	O	Y
13-Mar	16	16	2.5	700	PC	0	Y	STD	HO	N
15-Mar	**17**	**17**	**2.5**	**700**	**PC**	**0**	**Y**	**STD**	**C**	**N**
16-Mar	18	18	2.5	700	PC	0	N	STD	C	N
18-Mar	19	19	2.5	SUN	PC	0	Y	STD	C	N
19-Mar	20	20	4.5	700	PC	0	Y	STD	C	N

[12] GL = Glass, PC = Polycarbonate, AL = Aluminium
[13] Y = Yes, N = No
[14] STD = Standard Area (1 m^2), RDC = Reduced Area (0.0324 m^2)
[15] C = Closed, HO = Half Open, O = Open
[16] Y = Yes (Cool-down Profile recorded), N = No (Cool-down Profile not recorded)

Table A8.1 ctd: Test Variable Allocation Matrix										
Date	Test Number	Field Allocation in Code	Initial Water Mass	Lighting Power	Absorber Material	Salinity	Condenser Fan Operating	Evaporation Surface	Rig Open	Cool Down Profile
21-Mar	21	21	2.5	SUN	PC	0	Y	STD	C	N
22-Mar	22	22	2.5	SUN	PC	0	Y	STD	C	N
23-Mar	23	23	2.5	700	AL	0	Y	STD	C	N
28-Mar	24	24	2.5	700	AL	0	Y	STD	C	N
29-Mar	**25**	**25**	**2.5**	**700**	**PC**	**0**	**Y**	**STD**	**C**	**N**
30-Mar	26	26	2.5	700	PC	44	Y	STD	C	N

Notes:

Temperature sensors T1 and T8 became loose during Test 07

The load cells were zeroed after testing begun during Test13, so water in basin starts at zero and decreases. Add 2.12 *kg* to water mass at each data point to remedy this error.

No Condensate Collected during Test 19 due to wind whisking the drainage pipe out of the collection receptacle

Test 24 is the Aluminium cool-down profile only

For data processing purposes, the tests relevant to an identified variable of interest have been grouped together below in Tables A8.2 – A8.3.

Table A8.2: Test numbers ordered by relevant variable of interest				
Tested Variable	*Reference Test*	*Solar Incident Energy*	*Initial Water Mass*	*Reduced Energy Input*
Applicable Test Number	8	3	9	10
	17	4	17	12
	25	12		17
		17		
		19		
		21		
		22		

Table A8.3: Test numbers ordered by relevant variable of interest					
Tested Variable	Absorption Surface Material	Saline Water	Fan Off	Reduced Evaporative Area	Open Air Rig
Applicable Test Number	2	11	13	14	15
	17	12	17	17	16
	23	13	18		17
		17			
		26			

Appendix 09: Fault Analysis of Load Cell Arrangement

Figure A9.1 shows the brief fault analysis considered when dealing with the erroneous load cell measurements
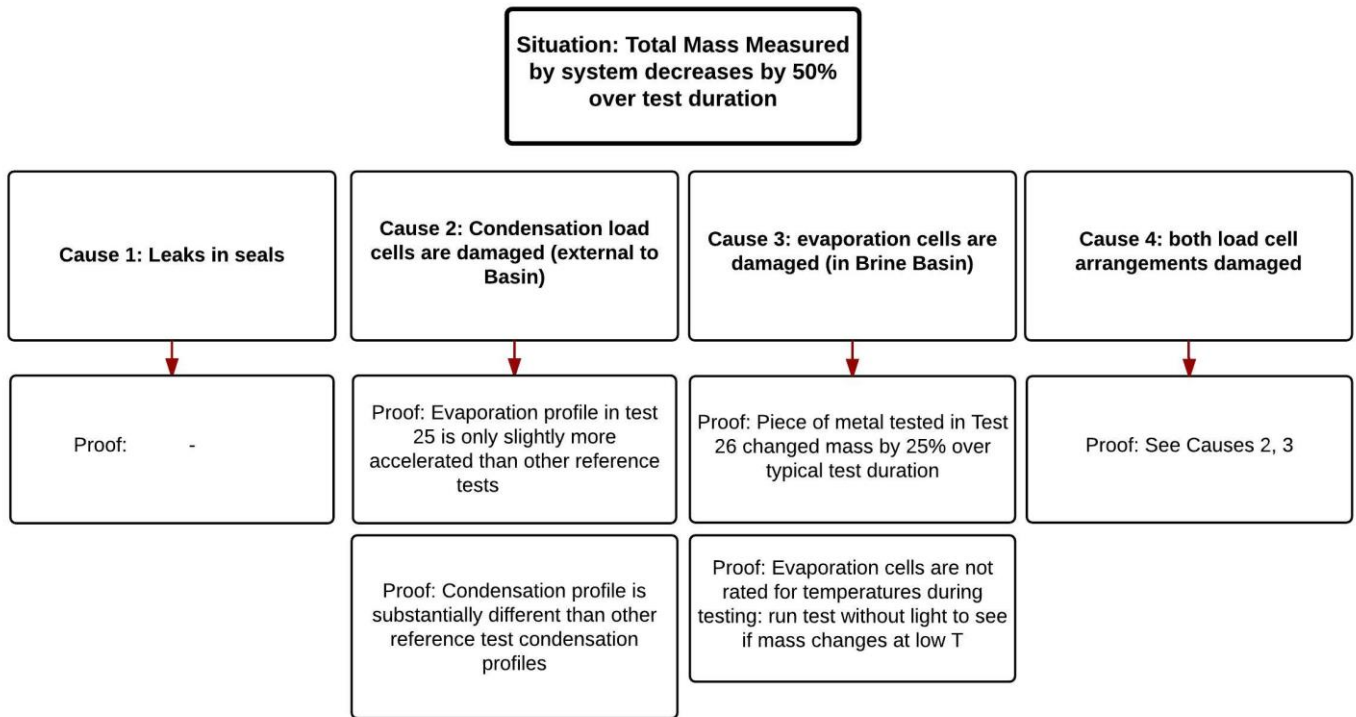
at the end of the test period

Figure A9.1: Fault analysis schematic detailing erroneous load cell measurements

Appendix 10: Energy Equivalence Calculations

A brief thermodynamic analysis was conducted to correlate the pyranometer readings from the halogen testing into equivalent solar energy values. The pyrnaometer used to measure the incident energy was calibrated to respond to a solar spectrum rather than a halogen spectrum, so was less sensitive based on how the values compared to the temperature values of the water in the basin. The energy-temperature relationship underpinning the analysis is provided by equation A10.1, where ΔE is the amount of energy required to cause a change in temperature of ΔT and α is the constant of proportionality that encompasses the thermal inertia of the rig and the internal air. The value of α has been assumed to be constant for all tests, independent of energy source.

$$\Delta E = \alpha \Delta T \hspace{4cm} \text{(A10.1)}$$

The analysis has assumed that heating the empty, sealed rig through a given temperature range requires effectively the same amount of energy to be input. At some instant during each of the sunshine tests, the temperature rise is equal to the temperature rise in the reference test. When the reference temperature difference became equal to the sunshine test differential, it was assumed that the cumulative energy input was the same for each. The ratio of cumulative sunshine energy to cumulative halogen energy was taken to find the scaling factor to correct the pyranometer readings for the halogen tests.

The minimum comparable temperature rise of the internal air between all sunshine tests and the reference test was calculated. A script written in MATLAB iterated through the data, recording the difference in accumulated energy that corresponded to this minimum temperature rise. Within the same data set, this minimum temperature rise occurred multiple times and this allowed an average change in energy to be calculated for the corresponding change in temperature.

The analysis has indicated that the expected calibration factor to ensure the pyranometer readings between the *in vitro* tests and the solar readings tests is approximately 2.9. This is a provisional value and dedicated testing needs to be undertaken to validate the method employed.

The code is included below for reproducing the analysis.

```matlab
%% Section 4.3.6.1 : Equating Incident Energy
clc; close all; clear all; load AllData_1.mat
fields = fieldnames(Data_1); nf = numel(fields);L = zeros(1,nf);
for i=1:nf
    L (i) = length(Data_1.(fields{i})(:,1));
end

time = max(L);
% Concatenates all tests to longest test length & removes trailing zeros
for i = 1:nf
    Data_1.t(:,i) = 1/3600*[Data_1.(fields{i})(:,1);...
        NaN*zeros([time-length(Data_1.(fields{i})(:,1)),1])];
    Data_1.M1(:,i) = [Data_1.(fields{i})(:,2);...
        NaN*zeros([time-length(Data_1.(fields{i})),1])];
    Data_1.M3(:,i) = [Data_1.(fields{i})(:,4);...
        NaN*zeros([time-length(Data_1.(fields{i})),1])];
    Data_1.T1(:,i) = [Data_1.(fields{i})(:,8);...
        NaN*zeros([time-length(Data_1.(fields{i})),1])];
    Data_1.T2(:,i) = [Data_1.(fields{i})(:,9);...
        NaN*zeros([time-length(Data_1.(fields{i})),1])];
    Data_1.T3(:,i) = [Data_1.(fields{i})(:,10);...
        NaN*zeros([time-length(Data_1.(fields{i})),1])];
    Data_1.T4(:,i) = [Data_1.(fields{i})(:,11);...
        NaN*zeros([time-length(Data_1.(fields{i})),1])];
    Data_1.I1(:,i) = [Data_1.(fields{i})(:,16);...
        NaN*zeros([time-length(Data_1.(fields{i})),1])];
end
m_i = repmat(Data_1.M1(1,:),length(Data_1.M1),1); % initial M1 values
%% Section 6: Legend Controls
af_IE = [6 3 1]; ColSet_IE = hsv(4*length(af_IE));
l_IE = cell(length(af_IE),1);
l_IE{1} = strcat(fields{af_IE(1)},' Polycarbonate (I_1 = 700 W)');
l_IE{2} = strcat(fields{af_IE(2)},' Glass_{} (Sunshine)');
l_IE{3} = strcat(fields{af_IE(3)},' Glass (I_1 = 700W)');
%% Figure 6.1: Incident Energy Mass Condensed & Evaporated
figure('Name','Figure 6.1: Incident Energy Tests - Mass','NumberTitle',...
    'off','units','normalized','outerposition',[0 0 1 1])
subplot(2,1,1)
[hLine031] = plot(Data_1.t(:,af_IE),Data_1.M3(:,af_IE));
title('Condensation Surface','FontSize',14);
ylabel(['Water Condensed',10,'at Collector [ kg ]'], 'FontSize', 14)
xlabel(['Time Elapsed [ hr ]',10,'   '], 'FontSize', 14);xlim([0,18]);
l=legend(l_IE, 'FontSize', 14,'Location','eastoutside'); grid on
a=get(l,'children');a=a([1 4 7 ]);set(a,'markersize',20);
set(gca,'Fontsize',18,'LineWidth',2)
for i =  1:length(af_IE)  % Line / Marker Properties
    set(hLine031(i),{'Color'},{ColSet_IE(4*i - 3,:)}',...
        {'LineStyle'},{'none'}',{'Marker'},{'.'}')
end

subplot(2,1,2)
[hLine032] = plot(Data_1.t(:,af_IE),Data_1.M1(:,af_IE)-m_i(:,af_IE));
title('Evaporation Surface','FontSize',14);
```

```matlab
ylabel(['Water Evaporated',10,'from Basin [ kg ]'], 'FontSize', 14)
xlabel('Time Elapsed [ hr ]', 'FontSize', 14);
l=legend(l_IE', 'FontSize', 14,'Location','eastoutside'); grid on
a=get(l,'children');a=a([1 4 7]);set(a,'markersize',20);
set(gca,'Fontsize',18,'LineWidth',2)
for i =  1:length(af_IE) % Line / Marker Properties
    set(hLine032(i),{'Color'},{ColSet_IE(4*i - 3,:)}',...
        {'LineStyle'},{'none'}',{'Marker'},{'.'}')
end

%% Figure 6.2 : Accumulated Incident Energy - Integral of power flux
figure('Name','Figure 6.2: Incident Energy Integral','NumberTitle',...
    'off','units','normalized','outerposition',[0 0 1 1])
subplot(2,1,1);
[hLine033] = plot(Data_1.t(:,af_IE),Data_1.I1(:,af_IE));
ylabel(['Incident Energy Rate',10,'[ W / m^2 ]'], 'FontSize', 14)
xlabel(['Time Elapsed [ hr ]',10,'   '], 'FontSize', 14);xlim([0,18]);
l=legend(l_IE', 'FontSize', 14,'Location','eastoutside'); grid on
a=get(l,'children');a=a([1 4 7 ]);set(a,'markersize',20);
set(gca,'Fontsize',18,'LineWidth',2)
for i =  1:length(af_IE) % Line / Marker Properties
    set(hLine033(i),{'Color'},{ColSet_IE(4*i - 3,:)}',...
        {'LineStyle'},{'none'}',{'Marker'},{'.'}')
end

% Incident Power Integral - ( Energy )
int_I1 = zeros(length(Data_1.I1),length(af_IE));h=zeros(length(af_IE),1);
int_t = Data_1.t; solI1=Data_1.I1;
for i = 1 : length(af_IE)
    h(i)=find(isnan(Data_1.t(:,af_IE(:,i))),1,'first');
    int_t(h:end,af_IE(i))=0;
    solI1(h:end,af_IE(i))=0;
    int_I1(:,i)= cumtrapz(Data_1.t(:,af_IE(:,i)),Data_1.I1(:,af_IE(:,i)));
end
subplot(2,1,2);
[hLine034] = plot(Data_1.t(:,af_IE),int_I1);
for i =  1:length(af_IE) % Line / Marker Properties
    set(hLine034(i),{'Color'},{ColSet_IE(4*i - 3,:)}',...
        {'LineStyle'},{'none'}',{'Marker'},{'.'}')
end
ylabel(['Cumulative Incident Energy',10,'[ J / m^2 ]'], 'FontSize', 14)
xlabel(['Time Elapsed [ hr ]',10,'   '], 'FontSize', 14);xlim([0,18]);
l=legend(l_IE', 'FontSize', 14,'Location','eastoutside'); grid on
a=get(l,'children');a=a([1 4 7]);set(a,'markersize',20);
set(gca,'Fontsize',18,'LineWidth',2)

%% Plot 6.3: Associated Temperature rise resulting from accumulated Energy
af_IET_dry = af_IE;
int_TI1_dry = int_I1;

% Colours are aligned with initial plot results; Ref Test plotted red
ColSet_IET = hsv(4*length(af_IET_dry));
figure('Name','Figure 6.3: Incident Energy
Integral','NumberTitle','off',...
    'units','normalized','outerposition',[0 0 1 1])
```

```matlab
subplot(4,1,1);
[hLine035] = plot(Data_1.t(:,af_IET_dry),int_TI1_dry);
ylabel(['Cumulative Incident Energy',10,'[ J / m^2 ]'], 'FontSize', 14)
xlabel(['Time Elapsed [ hr ]',10,'    '], 'FontSize', 14);xlim([0,7]);
l=legend(l_IE', 'FontSize', 14,'Location','eastoutside'); grid on
a=get(l,'children');a=a([1 4 7]);set(a,'markersize',20);
set(gca,'Fontsize',18,'LineWidth',2)
for i =  1:length(af_IET_dry) % Line / Marker Properties
    set(hLine035(i),{'Color'},{ColSet_IET(4*i - 3,:)}',...
        {'LineStyle'},{'none'}',{'Marker'},{'.'}')
end
subplot(4,1,2);
[hLine036] = plot(Data_1.t(:,af_IET_dry),Data_1.T4(:,af_IET_dry));
ylabel(['Water Temp',10,'[ ^oC ]'], 'FontSize', 14)
xlabel(['Time Elapsed [ hr ]',10,'    '], 'FontSize', 14);xlim([0,7]);
l=legend(l_IE', 'FontSize', 14,'Location','eastoutside'); grid on
a=get(l,'children');a=a([1 4 7]);set(a,'markersize',20);
set(gca,'Fontsize',18,'LineWidth',2)
for i =  1:length(af_IET_dry) % Line / Marker Properties
    set(hLine036(i),{'Color'},{ColSet_IET(4*i - 3,:)}',...
        {'LineStyle'},{'none'}',{'Marker'},{'.'}')
end


subplot(4,1,3);
[hLine037] = plot(Data_1.t(:,af_IET_dry),Data_1.T2(:,af_IET_dry));
ylabel(['Air Temp',10,'[ ^oC ]'], 'FontSize', 14)
xlabel(['Time Elapsed [ hr ]',10,'    '], 'FontSize', 14);xlim([0,7]);
l=legend(l_IE', 'FontSize', 14,'Location','eastoutside'); grid on
a=get(l,'children');a=a([1 4 7]);set(a,'markersize',20);
set(gca,'Fontsize',18,'LineWidth',2)
for i =  1:length(af_IET_dry) % Line / Marker Properties
    set(hLine037(i),{'Color'},{ColSet_IET(4*i - 3,:)}',...
        {'LineStyle'},{'none'}',{'Marker'},{'.'}')
end


subplot(4,1,4);
[hLine038] = plot(Data_1.t(:,af_IET_dry),Data_1.T1(:,af_IET_dry));
ylabel(['Absorber Temp',10,'[ ^oC ]'], 'FontSize', 14)
xlabel(['Time Elapsed [ hr ]',10,'    '], 'FontSize', 14);xlim([0,7]);
l=legend(l_IE', 'FontSize', 14,'Location','eastoutside'); grid on
a=get(l,'children');a=a([1 4 7]);set(a,'markersize',20);
set(gca,'Fontsize',18,'LineWidth',2)
for i =  1:length(af_IET_dry) % Line / Marker Properties
    set(hLine038(i),{'Color'},{ColSet_IET(4*i - 3,:)}',...
        {'LineStyle'},{'none'}',{'Marker'},{'.'}')
end
%% PLOT 06.4: Finding the point of equal energy input
l_diffIET_dry = cell(length(af_IET_dry)-1,1);
l_diffIET_dry{1} = strcat('\DeltaT_{PC-GL in vitro}
(_{',fields{af_IET_dry(1)},...
    ' - ',fields{af_IET_dry(2)},'})');
l_diffIET_dry{2} = strcat('\DeltaT_{PC-GL in vitro}
(_{',fields{af_IET_dry(1)},...
    ' - ',fields{af_IET_dry(3)},'})');
```

```matlab
% 'In' is a matrix of the initial experimental conditions, for comparison
% purposes
In{1,1} = 'T_water (t=0)';In{2,1} = 'T_air (t=0)';
In{3,1} = 'M_Brine(t=0)';In{4,1} = 'T_absorber (t=0)';
for i = 1 : length(af_IET_dry)
    In{1,i+1} = Data_1.T4(1,af_IET_dry(i));
    In{2,i+1} = Data_1.T2(1,af_IET_dry(i));
    In{3,i+1} = Data_1.M1(1,af_IET_dry(i));
    In{4,i+1} = Data_1.T1(1,af_IET_dry(i));
end


%temperature difference vectors dT
dT1 =zeros(length(Data_1.T1),length(af_IET_dry)-1);dT2 = dT1;dT4 = dT1;
for j = 2:length(af_IET_dry)
    for i = 1 : length(Data_1.T1(:,af_IET_dry(j)))
        dT1(i,j-1)= (Data_1.T1(i,af_IET_dry(1))...
            -Data_1.T1(1,af_IET_dry(1)))...
            - (Data_1.T1(i,af_IET_dry(j))-Data_1.T1(1,af_IET_dry(j)));
        dT2(i,j-1)= (Data_1.T2(i,af_IET_dry(1))...
            -Data_1.T2(1,af_IET_dry(1)))...
            - (Data_1.T2(i,af_IET_dry(j))-Data_1.T2(1,af_IET_dry(j)));
        dT4(i,j-1) =(Data_1.T4(i,af_IET_dry(1))...
            -Data_1.T4(1,af_IET_dry(1)))...
            - (Data_1.T4(i,af_IET_dry(j))-Data_1.T4(1,af_IET_dry(j)));
    end
end
% (extra +1,-1 added at end for processing)
dT4 = [dT4;ones(1,length(af_IET_dry)-1);-1*ones(1,length(af_IET_dry)-1)];
dT2 = [dT2;ones(1,length(af_IET_dry)-1);-1*ones(1,length(af_IET_dry)-1)];
dT1 = [dT1;ones(1,length(af_IET_dry)-1);-1*ones(1,length(af_IET_dry)-1)];


ColSetTrnc_IET=ColSet_IET(5:end,:);
figure('Name','Figure 6.4: Temperature Differences','NumberTitle',...
    'off','units','normalized','outerposition',[0 0 1 1]);
subplot(3,1,1);
[hLine039] =plot(Data_1.t(:,af_IET_dry(2:end)),dT2(1:length(Data_1.T2),:));
title('Temperature difference between Sunshine & Reference Tests',...
    'FontSize', 14)
ylabel(['Air Temp',10,'[ ^oC ]'], 'FontSize', 14)
xlabel(['Time Elapsed [ hr ]',10,'   '], 'FontSize', 14);xlim([0,7]);
l=legend(l_diffIET_dry', 'FontSize', 14,'Location','eastoutside');
grid on;a=get(l,'children');a=a([1 4]);set(a,'markersize',20);
set(gca,'Fontsize',18,'LineWidth',2)
for i =  1:length(af_IET_dry)-1 % Line / Marker Properties
    set(hLine039(i),{'Color'},{ColSetTrnc_IET(4*i - 3,:)}',...
        {'LineStyle'},{'none'}',{'Marker'},{'.'}')
end

subplot(3,1,2);
[hLine040] =plot(Data_1.t(:,af_IET_dry(2:end)),dT4(1:length(Data_1.T4),:));
ylabel(['Water Temp',10,'[ ^oC ]'], 'FontSize', 14)
xlabel(['Time Elapsed [ hr ]',10,'   '], 'FontSize', 14);xlim([0,7]);
l=legend(l_diffIET_dry', 'FontSize', 14,'Location','eastoutside');
grid on;a=get(l,'children');a=a([1 4]);set(a,'markersize',20);
set(gca,'Fontsize',18,'LineWidth',2)
```

```matlab
for i =  1:length(af_IET_dry)-1 % Line / Marker Properties
    set(hLine040(i),{'Color'},{ColSetTrnc_IET(4*i - 3,:)}',...
        {'LineStyle'},{'none'}',{'Marker'},{'.'}')
end


subplot(3,1,3);
[hLine041] =plot(Data_1.t(:,af_IET_dry(2:end)),dT1(1:length(Data_1.T1),:));
ylabel(['Absorber Temp',10,'[ ^oC ]'], 'FontSize', 14)
xlabel(['Time Elapsed [ hr ]',10,'    '], 'FontSize', 14);xlim([0,7]);
l=legend(l_diffIET_dry', 'FontSize', 14,'Location','eastoutside');
grid on;a=get(l,'children');a=a([1 4]);set(a,'markersize',20);
set(gca,'Fontsize',18,'LineWidth',2)
for i =  1:length(af_IET_dry)-1 % Line / Marker Properties
    set(hLine041(i),{'Color'},{ColSetTrnc_IET(4*i - 3,:)}',...
        {'LineStyle'},{'none'}',{'Marker'},{'.'}')
end


% The following script locates the first x-intercept in the data. This
% represents where the in vitro and sunshine test temperatures differntials
% are equal.

% It was assumed that the equal temperature difference corresponds to an
% equal amount of energy absorbed, as the initial water mass is effectively
% the same.
%                                E = M_w * Cp * DT

% Equal Temperature difference - Time - Energy vectors for each test set
eT_air = zeros(1,length(af_IET_dry)-1); t_air= eT_air; t_abs = t_air;
eT_water = eT_air; t_water = eT_water; eT_abs = eT_water;
eI_air = zeros(1,length(af_IET_dry)-1);eI_water = eI_air; eI_abs = eI_air;
index_air = eI_air; index_water = eI_water; index_abs = eI_abs;

% finding intercepts using the derivative of the sign of the data DT
for j= 1 : length(af_IET_dry)-1
    for i = 1:length(dT2)
        if isnan(dT2(i,j))== 1
            dT2(i,j) = 0;
        end
        if isnan(dT2(i,j))== 1
            dT2(i,j) = 0;
        end
    end
end
k2=diff(sign(dT2));   k4=diff(sign(dT4)); k1=diff(sign(dT1));
for j = 1 : length(af_IET_dry)-1
    start_value = 15;% offset to remove initial transient behaviour

% finding first intercept in each dataset, accounting for transient offset
    i2=find(k2(start_value:length(k2),j)~=0,1,'first')+1;
    i4=find(k4(start_value:length(k4),j)~=0,1,'first')+1;
    i1=find(k1(start_value:length(k1),j)~=0,1,'first')+1;
    if i2+start_value > length(Data_1.T4)
        i2 = length(Data_1.T4)-start_value;
    end
```

```matlab
    if i4+start_value > length(Data_1.T4)
        i4 = length(Data_1.T4)-start_value;
    end
    eT_air(j) =Data_1.T2(start_value+i2,af_IET_dry(j+1));
    t_air(j) = Data_1.t(start_value+i2,af_IET_dry(j+1));
    eI_air(j) = int_TI1_dry(start_value+i2,(j+1));
    index_air(j) = start_value+i2;
    eT_water(j) =Data_1.T4(start_value+i4,af_IET_dry(j+1));
    t_water(j) = Data_1.t(start_value+i4,af_IET_dry(j+1));
    eI_water(j) = int_TI1_dry(start_value+i4,(j+1));
    index_water(j) = start_value+i4;
    eT_abs(j) =Data_1.T4(start_value+i4,af_IET_dry(j+1));
    t_abs(j) = Data_1.t(start_value+i4,af_IET_dry(j+1));
    eI_abs(j) = int_TI1_dry(start_value+i4,(j+1));
    index_abs(j) = start_value+i1;
end

%% PLOT 6.4b All x-axis crossings in the 3rd dT2 Data set marked in red
% Does the result actually mean anything as there are multiple x-intercept
% crossings over the test period. I assumed the first one was significant
figure; B=k2~=0;
x_int = find(B(start_value : length(Data_1.T4),1) ~= 0); plot(dT2(:,1));
xlim([0,3520]); ylim([-5,10]); grid on; hold on;
plot(x_int + start_value,dT2(x_int(:) + start_value,1),'xr','markersize',9)

%% PLOT 6.5: Locating when Temperature rise is equal to Reference Test
figure('Name','Figure 6.5: Temperature Differences','NumberTitle',...
    'off','units','normalized','outerposition',[0 0 1 1]);
subplot(3,1,1)
[hLine042] = plot(Data_1.t(1:end,af_IET_dry(2:end)),...
    dT4(1:length(Data_1.T4),:));
title('Temperature difference between Sunshine & Reference Tests',...
    'FontSize', 14)
ylabel(['Water Temp',10,'[ ^oC ]'], 'FontSize', 14);ylim([-20,40]);
xlabel('Time Elapsed [ hr ]', 'FontSize', 14);xlim([0,7]);
l=legend(l_diffIET_dry', 'FontSize', 14,'Location','eastoutside');
grid on;a=get(l,'children');a=a([1 4]);set(a,'markersize',20);
set(gca,'Fontsize',18,'LineWidth',2)
for i =  1:length(af_IET_dry)-1 % Line / Marker Properties
    set(hLine042(i),{'Color'},{ColSetTrnc_IET(4*i - 3,:)}',...
        {'LineStyle'},{'none'}',{'Marker'},{'.'}')
    hold on
    h=plot([t_water(i) t_water(i)],[-100 100],'Color',...
        (ColSetTrnc_IET(4*i - 3,:))','LineStyle','--');
end

subplot(3,1,2)
[hLine043] = plot(Data_1.t(1:end,af_IET_dry(2:end)),...
    dT2(1:length(Data_1.T4),:));
ylabel(['Air Temp',10,'[ ^oC ]'], 'FontSize', 14); ylim([-20,40]);
xlabel('Time Elapsed [ hr ]', 'FontSize', 14);xlim([0,7]);
l=legend(l_diffIET_dry', 'FontSize', 14,'Location','eastoutside');
grid on;a=get(l,'children');a=a([1 4]);set(a,'markersize',20);
set(gca,'Fontsize',18,'LineWidth',2)
```

```matlab
for i =  1:length(af_IET_dry)-1 % Line / Marker Properties
    set(hLine043(i),{'Color'},{ColSetTrnc_IET(4*i - 3,:)}',...
        {'LineStyle'},{'none'}',{'Marker'},{'.'}')
    hold on;
    h = plot([t_air(i) t_air(i)],[-100 100],'Color',...
        (ColSetTrnc_IET(4*i - 3,:))','LineStyle','--');
end


subplot(3,1,3)
[hLine043] = plot(Data_1.t(1:end,af_IET_dry(2:end)),...
    dT1(1:length(Data_1.T1),:));
ylabel(['Absorber Temp',10,'[ ^oC ]', 'FontSize', 14); ylim([-20,40]);
xlabel('Time Elapsed [ hr ]', 'FontSize', 14);xlim([0,7]);
l=legend(l_diffIET_dry', 'FontSize', 14,'Location','eastoutside');
grid on;a=get(l,'children');a=a([1 4]);set(a,'markersize',20);
set(gca,'Fontsize',18,'LineWidth',2)
for i =  1:length(af_IET_dry)-1 % Line / Marker Properties
    set(hLine043(i),{'Color'},{ColSetTrnc_IET(4*i - 3,:)}',...
        {'LineStyle'},{'none'}',{'Marker'},{'.'}')
    hold on;
    h = plot([t_abs(i) t_abs(i)],[-100 100],'Color',...
        (ColSetTrnc_IET(4*i - 3,:))','LineStyle','--');
end
%% PLOT 6.6: Equating the incident energy based on first equal DT instance
figure('Name','Figure 6.6: Energy Equivalences','NumberTitle',...
    'off','units','normalized','outerposition',[0 0 1 1]);
[hLine042] = plot(Data_1.t(:,af_IET_dry(:)),...
    int_TI1_dry(:,1:length(af_IET_dry)));
title('Equivalent Energy Input Sunshine & Reference Tests',...
    'FontSize', 14)
ylabel(['Energy Accumulated',10,'[ J / m^2 ]','FontSize',14);
xlabel('Time Elapsed [ hr ]', 'FontSize', 14);xlim([0,7]);
l=legend(l_IE', 'FontSize', 14,'Location','eastoutside');
grid on;a=get(l,'children');a=a([1 4 7]);set(a,'markersize',20);
set(gca,'Fontsize',18,'LineWidth',2)
for i =  1:length(af_IET_dry) % Line / Marker Properties
    set(hLine042(i),{'Color'},{ColSet_IET(4*i - 3,:)}',...
        {'LineStyle'},{'none'}',{'Marker'},{'.'}')
    if i ~=1
        hold on
        h1 = plot(t_water(i-1),eI_water(i-1),'o','MarkerEdgeColor',...
            (ColSetTrnc_IET(4*(i-1) - 3,:))','markersize',12);
        h2 = plot(t_air(i-1),eI_air(i-1),'x','MarkerEdgeColor',...
            (ColSetTrnc_IET(4*(i-1) - 3,:))','markersize',12);
        h3 = plot(t_abs(i-1),eI_abs(i-1),'x','MarkerEdgeColor',...
            (ColSetTrnc_IET(4*(i-1) - 3,:))','markersize',12);
    end
end

% this script equates the accumulated energy values based on the
% temperature rise and scales the in vitro test readings by a corrective
% factor to obtain the equivalent expected Solar Energy value

ref_Iwater = zeros(1,length(eI_water));ref_Iair=ref_Iwater;
for i = 1 : length (eI_water)
```

```matlab
        % Using the indexed points of equal energy input, the corresponding
        % reference test cumulative energy value is located (first column of
        % int_I1 corresponds to teh 500 W data set)
        ref_Iwater(i) = int_I1(index_water(i),1);
        ref_Iair(i) = int_I1(index_air(i),1);
    end
% The scaling factor is the actual (solar) energy divided by the in
% vitro (halogen energy)
scale_air = eI_air ./ ref_Iair;
scale_water = eI_water ./ ref_Iwater;

for i = 1 : length(t_air)
    if isnan(scale_air(i))==1
        scale_air(i) = scale_water(i); %remove NaN from averaged value
    end
    scale_av = mean([scale_air;scale_water]);
    hold on;
    h3 =plot(Data_1.t(:,af_IET_dry(1)),...
        scale_av(i)*(int_TI1_dry(:,1)),'--',...
        'Color',(ColSetTrnc_IET(4*(i) - 3,:))');
end
scale_single=mean([scale_av(end-1);scale_av(end)]); %ignore T19 entry
scale_I1 = scale_single*Data_1.I1(:,af_IET_dry(1));

%% PLOT 6.7:   Scaling Factor to correct in vitro Incident Energy data

figure('Name','Figure 6.7: Scaled Incident Energy','NumberTitle','off',...
    'units','normalized','outerposition',[0 0 1 1]);
h4=plot(Data_1.t(:,17),[Data_1.I1(:,af_IET_dry(1)) scale_I1]);
title('Corrected in vitro Energy Input for Reference Tests',...
    'FontSize', 14)
ylabel(['Power Flux',10,'[ W / m^2 ]'],'FontSize',14);
xlabel('Time Elapsed [ hr ]', 'FontSize', 14);xlim([0,7]);
for i = 1:length(h4)
    set(h4(i),{'Color'},{ColSet_IET(4*i - 3,:)}',...
        {'LineStyle'},{'none'}',{'Marker'},{'.'}')
end
l_EqualE = cell(2,1);
l_EqualE{1} = strcat(fields{af_IE(1)},' (Raw Data)');
l_EqualE{2} = strcat(fields{af_IE(1)},' (Corrected Data)');
l=legend(l_EqualE', 'FontSize', 14,'Location','eastoutside');
grid on;a=get(l,'children');a=a([1 4]);set(a,'markersize',20);
set(gca,'Fontsize',18,'LineWidth',2)
```

Appendix 11: UV FLEX Datasheet

UV Flex TPE Coated Polyester Specifications reproduced under fair use

http://www.nzduct.co.nz/afawcs0145921/CATID=21/ID=6/SID=945907357/productdetails.html

Available Diameters: 32 to 508mm   Operable Temperature Range: -40ºC to 150ºC

- Ideal for suction of chemical fumes and gases, air conditioning, vehicle construction
- Very good resistance to acids
- Good tolerane to UV
- Rot proofed and withstands severe flexing
- Colour: Black

Maximum Vacuum Specifications (bar)

	Polyurethane				PVC		FoodGrade Flex	U V Flex	High Temp flex
Size mm	Light	Medium	Heavy	ExtraHeavy	Light	Heavy	Medium	Light	N/A
25	0.30	0.40	0.60	N/A	0.22	0.82	0.50	0.25	N/A
32	0.30	0.35	0.50	0.90	0.20	0.80	0.40	0.20	N/A
40	0.25	0.30	0.45	0.70	0.18	0.60	0.35	0.15	N/A
52	0.20	0.28	0.40	0.60	0.15	0.40	0.30	0.10	0.32
63	0.16	0.25	0.35	0.55	0.14	0.35	0.25	0.08	0.22
76	0.14	0.20	0.35	0.50	0.10	0.30	0.22	0.07	0.14
82	0.10	0.18	0.30	0.45	0.09	0.30	0.20	0.06	N/A
90	0.10	0.17	0.30	0.45	N/A	N/A	N/A	0.05	N/A
102	0.09	0.15	0.30	0.40	0.08	0.25	0.17	0.05	0.08
110	0.09	0.15	0.25	0.35	N/A	0.25	N/A	0.04	N/A
120	0.08	0.15	0.25	0.30	N/A	N/A	N/A	0.04	N/A
127	0.08	0.12	0.25	0.25	0.06	0.20	0.15	0.04	0.05
140	0.06	0.12	0.20	0.20	N/A	N/A	N/A	0.04	N/A
152	0.06	0.10	0.20	0.20	0.05	0.18	0.12	0.04	0.04

Size mm	Polyurethane Light	Medium	Heavy	ExtraHeavy	PVC Light	Heavy	FoodGrade Flex Medium	U V Flex Light	High Temp flex N/A
160	0.05	0.10	0.15	0.20	N/A	N/A	N/A	0.03	N/A

Maximum Vacuum Specifications (bar) continued

	Polyurethane				PVC		FoodGrade Flex	U V Flex	High Temp flex
Size mm	Light	Medium	Heavy	ExtraHeavy	Light	Heavy	Medium	Light	N/A
180	0.05	0.10	0.15	0.15	0.04	0.16	0.11	0.03	N/A
203	0.05	0.09	0.12	0.15	0.03	0.15	0.10	0.02	0.02
229	0.04	0.09	0.11	0.10	0.03	N/A	N/A	0.02	N/A
254	0.04	0.06	0.10	0.10	0.03	0.12	0.10	0.02	0.01
279	0.03	0.06	0.09	0.10	N/A	N/A	N/A	0.01	N/A
305	0.03	0.06	0.09	0.10	0.02	N/A	0.08	0.01	N/A
356	0.02	0.04	0.09	N/A	0.02	N/A	N/A	0.01	N/A
400	0.02	0.02	0.08	N/A	0.01	N/A	N/A	0.01	N/A
457	0.01	N/A	0.06	N/A	0.01	N/A	N/A	0.01	N/A
508	0.01	N/A	0.04	N/A	0.01	N/A	N/A	0.01	N/A

Appendix 12: Pressure – Evaporation Rate Relationship

A selection of the data from the study conducted by Vinnichenko *et al* have been reproduced in Figure A12.1. This data was analysed further to extract a greater amount of detail from the findings.
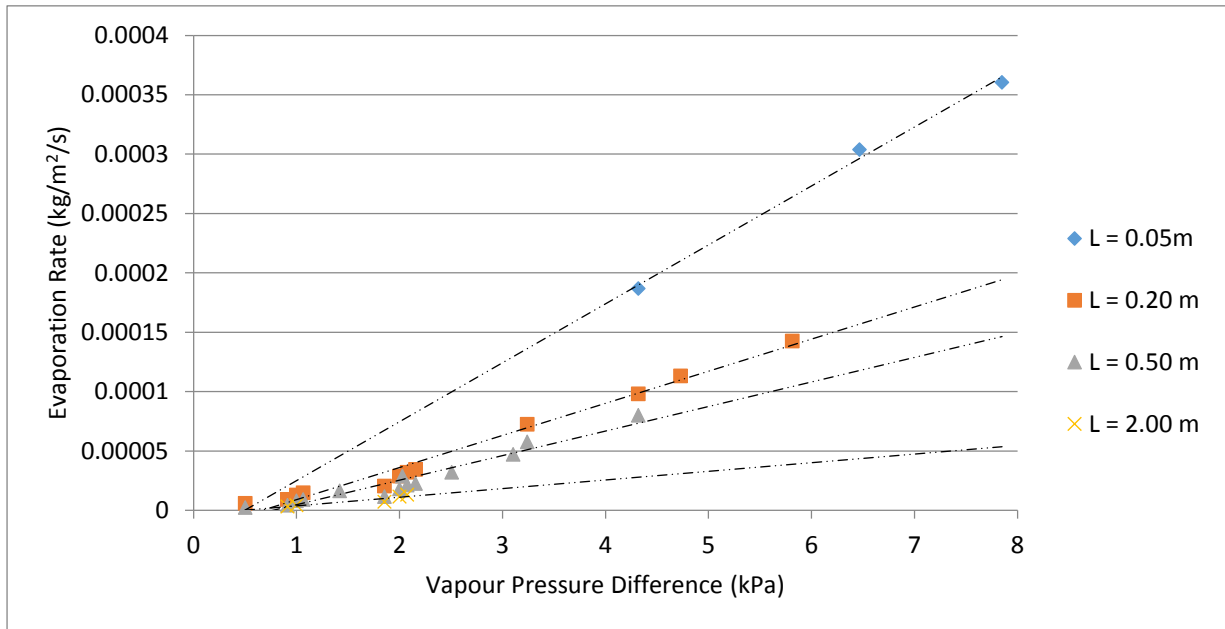
Figure A12.1: Relationship between pressure differential and evaporation rate as a function of characteristic length. Data: Vinnichenko *et al*.

The data presented indicates a strong linear dependence between evaporation rate and pressure difference for a given characteristic length (major dimension of evaporative surface area) over the range explored. This dependence becomes more pronounced as the tube diameter decreases which is indicative that at least one energy transferral mechanism does not scale linearly over the range of lengths considered. From these data, the connection between characteristic length and gradient of the evaporation – pressure relationship was established as shown in Figure A12.2.
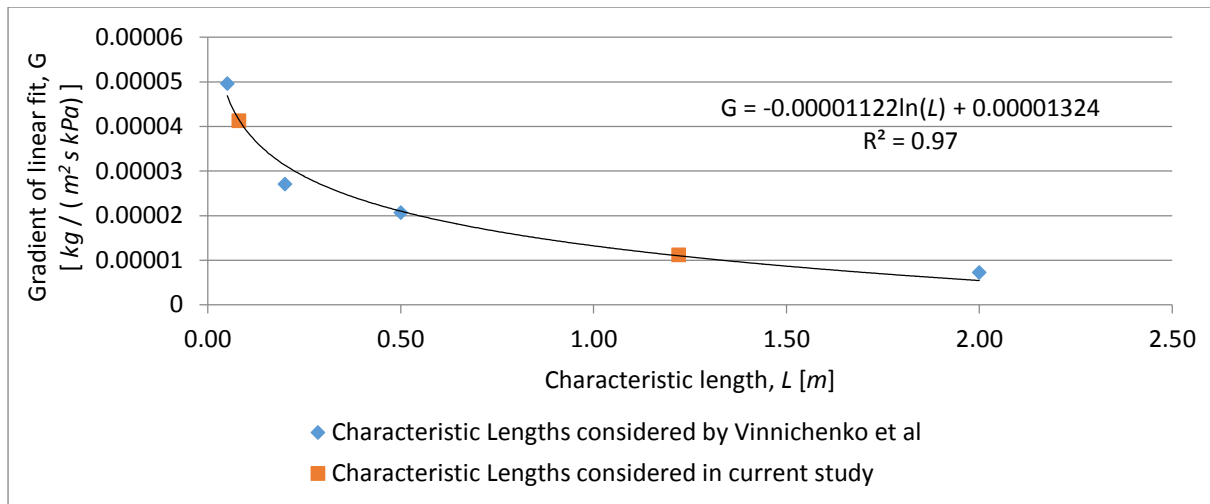
Figure A12.2: Inferred relationship and evaporation rate as a function of characteristic length.

The larger length considered in the current study corresponds to the primary test rig while the smaller length corresponds to the pressure testing rig. The relationship inferred from data in the previous study, as well as the regression coefficient are shown in Figure A12.2. Determination of the length-gradient relationship provided sufficient data to relate test rig operation back to expected evaporation rates for varying pressure differential conditions. The processed data is shown in Table A12.1, and the relationships for the experimental rig cases are plotted alongside the data from Figure A12.1 in Figure A12.3.

Table A12.1: Parameters for evaluating evaporation rate relationship (empirical cases in bold)						
Length, L $[m]$	0.05	**0.08**	0.2	0.5	**1.22**	2
Gradient, G $[kg / (m^2 s \, kPa)]$	4.96×10^{-5}	**4.13×10^{-5}**	2.70×10^{-5}	2.07×10^{-5}	**1.12×10^{-5}**	7.27×10^{-6}
Intercept $[kg / (m^2 s)]$	-2.47×10^{-5}	**-2.14×10^{-5}**	-1.81×10^{-5}	-1.59×10^{-5}	**-9.76×10^{-6}**	-3.56×10^{-6}
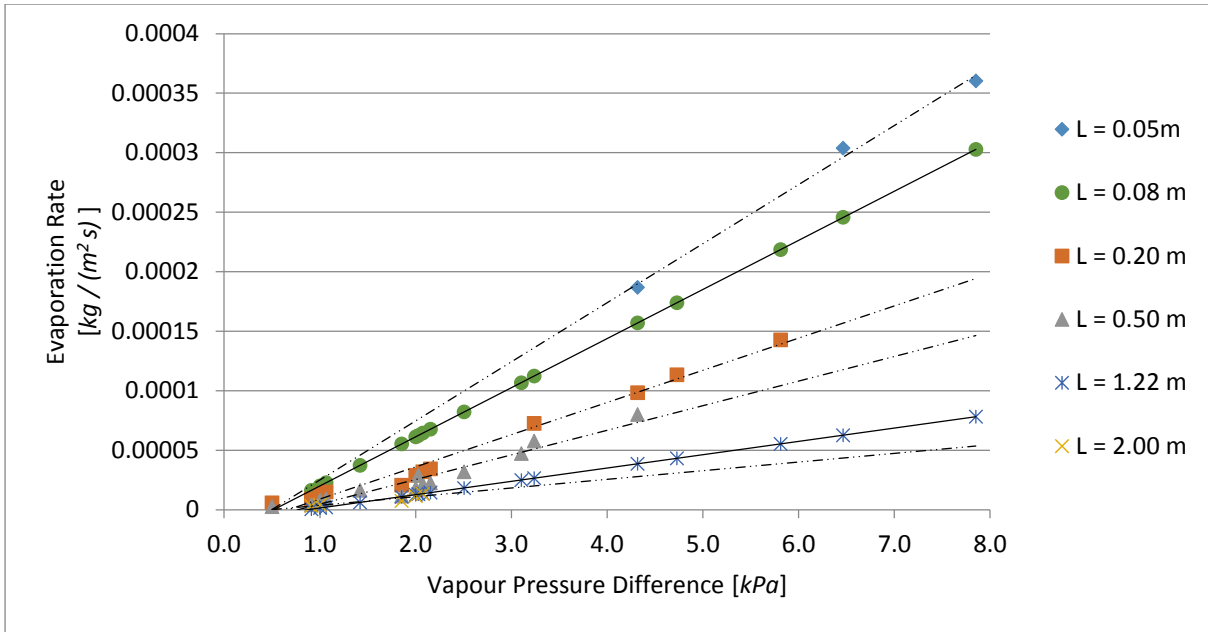
Figure A12.3: Expected evaporation rate – pressure difference relationships for test rigs (solid trend-lines), data from Figure A12.1 included for comparison (dashed trend-lines)

The gradient for the empirical cases is the most important outcome from this preliminary analysis. This term allows a change in pressure to be related back to a change in evaporation rate, and therefore still performance.

Appendix 13: Pressure Analysis

All tests displayed a high degree of noise on the pressure measurement as the transducer was strongly affected by minute air movements that could not be eliminated from the shared laboratory environment. The overall pressure trend was observed to be unaffected by changes to the system and oscillated about a mean point. The flatter regions coincide with times outside work hours. The typical pressure distribution observed during testing is shown in Figure A13.1
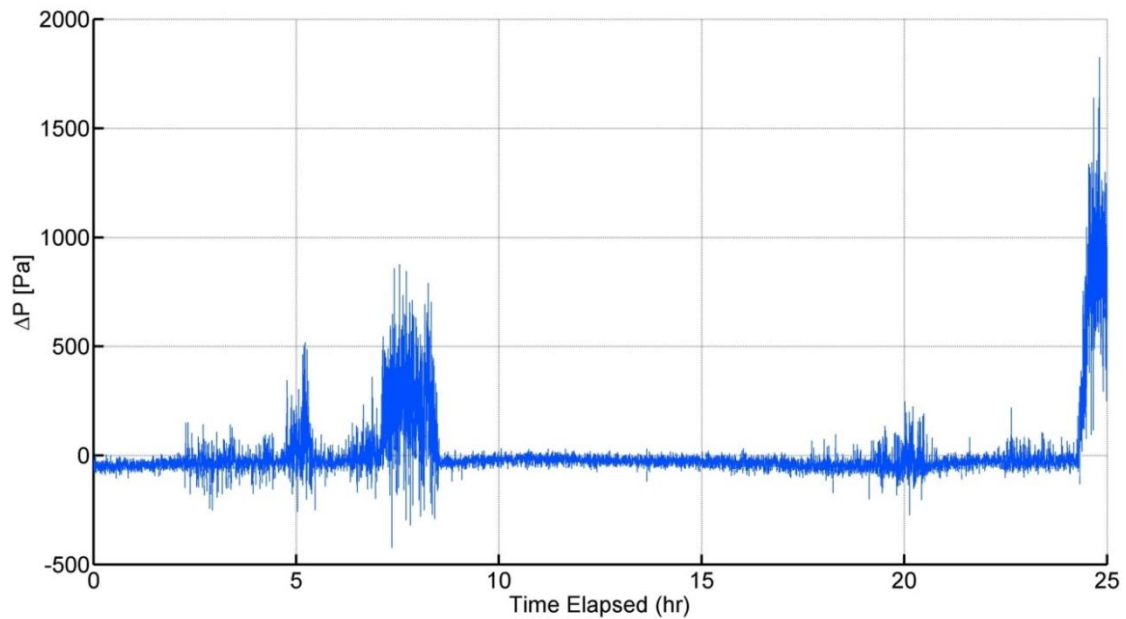
Figure A13.1: Typical pressure profile observed during reference test

As such, the average internal-external pressure difference for each test was obtained by numerically integrating the raw differential pressure data over the test period then dividing this by the time elapsed as shown in equation A13.1. This operation was repeated for each test and the time-averaged mean across all datasets. The script used to perform the calculations in MATLAB has been included at the end of Appendix 13.

$$\Delta P_{avg} = \frac{\sum_{i=1}^{n} \Delta P_i}{t_n - t_1} \qquad \text{(A13.1)}$$

From test to test, the mean pressure was found to vary substantially. This claim has been verified by the magnitude of the standard deviation on the mean pressure values. The relevant statistical quantities are presented in Table A13.1.

Table A13.1: Mean and standard deviation values for pressure differential during rig operation		
	$\overline{\Delta P}$	$s(\Delta P)$
Units	[kPa]	[kPa]
Reference Tests[17] [8, 17, 25]	13.0	27.6
All Tests	- 7.6	199.5

As a result of the inherent instability of the pressure transducer measurements, a more robust first principles approach was taken using psychrometric and thermodynamic considerations. The method involved finding the saturation pressure at the evaporative surface, then the partial vapour pressures at both the condensation and evaporation surfaces. These quantities were obtained using only the relative humidity and temperature measurements and were deemed much more reliable for the analysis. The MATLAB script used to perform these calculations has been included at the end of Appendix 13.

It is important to note that such wild variation in pressure transducer measurement was unapparent when an externally acting agent was providing forcing to maintain a differential; as was the case when the secondary pressure rig was being tested. Once the rig seal was broken and the system pressure equalised, the noise in the readings tended to increase.

The psychrometric relations for obtaining the relevant pressure terms yielded the values presented in Table A13.2 which were then integrated back into the evaporation analysis using the relationships derived from the Vinnichenko *et al* dataset. The necessary terms are the saturation pressure, P_S, and the partial vapour pressure, P_V, which have been both evaluated at both the evaporation (*evap*) and condensation (*cdns*) surfaces for completeness.

---

[17] The Reference Tests simulate the basic Rig operating condition mentioned in section 4.3.7)

Table A13.2: Partial and Saturation Pressures at relevant surfaces obtained through first principles analysis			$\overline{P_i}$	$s(P_i)$
Relevant pressure at surface of interest			[kPa]	[kPa]
Reference Tests	Partial Vapour Pressure (Evaporation Surface)	$P_{V\,(evap)}$	5.7	2.1
	Saturation Pressure (Evaporation Surface)	$P_{S\,(evap)}$	12.0	0.7
	Partial Vapour Pressure (Condensation Surface)	$P_{V\,(cnds)}$	3.2	1.2
	Saturation Pressure (Condensation Surface)	$P_{S\,(cnds)}$	4.0	1.2
All Tests	Partial Vapour Pressure (Evaporation Surface)	$P_{V\,(evap)}$	4.9	7.5
	Saturation Pressure (Evaporation Surface)	$P_{S\,(evap)}$	9.8	17.4
	Partial Vapour Pressure (Condensation Surface)	$P_{V\,(cnds)}$	3.5	4.2
	Saturation Pressure (Condensation Surface)	$P_{S\,(cnds)}$	4.6	5.0

An appreciable amount of variation still exists in the mean pressure terms when all tests are considered. However, the magnitude of the standard deviation compared to the magnitude of the corresponding pressure term is much lower than using the previous method. The most likely reason for this variation is that different operating conditions, as apparent during the testing result in different pressure profiles. Grouping all terms together in a single mean may be too crude of an analysis. These 'All Test' values have been provided only for comparative purposes against the initial pressure transducer method of analysis.

The results relating to the reference tests only, display considerably less variance and have been deemed valid for the purpose of the pressure analysis. These tests are also more relevant for this analysis as the reference case represents the current state of the basic System, described in section 4.3.7.1.

The pressure differential of interest was defined by Vinnichenko *et al* as the differential between saturation pressure at the water surface and the partial vapour pressure far from this surface; termed the Vapour Pressure Difference, $\Delta P_{S\text{-}V}$, in section 4.3.7.4. In accordance with this definition, the condensation surface vapour pressure has been judged to represent the pressure far from the evaporation surface. The vapour pressure difference is therefore given by equation A13.2 and allows a corresponding evaporation rate under basic operation conditions of the system to be identified.

$$\Delta P_{S-V} = P_{s\,(evap)} - P_{V\,(cdns)} = 12.0 \pm 0.7 - 3.2 \pm 1.2 = 8.8 \pm 1.4 \, kPa \qquad \text{(A13.2)}$$

```matlab
%% Script for obtaining mean and standard deviation of pressure values


load AllData_1.mat
%% Data Loading and Relevant Data Truncation
fields = fieldnames(Data_1); nf = numel(fields);L = zeros(1,nf);
for i=1:nf
    L (i) = length(Data_1.(fields{i})(:,1));
end

time = max(L);P_int = zeros(time,nf); LastP = P_int; P_av = P_int;
for i = 1:nf    % Concatenates all tests to length of longest test
                % and removes trailing zeros from plot
    Data_1.t(:,i) = 1/3600*[Data_1.(fields{i})(:,1);...
        NaN*zeros([time-length(Data_1.(fields{i})(:,1)),1])];
    Data_1.P1(:,i) = [Data_1.(fields{i})(:,7);...
        NaN*zeros([time-length(Data_1.(fields{i})),1])];
    LastP(:,i)=find(isnan([Data_1.P1(:,i);NaN]),1,'first')-1;
    P_av(:,i) = P_int(LastP(i),i)/Data_1.t(LastP(i),i);
    Data_1.P_av = P_av';
    Data_1.P_total = 101325+P_av';
end
%% Pressure Manipulations
close all

 %Active Fields (af) - select the tests of interest using Appendix 08b
af = [8 17 25];
c = 0;
P_av = zeros(1,length(af));
LastP = zeros(1,length(af));
for i = af
    c = c+1;
 figure(af(c))
 subplot(2,1,1)
    plot(Data_1.t(:,i),Data_1.P1(:,i))
    P_int(:,i) = cumtrapz(Data_1.t(:,i),Data_1.P1(:,i));
    LastP(1,i)=find(isnan([Data_1.P1(:,i);NaN]),1,'first')-1;
    P_av(1,c) = P_int(LastP(i),i)/Data_1.t(LastP(i),i);
subplot(2,1,2)
    plot(Data_1.t(:,i),P_int(:,i))

end
mean(P_av)
std(P_av)
close all

%% Script for obtaining Saturated and Partial Pressure values

%% Geometric Properties specific to test rig
L = 1.2; W1 = .838; h1 = .55; h2 = .115; h4 = .993; h3 = h4-h2; W2 = .238;
% [m] Cavity geometry
V_air = L * W1 * (.5*(h1 + h3)) + L * W2 * h2; % [m^3] Air Cavity volume
```

```matlab
%% Thermodynamic Properties and relationships
Cp=4180; % [J/kg/K] Heat Capacity of water
R = 8.314; % [J/K/mol] Gas Constant
M_D = 0.028964; % [kg/mol] Molar Mass of Dry Air
M_V = 0.018016; % [kg/mol] Molar Mass of Water Vapour


%% Partial and Saturation Pressures

% Saturation Pressures are based only on the temperature of interest
% (either the Water or Internal Condenser Surface Temperature)

%Saturation Pressure Evap Surface
P_sat_evp1 = 610.78 * 10 .^ (7.5.*TW./(TW+237.5)); % [Pa]
P_sat_evp2=exp(77.345+0.0057.*(273+TW)-7235./(273+TW))./(273+TW).^8.2;%[Pa]
P_v_evap_ant = 10.^(8.07131-1730.63./(233.426+TW)).*133.322365;
P_d_evap_ant = P_tot - P_v_evap_ant; % [Pa] via Antoine Eqn
err_E = [abs(P_sat_evp1 - P_sat_evp1)./P_sat_evp1,...
         abs(P_sat_evp2-P_sat_evp1)./P_sat_evp1,...
         abs(P_v_evap_ant-P_sat_evp1)./P_sat_evp1];


%Saturation Pressure Cnds Surface
P_sat_cds1 = 610.78 * 10 .^ (7.5.*TC./(TC+237.5)); % [Pa]
P_sat_cds2=exp(77.345+0.0057.*(273+TC)-7235./(273+TC))./(273+TC).^8.2;%[Pa]
P_v_cdns_ant = 10.^(8.07131-1730.63./(233.426+TC)).*133.322365;
P_d_cdns_ant = P_tot - P_v_cdns_ant;% [Pa]  via  Antoine Eqn (cdns)
err_C = [abs(P_sat_cds1 - P_sat_cds1)./P_sat_cds1,...
         abs(P_sat_cds2-P_sat_cds1)./P_sat_cds1,...
         abs(P_v_cdns_ant-P_sat_cds1)./P_sat_cds1];


%% Figure 01 - Calculation Methods for Saturation Pressure
figure('units','normalized','outerposition',[0 0 1 1])
subplot(2,1,1);
plot(t,0.001.*[P_sat_evp1 P_sat_evp2 P_v_evap_ant],'LineWidth',2);
title('Theoretical Saturation Pressure at Evap. Surface','Fontsize',16);
l=legend('P_{E (sat)} = 610.78\times10 ^{(7.5T_E/(T_E+237.5))}',...
'P_{E2 (sat)} = e^{(77.3+0.0057\times(273+T_E)-
7235/(273+T_E))}/(273+T_E)^{8.2}',...
'P_{E3 (sat)} = 133\times10 ^{(8.07-1731/(233.426+T_E))} \it(Antoine
Eqn)');
 ylabel('Saturation Pressure [kPa]','Fontsize',16,'LineWidth',2);
set(l,'Location','eastoutside');set(gca,'Fontsize',16,'LineWidth',2);grid
on;
subplot(2,1,2);plot(t,0.001.*[P_sat_cds1 P_sat_cds2
P_v_cdns_ant],'LineWidth',2);
title('Theoretical Saturation Pressure at Cond.
Surface','Fontsize',16,'LineWidth',2)
l=legend('P_{C (sat)} = 610.78\times10 ^{((7.5T_c/(T_c+237.5)}',...
'P_{C2 (sat)} = e^{(77.3+0.0057\times(273+T_c)-
7235/(273+T_c))}/(273+T_c)^{8.2}',...
'P_{C3 (sat)} = 133\times10 ^{(8.07-1731/(233.426+T_c))} \it(Antoine
Eqn)');
ylabel('Saturation Pressure [kPa]','Fontsize',16,'LineWidth',2);
set(l,'Location','eastoutside');set(gca,'Fontsize',16,'LineWidth',2)
grid on;
```

```matlab
%% Figure 02 - Error between Calculation Methods for Saturation Pressure
figure('units','normalized','outerposition',[0 0 1 1]) %1
subplot(2,1,1);plot(t,100.*err_E,'LineWidth',2);
title('Error between theoretical Saturation Pressure Methods at Evaporation
Surface','Fontsize',16,'LineWidth',2);
set(gca,'Fontsize',16,'LineWidth',2);grid on;
l=legend('| (P_{E (sat)} - P_{E (sat)}) | / P_{E (sat)}',...
    '| (P_{E2 (sat)} - P_{E (sat)}) | / P_{E (sat)}',...
    '| (P_{E3 (sat)} - P_{E (sat)}) | / P_{E (sat)}');
ylabel('Relative Error [%]','Fontsize',16,'LineWidth',2);
set(l,'Location','eastoutside');
subplot(2,1,2);plot(t,100.*err_C,'LineWidth',2);
title('Error between theoretical Saturation Pressure Methods at
Condensation Surface','Fontsize',16,'LineWidth',2)
l=legend('| (P_{C (sat)} - P_{C (sat)}) | / P_{C (sat)}',...
    '| (P_{C2 (sat)} - P_{C (sat)}) | / P_{C (sat)}',...
    '| (P_{C3 (sat)} - P_{C (sat)}) | / P_{C (sat)}');
ylabel('Relative Error [%]','Fontsize',16,'LineWidth',2);
set(l,'Location','eastoutside');set(gca,'Fontsize',16,'LineWidth',2);
grid on;

% The theoretical Saturation Pressure at each surface is very similar
% irrespective of what calculation method is used
%                           max(err_E) = 0.3 %
%                           max(err_C) = 1.1 %

% For subsequent calculations, the first method P_sat_1 will be used
%% Vapour Pressure

% The vapour pressure is calculated using both the experimental Relative
% Humidity and implicitly using the relevant temperature in the Saturation
% Pressure Eqn.
% The dry air pressure is calculated as the difference between the Total
% Pressure[assumed to be constant with magnitude (P_av+P_atm) where P_av is
% the average pressure during testing] and the Vapour Pressure, calculated
% prior

% Partial Pressures @ Evap Surface(using Ideal Gas(IG) eqn)
P_v_evap = RHE./100 .* P_sat_evp1; P_d_evap = P_tot - P_v_evap; % [Pa]

% Partial Pressures @ Cnds Surface(using Ideal Gas(IG) eqn)
P_v_cdns = RHC./100 .* P_sat_cds1; P_d_cdns = P_tot - P_v_cdns; % [Pa]

Basic_eV = [mean(P_v_evap),std(P_v_evap)];
Basic_cV = [mean(P_v_cdns),std(P_v_cdns)];

Sat_eV = [mean(P_sat_evp1),std(P_sat_evp1)];
Sat_cV = [mean(P_sat_cds1),std(P_sat_cds1)];
%% Figure 03 - Vapour Partial Pressures
figure('units','normalized','outerposition',[0 0 1 1]);
subplot(2,1,1);plot(t,0.001.*[P_v_evap P_sat_evp1],'LineWidth',2);
title('Evaporation Surface','Fontsize',16,'LineWidth',2);
xlabel('Time Elapsed (hr)','Fontsize',16);
l=legend('P_{v (E)} = RH_E \times (P_{(E) (sat)})','P_{(E) (sat)} \it');
```

```matlab
ylabel('Vapour Pressure [kPa]','Fontsize',16,'LineWidth',2);
set(gca,'Fontsize',16,'LineWidth',2);grid on;
set(l,'Location','eastoutside');
subplot(2,1,2);plot(t,0.001.*[P_v_cdns P_sat_cds1],'LineWidth',2);
title('Condensation Surface','Fontsize',16);
l=legend('P_{v (C)} = RH_C \times (P_{(C) (sat)})','P_{(C) (sat)} \it');
xlabel('Time Elapsed (hr)','Fontsize',16);grid on;
ylabel('Vapour Pressure [kPa]','Fontsize',16,'LineWidth',2);
set(l,'Location','eastoutside');set(gca,'Fontsize',16,'LineWidth',2);
% As expected, both the evaporation and the condensation surfaces exhibit
% vapour pressures below the theoretical maximum. This result was expected
% as neither surface is at 100 % relative humidity
```

Appendix 14: Quantifying Performance Increase in Evaporation Rate
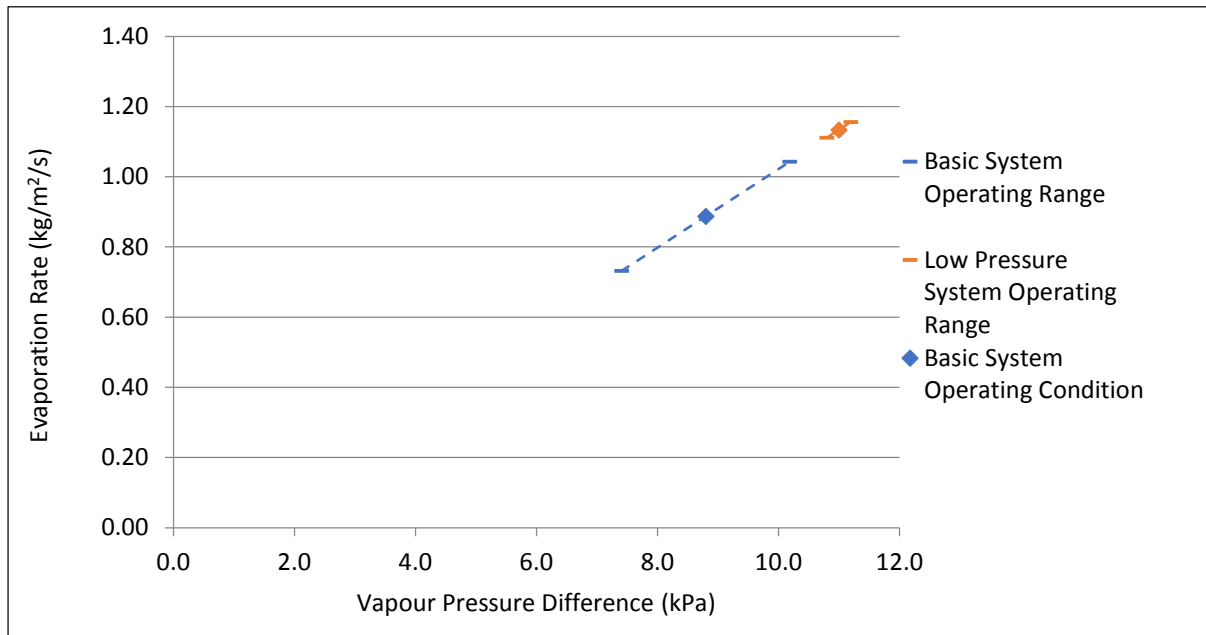
Figure A14.1: Processed empirical data relationship between evaporation rate and vapour pressure difference for both basic and Low Pressure system operation

Table A14.1: Vapour Pressure Difference and Evaporation Rate data for basic System					
Description	Term	Units	Lower Limit	Mean Value	Upper Limit
Vapour Pressure Difference	P_{S-V}	[kPa]	7.41	8.8	10.19
Evaporation Rate x 10^4	E	[kg /(m^2 s)]	0.73	0.89	1.04

Table A14.2: Vapour Pressure Difference and Evaporation Rate data for Low Pressure System, performance increase from basic System					
Description	Term	Units	Lower Limit	Mean Value	Upper Limit
Vapour Pressure Difference	P_{S-V}	[kPa]	10.8	11.0	11.2
Evaporation Rate x 10^4	E	[kg /(m^2 s)]	1.11	1.13	1.16
Increase from Basic System Mean Value	-	[%]	25.2%	**27.8%**	30.3%

The mean performance increase of the Low Pressure addition based on the empirical testing data and the relationships inferred from Vinnichenko *et al* is found to be 27.8 ±2.5 *%*.

Appendix 15: Component Reliability Analysis

Appendix 15 summarises the calculation methods employed to ascertain the probabilities for component success and failure in the expected operating conditions of the Low Pressure System when placed *in situ*. The methods are aligned with those presented in the Handbook of Reliability Prediction Procedures for Mechanical Equipment[18]. These component reliability values were combined according to the approach presented in section 4.3.7.5.

Component: Concentric LACT12-12V-20 Linear Actuator: 12" Stroke, 12V, 0.5"/s

Source: https://www.pololu.com/product/2312/resources

Notes: Actuator analysis conducted using theory and equations presented in Chapter 9: Actuators of the Handbook of Reliability Prediction Procedures for Mechanical Equipment

Analysis:

Description	Symbol	Units	Value
Number of cycles in Constant wear phase	N_o	-	769
Lubrication Constant	k_2	-	17700
wear factor (worst case scenario assumed)	γ	-	0.2
Yield Strength of softer material	F_y	psi	35000
Compressive stress between surfaces	S_C	lbs/in^2	7785
Load on Actuator	W_S	lbf	130
Cylinder Diameter (Cylinder 20.2mm)	D_1	in	0.80
Piston Diamter (Piston 20 mm)	D_2	in	0.79
Elastic Modulus Cylinder	E_1	lbs/in^2	10000000
Elastic Modulus Piston	E_2	lbs/in^2	10000000
Poisson's Ratio Cylinder	η_1	-	0.33
Poisson's Ratio Piston	η_2	-	0.33
Intermediate Equation 9.6 – Numerator	$N_{9.6}$	lbs/in^2	0.0206
Intermediate Equation 9.6 - Denominator	$D_{9.6}$	lbs/in^2	3×10^{-14}

Component: Concentric LACT12-12V-20 Linear Actuator: 12" Stroke, 12V, 0.5"/s

Analysis ctd:

Description	Symbol	Units	Value
Base Failure Rate	$\lambda_{B, Actuator}$	Failures/10^6 cycles	1301
Corrected Failure Rate	$\lambda_{Actuator}$	Failures/10^6 cycles	7327
Operating Temperature	T	^oC	34
Thermal Concentration Factor	C_T	-	2.82
Hardness (Cylinder)	H_C	lbs/in^2	25
Hardness (Piston)	H_P	lbs/in^2	25
Filtration Factor	C_S	-	1
Particle Hardness Factor	C_H	-	1
Particle Size Factor	C_N	-	2
Contamination Concentrator	C_{CP}	-	2
Duty Cycles	#	Cycles/yr	730
Probability of Failure	P (Failure per cycle)	-	0.01
Probability of Success	**P (Reliability per cycle)**	**-**	**0.99**

Component: PV Panel

Source: Industry Client (John Wilson) + Local Expert (Prof. Pat Bodger)

Notes: The current author contacted Prof. Pat Bodger, who has installed PV panels on schools in Tonga and as far as he is aware, there have been no failures since their commissioning in 2012-2013, so the accuracy of John's estimates will provide a conservative upper bound

Analysis:

	Unit Quantities	
Units Installed	500	(1)
PV Panels Required Servicing	5	(1)
Controllers Required Servicing/ year	5	(1)

	Reliability Statistics
P('Failure' of controller in a year)	0.01
P('Failure' of PV panel in a year)	0.01
P(Successful Controller)	0.99
P(Successful PV Panel)	**0.99**

(1). Unit quantities were provided by the industry client. The sample size is relatively small, and more accurate results could be obtained from a larger sample

This figure has been provisionally revised to 0.9 after discussion with the primary supervisor, in light of the small sample sizes from both prior sources

Component: Rubber Nitrile Seals

Source: https://www.amazon.co.uk/Flexible-Nitrile-Rubber-Washers-Grommets-y/dp/B008AGN1J8

Notes: Poppet Valve analysis conducted using equations presented in Chapter 3: Seals and Gaskets of the Handbook of Reliability Prediction Procedures for Mechanical Equipment

Analysis:

Description	Symbol	Units	Value	
Fluid Leakage	Q_a	in^3/min	2.25 x10^{-4}	
Allowable Fluid Leakage	Q_F	in^3/min	0.001	
Upstream Pressure	P_1	lb/in^2	14.7	(1)
Downstream Pressure	P_2	lb/in^2	12.7	
Absolute viscosity	v_a	$lbf\text{-}min/in^2$	1.60 x10^{-7}	
Inside Radius	r_i	in	0.08	
Outside Radius	r_o	in	0.175	
Mean Surface Finish of opposing surfaces	F	in	0.000064	
Conductance Parameter	H	in	2.89 x10^{-4}	
Meyers Hardness	M	lbs/in^2	1450	(2)
Contact Stress	C	lbs/in^2	1704	
Force Compressing Seals	F_C	lb	130	

Component: Rubber Nitrile Seals

Analysis ctd:

			Dynamic	Static	
Term	Symbol	Units	Value	Value	
Constant	K_1	-	-	3.3×10^{-4}	
Fluid Pressure Factor	C_P	-	0.25	-	
Allowable Leakage Factor	C_Q	-	4.22	-	
Seal Size Factor	C_{DL}	-	1.00	-	
Contact Stress and Hardness Factor	C_H	-	1.00	-	
Surface Finish Factor	C_F	-	2.68	-	
Fluid Viscosity Factor	C_v	-	0.02	-	
Temperature Factor	C_T	-	0.86	-	
Contaminant Factor	C_N	-	5.00		(3)
Pressure Velocity Factor	C_{PV}	-	1.00	-	
Base failure rate dynamic seal	$\lambda_{B,SEAL}$	Failures/10^6 hours	22.80	2.4	
Failure rate of dynamic seal	λ_{SEAL}	Failures/114 yrs (=10^6 hours)	6.04	0.001406	
Failure rate of dynamic seal	λ_{SEAL}	Failures/year	0.05	0.00	
Expected failures per year	λ_{SEAL}	Failures/cycle	7.25×10^{-5}	1.69×10^{-8}	
P(successful performance)	**-**	**-**	**0.95**	1.00	(4)

(1)   Air is the working fluid

(2)   Young's Modulus suitable for rubber materials according to Reliability Handbook

(3)   Due to the harsh saline environment which the system is exposed to, degradation of the seals are expected and higher weighting has been given to the Contamination factor than calculated

(4)   The conservative option is to consider the seal under dynamic conditions, which it will experience when the valves are opened and closed for filling the unit

Further seals will be required, therefore the successful performance probability is raised to the number of seals. Assuming three elements to completely seal the unit, this gives a total probability of successful performance of 85 *%* for the unit seals.

Component: Poppet Valve Assembly

Source: http://www.industrialtooling.co.nz/products/cum
5163

Notes: Poppet Valve analysis conducted using equations presented in Chapter 6: Valve Assemblies of the
Handbook of Reliability Prediction Procedures for Mechanical Equipment

Analysis:

Term	Symbol	Units	Value	
Fluid Leakage	Q_a	in^3/min	0.004	(1)
Allowable Fluid Leakage	Q_F	in^3/min	0.008	
Mean seat diameter	D_M	In	0.358	
Outer Diameter of Poppet	D_1	In	0.5112	
Diameter of Poppet Shaft	D_2	In	0.128	
Inside Diameter of Valve Outlet	D_3	In	0.204	
Mean Surface Finish of opposing surfaces	F	In	0.000064	
Upstream Pressure	P_1	lb/in^2	14.7	
Downstream Pressure	P_2	lb/in^2	12.7	
Absolute viscosity	v_a	$lbf\text{-}min/in^2$	1.60E-07	
Radial seat Land Width	L_W	in	0.472	
Seat Stress	S_s	lb/in^2	2.281	
Impact of Contaminant (size, hardness, quantity)	K_1	-	1	
Seat Area	A_{ST}	in^2	0.192876994	
Seat Land Area	A_{SL}	in^2	0.172958711	(2)
Viscosity /Temp Factor	C_v	-	446.5	
Friction Factor(steel on Steel)	C_μ	-	0.5	
Surface Finish Factor	C_F	-	2.706588621	
Pressure Factor	C_P	-	0.000001	
Leakage Factor	C_Q	-	6.875	
Contaminant Factor	C_N	-	0.0004	
Seat Stress Factor	C_S	-	64458.46623	
Seat Diameter Factor	C_{DT}	-	0.882992126	
Seat Land Width Factor	C_{SW}	-	0.25	
Flow Rate Factor	C_W	-	2	
Failure Rate		$failures/10^6$ operations	33372	
Failure Rate	P (failure per cycle)	-	0.033	
P(no failure, t = 1 yr)	**P (no failure)**	**-**	**0.967**	

Conversion between viscosity units

(1)   Air is the working fluid

(2)   75 °F = 24 °C

lbf s /ft²	min/s	ft²/in²
3.84 x10⁻⁰⁷	0.0167	0.00694

Component: UV Flex PTE flexible ducting

Source: Datasheet provided in Appendix 11

Notes: A provisional probability of success of 90 *%* has been given, as this is the general standard for non-medical engineering solutions

Analysis:

Description	Term	Units	Value
Probability of Failure	*P(failure)*	-	0.1
Probability of Success	***P(successful Operation)***	**-**	**0.9**

Component: Extra Frame elements to support volume change mechanism

Source: N/A

Notes: A provisional probability of success of 90 *%* has been given, as this is the general standard for non-medical engineering solutions

The loads experienced during operation are not expected to exceed 80*kg* gross weight borne by the structure. Wind loading and potentially corrosive exposure to saline water is also expected

Analysis:

Description	Term	Units	Value
Probability of Failure	*P(failure)*	-	0.1
Probability of Success	***P(successful Operation)***	**-**	**0.9**

Appendix 16: Forward Simulation Script used to Process Data

The following script was devised to as a more robust means to process the experimental data than the inbuilt Levenberg-Marquardt algorithm (lsqnonlin) that was initially used in MATLAB. This script processes the time period in a piecewise fashion (in steps of 1000 data points) rather than solving it all at once as did the previous algorithm. This version of the code was used to forward simulate for the water temperature equation

```matlab
% x = initial parameter guess
% MW = Mass of Water in the basin vector
% II = Solar incidence vector
% t = time vector
% TW = Water Temperature vector
function psi=FS_may26(x,MW,II,t,TW)
global Tw TA
dH_vap = 2257e3 ;  % Heat of Vaporization [J/kg]
Cp = 4185 ;        % Heat Capacity [J/(kg.K)]

Twi=Tw(1)*ones(1,1001);
L=length(Tw);
Tw(end+1:1000*ceil(length(Tw)/1000)+1)=Tw(end);
MW(end+1:length(Tw))=MW(end);
TA(end+1:length(Tw))=TA(end);
II(end+1:length(Tw))=II(end);

for I=1:ceil(length(TW)/1000)
    Twii=Twi(end);
    Twi=Tw(1000*(I-1)+(1:1001));
    MWi=MW(1000*(I-1)+(1:1001));
    TAi=TA(1000*(I-1)+(1:1001));
    IIi=II(1000*(I-1)+(1:1001));

    for JJ=1:100
        Twi=0.5*(Twi+Twii+cumtrapz(x(2)/Cp*IIi-x(1)*(Twi-TAi))-(MWi-
MWi(1))./MWi*dH_vap/Cp);
%    Tw(1000*(I-1)+(1:1001))=Twi;
%    plot(Tw);ylim([0 70]);drawnow
    end
    Tw(1000*(I-1)+(1:1001))=Twi;
end

Tw=Tw(1:L);
psi=Tw-TW;
```
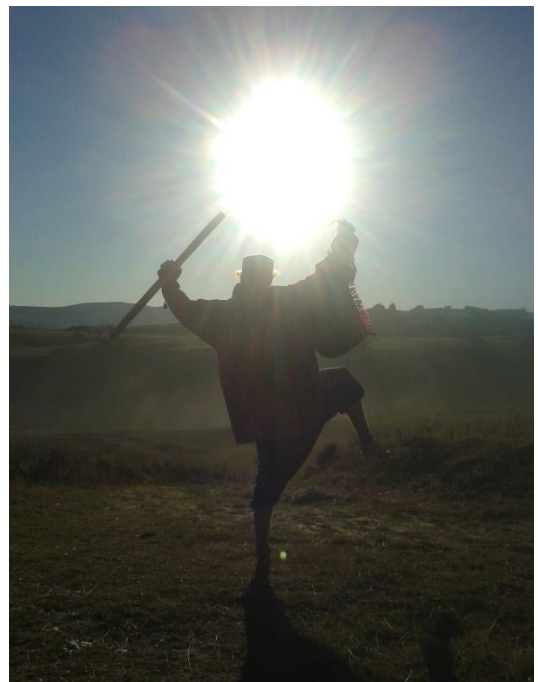
Appendix 17: Further Implications

Sun dances were left largely unexplored during the current study, despite holding possession of the crow totem for the latter stages of the work. Their effect on solar still productivity is unknown.

'E ra kaha, homai tōu mana!' – *Mighty sun give us your power!*